Universidade do Minho
Escola de Medicina

Sónia Isabel Nunes Guerra Gomes

The impact of astrocyte calcium signaling in cortico-limbic function and behavior

outubro de 2019

Sónia Isabel Nunes Guerra Gomes **The impact of astrocyte calcium signaling in cortico-limbic function and behavior**

UMinho | 2019

Universidade do Minho
Escola de Medicina

Sónia Isabel Nunes Guerra Gomes

The impact of astrocyte calcium signaling in cortico-limbic function and behavior

Tese de Doutoramento
Doutoramento em Ciências da Saúde

Trabalho efetuado sob a orientação do
Doutor João Filipe Pedreira de Oliveira
e da
Doutora Luísa Alexandra Meireles Pinto

outubro de 2019

DIREITOS DE AUTOR E CONDIÇÕES DE UTILIZAÇÃO DO TRABALHO POR TERCEIROS

Agradecimentos/Acknowledgments

Chegada ao final desta caminhada, quero agradecer a todos aqueles que, no momento certo, me souberam dar uma palavra de aconchego e de orientação, força e confiança para que este trabalho chegasse a bom porto. Ao Doutor João Filipe Oliveira por me ter contagiado com a sua paixão pelo mundo dos astrócitos! Obrigada pela partilha de conhecimentos, pela orientação, pela boa disposição e pelo entusiasmo! À Doutora Luísa Pinto por ter aceite ser minha orientadora! Obrigada pelas sugestões, pelas discussões científicas e pelo apoio constante! Aos Professores Nuno Sousa e João Bessa, pelo trabalho desenvolvido como coordenadores dos NERDs. Aos Professores Fernando Rodrigues, Margarida Correia-Neves e Joana Palha pela confiança que depositaram em mim como Representante dos alunos dos anos avançados do PhDCS. Aos Professores Jorge Pedrosa e Jorge Correia Pinto por trabalharem diariamente no sentido de nos proporcionarem as melhores condições de trabalho, mesmo em dias menos risonhos. A todos os funcionários do ICVS e da Escola de Medicina, com especial agradecimento às tratadoras do Biotério e à Doutora Alice Miranda. À Doutora Teresa Summavielle por ter aceite ser membro externo da Comissão que acompanhou esta tese. À Doutora Andreia Teixeira-Castro pelo apoio no trabalho experimental, pelas discussões, por ser um exemplo de cientista a seguir! Ao meu Astrogang, atuais membros: Inês "a engenheira", João Viana "o vírus" e Diana "a poveirinha"; e anteriores membros: Gabriela, Manuella, Daniel, Pedro Pinto, Joana Correia, Ana Oliveira e Ana Lima. À Vanessa, que foi uma das maiores conquistas deste doutoramento! Ganhei uma irmã para a vida, e se cheguei até aqui muito te devo a ti! Aos melhores vizinhos de secretária ever: Bárbara Pinheiro, Sofia Serra e Eduardo Gomes. Aos amigos que este doutoramento me deu: Cláudia Antunes, Luísa Santa Marinha, Jorge Silva, Marco Guimarães, Sofia Neves, Susana Monteiro, Dulce Almeida, Rita Silva, Marta Guedes, Isabel Castanho, Sara Pinheiro, Fátima Ramalhosa, Filipe Marques, João Costa, André Lopes, Mónica Morais e Francisca Bravo. Ao Eduardo Campos e ao Dinis Alves por todas as vezes que me ajudaram no biotério. Aos meus amigos de Aveiro: Ana Macedo, Carla Pereira, João Carvalho, Sara Marques e Tamira Cruz. Aos alcoólicos anónimos: Sílvia e Diogo, Samuel e Sofia, Rui e Tânia, Andreia e Daniel. Aos meus amigos de Braga: Carla, César e Francisca, Diogo, Manuel, José Antunes e Dominique. Ao meu afilhado Francisco. À minha família da Póvoa e Cabeceiras, em especial avós, tios e primos. Aos meus pais e ao meu irmão, que sempre acreditaram em mim e me deram todo o amor, força e confiança que precisei ao longo da vida. Ao Pedro, sem ti nada disto seria possível! Juntos somos mais fortes e a chegada ao final desta etapa é a prova disso. Esta tese é tua!

The work presented in this thesis was performed in the Life and Health Sciences Research Institute (ICVS), at the School of Medicine, University of Minho. Financial support was provided by a PhD grant (SFRH/BD/101298/2014 to SGG), FCT Investigator grants (IF/00328/2015 to JO, IF/01079/2014 to LP) and PTDC/MED-NEU/31417/2017 from the FCT – Foundation for Science and Technology, by BIAL Foundation grants (207/14 to JO and 427/14 to LP), by Northern Portugal Regional Operational Programme (NORTE 2020), under the Portugal 2020 Partnership Agreement, through the European Regional Development Fund (FEDER) (NORTE-01-0145-FEDER-000013); FEDER Funds, through the Competitiveness Factors Operational Programme (COMPETE), and The National Fund, through the FCT (POCI-01-0145-FEDER-007038).

STATEMENT OF INTEGRITY

I hereby declare having conducted this academic work with integrity. I confirm that I have not used plagiarism or any form of undue use of information or falsification of results along the process leading to its elaboration.

I further declare that I have fully acknowledged the Code of Ethical Conduct of the University of Minho.

O impacto da sinalização de cálcio nos astrócitos na função cortico-límbica e no comportamento

Resumo

Os astrócitos desempenham múltiplas funções desde a homeostasia cerebral ao controlo e processamento da atividade sináptica. Eles integram sinais neuronais por elevações complexas de cálcio (Ca^{2+}) com impacto na comunicação neurónio-astrócito. As elevações de Ca^{2+} nos astrócitos podem ser divididas em dois tipos: globais (presentes no soma e principais processos) e/ou focais (presentes nos microdomínios). Apesar de estar descrito que as elevações globais de Ca^{2+} nos astrócitos podem modular a comunicação sináptica, continuam por esclarecer quais os mecanismos moleculares envolvidos. Desta forma, urge uma caracterização comportamental, estrutural e molecular detalhada para compreender esses mecanismos. Nesta tese, utilizámos o modelo de murganho que apresenta a deleção constitutiva do receptor 2 do inositol 1,4,5-trifosfato (IP_3R2 KO), no qual as elevações globais de Ca^{2+} nos astrócitos estão ausentes. Na primeira parte deste trabalho (Capítulo 2) demonstramos que os murganhos IP_3R2 KO têm um desenvolvimento somático e neurológico normal. Em seguida, a caracterização comportamental deste modelo transgénico (Capítulo 3) revelou que os murganhos IP_3R2 KO apresentam uma melhoria do desempenho cognitivo em tarefas dependentes do hipocampo. Identificámos o factor de transcrição *Foxo1* como modulador da expressão de genes específicos de astrócitos, responsáveis pela regulação do citoesqueleto e de espinhas dendríticas. A sobre-expressão do FOXO1 em astrócitos do hipocampo de murganho C57BL/6J foi suficiente para mimetizar a melhoria cognitiva verificada no modelo IP_3R2 KO. Este resultado levou-nos a avaliar o papel da sinalização global de Ca^{2+} no contexto da depressão, uma doença que afeta comportamento dependente das regiões cortico-límbicas (Capítulo 4). Os murganhos IP_3R2 KO apresentam uma surpreendente resiliência ao efeito ansiogénico do stress crónico. Por fim, explorámos o papel da sinalização de Ca^{2+} nos astrócitos no envelhecimento cognitivo (Capítulo 5). Os nossos resultados demonstram uma preservação do desempenho cognitivo em murganhos IP_3R2 KO envelhecidos, caracterizado por alteração do rácio neurónio/astrócito e por refinamento dendrítico dos neurónios da camada V do córtex pré-frontal. Em suma, este trabalho contribuiu para uma melhor compreensão do papel da sinalização global de Ca^{2+} nos astrócitos desde o desenvolvimento até ao envelhecimento, num contexto de saúde e doença. Os resultados revelaram um alvo terapêutico específico em astrócitos com potencial aplicação em contextos de depressão e envelhecimento cognitivo.

Palavras-chave: astrócito, cálcio, cérebro, comportamento, IP_3R2

The impact of astrocyte calcium signaling in cortico-limbic function and behavior

Abstract

Astrocytes are responsible for distinct functions ranging from brain homeostasis to the modulation of synaptic functioning. They integrate neuronal signals by complex calcium (Ca^{2+}) elevations that control intracellular mechanisms that in turn drive the neuron-astrocyte dialogue, modulating the activity of cells and networks. It is now recognized that Ca^{2+} elevations in astrocytes appear spatially distributed in global (soma and main processes) and/or focal regions (microdomains). Although it is observed that global astrocytic Ca^{2+} signaling contributes to synaptic communication, its role in circuit computation and behavioral performance is still poorly understood. A detailed behavioral, structural and molecular characterization should provide us with putative mechanisms underlying the roles of astrocytic Ca^{2+}.

In this thesis, we took advantage of the inositol 1,4,5-trisphosphate receptor type 2 knockout (IP_3R2 KO) mouse model, which lacks global Ca^{2+} signaling in astrocytes. In the first part of this work (Chapter 2), we demonstrate that IP_3R2 KO mice retain a normal developmental maturation, as compared with WT littermates. Next, a detailed behavioral characterization of this mouse model (Chapter 3) showed that IP_3R2 KO mice display enhanced cognitive performance in hippocampal-dependent tasks. We found *Foxo1* as the most active transcription factor controlling the increased expression of astrocyte-specific genes related with fine cytoskeleton modulation and spinogenesis, which could underlie the cognitive enhancement observed. Moreover, specific overexpression of FOXO1 in hippocampal astrocytes of C57BL/6J mice was enough to recapitulate the enhanced fear memory observed in IP_3R2 KO mice. This striking observation prompted us to test the role of global Ca^{2+} signaling in the context of depression, which affects cortico-limbic regions (Chapter 4). IP_3R2 KO mice present an unexpected resilience to the installation of stress effects, namely translated into an increased self-care and a reduced anxious-like phenotype. Finally, we explored the role of astrocytic Ca^{2+} signaling in cortico-limbic performance in aged mice that display cognitive decline (Chapter 5). We observed a preserved cognitive performance in aged IP_3R2 KO mice, an altered neuron/astrocyte ratio and a dendritic refinement of mPFC neurons. Overall, this work contributed to a better understanding on the role of global astrocytic Ca^{2+} signaling from development to aging, both in a health and disease context. We found a putative astrocyte-specific therapeutic target that could be used to prevent depression- and aging-related deficits.

Keywords: astrocyte, behavior, brain, calcium, IP_3R2

Contents

Abbreviations list

2TPR	-	Two-trial Place Recognition
AAV5	-	Adeno-Associated Virus 5
AD	-	Alzheimer's disease
AKT	-	Protein kinase B
Aldh1L1	-	Aldehyde dehydrogenase 1 family member L1
AMPA	-	Alpha-amino-3-hydroxy-5-methyl-4-isoxazole propionic acid
ANOVA	-	Analysis of variance
ATP	-	Adenosine triphosphate
AV	-	Average expression
BBB	-	Blood Brain Barrier
CA1	-	Cornu ammonis 1
Ca^{2+}	-	Calcium ion
CB1R	-	Cannabinoid receptor type 1
cDNA	-	Complementary DNA
CFC	-	Contextual Fear Conditioning
CNS	-	Central Nervous System
CORT	-	Corticosterone
CREB	-	cAMP response element-binding protein
CRS	-	Chronic Restraint Stress
Cx30	-	Connexin 30
Cx43	-	Connexin 43
Cxs	-	Connexins
D.I.	-	Discrimination Index
DAG	-	Diacylglycerol
DG	-	Dentate gyrus
dHIP	-	dorsal Hippocampus
dnSNARE	-	dominant negative domain of vesicular SNARE
DREADD	-	Designer Receptor Exclusively Activated by Designer Drugs
EPM	-	Elevated Plus Maze
ER	-	Endoplasmic Reticulum

Ezr	-	Ezrin
FC	-	Fold Change
FDR	-	False Discovery Rate
FOXO	-	Forkhead box protein O
FOXO1	-	Forkhead box protein O1
FST	-	Forced Swim Test
GABA	-	Gamma-aminobutyric acid
GECIs	-	Genetically Encoded Calcium Indicators
GFAP	-	Glial Fibrillary Acidic Protein
GLAST/EAAT1	-	Glutamate aspartate transporter/excitatory amino acid transporter 1
GLT-1/EAAT2	-	Glutamate transporter/excitatory amino acid transporter 2
GPCR	-	G protein-coupled receptor
GS	-	Glutamine Synthetase
HIP	-	Hippocampus
HPA	-	Hypothalamic–Pituitary–Adrenal axis
i.p.	-	Intraperitoneal
IP_3	-	Inositol 1,4,5-trisphosphate
IP_3R	-	Inositol 1,4,5-trisphosphate receptor
IP_3R2	-	Inositol 1,4,5-trisphosphate receptor type 2
IP_3R2 KO	-	Inositol 1,4,5-trisphosphate receptor type 2 knock-out
K^+	-	Potassium ion
Kir	-	Inward-rectifier potassium channel
LD Box	-	Light-Dark Box
LTD	-	Long-term Depression
LTP	-	Long-term Potentiation
MAPK	-	Mitogen-activated protein kinase
mGluR	-	Metabotropic glutamate receptor
mPFC	-	medial Prefrontal cortex
MWM	-	Morris Water Maze
Na^+	-	Sodium ion
NCX	-	Na^+/Ca^{2+} exchanger
NEP	-	Neuroepithelial cells

NES	-	Enrichment score threshold
NG2	-	Neuron-glia antigen 2 glia
NMDA	-	N-methyl-D-aspartate
NOR	-	Novel Object Recognition
OF	-	Open Field
PAP	-	Perisynaptic Astrocyte Process
PBS	-	Phosphate Buffered Saline
PCR	-	Polymerase Chain Reaction
PFC	-	Prefrontal cortex
PIP2	-	Phosphatidylinositol 4,5-bisphosphate
PKC	-	Protein kinase C
PLC	-	Phospholipase C
PMCA	-	Plasma membrane Ca^{2+}-ATPase channels
PND	-	Postnatal day
PTM	-	Post-translational modifications
RG	-	Radial glia
RIN	-	RNA integrity number
RM	-	Reference memory
RT-qPCR	-	Real-time quantitative PCR
S100β	-	S100 calcium-binding protein B
Sdc2	-	Syndecan-2
SDS	-	Sodium Dodecyl Sulfate
SEM	-	Standard Error of the Mean
SERCA	-	Sarcoendoplasmic reticulum calcium transport ATPase
SICs	-	Slow Inward Currents
SOCE	-	Store-operated Ca^{2+} entry
SOCs	-	Store-operated channels
TBS	-	Tris-buffered saline
tDCS	-	Transcranial direct current stimulation
TF	-	Transcription factor
TREK	-	TWIK-related K^{+} channel
TRP	-	Transient receptor potential channel

TRPA1	-	Transient receptor potential cation channel subfamily A member 1
TRPC	-	Transient receptor potential-canonical channel
TSS	-	Transcription Start Site
TST	-	Tail Suspension Test
uCMS	-	unpredictable Chronic mild stress
WM	-	Working memory
WT	-	Wild-type

Figures and tables list

CHAPTER 1

Introduction

1. Glial cells in the brain

The brain is the most complex organ, composed by a diversity of cell types organized in a defined structure. These unique characteristics allow it to regulate and dynamically respond to environmental changes and to coordinate several biological responses. During many years, neurons were recognized as the main cellular elements in the brain, responsible for transmitting and processing information through electrical impulses. Neurons are well organized into circuits and communicate by specialized structures called synapses. One hundred and sixty years ago, Rudolf Virchow revolutionized the neuroscience field by introducing the term "neuroglia", as non-neuronal cells of the central nervous system (CNS). During many years, glial cells were considered to play a passive role in brain functioning, mainly due to the absence of electrical excitability. They were described as a connective material responsible for filling the interstitial space and for playing a supportive role (Kettenmann and Verkhratsky 2008; McIver et al. 2013). However, several studies revealed that glial cells are not only important for homeostatic brain functions, but they are also active partners in the modulation of synaptic function (Perea et al. 2014). This fact was demonstrated due to the development of calcium (Ca^{2+}) dyes, which uncovered the observation that glial cells respond to the surrounding activity by elevating its intracellular Ca^{2+} levels (Cornell-Bell et al. 1990; Charles et al. 1991). Several reports described differences in the number, form, and function of glial cells pointing to an increase in the glia to neuron ratio in phylogenetically evolved species (Verkhratsky and Parpura 2014; Verkhratsky and Nedergaard 2016). Glial cells are a heterogeneous population that can be distinguished according to their morphology and associated functions. Microglia act as the immune and phagocytic cells of the brain, oligodendrocytes and Schwann cells play a role in axonal myelination, NG2-glia are acknowledged for their role as progenitor cells and astrocytes are the most abundant glial cell type population in the brain and the main focus of this thesis (Verkhratsky 2006; Jakel and Dimou 2017). A growing body of evidence has shown that astrocytes can sense (be activated by several signals), integrate (elevate its intracellular Ca^{2+} levels) and respond (release of gliotransmitters) to neuronal activity (Araque et al. 1999; Araque et al. 2014; Perea et al. 2014; Guerra-Gomes et al. 2017).

The main aim of this thesis was to assess the impact of astrocytic Ca^{2+} signaling in cortico-limbic function and behavior. Throughout this chapter, we will review the main topics related to astrocytic functions, mainly focusing on intracellular Ca^{2+} signaling and its role in the health and disease conditions.

1.1. Astrocytes

Astrocytes are the most numerous glial cell type in the CNS. These cells were termed astrocytes by Michael von Lenhossek in the 1890s due to their star-shaped morphology (Verkhratsky et al. 2016a). They correspond to a heterogeneous population that can be classified into protoplasmic astrocytes of the grey matter and fibrous astrocytes of the white matter. Moreover, in distinct brain regions, astrocytes display specific structural and functional properties as an adaptation to local circuit requirements, such as the Müller cells in the retina and Bergmann glia in the cerebellum (Emsley and Macklis 2006; Matyash and Kettenmann 2010; Oberheim et al. 2012; Verkhratsky and Parpura 2014; Ben Haim and Rowitch 2017; Farmer and Murai 2017; Mederos et al. 2018). Astrocytes are responsible for distinct functions from brain homeostasis to the control and processing of synaptic functioning. These glial cells regulate brain homeostasis by interacting in close proximity to neuronal cell bodies, dendrites, axons and synapses (Perea et al. 2009). They interact with blood vessels by enwrapping endothelial cells and pericytes with their endfeet, thus controlling neurovascular coupling (McIver et al. 2013). Astrocytes occupy a unique territory without a structural overlap between neighbor cells, in several brain regions. This morphological organization favors a locally and specific astrocytic response, which is important to respond and regulate the activity of a given brain region (Ben Haim and Rowitch 2017). Due to their spatial organization in individual territories, astrocytes display an efficient cell-to-cell communication mechanism through gap junctions, forming a syncytium. These gap junction channels are formed by connexins (Cxs), with Cx30 and Cx43 being the most expressed in astrocytes (Nagy et al. 1999; Giaume et al. 2010; Pannasch and Rouach 2013). These channels allow the diffusion of several small molecules (up to 1.5 kDa) between neighboring astrocytes, such as ions, neurotransmitters and energy metabolites. (Pannasch et al. 2011; Pannasch and Rouach 2013). Astrocytes may also communicate with vicinal astrocytes by generating intercellular Ca^{2+} waves through ATP release that will act on Gq-G-protein-coupled receptors (GPCR) present in neighboring cells, eliciting a Ca^{2+} response (Bowser and Khakh 2007). Thus, instead of responding to the surrounding stimuli by generating action potentials, astrocytes display a Ca^{2+}- and Na^{+}-based excitability. Besides Ca^{2+} elevations, the intracellular concentration of Na^{+} in astrocytes can be regulated by plasmalemmal channels, ATP-dependent pumps and ion exchangers (Parpura and Verkhratsky 2012).

Astrocytes express several membrane receptors, cell surface molecules, voltage- and ligand-gated ion channels. However, these ion channels are poorly expressed and consequently they do not present membrane excitability (Araque and Navarrete 2010). Astrocytes broadly express inwardly-retifying potassium (K^{+}) channel 4.1 (Kir4.1) and their membrane is highly permeable to this ion. These cells have

the ability to buffer excess extracellular K^+ resultant from neuronal activity and to distribute it to sites where its concentration is lower (Seifert et al. 2018).

Briefly, astrocytes are actively involved in brain homeostasis and participate in information processing by forming a network that allows an orchestrated response specific for each brain region and adapted to a physiological or pathological state (Araque 2008; Wang and Bordey 2008; Ben Haim and Rowitch 2017). Moreover, it was recently demonstrated that the developmental origin of astrocytes determines its organization as an intercellular network (Gutierrez et al. 2019).

1.1.1. Developmental origin and heterogeneity

The complexity of the adult CNS generation forecasts a diversity of mechanisms that give rise to different cell types during development. Several extrinsic developmental signals and intrinsic signaling cascades determine cell fate and consequently the generation of distinct neuronal cells with specific functional, morphological and molecular characteristics (Edlund and Jessell 1999; Molofsky et al. 2012). Astrocytes have been described as being as heterogeneous as neurons, with unique properties in different brain regions. Interestingly, a growing body of evidence showed that neurons and glial cells are generated in a temporarily distinct, yet overlapping pattern. In fact, the CNS is originated from the neuroepithelium, which consists of a thin monolayer of epithelial cells – the neural plate. From these neuroepithelial (NEP) cells, radial glia (RG) cells emerge (Kettenmann and Ransom 2005). The progenitor domains associated with both NEP and RG cells are determined by several environmental signals, indicating positional information about both dorsal-ventral and anterior-posterior axes. Among these signals are members of the dorsal bone morphogenetic protein and Sonic hedgehog (Kessaris et al. 2008; Bayraktar et al. 2014). During mammalian CNS development, neural stem cells are primarily generated, followed by glial cells (Figure 1.1). This allows the adjustment of glial cell number and organization into the newly formed neuronal circuit (Miller and Gauthier 2007; Kessaris et al. 2008). By the onset of neurogenesis, RG cells begin to express several astrocytic markers such as vimentin, glial fibrillary acidic protein (GFAP), glutamate aspartate transporter (GLAST) and glutamate transporter 1 (GLT-1) and glutamine synthetase (GS) (Dimou and Gotz 2014). In the mammalian CNS, gliogenesis begins in later periods of embryonic development and continues until late postnatal period. More specifically, astrocytes are generated around embryonic day 18, and their proliferation is almost complete at early postnatal stages (Miller and Gauthier 2007; Wang and Bordey 2008). However, their maturation continues throughout development and coincides with the establishment of synaptic and vascular connections, where astrocytes exert an

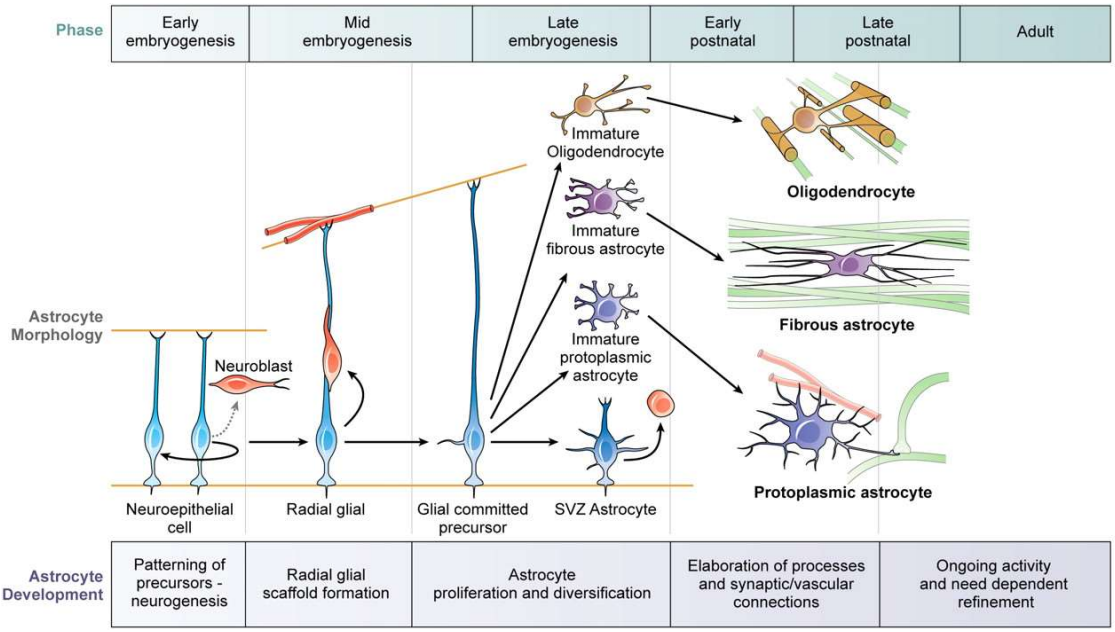

Figure 1.1 - The developmental origin of astrocytes.

Schematic drawing depicting several phases associated with pre- and postnatal astrocytic development. Radial glial cells develop from early neuroepithelial cells, which initially generate neurons, and at later stages give rise to glial-committed precursor cells to produce astrocytes. These precursors proliferate and can generate immature oligodendrocytes and immature fibrous or protoplasmic astrocytes. At the postnatal stage, these cells reach a mature state into oligodendrocytes, fibrous and protoplasmic astrocytes, which coincides with important phases of development like synaptogenesis and angiogenesis. During the late postnatal stage, astrocytes also participate in other important functions such as neuronal migration and synapse elimination. Adapted from Molofsky et al. (2012).

important role. During this phase, the expression of astrocytic markers such as GFAP, Aquaporin-4, and S100β significantly increases (Molofsky et al. 2012).

Several reports indicate that astrocytic heterogeneity is due to their derivation from regionally patterned RG cells (Bayraktar et al. 2014). Astrocytes display a regional morphological and genetic profile that was shown to be linked to their location and function within the CNS (Ben Haim and Rowitch 2017). They also present intrinsic functional features according to specific brain regions that allow them to build a concerted response to network changes. For instance, astrocytes from distinct brain regions exhibit distinct electrophysiological responses (Chai et al. 2017). Likewise, during running activity, Bergmann glia and neocortical astrocytes display contrasting Ca^{2+} responses (Nimmerjahn et al. 2009). Furthermore, in the rodent cortex, a stratification of Ca^{2+} responses is observed among the different cortical layers (Takata and Hirase 2008). More so, Cai et al. (2007) demonstrated that in the absence of a transcription

factor – Olig2 – the formation of white matter astrocytes is compromised, but gray matter astrocytes remain intact, pointing to a differential mechanism related with the generation of both types of astrocytes. Recently, it was shown that the developmental cell lineage also determines the establishment of a gap junctional network between sibling astrocytes (Gutierrez et al. 2019).

A growing number of markers have been helping the study of both morphological and molecular profiles of astrocytes. The first molecular marker described for astrocytes was GFAP, a hallmark cytoskeletal intermediate filament. GFAP is composed by 10 isoforms (α, β, γ, GFAPΔexon6, GFAPΔ164, GFAPΔexon7, GFAPΔ135, δ, κ, and ζ) and astrocytes differentially express these isoforms (Kamphuis et al. 2012; Hol and Pekny 2015). Several reports suggest caution for the use of this astrocytic marker, mainly due to astrocyte molecular diversity. In fact, some astrocytes do not stain for GFAP but are positive for other astrocytic markers such as S100β, GS or aldehyde dehydrogenase 1 family member L1 (Aldh1L1). The main reason behind this fact is the GFAP differential expression across brain regions. For example, most hippocampal astrocytes are GFAP-positive, while few thalamic astrocytes are detected by GFAP immunostaining (Sofroniew and Vinters 2010; Khakh and Sofroniew 2015). Similarly, an almost undetectable immunoreactivity of GFAP in the dorsal and ventral mouse cortex was described (Zhang et al. 2019). Other cell types in the nervous system (central and peripheral) may display positive staining for GFAP. In the CNS, detection of GFAP staining is also observed in RG cells in late embryogenic stages, while in the peripheral nervous system non-myelinating Schwann cells were found to be GFAP-positive (Khakh and Sofroniew 2015; Yang and Wang 2015).

Regarding morphology, it is important to note that GFAP only labels astrocyte main processes, which covers around 15% of the astrocyte total area (Khakh and Sofroniew 2015). However, the reconstruction of GFAP-stained structures allows a fast and reliable assessment of gross structural alterations in astrocytes (Tavares et al. 2017).

Technical advances in the field have allowed unveiling a diversity of molecular markers for astrocytes, which have proven to be pivotal for the development of new genetic targeting strategies (Cahoy et al. 2008; Zhang et al. 2014; Boisvert et al. 2018).

1.1.2. Homeostatic functions

Several lines of evidence point to astrocytes as the multitasking cells of the brain. Astrocytes are involved in the regulation of several CNS functions, from development to adulthood (Allen and Lyons 2018). They actively participate in brain homeostatic processes such as maintenance of the blood-brain barrier (BBB), control of local cerebral blood flow, angiogenesis, modulation of the extracellular matrix, neurotransmitter

uptake, extracellular ion buffering and metabolic support (Wang and Bordey 2008; Araque and Navarrete 2010).

Astrocytes directly contact with CNS microvasculature by extending long processes and enwrapping them with their endfeet. This close interaction allows the control of BBB integrity and modulates neurovascular coupling through the release of several gliotransmitters (Alvarez et al. 2013). This strategic location allows astrocytes to supply neuronal cells with nutrients (Allen and Lyons 2018). Astrocytes contribute to vasculature formation by promoting angiogenesis. A good example of this contribution is observed in the retina. More specifically, the platelet-derived growth factor released by retinal neurons triggers the astrocytic release of vascular endothelial cell growth factor that in turn stimulate blood vessel growth (Wang and Bordey 2008). Furthermore, astrocytes can shape the extracellular matrix by promoting neurite growth and contributing to extracellular matrix degradation and remodeling. Specifically, they express a wide range of extracellular matrix and adhesion molecules, such as N-cadherin and matrix metalloproteinases (Wang and Bordey 2008). Astrocytes secrete several growth factors, such as the brain-derived neurotrophic factor, glial cell line-derived neurotrophic factor, nerve growth factor, and basic fibroblast growth factor. These growth factors are fundamental to maintain cell viability, oxidant-antioxidant balance, metabolic functioning and gene expression control (Cabezas et al. 2016).

Besides their role in cell support, astrocytes can control neuronal excitability. They clear the byproducts of metabolism (e.g. ammonium, NH_4^+) and neurotransmitters (e.g. glutamate, gamma-aminobutyric acid (GABA), dopamine, noradrenaline) released to the synaptic cleft through the expression of protein transporters, predominantly GLT-1/EAAT2 and GLAST/EAAT1. Under physiological conditions, glutamate uptake occurs through an electrochemical gradient (3 Na^+/1H^+ in exchange for 1 K^+), which alters astrocyte membrane potential (Kreft et al. 2009; Allen 2014; Weber and Barros 2015). The expression levels of glutamate transporters are highly dynamic, dependent on the level of neuronal activity (Benediktsson et al. 2012; Allen and Lyons 2018). Conversely, GLT-1 ablation in mice leads to increased levels of extracellular glutamate, and consequently to spontaneous seizure episodes (Tanaka et al. 1997; Allen 2014). Another important astrocytic housekeeping function is the extracellular K^+ buffering. The major K^+ buffer present in astrocytes is Kir4.1. During periods of intense neuronal activity, K^+ accumulation leads to enhanced neuronal excitability and consequently to seizures. In line with these observations, mice lacking Kir4.1 specifically in astrocytes have an accumulation of extracellular K^+, impaired glutamate uptake and develop seizures due to increased excitotoxicity (Djukic et al. 2007; Allen 2014). Additionally, another class of K^+ channels (TREK-1 and TREK-2) was reported to be present in astrocytes and to contribute to K^+ buffering (Rivera-Pagan et al. 2015).

Interestingly, astrocytes not only regulate extracellular neurotransmitter concentration but also control its recycling. For example, glutamate is taken up by transporters and metabolized via the glutamate-glutamine shuttle. This mechanism leads to the production of glutamine via GS action. Glutamine is redistributed to glutamatergic/GABAergic neurons so that the neuronal production of glutamate/GABA is ensured (Wang and Bordey 2008; Allen 2014). In the same way, astrocytes are important providers of precursor molecules for neurons. For example, they are enriched in lipid synthesis pathways and produce molecules such as, for instance, cholesterol that is essential for presynaptic function maintenance (Allen 2014). Moreover, astrocytes uptake glucose from the blood stream and produce lactate via two pathways: glycogenolysis and glycolysis. Lactate is formed by astrocytes as a response to neuronal activity. The transport of lactate from astrocytes to neurons occurs through monocarboxylate transporters, fulfilling the neuronal energetic needs and providing signals that modulate synaptic function, the astrocyte-neuron lactate shuttle. For instance, in the hippocampus, astrocytic lactate release is essential to memory formation (Suzuki et al. 2011; Magistretti and Allaman 2018).

1.1.3. The tripartite synapse

The tripartite synapse concept emerged to describe the bidirectional communication between neurons and astrocytes in brain function control (Araque et al. 1999). This view completely challenged the classically accepted paradigm claiming that brain function relies exclusively on neuronal activity. In fact, astrocytes are intimately close to synapses and it is described that one astrocyte is able to make contact with over 100.000 synapses (Bushong et al. 2002). The tripartite synapse concept is based on three main astrocytic features: (i) expression of functional neurotransmitter receptors (e.g. for glutamate, ATP, GABA); (ii) ability to process complex Ca^{2+} signaling and communicate with vicinal astrocytes, through "Ca^{2+} waves" and (iii) release of active substances called "gliotransmitters" (e.g. glutamate, D-serine, ATP, GABA) to feedback to neurons (Figure 1.2).

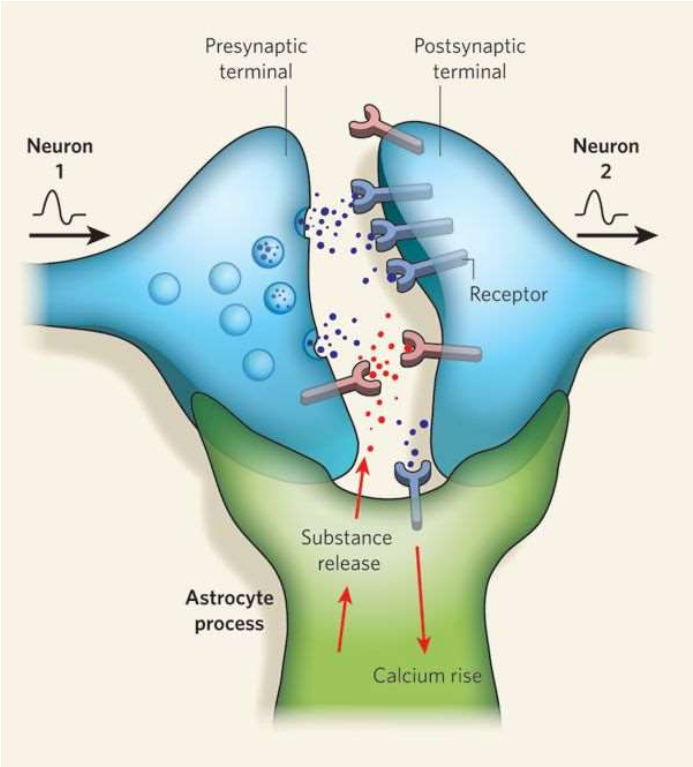

Figure 1.2 - The tripartite synapse.

Astrocytes closely enwrap pre- and postsynaptic terminals. They express several neurotransmitter receptors that allow them to sense and respond to neuronal activity. Neurotransmitters released to the synaptic cleft activate astrocytes, through binding to the receptors present on their membrane. Consequently, astrocytic intracellular Ca^{2+} levels increase. This Ca^{2+} rise in astrocytes may trigger the release of several substances, named "gliotransmitters", such as glutamate, ATP, and D-serine, which feedback to neurons to modulate network activity. Furthermore, astrocytes actively participate in other brain functions such as synaptogenesis, regulation of presynaptic function and modulation of the postsynaptic neuron response to neurotransmitters. Adapted from Allen and Barres (2009).

Astrocytes sense neuronal activity through a wide variety of neurotransmitter receptors, ion channels and transporters expressed in their membranes (Pannasch and Rouach 2013; Verkhratsky and Parpura 2014; De Pitta et al. 2016). These receptors can be activated by neurotransmitters, "gliotransmitters" or volume transmitters, which consequently trigger astrocyte excitability (Verkhratsky 2009). Astrocytes express a large number of GPCRs for different neurotransmitters such as glutamate, GABA, purines, norepinephrine, dopamine, and cannabinoids (Verkhratsky and Parpura 2014). Among those, activation of a GPCR coupled to a Gq-protein stimulates phospholipase C (PLC), leading to the production of inositol 1,4,5-trisphosphate (IP_3), which, in turn, will activate IP_3 receptors (IP_3Rs) present in the endoplasmic reticulum (ER). Consequently, Ca^{2+} is released from astrocytic internal stores and its intracellular Ca^{2+}

concentration increases (Wang and Bordey 2008; Perea et al. 2009). With the development of Ca^{2+}-imaging tools, it was demonstrated that, in several brain regions, excitatory and/or inhibitory signals trigger Ca^{2+} elevations in astrocytes and lead to gliotransmitter release (Guerra-Gomes et al. 2017). Furthermore, it was identified that astrocytes display not only Ca^{2+}-dependent but also Ca^{2+}-independent release of gliotransmitters (Parpura and Zorec 2010; Santello et al. 2012; Martineau 2013; Araque et al. 2014; Petrelli and Bezzi 2016). However, the occurrence of these mechanisms in physiological and/or pathological conditions is still under debate (Savtchouk and Volterra 2018; Fiacco and McCarthy 2018). Gliotransmitters are active substances that include glutamate, ATP, GABA, D-serine, tumor necrosis factor alpha, prostaglandins, proteins, and peptides. The release of gliotransmitters occur within a specific spatio-temporal range and control synaptic functioning and plasticity (Araque et al. 2014; Mederos et al. 2018). On one hand, low-frequency neuronal activity stimulates a local astrocytic Ca^{2+} response and consequently a local release of gliotransmitters. On the other hand, high-frequency synaptic activity triggers a broader astrocytic Ca^{2+} response, exerting long-range effects at distant synapses (Araque et al. 2014). In addition, astrocytes have the ability to control the spatial propagation of Ca^{2+} elevations through intracellular signaling pathways. Evidences supporting this effect show that simultaneous activation of glutamatergic and cholinergic inputs lead to decreased Ca^{2+} response in astrocytes, as compared with the independent activation of both pathways (Durkee and Araque 2019).

Due to the high complexity of astrocytic Ca^{2+} signaling, a detailed and comprehensive review on this astrocytic feature will be assessed in the next subchapter. More recently, a new concept postulated that astrocytes not only modulate active synapses but can also influence adjacent synapses. This process is called lateral astrocyte synaptic regulation and consists of a form of paracrine signaling that depends on the morphological and functional features of astrocytes (Covelo and Araque 2016). This notion broadened the view of the tripartite synapse concept, demonstrating that astrocytes are able to integrate and respond to signals resulting from one synapse to adjacent synapses.

1.2. Astrocytic calcium signaling

Despite being electrically silent, astrocytes display a high level of excitability in the form of dynamic intracellular Ca^{2+} elevations. Early studies, led by the Stephen Smith and Michael Sanderson labs, paved the way to this astrocytic function by using Ca^{2+} imaging techniques to study glial cell cultures (Cornell-Bell et al. 1990; Charles et al. 1991). A few years later, two elegant studies demonstrated the role of astrocytic Ca^{2+} signaling in the modulation of neuronal Ca^{2+} activity (Nedergaard 1994; Parpura et al. 1994). Nowadays, it is known that astrocytic Ca^{2+} signaling is incredibly complex (Volterra et al. 2014).

The development of several methodologies to tackle astrocytic Ca^{2+} signaling, as the genetically encoded Ca^{2+} indicators (GECIs), allowed the study of compartmental Ca^{2+} dynamics and to perform chronic imaging studies *in vivo* (Shigetomi et al. 2016). Although it is already accepted that the morphological and molecular heterogeneity of astrocytes is key to shape Ca^{2+} elevations, we are still far from decoding the complexity of astrocytic Ca^{2+} signaling and its functional consequences. For instance, it was shown that Ca^{2+} elevations in astrocytes may lead to differential responses in different brain regions (Volterra et al. 2014; Rusakov 2015; Khakh and Sofroniew 2015; Bazargani and Attwell 2016; Shigetomi et al. 2016). Moreover, Ca^{2+} dynamics in astrocytes are spatiotemporally regulated, which may account for the generation of diverse output signals (Santello et al. 2012; Volterra et al. 2014).

The complexity of Ca^{2+} elevations in astrocytes will be detailed in the next sections focusing on their mechanisms, shapes and functional consequences.

1.2.1. Mechanisms that trigger astrocytic calcium elevations

Recent technical advances in Ca^{2+} imaging tools allowed the discovery of complex spatiotemporal properties of astrocytic Ca^{2+} responses (Volterra et al. 2014; Shigetomi et al. 2016). Astrocytes elevate its intracellular Ca^{2+} levels in response to sensory stimulation, locomotor activity, autonomic responses, and synaptic transmission [for review, (Volterra et al. 2014; Guerra-Gomes et al. 2017)]. The most studied mechanism responsible for intracellular Ca^{2+} elevations in astrocytes is the PLC/IP_3 pathway. It occurs through a Gq-GPCR activation that will consequently activate PLC to hydrolyze the membrane lipid phosphatidylinositol 4,5-bisphosphate (PIP2) to generate diacylglycerol (DAG) and IP_3. The IP_3 molecule will bind to the IP_3Rs and elicit Ca^{2+} release from the ER (Agulhon et al. 2008). Besides IP_3Rs, other local ER structures, as the ryanodine receptors and sarcoplasmic/ER Ca^{2+} ATPase (SERCA) pumps, also contribute to intracellular Ca^{2+} turnover (Figure 1.3) (Parpura and Verkhratsky 2012; Rusakov 2015).

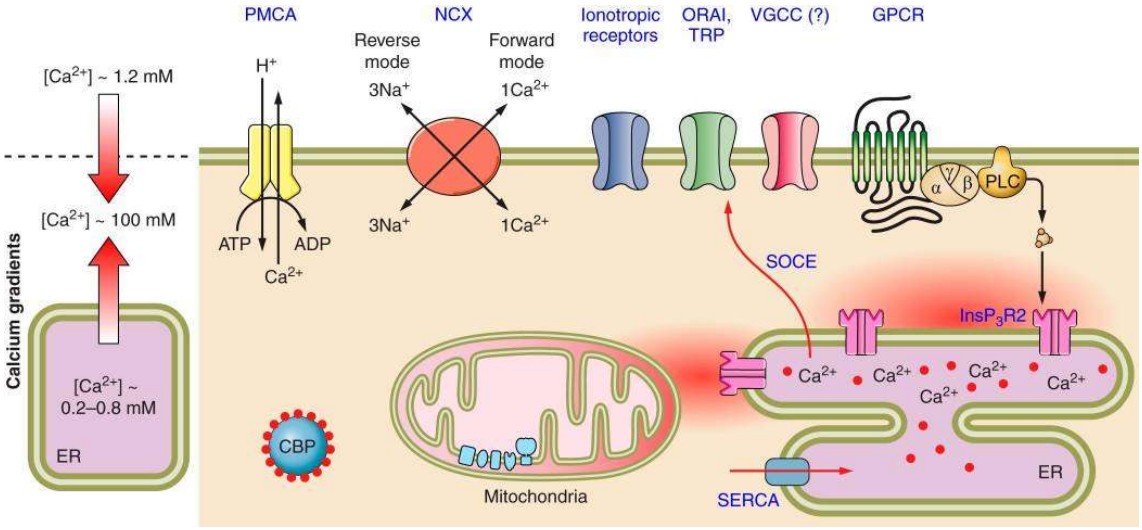

Figure 1.3 - Mechanisms of intracellular astrocytic Ca^{2+} elevations.

Calcium signaling in astrocytes is ensured by the coordinated activity of Ca^{2+} release from the endoplasmic reticulum (ER) mainly via a Gq-GPCR/PLC/IP_3R2 signaling pathway, or Ca^{2+} entry via plasma membrane Ca^{2+}-ATPase channels (PMCA), reversed Na^{+}-Ca^{2+} exchangers (NCX), ionotropic receptors (e.g. P2X4 and P2X7) and Ca^{2+} channels (ORAI, TRP, VGCC). Synaptic activity activates the Gq-GPCR pathway, which triggers a signaling cascade that will lead to the production of IP_3 and consequently activate IP_3R2 present in the ER to release Ca^{2+} to the cytosol. This reduction in ER Ca^{2+} content stimulates an important regulatory Ca^{2+} mechanism denominated store-operated Ca^{2+} entry (SOCE). This process is dependent on the action of Ca^{2+} sensors (e.g. Stim) and Ca^{2+} channels (ORAI and TRP). Ca^{2+} elevations control the initiation of several cellular reactions by interacting with Ca^{2+}-binding proteins (CBP) in the cytosol. These cytosolic Ca^{2+} signals are extinguished by Ca^{2+} extrusion to the extracellular space through Ca^{2+} pumps and NCX exchangers, and Ca^{2+} uptake into the ER by SERCA pumps and mitochondrial Ca^{2+} uniporters. Adapted from Verkhratsky and Nedergaard (2018).

Moreover, astrocytes are able to elevate its intracellular Ca^{2+} levels via external sources through plasma membrane Ca^{2+} channels, ionotropic receptors or store-operated channels (SOCs) (Verkhratsky and Nedergaard 2018). Astrocytes also express several types of transient receptor potential channels (TRP) channels (Verkhratsky et al. 2014). The spontaneous opening of transient receptor potential cation channel subfamily A member 1 (TRPA1) was shown to trigger Ca^{2+} transients that contribute to basal Ca^{2+} levels and to a fraction of intrinsic fluctuations (Shigetomi et al. 2011; Shigetomi et al. 2013; Khakh and McCarthy 2015). Furthermore, transient receptor potential-canonical (TRPC) channels contribute to the generation of store-operated Ca^{2+} entry (SOCE) by modulating Ca^{2+}-dependent vesicular glutamate release in cortical astrocytes (Parpura et al. 2011; Zorec et al. 2012; Reyes et al. 2013).

Astrocytic Ca^{2+} elevations may occur spontaneously or as a result of neuronal activity. Spontaneous Ca^{2+} responses occur sporadically in individual astrocytes and do not require neuronal activity to be elicited.

Several reports using cell culture, brain slices or *in vivo* two-photon imaging demonstrated that astrocytes are able to spontaneously increase Ca^{2+} levels from internal stores (Aguado et al. 2002; Nett et al. 2002; Hirase et al. 2004; Perea and Araque 2005; Wang et al. 2006a; Panatier et al. 2011; Kuga et al. 2011; Srinivasan et al. 2015). These events are more frequent in astrocytic processes and precede glutamate release (Panatier et al. 2011).

During many years, somatic Ca^{2+} elevations were the focus of glia research, mainly due to technical issues related to its accessibility and detection sensitivity. With the advent of novel Ca^{2+} imaging tools it was possible to disclose that, under physiological conditions, Ca^{2+} elevations in astrocytic soma differ from those of thinner processes. In distal regions, Ca^{2+} elevations are enclosed in localized microdomains and can occur spontaneously or in response to neuronal activity (Verkhratsky and Nedergaard 2018). A recent study has demonstrated that at far astrocytic processes (microdomains) the main active Ca^{2+} source derives from the mitochondria (Agarwal et al. 2017).

The development of molecular and live imaging techniques allowed for the recognition of distinct spatio-temporal features within somatic and microdomain Ca^{2+} elevations in astrocytes. Accordingly, astrocytic Ca^{2+} elevations can be classified as "global" (mainly observed in the soma and main processes) or "focal" (restricted to thin processes and microdomains) (Volterra et al. 2014). The main hallmarks associated to both "global" and "focal" Ca^{2+} events in astrocytes are summarized in Table 1.1.

Table 1.1 - Hallmarks of distinct Ca^{2+} responses present in the complex astrocytic morphology

Adapted from (Shigetomi et al. 2011; Di Castro et al. 2011; Volterra et al. 2014; Agarwal et al. 2017).

Hallmarks	"Global" Ca^{2+}	"Focal" Ca^{2+}
Characteristics	Larger in amplitude, duration and spatial extent), somatic	Faster, local
	Sensitive to neuronal firing	May occur independently of neuronal firing
	Generated by neuronal activity	Sensitive to pharmacological or IP_3Rs genetic deletion
	Activation occurs above a certain threshold of cell activation	Could originate from spontaneous neurotransmitter release from neighboring synapses
Trigger(s)	Gq-GPCR/IP_3Rs-dependent	IP_3Rs, TRPA1 channels, mitochondria (transient opening of the permeability transition pore)
Functional consequences	Increased gliotransmitter release probability	Not fully understood. Hypothesis = Synaptic stabilization and coordination of synaptic plasticity events

The following subchapters will cover the consequences of complex astrocytic Ca^{2+} signaling for synapses, circuit functioning and behavioral performance. This literature review is published (Guerra-Gomes et al. 2017) (in annex). Although some information may partially overlap with the previous subchapter, we include the review text *ipsis verbis* since is required to link with the functional consequences described.

1.2.2. Different forms of Ca^{2+} elevations in astrocytes: the complexity of simplicity

Astrocytes have emerged as key players in the regulation of synaptic physiology. They display complex and heterogeneous morphological structures and are able to sense and respond to environmental signals, modulate neuronal activity, synaptic transmission, and vascular function (Araque et al. 2014; Perea et al. 2014; Petrelli and Bezzi 2016); [for review (Petzold and Murthy 2011; Zorec et al. 2012)]. Synaptic activity is integrated by astrocytes (Perea and Araque 2005) and might result in intracellular Ca^{2+} elevations with specific spatial and temporal properties. These might appear as "global" and/or "focal" responses within the astrocytic complex morphology. It is yet unclear if global Ca^{2+} elevations are more representative of an integrative response or if they are the result of a linear summation of Ca^{2+} fluctuations or inositol 1,4,5-trisphosphate (IP_3) levels; nevertheless, these have been used for over two decades as a readout of astrocytic function [(Khakh and McCarthy 2015); [for review (Rusakov et al. 2014; Volterra et al. 2014)]. Ca^{2+} elevations may appear spontaneously or may be triggered by endogenous or exogenous stimuli. Traditionally, the use of Ca^{2+} indicator dyes allowed for the detection of Ca^{2+} elevations within astrocyte somata, but failed to efficiently track them in the fine processes (Wang et al. 2006b; Takata and Hirase 2008; Nizar et al. 2013). This hindered the complete interpretation of Ca^{2+} dynamics. More refined methods to image astrocyte Ca^{2+} signals have been recently described (Kanemaru et al. 2014; Srinivasan et al. 2016; Bindocci et al. 2017); [for review (Shigetomi et al. 2016)].

There are several mechanisms that trigger the elevation of astrocyte intracellular Ca^{2+} levels. The activation of Gq-GPCRs triggers the IP_3 signaling cascade and results in robust intracellular Ca^{2+} elevations, mainly via the IP_3 receptor type 2 activation (IP_3R2) (Petravicz et al. 2008; Takata et al. 2011; Navarrete et al. 2012); [for review (Parpura et al. 2011)]. Curiously, $GABA_B$ receptor (Gi-coupled GPCRs) activation was also shown to trigger intracellular Ca^{2+} elevations in astrocytes (Serrano et al. 2006; Mariotti et al. 2016; Perea et al. 2016). Moreover, astrocytes express several types of transient receptor potential (TRP) channels (Verkhratsky et al. 2014). The spontaneous opening of TRPA1 channels was shown to contribute to basal Ca^{2+} levels and to a fraction of intrinsic fluctuations (Shigetomi et al. 2011; Shigetomi et al. 2013), and their blockade contributes to a slight decrease in resting Ca^{2+} levels (Agarwal et al. 2017). Additionally, TRPC channels modulate Ca^{2+}-dependent vesicular glutamate release in cortical astrocytes by contributing

to the generation of store-operated Ca^{2+} entry (SOCE) (Reyes et al. 2013). More recently, Agarwal et al. (2017) reported that mitochondria, which are abundant in astrocytic processes, are the main active source of Ca^{2+} for localized events in far distant microdomains. While our understanding of the origin and features of astrocytic Ca^{2+} signaling is steadily growing, its functional consequences to the surrounding cellular circuits remain poorly understood. Therefore, this review will focus on the available data showing functional outputs of astrocytic Ca^{2+} elevations. The reader may find useful reviews and discussions elsewhere on the origin and features of astrocyte Ca^{2+} elevations (Scemes and Giaume 2006; Agulhon et al. 2008; Leybaert and Sanderson 2012; Volterra et al. 2014; Khakh and McCarthy 2015; Bazargani and Attwell 2016; Shigetomi et al. 2016) and on the role of astrocyte Ca^{2+} in pathology (Nedergaard et al. 2010; Agulhon et al. 2012; Vardjan et al. 2017).

1.2.3. Functional roles of astrocyte calcium elevations

The advent of novel techniques and approaches allowed for the quantification of astrocytic Ca^{2+} elevations and the characterization of their spatiotemporal dynamics in several brain regions. Below, we will discuss relevant studies that report on the functional influence of astrocytic Ca^{2+} elevations on synapses, circuits, and behavior.

Astrocyte Calcium and Synapses

The studies reviewed in this section describe experiments performed in rat and mouse brain slices. Several pieces of evidence indicate that astrocytic Ca^{2+} elevations precede the release of gliotransmitters, which may ultimately modulate synaptic transmission (Figure 1.4).

Different levels of neuronal activity appear to scale astrocytic Ca^{2+} levels, leading to orchestrated (multi)synaptic responses [for review, Araque et al. (2014)]. In the hippocampus, ATP-evoked astrocyte Ca^{2+} was shown to promote glutamate release, which consequently facilitates synaptic transmission through the activation of metabotropic glutamate receptors (mGluRs) (Perea and Araque 2007). Although further attempts to control astrocytic Ca^{2+} signaling failed either to affect general readouts of synaptic transmission and plasticity in the hippocampus [using MrgA1 and IP_3R2 KO mouse models (Petravicz et al. 2008; Agulhon et al. 2010)] or to detect glutamate release in the hippocampus or striatum [upon Designer Receptor Exclusively Activated by Designer Drugs (DREADD) activation (Chai et al. 2017)], a series of studies have supported this hypothesis. In fact, the tight modulation of astrocytic intracellular Ca^{2+} is crucial for D-serine-dependent long-term potentiation (LTP) of hippocampal CA1 pyramidal cells (Henneberger et al. 2010).

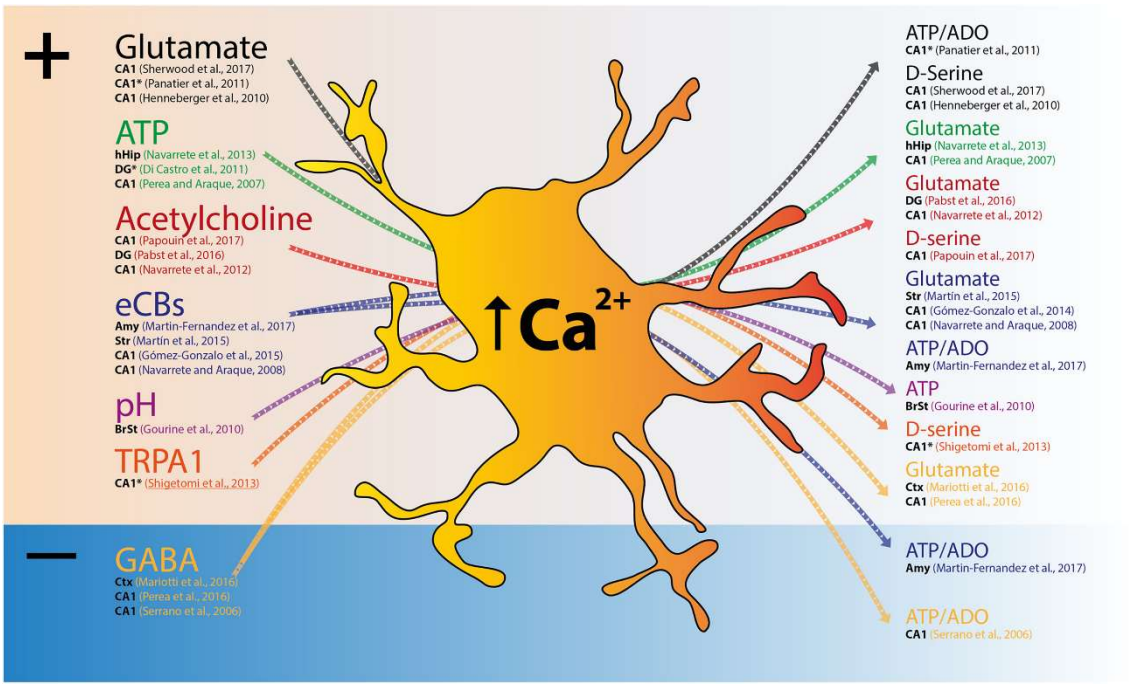

Figure 1.4 - Excitatory and/or inhibitory signals trigger Ca^{2+} elevations in astrocytes and lead to gliotransmitter release.

Scheme depicting input signals that trigger astrocyte Ca^{2+} elevations and respective transmitter release. Both excitatory (+) and inhibitory (–) signals cause global or focal Ca^{2+} elevations in astrocytes (Left), and precede gliotransmitter release that might exert excitation or inhibition of neighboring synapses (Right). For each reference, the region studied is indicated in black (Amy, Amygdala; BrSt, brainstem; CA1, CA1 subfield of the hippocampus; Ctx, cortex; DG, dentate gyrus; hHip, human hippocampus; Str, Striatum). *Indicates the studies that described functional consequences to focal Ca^{2+}, rather than global Ca^{2+} responses.

Accordingly, a recent study has showed that acute blockade of Ca^{2+}-dependent IP_3 mechanisms impairs LTP, but that this can be rescued by exogenous D-serine (Sherwood et al. 2017).

Astrocytic Ca^{2+} elevations appear to also promote alternative forms of plasticity in the brain. In the hippocampus, cholinergic afferents from the medial septum modulate CA1 synaptic plasticity via an astrocytic Ca^{2+}-dependent mechanism that triggers glutamate release and consequent activation of mGluRs in neurons (Navarrete et al. 2012). This mechanism of synaptic modulation is not restricted to the hippocampus since astrocytic Ca^{2+} elevations also mediate muscarinic acetylcholine receptor-dependent plasticity in the somatosensory cortex (Takata et al. 2011), as it will be discussed in the next chapter. Moreover, a recent study showed that the cholinergic input to astrocytes, driven by active/sleep phases, controls Ca^{2+}-dependent D-serine release, ultimately gearing up N-methyl-D-aspartate receptor

(NMDA) receptor activation at CA1 synapses (Papouin et al. 2017). In a different hippocampal subfield, the cholinergic activation of hilar astrocytes triggers intracellular Ca^{2+} elevations that precede the activation of hilar inhibitory interneurons, causing a long-lasting GABAergic inhibition of dentate granule cells (Pabst et al. 2016). Further evidences point out that astrocytic Ca^{2+} mediates endocannabinoid-dependent plasticity. Navarrete and Araque (2008) reported that the activation of astrocytic cannabinoid type 1 receptors (CB1R) leads to intracellular Ca^{2+} elevations, triggering glutamate release and slow inward currents (SICs) in vicinal pyramidal neurons. Furthermore, endocannabinoid-triggered elevation of astrocytic Ca^{2+} levels contributes to heteroneuronal LTP (Gomez-Gonzalo et al. 2015). In the striatum, a circuit-specific astrocyte-neuron signaling takes place in which the release of endocannabinoids promotes Ca^{2+} elevations in a specific population of astrocytes, triggering the release of glutamate that modulates excitability and synaptic transmission (Martin et al. 2015). Finally, in the medial central amygdala, astrocytes receive endocannabinoid signaling to release ATP and depress excitatory synapses from basolateral amygdala via A_1 adenosine receptor activation, and enhance inhibitory synapses from the lateral subdivision of the central amygdala via A_{2A} receptor activation. This redundancy system results in medial central amygdala neuronal inhibition with impact in animal behavior (Martin-Fernandez et al. 2017).

Interestingly, astrocytic Ca^{2+} elevations are not exclusive to the action of classic excitatory transmitters. Activation of GABA receptors in astrocytes was shown by different research groups to trigger Ca^{2+} elevations with functional synaptic consequences. Specifically, GABAergic heterosynaptic depression in the hippocampal CA1 subfield requires astrocytic Ca^{2+} elevations and ATP release, whose metabolite adenosine will activate A_1 receptors (Serrano et al. 2006). More recently, Mariotti et al. (2016) showed that the activation of $GABA_B$ receptors evoked somatic Ca^{2+} elevations, consequently leading to the occurrence of SICs in cortical pyramidal neurons. Curiously, these effects were absent in IP_3R2 KO mice suggesting a relationship between G_i-coupled GPCRs and IP_3 signaling in astrocytes. Moreover, the activation of astrocytic $GABA_B$ receptors triggered intracellular Ca^{2+} elevations in hippocampal CA1 astrocytes, which led to synaptic potentiation via glutamate release and modulation of presynaptic group I mGluRs (Perea et al. 2016).

Astrocytic Ca^{2+} signaling also plays a role in structural integrity of synapses. It was reported that the IP_3 "sponge" mouse model, whose astrocytic IP_3 signaling is impaired, has a reduced astrocytic coverage of asymmetric synapses leading to modulation of glutamatergic transmission (Tanaka et al. 2013). In accordance, activity-related structural remodeling of astrocytic processes in the vicinity of synapses was

shown to depend on presynaptic activity and to require G-protein-mediated Ca^{2+} elevations in astrocytes, both in the hippocampus and in the cortex (Perez-Alvarez et al. 2014).

Finally, Navarrete et al. (2013) studied cortical and hippocampal human brain samples and showed that increases in intracellular Ca^{2+} levels of both cortical and hippocampal astrocytes are accompanied by an increase in SICs frequency. These observations confirm that, at least partially, astrocyte Ca^{2+} elevations are also required to modulate synapses in the human brain.

Most of the studies mentioned above regarding synaptic modulation reported consequences of somatic (or in major processes) Ca^{2+} elevations. Recently, several elegant studies suggested that Ca^{2+} signals occurring only at astrocyte microdomains are sufficient to modulate synaptic events. Specifically, Ca^{2+} signals in astrocyte processes of the hippocampal DG are relevant for basal synaptic function, since the application of a Ca^{2+} chelator or an antagonist for a GPCR predominantly expressed in astrocyte processes decreased synaptic efficacy (Di Castro et al. 2011). Similarly, mGluR-dependent astrocytic Ca^{2+} signaling was shown to mediate the regulation of basal transmission in CA1 pyramidal neuron synapses (Panatier et al. 2011). The Ca^{2+} signaling that occurs at the distant processes appears to originate from distinct sources, other than the ER. For instance, TRPA1 channels mediate a transmembrane Ca^{2+} flux pathway with contributions to basal Ca^{2+} levels and regulation of interneuron inhibitory synapse efficacy via GABA transporter type 3 (Shigetomi et al. 2011). In addition, the same group showed that TRPA1 activation contributes to the release of D-serine into the extracellular space, which consequently influences NMDA-dependent hippocampal plasticity (Shigetomi et al. 2013).

Most of the available data resulted from experimental approaches that block general astrocyte Ca^{2+} elevations, namely by using Ca^{2+} chelators or genetic IP_3R2 deletion. This may explain the current bias toward effects of global (soma and main processes) Ca^{2+} signals rather than that of focal events (restricted to cellular microdomains). Nevertheless, it is now clear that global and focal signals coexist in specific spatio-temporal maps. Despite the 10- to 100-fold scale that distinguishes global and focal signals, both have been shown to precede transmitter release and modulate different forms of synaptic transmission [for review, Volterra et al. (2014)]. Future studies are needed to further discriminate their functional consequences.

Altogether, these sets of data suggest that astrocytes integrate brain circuits following two physiological mechanisms (Figure 1.4). First, the activation of astrocytes appears to represent a novel integration mechanism. Astrocyte Ca^{2+} elevations not only occur upon activation through various excitatory transmitters (e.g. glutamate, ATP, or acetylcholine), but can also be triggered by the inhibitory transmitter GABA. This means that, independently of the nature of the transmitter, astrocytes will be excited/activated

(Figure 1.4, left), suggesting they integrate some brain circuits as a redundant layer that reads excitatory and inhibitory neuronal inputs similarly. This concept may add up to the mechanisms of coincidence detection proposed a decade ago by Perea and Araque (Perea and Araque 2005; Perea and Araque 2007). Second, upon activation and Ca^{2+} elevation, astrocytes release gliotransmitters that ultimately cause either neuronal excitation (e.g. glutamate or D-serine) or inhibition (e.g. ATP degraded to adenosine). Curiously, the available literature indicates that astrocytes provide, in most cases, an excitatory output. Nevertheless, astrocytes also release ATP, which is readily degraded to adenosine and in turn activates A_1 receptor leading to synaptic inhibition (Serrano et al. 2006; Martin-Fernandez et al. 2017). This suggests that the type of modulation performed by astrocytes relies not only on the type of transmitter released (which is an intrinsic specificity of the astrocyte), but also on the nature of the receptors expressed by the neighboring cells (which depends on the nature of the neural circuit). In accordance, Martin-Fernandez et al. (2017) also showed that astrocyte-derived ATP results ultimately in excitation or inhibition, depending on the type of receptors found by adenosine. Whether brain circuits are endowed with exclusively excitatory and/or exclusively inhibitory astrocytes, or if these cells play both roles simultaneously (i.e., express machinery to produce, load, and release different transmitters), is still unknown. The first case would not be surprising, since it is the reality for the different neuronal cells (e.g. excitatory glutamatergic vs. inhibitory GABAergic). While recent technical advances have provided fruitful reports of unexpected physiological processes, future studies are needed to confirm their relevance for circuit function.

Astrocyte Calcium and Neural Circuits

The difficulty to measure and/or manipulate intracellular astrocytic Ca^{2+} in the intact brain may explain the lack of studies that report on its functional consequences for circuit and behavior computation. Still, recent reports indicate that the Ca^{2+}-dependent modulation of single synapses (as reviewed above) also have an expected impact on brain circuits.

Regarding the control of cortical synchronization, it was observed that astrocyte Ca^{2+} elevations *in vivo* regulate extracellular glutamate levels, which consequently triggers a slow neuronal rhythm in the brain. This event is characterized by synchronized neuronal firing across different behavioral states, and points to an important regulatory role of astrocytes in cortical circuits (Poskanzer and Yuste 2016). This observation is in line with previous studies performed in brain slices of the cortex and hippocampus that showed reduced neural synchrony upon disruption of astrocytic Ca^{2+} elevations (Poskanzer and Yuste 2011; Sasaki et al. 2014). Neural rhythmicity in these regions is essential for several behavioral functions

such as attention, learning, memory, and control of sleep/wake cycles [for review, Oliveira et al. (2015)]. IP_3R2-dependent signaling appears to support ripple-type events that occur during non-theta periods in the CA1 of rodents, a mechanism that might be related to the emotional consequences of social isolation (Tanaka et al. 2017).

In the rat trigeminal sensorimotor circuit for mastication, neural rhythmicity arises after sensory encoding. In this circuit, astrocytes actively respond to sensory stimuli by elevating their intracellular Ca^{2+} levels and, thus, regulating neuronal rhythmic activity, in brainstem slices (Morquette et al. 2015). Furthermore, in thalamo-cortical circuits, astrocytic Ca^{2+} elevations contributed to the modulation of sensory transmission. More specifically, the activation of mGluR2 triggers intracellular Ca^{2+} elevations in astrocytes, which are blocked by the astrocyte-specific toxin fluorocitrate. This effect described *in vivo* and in brain slices is linked to sensory inhibition in the rodent thalamus (Copeland et al. 2017). Furthermore, simultaneous stimulation of whiskers and the nucleus basalis of Meynert revealed that astrocytic Ca^{2+} elevations precede muscarinic acetylcholine receptor-dependent plasticity in the somatosensory cortex *in vivo*. This process is dependent on IP_3R2 signaling and extracellular D-serine (Takata et al. 2011). In the visual cortex, IP_3R2-mediated astrocytic Ca^{2+} elevations are also critical for the integration of visual sensory inputs with the nucleus basalis afferent information (Chen et al. 2012). Moreover, transcranial direct current stimulation (tDCS) was shown to enhance sensory-evoked cortical responses, through elevation of astrocytic intracellular Ca^{2+} via IP_3R2 (Monai et al. 2016). Thus, the authors propose that astrocytic Ca^{2+} elevations might mediate, at least in part, the recognized improvements obtained by tDCS in neuropsychiatric and neurological conditions. Finally, astrocyte Ca^{2+} elevation appears to also be involved in the maintenance of homeostatic mechanisms. Astrocytes in brainstem chemoreceptor areas respond to physiological decreases in pH with vigorous elevations in intracellular Ca^{2+}. These were shown to trigger the release of ATP, inducing adaptive increases in breathing (Gourine et al. 2010).

Astrocyte Ca^{2+} elevations appear to control the function of brain circuits at least in two different forms. On one hand, astrocytes appear to control plasticity in synapses occurring between neurons projecting to long distances, similarly to the control of local synapses within one brain region, as discussed above. On the other hand, astrocytes of a specific region appear to support local neural synchronization states, controlling the circuit output, most likely in a multi-synaptic process. Whether the two forms of modulation use similar mechanisms, i.e., whether regional integration is a product of 10 to 1000 of synapses being similarly integrated, is still unknown. However, it seems that both temporal and spatial properties of Ca^{2+} signals are important for this modulation to occur.

Astrocyte Calcium Effects on Behavior

The study of rodent models that display altered astrocyte function indicated that astrocytes play important roles in the production of behavior outputs in different dimensions (cognition, emotion, motor, and sensory processing) [(for review, Oliveira et al. (2015)]. As reviewed above, astrocytic Ca^{2+} signaling is reported to mediate synaptic modulation in different brain circuits. Genetic interference in this astrocytic hallmark has been the main strategy used to assess the role played by astrocyte Ca^{2+} elevations in behavior, with different laboratories using mostly two approaches: (1) triggering intracellular Ca^{2+} elevations via chemogenetic activation of GPCR signaling, and (2) inhibiting IP_3 signaling by deletion of IP_3 receptors or by buffering IP_3.

The genetic deletion of IP_3R2, specifically in about 80% of GFAP-positive cells (at least in the cortex, hippocampus, and substantia nigra), does not appear to influence spatial memory (Petravicz et al. 2014). However, the attenuation of IP_3 signaling in GLT1-positive cells led to partial cognitive impairment (Tanaka et al. 2013). Despite the extensive evidence showing a clear influence of astrocyte Ca^{2+} events on synapses and circuits involved in cognitive behavior (e.g. hippocampus), these two studies provided only modest evidence to support it. We believe that further studies using more specific tools to modulate astrocyte Ca^{2+} will reveal additional links to cognition. Indeed, we recently showed that spatial learning and memory rely on astrocyte exocytosis, which is a Ca^{2+}-dependent mechanism, and therefore might be dependent on astrocyte integration of surrounding activity (Sardinha et al. 2017).

IP_3-dependent astrocytic Ca^{2+} signaling does not seem to be related to anxiety-like behavior as indicated by studies using a constitutive (Cao et al. 2013; Tanaka et al. 2013) or conditional (Petravicz et al. 2014) IP_3R2 deletion. Regarding the depressive-like behavior, the available data is not consistent. While the constitutive deletion of IP_3R2 was shown to trigger some forms of a depressive phenotype (Cao et al. 2013), these are completely absent in the model with conditional deletion (Petravicz et al. 2014). Curiously, the GFAP-MrgA1 model that allows stimulation of astrocyte Ca^{2+} displayed decreased learned helplessness in the forced swim test (Cao et al. 2013). Further experimentation is required to clarify these apparently contradictory results. Finally, a recent study indicated that the astrocytic control of excitatory/inhibitory inputs to the central amygdala is crucial for fear-related behavior (Martin-Fernandez et al. 2017).

Regarding motor function, the activation of IP_3 "sponge" or deletion of IP_3R2 does not seem to interfere with exploratory behavior (Cao et al. 2013; Tanaka et al. 2013; Petravicz et al. 2014). Interestingly, the chemogenetic activation of astrocyte G_q-coupled signaling led to an impairment in motor coordination in an IP_3R2-independent manner (Agulhon et al. 2013). The specific ablation of IP_3R2 in GLAST-positive cells

resulted in an impairment in motor-skill learning of a forelimb reaching task (Padmashri et al. 2015). More so, the attenuation of IP_3/Ca^{2+} signaling in astrocytes resulted in modulation of the rodent sleep, by increasing the time spent and frequency periods in rapid eye movement phase (Foley et al. 2017).

While the research carried out so far has provided us with critical knowledge of the influence of astrocytic Ca^{2+} in synaptic or circuit function, further research should be performed to complement the rather sparse evidence on the influence of astrocytes on behavior. Moreover, further evidence will help clarify the discrepant results and reconcile the existent observations. For instance, the different observed cognitive outcomes might be related to the different mechanism used to target intracellular Ca^{2+} (full deletion of IP_3R2 vs. IP_3 "sponge"), or by the promotor used to drive astrocyte specificity (GFAP vs. GLT-1) that could result in differential regional expression. Moreover, there are at least five different IP_3R2 KO strains with different genetic backgrounds (Oliveira et al. 2015); this might not be critically relevant for studies of synaptic plasticity in brain slices, but it may easily lead to distinct observations in behavior tests. Additionally, the different studies should be conducted in a standardized form to allow the linear comparison of the results.

All rodent models reported above result on drastic modulation of global Ca^{2+} elevations. Intracellular Ca^{2+} rises may trigger a multitude of signaling pathways. Thus, it must always be considered that the interference with global Ca^{2+} events may trigger several simultaneous consequences, which might lead to confounding results. Although these models might be very useful when carefully assessed, the research field requires the development of more specific models to allow temporal and, more importantly, local control of Ca^{2+} signals in physiological processes.

1.2.4. The IP_3R2 KO mouse model

Due to the high expression of IP_3R2 specifically in astrocytes, the IP_3R2 knockout (IP_3R2 KO) mouse model naturally emerged as a tool to study astrocytic Ca^{2+} signaling (Li et al. 2005; Petravicz et al. 2008). These mice lack global Ca^{2+} elevations, which correspond to the slower, long-lasting events that are mainly confined to the soma and main processes. However, they still display IP_3R2-independent Ca^{2+} signals in astrocytic microdomains. These signals derive from alternative Ca^{2+} sources as the plasmalemmal Ca^{2+} influx or the mitochondria (Srinivasan et al. 2015; Rungta et al. 2016; Agarwal et al. 2017). The IP_3R2 KO mouse model was generated at the Ju Chen laboratory (Li et al. 2005). It had a strong Black Swiss background, that could cause retinal degeneration and blindness with a negative impact on behavioral performance (Clapcote et al. 2005). Our lab and others circumvented this constraint by backcrossing the founder line to C57BL/6J mice (Wang et al. 2012b; Chen et al. 2012; Petravicz et al. 2014; Feriod et al.

2014; Biesecker et al. 2016; Guerra-Gomes et al. 2018; Pinto-Duarte et al. 2019). The variety of strains derived from the initial models generated in Prof. Ju Chen (Li et al. 2005) and Prof. Katsuhiko Mikoshiba (Futatsugi et al. 2005) are summarized in Table 1.2. For the sake of simplicity, the mouse line generated by Li et al. (2005) is referred as IP_3R2 KO, and whenever crossed with C57BL/6J wild-type mice as IP_3R2 KO (C57BL/6). The mouse line generated by Futatsugi et al. (2005) has this reference added to the IP_3R2 KO designation and crossings with other mouse lines are specifically mentioned.

The IP_3R2 KO mice generated by Li et al. (2005) are viable and fertile and display no overt behavioral abnormalities (Petravicz et al. 2008). Due to the importance of IP_3R2 in hepatocytes, Feriod and co-authors (2014) dissected the role of this receptor in metabolic functionality. They observed that C57BL/6 IP_3R2 KO mice had a normal energy balance, glucose production and tolerance, and insulin sensitivity. Moreover, no alterations in liver morphology were found. Despite the recognized importance of the IP_3 signaling for astrocytic Ca^{2+} elevations, contrasting results were reported regarding synaptic transmission and plasticity in these mice. For instance, cholinergic-induced presynaptic LTP in cortical (Takata et al. 2011) and hippocampal (Navarrete et al. 2012) regions was shown to be affected, while induction of NMDAR-dependent LTP was not (Agulhon et al. 2010). Recently, two studies demonstrated that IP_3R2 KO mice present an impaired NMDAR-dependent hippocampal long-term depression (LTD) (Pinto-Duarte et al. 2019; Navarrete et al. 2019).

Depending on the IP_3R2 KO model used, several laboratories reported distinct observations for different behavioral dimensions. The outcomes obtained from studies using IP_3R2 KO mouse model or IP_3R2 KO crossed with other models are summarized in Table 1.2. Several studies have demonstrated that interfering with IP_3-dependent Ca^{2+} signaling affects synaptic, circuit and behavioral functioning, while others report no changes related to these brain functions (Guerra-Gomes et al. 2017). Moreover, some evidences point to a role of IP_3R2-dependent Ca^{2+} in K^+ homeostasis and in pathological conditions (e.g. stroke, injury, neurodegenerative disorders) (Wang et al. 2012a; Dong et al. 2013a; Kanemaru et al. 2013; Li et al. 2015; Kim et al. 2016; Rakers and Petzold 2017; Heuser et al. 2018). Interestingly, an overall role of neuroprotection against an insult or a pathological state was observed in these studies. Contrarily, the control of neurovascular coupling was shown to be independent of an IP_3R2-Ca^{2+} mechanism (Nizar et al. 2013; Bonder and McCarthy 2014).

Novel tools are needed to draw further conclusions regarding the functional influence of astrocytic Ca^{2+} signals. Recently, Yu et al. (2018) developed a mouse model that constitutively extrude cytosolic Ca^{2+} in astrocytes, targeting specific spatiotemporal aspects of astrocyte Ca^{2+} signaling in the striatum. This approach revealed an important role for astrocytic Ca^{2+} in the control of a striatum-dependent behavior.

Thus, the development of novel genetic tools with higher spatial and temporal resolution will be pivotal to dissect the role of astrocytic Ca^{2+} signaling in brain functioning.

Table 1.2 - Functional consequences of the interference with IP_3R2 expression

Symbol legend: ↑, increased; ↓, decreased; =, no change.

Model	Alteration/modulation	Approach	Phenotype	References
BEHAVIOR				
COGNITION				
GFAP-IP_3R2 cKO (C57BL/6)	Lack of intracellular global Ca^{2+} signaling in $GFAP^+$ astrocytes; C57BL/6 background;	Spatial Reference Memory and Reversal Learning (MWM)	= long-term spatial memory = reversal learning	(Petravicz et al. 2014)
GLT1-IP_3 "sponge"	Attenuation of intracellular global Ca^{2+} signaling in GLT-1^+ astrocytes	Spatial Reference Memory (MWM) and Fear Conditioning	↓ long-term memory	(Tanaka et al. 2013)
$Appps1^{+/-}$ x IP_3R2 KO	Lack of intracellular global Ca^{2+} signaling in astrocytes in a mouse model of Alzheimer's disease (AD)	Spatial Reference Memory (MWM)	↑ spatial memory and network hyperactivity in a mouse model of AD	(Reichenbach et al. 2018)
IP_3R2 KO (C57BL/6)	Lack of intracellular global Ca^{2+} signaling in astrocytes	Y-maze Two-Trial Place Recognition (2TPR)	= cognitive performance (PFC-dependent) with aging	(Guerra-Gomes et al. 2018)
IP_3R2 KO (C57BL/6)	Lack of intracellular global Ca^{2+} signaling in astrocytes	Y-maze (spontaneous alternations)	↓ spontaneous alternations (working memory)	(Pinto-Duarte et al. 2019)
		Barnes maze test	↓ remote spatial memory = recent spatial memory	
		Cued and contextual fear conditioning	↓ remote fear memory = recent fear memory	
		Novel object recognition	↓ long-term recognition memory	
EMOTION				
Anxious-like behavior				
IP_3R2 KO	Lack of intracellular global Ca^{2+} signaling in astrocytes	Elevated Plus Maze	= anxious-like behavior ↓ ATP levels	(Cao et al. 2013)
GLT1-IP_3 "sponge"	Attenuation of intracellular global Ca^{2+} signaling in GLT-1^+ astrocytes	Open Field	= anxious-like behavior	(Tanaka et al. 2013)
GFAP-IP_3R2 cKO (C57BL/6)	Lack of intracellular global Ca^{2+} signaling in $GFAP^+$ astrocytes	Elevated Plus Maze Activity Box	= anxious-like behavior	(Petravicz et al. 2014)
IP_3R2 KO (C57BL/6)	Lack of intracellular global Ca^{2+} signaling in astrocytes	Light/dark box	= anxious-like behavior	(Pinto-Duarte et al. 2019)

Depressive-like behavior				
IP_3R2 KO	Lack of intracellular global Ca^{2+} signaling in astrocytes	Sucrose Preference Test	↑ anhedonia	(Cao et al. 2013)
		Forced Swim Test	↑ learned helplessness	(Cao et al. 2013)
		Coat Score	↑ depressive behavior	(Cao et al. 2013)
IP_3R1, IP_3R2 and IP_3R3 knockdown	Mice carrying a cerebral knockdown for each IP_3R isoform	Forced Swim Test	↓ depressive behavior	(Galeotti et al. 2008)
GFAP-IP_3R2 cKO (C57BL/6)	Lack of intracellular global Ca^{2+} signaling in $GFAP^+$ astrocytes	Tail Suspension	= depressive-like behavior	(Petravicz et al. 2014)
Impulsivity				
GFAP-IP_3R2 cKO (C57BL/6)	Lack of intracellular global Ca^{2+} signaling in $GFAP^+$ astrocytes	Acoustic startle	= sensory-motor gating and prepulse inhibition	(Petravicz et al. 2014)
MOTOR				
Motor activity and coordination				
IP_3R2 KO	Lack of intracellular global Ca^{2+} signaling in astrocytes	Open Field	= exploratory/locomotor behavior	(Cao et al. 2013)
GLT1-IP_3 "sponge"	Attenuation of intracellular global Ca^{2+} signaling in $GLT\text{-}1^+$ astrocytes	Open Field	= exploratory behavior	(Tanaka et al. 2013)
GFAP-hM3Dq x IP_3R2 KO	Chemogenetic control of astrocytic Gq-coupled signaling independent of IP_3	Open Field	= exploratory behavior	(Agulhon et al. 2013)
		Rotarod	↓ motor coordination	
		Righting reflex analysis	↓ motor coordination	
IP_3R2 KO (C57BL/6)	Lack of intracellular global Ca^{2+} signaling in astrocytes	Electrocorticogram	↓ astrocyte-cortical upstate synchrony	(Wang et al. 2012b)
GLASTCre-$IP_3R2^{fl/fl}$	Lack of intracellular global Ca^{2+} signaling in $GLAST^+$ astrocytes	Forelimb Reaching Task	↓ motor-skill learning	(Padmashri et al. 2015)
GFAP-IP_3R2 cKO (C57BL/6)	Lack of intracellular global Ca^{2+} signaling in $GFAP^+$ astrocytes	Open Field Rotarod	= motor function and exploratory behavior = motor coordination and learning	(Petravicz et al. 2014)
IP_3R2 KO (C57BL/6) (Futatsugi et al. 2005)	Lack of intracellular global Ca^{2+} signaling in astrocytes	Rotarod	= motor function	(Kim et al. 2016)
IP_3R2 KO (C57BL/6)	Lack of intracellular global Ca^{2+} signaling in astrocytes	Locomotor activity test	= motor function	(Pinto-Duarte et al. 2019)

SENSORIAL				
Whisker + Tail pinch				
IP_3R2 KO	Lack of intracellular global Ca^{2+} signaling in astrocytes	Whisker stimulation + *in vivo* electrophysiology	↓ somatosensory plasticity, rescued by D-Serine administration;	(Takata et al. 2011)
		Tail stimulation + *in vivo* electrophysiology	↓ cholinergic-dependent hippocampal plasticity	(Navarrete et al. 2012)
IP_3R2 KO (C57BL/6) (Futatsugi et al. 2005)	Lack of intracellular global Ca^{2+} signaling in astrocytes	Whisker stimulation	= neural activity-driven CBF modulation	(Takata et al. 2013)
$IP_3R2^{-/-}$ x Thy1-eGFP-M mice	Lack of intracellular global Ca^{2+} signaling in astrocytes	*In vivo* sensory stimulation	↓ sensory stimulation-induced PDAP motility increase	(Perez-Alvarez et al. 2014)
Pain				
IP_3R2 KO (C57BL/6) (Futatsugi et al. 2005)	Lack of intracellular global Ca^{2+} signaling in astrocytes	Partial ligation of the right sciatic nerve (PSL injury)	↓ mechanical allodynia absence of enhanced S1 neuronal excitability following injury	(Kim et al. 2016)
Vision				
GFAP-IP_3R2 cKO (C57BL/6)	Lack of intracellular global Ca^{2+} signaling in $GFAP^+$ astrocytes	Visual stimulation + *in vivo* electrophysiology	↓ Nucleus basalis-induced potentiation of visual responses	(Chen et al. 2012)
Mlc1-YC-Nano50-IP_3R2 KO	Expression of the Ca^{2+} indicator Yellow Cameleon-Nano 50 in astrocytes lacking global Ca^{2+} signaling in astrocytes	Tail stimulation + two photon imaging	Ø astrocytic Ca^{2+} response to sensory stimulation	(Kanemaru et al. 2014)
IP_3R2 KO (C57BL/6) X GLAST-CreER;R26-lsl-GCaMP3	Lack of intracellular global Ca^{2+} signaling in astrocytes	Sensory stimulation (retina)	↑ Ca^{2+} in the glial endfeet contacting capillaries Ø light-evoked capillary dilation	(Biesecker et al. 2016)
IP_3R2 KO	Lack of intracellular global Ca^{2+} signaling in astrocytes	Multiphoton imaging visual cortex (OGB-1/SR-101) + visual stimulation	= neurovascular coupling = functional hyperemia	(Bonder and McCarthy 2014)
IP_3R2 KO	Lack of intracellular global Ca^{2+} signaling in astrocytes	*In vivo* two-photon microscopy (somatosensory cortex + forepaw stimulation)	= stimulus-induced vasodilation	(Nizar et al. 2013)
IP_3R2 KO (C57BL/6)	Lack of intracellular global Ca^{2+} signaling in astrocytes	Optomotor	= visual ability	(Pinto-Duarte et al. 2019)

FUNCTIONAL				
fMRI				
IP_3R2 KO (WT not littermates)	Lack of intracellular global Ca^{2+} signaling in astrocytes	Electrophysiology (LFP) + fMRI	= EPSP and population spikes responses	(Jego et al. 2014)
Electrophysiology				
IP_3R2 KO	Lack of intracellular global Ca^{2+} signaling in astrocytes	Brain slice electrophysiology	= hippocampal spontaneous/evoked activity; = synaptic plasticity;	(Petravicz et al. 2008; Agulhon et al. 2010)
IP_3R2 KO (C57BL/6) (Futatsugi et al. 2005)	Lack of intracellular global Ca^{2+} signaling in astrocytes	LFP recordings + enriched/isolated environment	↓ Hippocampal ripple events, in magnitude and frequency	(Tanaka et al. 2017)
IP_3R2 KO (C57BL/6) (Futatsugi et al. 2005)	Lack of intracellular global Ca^{2+} signaling in astrocytes	Transcranial direct current stimulation (tDCS)-induced visual flash evoked potential	= tDCS-induced plasticity	(Monai et al. 2016)
IP_3R2 KO	Lack of intracellular global Ca^{2+} signaling in astrocytes	Electrophysiology (EPSCs)	Ø AMPAR-EPSCs, NMDA-EPSCs and AMPAR-EPSC/NMDAR-EPSC at VPm relay synapses Affected synaptic strengthening during development	(Yang et al. 2016)
IP_3R2 KO (C57BL/6)	Lack of intracellular global Ca^{2+} signaling in astrocytes	Electrophysiology (LTP/LTD)	↓ CA1 hippocampal LTD induction, rescued by D-serine application = CA1 hippocampal LTP induction	(Pinto-Duarte et al. 2019)
IP_3R2 KO	Lack of intracellular global Ca^{2+} signaling in astrocytes	Electrophysiology (LTD)	↓ NMDAR-dependent hippocampal LTD	(Navarrete et al. 2019)
PATHOLOGY				
Injury				
IP_3R2 KO	Lack of intracellular global Ca^{2+} signaling in astrocytes	Photothrombosis-induced ischemia (Stroke therapy)	↓ infarction in acute and chronic phase of ischemia ↓ neuronal apoptosis, reactive astrogliosis and tissue loss ↑ performance in cylinder, hanging wire, pole and adhesive behavioral tests after injury	(Li et al. 2015)
IP_3R2 KO	Lack of intracellular global Ca^{2+} signaling in astrocytes	Focal ischemia	↓ peri-infarct depolarizations frequency and overall peri - infarct depolarizations burden ↑ neuronal survival after stroke ↓ glutamate accumulation during PIDs	(Rakers and Petzold 2017)
IP_3R2 KO	Lack of intracellular global Ca^{2+} signaling in astrocytes	Permanent middle cerebral artery occlusion – ischemic model	↓ injured ↓ infarct volume	(Dong et al. 2013a)
IP_3R2 KO	Lack of intracellular global Ca^{2+} signaling in astrocytes	Stab wound injury	↓ astrogliosis; ↑ injury associated neuronal death	(Kanemaru et al. 2013)

IP_3R2 KO	Lack of intracellular global Ca^{2+} signaling in astrocytes	Kainate-induced seizures	↓ hypersynchronous neuronal activity ↓ epileptic activity ↓ seizure burden	(Heuser et al. 2018)
Alexander disease				
60TM:: IP_3R2 KO mice	Lack of intracellular global Ca^{2+} signaling in astrocytes in a mouse model of Alexander disease	Two-photon microscopy	↓ Ca^{2+} signals in *stratum radiatum;* ↓ aberrant extra-large Ca^{2+} signals present in Alexander disease	(Saito et al. 2018)

1.3.Cognition: learning and memory

Cognitive science encompasses different domains as perception, action, decision-making, language, attention, learning and memory, which are important functions for our everyday lives. Learning allows us to acquire new knowledge, while memory consists of retaining and recall this acquired information over time (Kandel et al. 2013; Kandel et al. 2014). Learning is a process that occurs simultaneously whenever the brain is perceiving, thinking and/or feeling. In fact, brain processing has the ability to choose if it is worth to store information, in order to use it for guidance of future behavior based on previous experience (Spitzer 2006). Early observations from Ramon y Cajal and subsequent behavioral studies provided direct evidence that synaptic network connections change in response to the learning process and that these modifications underlie the mechanisms related to memory storage (Mayford et al. 2012). Memory can be categorized into two dimensions according to the time course to learn and the nature of the stored memory (Kandel et al. 2013). Short-term memory involves temporary changes in synaptic transmission (lasting minutes to hours) and is related to goal-relevant knowledge. In contrast, long-term memory requires longer retention delays (lasting days to weeks) and can be divided into explicit (declarative) or implicit (non-declarative) (Mayford et al. 2012; Kandel et al. 2013). Explicit memory is related to facts, events, people, places and objects, whereas implicit memory is associated with perceptual and motor skills. The former is dependent on hippocampal and adjacent cortical regions, while implicit memory relies more on the cerebellum, striatum, and amygdala (Kandel et al. 2014). Looking deeper into explicit memory, we can further classify it into episodic (related to events) and semantic (related to facts) memory (Figure 1.5) (Kandel et al. 2013).

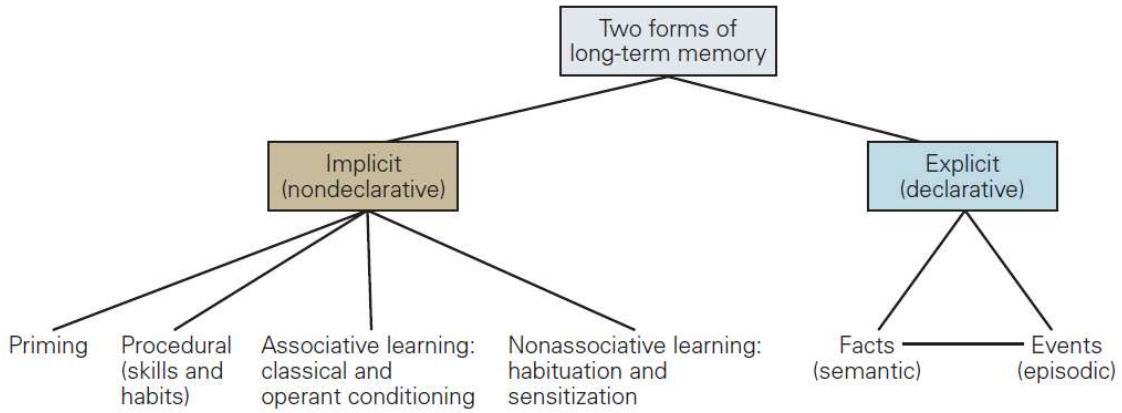

Figure 1.5 – Different forms of long-term memory.

Implicit memories are those related to unconscious actions, as the procedural tasks (skills and habits). These correspond to automatic processes, and its distinct forms give rise to priming, skill learning, habit memory, and conditioning. In opposition, explicit memories are the result of a conscious retrieval of past stored information. This recalled information can be related to people, places and things. Explicit memory is more flexible as compared with implicit since it allows the association of different pieces of information under different circumstances. Adapted from Kandel et al. (2013).

Both memory processes comprise synaptic and molecular changes, fundamentally to strengthen synaptic connections. While for short-term memory a strengthening of synaptic connections and a modification of pre-existing proteins occurs, long-term memory processing requires synaptogenesis and synthesis of new molecules. The signaling pathways involved in the conversion from short- to long-term memory are protein kinase A, mitogen-activated protein kinase (MAPK), CREB-1, and CREB-2 (Bailey et al. 2008; Mayford et al. 2012). Of notice, the use of transgenic mouse models revealed key signaling molecules and pathways that upon manipulation promote stability of synaptic plasticity, and enhance learning and memory acquisition (Lee and Silva 2009).

Among the brain regions involved in memory processing, the hippocampus and prefrontal cortex (PFC) play critical roles and have been extensively studied. Most studies in rodents tackle their performance in working memory (WM) and reference memory (RM) tasks. On one hand, WM is a form of short-term memory that depends on transient storage and manipulation of information to guide a behavioral action. On the other hand, RM corresponds to a long-term acquisition of information that remains unchanged during trials and relies on the presence of a discriminative stimulus (e.g. visual cue) (Lima et al. 2014; Sardinha et al. 2017).

One of the goals of this thesis is to understand the role of global astrocyte Ca^{2+} signaling in cognitive function dependent on the hippocampus and PFC. Therefore, in the next subchapters we will review the main features and functions associated with both brain regions.

1.3.1.The hippocampus

The hippocampal formation, localized in the medial temporal lobe of the brain, is composed by the hippocampus, dentate gyrus (DG) and subiculum (Kandel et al. 2013). All these structures participate in the formation of episodic memories (daily experiences) but do not constitute the permanent storage unit for these memories. Accordingly, a lesion in the hippocampal formation may affect the acquisition of new memories, without necessarily impairing the retrieval of old memories. This phenomenon is called anterograde amnesia (Kandel et al. 2013). The hippocampus is responsible for the computation of distinct behavioral readouts as spatial memory, anxiety or reward (Ciocchi et al. 2015). An important finding connecting the hippocampus to spatial navigation was the discovery of place cells (O'Keefe and Dostrovsky 1971). These hippocampal neurons were shown to specifically fire at a particular spatial location, comprising a cognitive map of the environment (Knierim 2010; Ciocchi et al. 2015). Moreover, a fascinating work showed that high-frequency stimulation of hippocampal input fibers induces the LTP phenomenon that strengthens synaptic connections (Bliss and Lomo 1973). Contrarily, the LTD is a form of synaptic plasticity that weakens previous established synaptic contacts (Kandel et al. 2013).

Both human and rodent brains present a relatively conserved intrinsic hippocampal circuit organization. It receives sensory and spatial inputs from the entorhinal cortex. Then, these signals follow a direct or indirect pathway to reach CA1 pyramidal neurons. After receiving this information, CA1 neurons classically project to the entorhinal cortex and to the subiculum (Kandel et al. 2013; Ciocchi et al. 2015). Furthermore, the ventral part of the hippocampus projects to other brain areas, such as the mPFC, nucleus accumbens and amygdala. Functionally, the ventral hippocampus is associated with the control of affective and motivational behaviors, while the dorsal hippocampus (dHIP) is associated with cognitive functions, such as spatial navigation and episodic memory (Cenquizca and Swanson 2007; Fanselow and Dong 2010; Ciocchi et al. 2015).

The study of animal models of astrocytic dysfunction revealed a striking role for astrocytes in the integration of spatio-temporal outputs controlling cognitive performance [for review, (Oliveira et al. 2015)]. In particular, our lab has recently shown that the blockade of gliotransmitter release in astrocytes leads to a decrease in hippocampal-PFC theta synchrony, leading to an impairment in tasks that require the processing of spatial memory by the hippocampus (Sardinha et al. 2017).

1.3.2. The prefrontal cortex

The PFC is the anterior portion of the frontal lobes and acts as a neocortical connecting point that sends and receives several projections from many subcortical structures and cortical systems related to sensorial and motor functions (Miller and Cohen 2001; Wilson et al. 2010). It is involved in the control of high-level cognitive functions, such as executive function (behavioral flexibility and working memory), behavioral inhibition and general intelligence (Cerqueira et al. 2005; Wilson et al. 2010). Furthermore, the medial PFC (mPFC) is intimately connected with other components of the limbic system, controlling cognitive, mnesic and emotional processing (Heidbreder and Groenewegen 2003; Hoover and Vertes 2007). This brain region is not required for simple, automatic behaviors, but rather for the guidance of internal states or intentions in order to form an attentional set and to learn the "rules of the game" (Miller and Cohen 2001). For example, the Wisconsin card sort task is a classical task to assess PFC function in humans. In this test, the rule is continuously changing; subjects need to choose a card according to a prevailing category: shape, color or number of symbols. Patients with frontal lobe deficiencies (autism, schizophrenia, Parkinson's disease) have great difficulty performing this task once the relevant category changes (Bissonette et al. 2008). Similarly, our lab has previously shown that the ablation of astrocytes in the PFC leads to impairments in spatial working memory, attention and behavioral flexibility (Lima et al. 2014). Moreover, astrocytic ablation in this brain region also affects emotional dimensions, namely anxious and depressive-like behaviors (Banasr and Duman 2008). These studies provide compelling evidence supporting the idea that astrocytes are important partners in the control of PFC-dependent functions.

1.3.3. Behavior tests to assess cognition in mouse models

Rodent models play a pivotal role in the biomedical research field, namely in the study of cognition in health and disease. With the emergence of pharmacological, environmental and genetic manipulation, it became necessary to develop valid, reliable and brain-region directed behavioral tests to evaluate cognitive performance. Generally, in these paradigms, experimental groups are compared with controls to estimate the impact of such manipulation by extracting a cognitive readout. Importantly, these procedures require careful design and execution in order to avoid biased results. Thus, it is pivotal to control experimental parameters as genetic background, gender, animal husbandry (housing and handling), place and time of testing, external noise and testing conditions (light, temperature, humidity). When designing experiments to assess behavior in mouse models, one should take into account that the performance in a particular paradigm is dependent on the contribution of specific brain regions. For

instance, the hippocampus has a recognized role in the spatial and temporal distinction of different stimuli (e.g. textures or shapes) and is implicated in avoidance tests. It is further described as necessary to suppress an originally formed memory, and for memory recall over 3-4 weeks after acquisition. Another limbic region involved in cognitive processing is the amygdala. This brain region is important in learning and memory processes usually associated with an aversive stimulus (e.g. footshock). Due to its close implication in motor functions, the cerebellum is required for motor learning, whereas the striatum is critical for motor and reward system functioning. The rhinal cortex, a cortical region of the medial temporal lobe, has been implicated in object recognition and the cortical regions that receive direct outputs from the ventral hippocampus – the PFC – are fundamental for working memory and memory extinction tasks (Sousa et al. 2006).

An important concern when working with full knockout models is the relevance of the deleted gene during developmental stages. Genetic manipulation can also lead to early developmental alterations that could influence adult cognitive behavior. Thus, the achievement of milestones through an examination of somatic parameters and neurological reflexes should be addressed to evaluate the developmental progression (Hill et al. 2008). Additionally, this analysis can be complemented by assessing general phenotypical behavior in adult mice through the assessment of motor behavior and exploratory drive.

Cognitive tests encompass interacting aspects of learning and memory, so by testing several paradigms we will be able to obtain a comprehensive readout of cognitive function. Learning and memory functions can be assessed through different mazes and paradigms. In this thesis, we tested several PFC and/or hippocampal-dependent cognitive tasks. Each of the cognitive tests used is depicted in Figure 1.6.

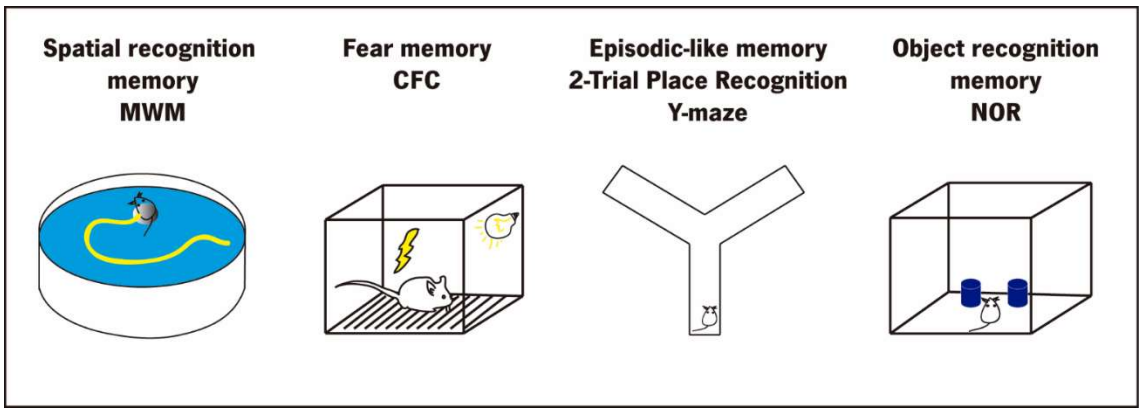

Figure 1.6 - Illustrative scheme of the behavioral tests used for cognitive assessment.

The scheme represents the behavioral tests used to assess cognitive function in this thesis. Morris Water Maze (MWM) evaluates spatial recognition memory, as the animal needs to find a hidden platform in a pool guided by spatial cues. Contextual Fear Conditioning (CFC) allows the assessment of fear memory acquisition since animals are exposed to an aversive stimulus (light followed by a shock). Y-maze 2-Trial Place Recognition (2TPR) takes advantage of the ability of rodents to explore novelty, to evaluate their memory for novel locations. Novel object recognition task (NOR) evaluates the ability of rodents to memorize a familiar (previously explored) and novel object in an arena.

The Morris Water Maze (MWM) is a gold-standard test to evaluate spatial navigation in an open swimming area surrounded by visual cues. In this test, several paradigms can be assessed: RM, WM and reversal learning. All of these involve the use of visual cues to successfully reach a hidden platform that can maintain (RM) or shift (WM) its location during several trials (Vorhees and Williams 2006). Cognitive tests are designed with the premise that animals will have willingness to participate, either because they are exposed to a positive (sugary pellet vs regular food) or negative (footshock) reinforcer. A great example of a learning test associated with a negative reinforcer is the Contextual Fear Conditioning (CFC). In this test, animals associate an aversive electric shock with a cue (light or tone) and a specific context (Gu et al. 2012). In contrast, both the Y-maze task and the Novel Object Recognition (NOR) test are based on the natural drive of rodents to explore novelty (Leger et al. 2013; Holter et al. 2015)

1.3.4. Astrocytic modulation of cognitive behavior

Astrocytic signaling plays a key role in the control of brain homeostasis and communication. Growing evidence point to astrocytes as key regulators of cognitive processing (Gibbs et al. 2008; Pannasch and Rouach 2013; Fields et al. 2014; Oliveira et al. 2015; Dallerac and Rouach 2016; Santello et al. 2019). Over the past years, pharmacological and genetic tools were developed to study astrocytic function,

targeting specific features such as: i) astrocytes' ability to “sense”; ii) elevate its intracellular Ca^{2+} levels in response to neuronal activity and iii) respond to the surrounding activity by releasing gliotransmitters. These tools allowed a better comprehension of the role of astrocytes in brain functioning, by tackling specific astrocytic functions and exploring its implications, for instance, in cognitive performance. For example, astrocytes express a variety of functional receptors in their membranes. Robin and co-authors (2018) showed that genetic deletion of CB1R specifically in astrocytes impairs hippocampal LTP and long-term recognition memory. These observations were rescued by application of the gliotransmitter, D-serine. Similarly, we previously demonstrated that conditional blockade of exocytosis in astrocytes, using the dnSNARE mouse model, critically impairs cognitive function. These deficits were completely restored after D-serine application (Sardinha et al. 2017). A study using another approach to interfere with astrocytic exocytosis, through the expression of tetanus toxin, revealed that these animals presented an impairment in the performance of a recognition memory task (Lee et al. 2014). Contrastingly, modulation of astrocytic function can also result in cognitive enhancement. This was elegantly shown by Mederos et al. (2019), using the specific expression of a G-protein-coupled photopigment to trigger astrocytic Ca^{2+} elevations. This approach enhanced episodic-like memory in an object recognition task. In the same way, the expression of a modified form of the human M3 muscarinic receptor in CA1 astrocytes was able to enhance fear memory, in the CFC paradigm and spatial recognition memory in the T-maze (Adamsky et al. 2018).

The role of astrocytes in the maintenance of neuronal networks has also been reported to change in response to a pathological state. In such cases, neuron-astrocyte interaction undergoes functional, morphological and molecular changes that strongly affect cognitive function. For example, Alzheimer’s disease (AD) is a known neurodegenerative disorder characterized by marked cognitive deficits. Orr and colleagues (2015) found that an AD mouse model presented increased expression of astrocytic A_{2A} receptors that contributed to the observed cognitive impairments. The genetic deletion of these receptors in astrocytes was able to enhance memory performance in the MWM test. Moreover, the lack of IP_3-dependent Ca^{2+} signaling in astrocytes in a mouse model of AD enabled the restoration of both spatial memory and network hyperactivity (Reichenbach et al. 2018). Furthermore, in the experimental autoimmune encephalomyelitis model of multiple sclerosis, the astrocytic TNF receptor type 1 signaling was shown to be implicated in the impaired fear memory observed (Habbas et al. 2015). Accordingly, several brain diseases lead to impaired cognitive processing. An aberrant astrocytic activity has been demonstrated to influence these outputs and even accelerate the undesirable events that occur through a pathological state.

1.4. Astrocytes in disease: involvement in depression

Astrocytes participate in the control of several functions related to CNS normal development and functioning. Upon injury or under pathological conditions, astrocytes undergo a phenotypical alteration, changing their morphology and molecular profile, which can be protective or detrimental to the diseased tissue (Khakh and Sofroniew 2015). Generally, it is considered that after being exposed to an insult, astrocytes become "reactive" and respond through a process called astrogliosis (Sofroniew 2014). Further analysis into the molecular profile of reactive astrocytes revealed an A1 (neurotoxic) or A2 (neuroprotective) astrocytic phenotype (Zamanian et al. 2012; Liddelow et al. 2017). A growing body of evidence reported an altered astrocytic Ca^{2+} signaling in response to brain diseases, such as neurological and psychiatric disorders (Nedergaard et al. 2010; Shigetomi et al. 2016). However, the mechanisms underlying the development of the deleterious effects after a pathological insult are still unexplored. In this thesis, after observing a positive modulation of hippocampal-dependent behavior, we decided to test its modulatory potential in a model of depression, which is a disease that affects cortico-limbic circuits with impact both in cognitive and emotional behavior.

Depression is a neurobiological, multidimensional disorder and the leading cause of disability worldwide (WHO 2017). This is a highly heterogeneous disorder, with a variable course and an inconsistent response to treatment. Depressive patients present alterations in distinct behavioral domains such as mood, anxiety, and cognition (Bessa et al. 2009b). The unpredictable chronic mild stress (uCMS) protocol developed by Willner et al. (1987) induces a depressive-like phenotype in mice and rats, due to the exposure to several stressors in a random and unpredictable fashion. This protocol is highly translatable to the human disease since it has a multi-dimensional behavioral impact (Bessa et al. 2009b). In fact, studies performed in our lab using the uCMS animal model of depression have reported alterations in mood, anxiety, and cognition. Moreover, rats exposure to uCMS leads to alterations in the hypothalamic–pituitary–adrenal (HPA) axis activation, neural plasticity, cytogenesis and different molecular profiles (Bessa et al. 2009b; Mateus-Pinheiro et al. 2013; Patricio et al. 2015; Alves et al. 2017).

The hippocampal formation is affected by chronic stress, which paved the way to look to other interconnected brain regions, such as the PFC and the amygdala (McEwen et al. 2016). In fact, our lab has previously shown a clear neuronal compromise in the PFC (Dias-Ferreira et al. 2009) and the hippocampus (Mateus-Pinheiro et al. 2013) after exposure to chronic stress. In addition, imaging studies performed in our lab support these observations by reporting structural atrophy in cortico-limbic regions and others, after stress exposure (Magalhaes et al. 2018).

The recognized role of astrocytes in brain function led to the disclosure of its importance in mood disorders. A reduced immunoreactivity of specific astrocytic markers (GFAP and GS) was observed in cortico-limbic regions in rodent models of depression (Musholt et al. 2009; Gosselin et al. 2009) and human patients (Miguel-Hidalgo et al. 2000; Cotter et al. 2002). Furthermore, Golgi-Cox staining analysis revealed an altered astrocytic cortical morphology in samples from depressed suicides (Torres-Platas et al. 2011). Our group and others demonstrated that, in rats, the specific ablation of astrocytes in the PFC leads to cognitive deficits in a WM task (Lima et al. 2014) and induce an anhedonic phenotype (Banasr and Duman 2008; Banasr et al. 2010), two major hallmarks of depression. Additionally, glutamatergic excitotoxicity has been described as an important feature in the installation of the disease, due to the defective neurotransmitter uptake by astrocytes (Rajkowska and Stockmeier 2013). In line with this, the administration of a drug that induces the overexpression of the astrocyte glutamate transporter GLT-1 – ceftriaxone – was shown to be able to exert an anti-depressant effect (Mineur et al. 2007). Contrarily, interfering with glutamate uptake namely by blocking GLT-1, leads to a depressive-like phenotype (Lee et al. 2007; John et al. 2012) and impairs spatial memory (Bechtholt-Gompf et al. 2010). Despite the emerging importance of astrocytes in the context of brain disorders, it is still unexplored the functional mechanisms underlying its contribution to the pathophysiology of depression. So far, the role of signaling dependent on global astrocyte Ca^{2+} in the context of mood disorders, namely depression is poorly understood.

1.5. Astrocytes in aging

Aging is a lifelong process characterized by an accumulation of several detrimental changes that lead to an increased risk of disease and death (Tosato et al. 2007). In the brain, aging alters molecules, cells, vasculature, brain size and cognition (Peters 2006). Imaging studies revealed that aging is accompanied by alterations in regional brain volumes in areas related to cognitive function, motor behavior and emotional processing (Amorim et al. 2018). Specifically, the PFC and basal ganglia show a particular vulnerability to the aging process, translated into functional and morphological (atrophic) alterations (Burke and Barnes 2006; Berchtold and Cotman 2009). Based on this, heathy aging affects cognitive functions mainly related with memory, executive function, and processing speed. Contrastingly, in pathological aging, a global cognitive dysfunction is observed (Berchtold and Cotman 2009). In healthy aging, several brain cell types become compromised and contribute to cognitive impairments. Several studies tried to dissect the underlying morphological and molecular alterations occurring in the aging body. However, conflicting results lead to a myriad of controversial observations. Regarding neuronal cell

number, some reports suggested a decrease in the dorsal PFC (Stranahan et al. 2012), mPFC and primary visual cortex of rodents (Yates et al. 2008), while others revealed no changes in neuronal counts in neocortical regions of human aged brains (Freeman et al. 2008). Similarly, dendritic morphology and spine analysis revealed a huge variability of results, from no changes to an increased dendritic complexity upon aging (Konsolaki and Skaliora 2015). The lack of a clear neuronal influence that could explain the behavioral results observed with aging, led some authors to explore the role of other cells involved in synaptic control such as astrocytes. Aging triggers functional, morphological and molecular alterations in astrocytes (Palmer and Ousman 2018). Age-related changes alter astrocytic ability to properly maintain a homeostatic brain environment. A reduction in astrocytic - synaptic coverage, neurovascular and metabolic support has been observed and their consequences in the aged hippocampus were reviewed by Ojo et al. (2015). In addition, age-dependent oxidative stress in middle-aged mice was shown to lead to an increase in reactive oxygen species and Ca^{2+} overload in astrocytes (Ishii et al. 2017). Recently, Gomez-Gonzalo et al. (2017) demonstrated that spontaneous and neuronal-activity evoked astrocytic Ca^{2+} signals remain unaltered with normal aging, using hippocampal and cortical slices. Moreover, authors showed that in the context of AD, interfering with IP_3R2-dependent Ca^{2+} signaling in astrocytes contributes to the disease installation. Contrastingly, neocortical astrocytes from WT and dnSNARE mice displayed an age-related decrease in spontaneous Ca^{2+} elevations. This alteration was counterbalanced by exposing animals to an environmental enrichment or caloric restriction approach (Lalo et al. 2018).

Astrocytes are recognized to undergo alterations in their main structure with aging. Typically a process called astrogliosis occurs and a general hypertrophy is observed (Cotrina and Nedergaard 2002). A comprehensive analysis studied GFAP-immunostaining in three brain regions (entorhinal cortex, DG and CA1 hippocampus) from young and aged mice (Rodriguez et al. 2014). These authors strikingly showed an increase in GFAP-stained astrocytic structure in DG and CA1 regions, contrasting with a reduction in this staining at the entorhinal cortex. These results point to a heterogeneous response of astrocytes to age-dependent changes. The breakthrough of transcriptomic analysis revealed that aging alters astrocytic gene expression patterns in humans (Soreq et al. 2017) and mice (Boisvert et al. 2018). Astrocytes specifically isolated from aged mice display an upregulation of genes related with synapse elimination and immune pathways, a decrease in the expression of genes associated with cholesterol production, and major gene alterations in brain areas intimately related to the aging process, as the cerebellum and the hypothalamus (Boisvert et al. 2018). Clarke et al. (2018) added that, in healthy aging, astrocytes take on an A1 phenotype and have an increased number of differentially expressed genes, particularly in the hippocampus and striatum.

Together, compelling evidences point to an important role of astrocytes in brain function control in the context of depression and aging. Thus, it urges to explore the potential of global astrocyte Ca^{2+} signaling to modulate aging-related molecular, structural and cognitive deficits.

1.6. Aims of this thesis

Astrocytes are acknowledged for their role in brain function, mainly due to the identification of their intracellular Ca^{2+} dynamics and the development of imaging techniques. The view of these cells as simple passive, non-excitable cells, supporting neuronal activity is now outdated. About 30 years ago, the discovery of astrocyte intracellular Ca^{2+} elevations completely revolutionized the field (Cornell-Bell et al. 1990; Charles et al. 1991). These elevations represent a proxy of astrocyte activity and prompted neuroscientists to study its role in physiological and pathological conditions. Astrocytic Ca^{2+} elevations were found to emerge from different sources and display complex spatio-temporal properties (Bazargani and Attwell 2016). In the brain, astrocytes are an organized network that respond to activation via Ca^{2+} signaling, driving orchestrated responses. Therefore, astrocytic Ca^{2+} impacts synapses, circuits and behavior (Guerra-Gomes et al. 2017). Global astrocytic Ca^{2+} elevations occur mainly through a Gq-GPCR signaling pathway that leads to the production of IP_3, following the activation of IP_3R2, which triggers the release of Ca^{2+} from the ER. These global Ca^{2+} signals were shown to modulate different forms of synaptic transmission in several brain regions, with a potential impact to modulate circuits and behavior.

The main goal of this thesis was to investigate the role of global astrocytic Ca^{2+} signaling in cortico-limbic function and behavior. For that, we took advantage of the IP_3R2 KO mouse model that lacks global Ca^{2+} signaling in astrocytes. We performed a longitudinal characterization of this mouse model by assessing its impact during postnatal development, adulthood (healthy and in a depression context) and aging, at behavioral, structural and molecular levels. We were interested in understanding the impact of astrocytic Ca^{2+} signaling in cognitive function, mainly dependent on the hippocampus and the PFC.

To address this main goal we aimed at:

i) Characterize the impact of IP_3R2 deletion during postnatal development **(Chapter 2)**;

ii) Evaluate the role of IP_3R2-dependent astrocytic Ca^{2+} signaling in cognitive function by performing a detailed behavioral, structural and molecular characterization **(Chapter 3)**;

iii) Test a putative involvement of astrocytic IP_3R2-dependent Ca^{2+} signaling in the deleterious effects of uCMS exposure **(Chapter 4)**.

iv) Test the protective potential of IP_3R2-dependent Ca^{2+} signaling in astrocytes during aging **(Chapter 5)**;

CHAPTER 2

Sónia Guerra-Gomes, Eduardo Loureiro-Campos, Vanessa Morais Sardinha, Diana Sofia Marques Nascimento, João Filipe Viana, Nuno Sousa, Luísa Pinto, João Filipe Oliveira

IP_3R2 KO mice display a normal somatic and neurological development

(Manuscript submitted)

(2019)

Title: IP_3R2 KO mice display a normal somatic and neurological development

Authors:

Sónia Guerra-Gomes[1,2], Eduardo Loureiro-Campos[1,2], Vanessa Morais Sardinha[1,2], Diana Sofia Marques Nascimento[1,2], João Filipe Viana[1,2], Nuno Sousa[1,2], Luísa Pinto[1,2], João Filipe Oliveira[1,2,3]

Affiliations:

1 - Life and Health Sciences Research Institute (ICVS), School of Medicine, University of Minho, 4710-057 Braga, Portugal

2 - ICVS/3B's - PT Government Associate Laboratory, Braga/Guimarães, Portugal

3 - IPCA-EST-2Ai, Polytechnic Institute of Cávado and Ave, Applied Artificial Intelligence Laboratory, Campus of IPCA, Barcelos, Portugal

Corresponding author:

João Filipe Pedreira de Oliveira (PhD), Life and Health Sciences Research Institute (ICVS), School of Medicine, University of Minho, Campus de Gualtar, 4710-057 Braga, Portugal, Tel: +351-253-604871, Fax: +351-253-604809, joaooliveira@med.uminho.pt

ACKNOWLEDGMENTS

The authors are grateful to Prof. Alfonso Araque and Prof. Ju Chen for sharing the mice line. They acknowledge also funding from national funds through Foundation for Science and Technology (FCT) fellowships to SGG, ELC, VMS, CEEC to DSMN and IF grants to LP (IF/01079/2014) and JFO (IF/00328/2015); Bial Foundation Grants 207/14 and 037/18 to JO, and 427/14 to LP; Northern Portugal Regional Operational Programme (NORTE 2020), under the Portugal 2020 Partnership Agreement, through the European Regional Development Fund (FEDER) (NORTE-01-0145-FEDER-000013); FEDER Funds, through the Competitiveness Factors Operational Programme (COMPETE), and The National Fund, through the FCT (POCI-01-0145-FEDER-007038).

Abstract

Astrocytes are key players in the regulation of brain development and function. They sense and respond to the surrounding activity by elevating their intracellular calcium (Ca^{2+}) levels. These astrocytic Ca^{2+} elevations emerge from different sources and display complex spatio-temporal properties. Ca^{2+} elevations appear spatially distributed in global (soma and main processes) and/or focal regions (microdomains). The inositol 1,4,5-triphosphate receptor type 2 knockout (IP_3R2 KO) mouse model lacks global Ca^{2+} elevations in astrocytes and it has been recently used by different laboratories in the glia field. However, this model is a constitutive knockout posing the natural concern that the absence of IP_3R2 during development may trigger compensating phenotypes, which could bias results of experiments using developing or adult mice. Therefore, we performed a detailed neurodevelopmental evaluation of male and female IP_3R2 KO mice, during the first 21 days of life. This evaluation consisted of a detailed examination of somatic parameters and neurological reflexes. Our results show that male and female IP_3R2 KO mice display a normal growth, as compared with wild-type (WT) mice. IP_3R2 KO mice reached all mature neurological reflexes within the time windows of WT mice. As expected, this normal development results in normal locomotion and exploratory drive in this mouse model in adulthood. Overall, our results show that the IP_3R2 KO mouse is a reliable model to study the functional impact of global IP_3R2-dependent astrocytic Ca^{2+} elevations.

Keywords

Astrocytes, calcium signaling, IP_3R2, development, behavior

Introduction

Astrocytes, the most abundant glial cell type in the nervous system, play a pivotal role in integrating and responding to network activity (Perea et al. 2009; Oliveira et al. 2015; Mederos et al. 2018). Phylogenetic evidences showing an increased glia-to-neuron ratio, namely in species with larger brains (Verkhratsky and Nedergaard 2016), support the importance of this role of astrocytes. These glial cells sense and integrate the surrounding activity by elevating its intracellular calcium (Ca^{2+}) levels. The discovery of this particular astrocytic feature and the development of tools to allow its quantification (Cornell-Bell et al. 1990; Nedergaard 1994; Parpura et al. 1994) paved the way for a better understanding of the spatio-temporal dynamics of astrocytic modulation (Volterra et al. 2014; Shigetomi et al. 2016). Since then, several studies described important contributions of astrocytic Ca^{2+} signaling for the control of synaptic communication, circuit computation and behavioral performance (Guerra-Gomes et al. 2017). Astrocyte activation can elicit complex Ca^{2+} events that vary from global (mainly observed in the soma and main processes) to focal (restricted to thin processes and microdomains), whose complexity and functional consequences are being studied by multiple laboratories (Volterra et al. 2014; Shigetomi et al. 2016). Taking advantage of the high predominance of inositol 1,4,5-triphosphate receptor type 2 (IP_3R2) in astrocytes, the most used animal model to study the role of global IP_3-dependent Ca^{2+} elevations in astrocytes is the knockout mouse for this receptor (IP_3R2 KO) (Li et al. 2005). This model displays a normal neuronal Ca^{2+} activity, but critically impaired global astrocytic Ca^{2+} signals, and therefore it has been extensively used both in health and disease contexts (Petravicz et al. 2008; Agulhon et al. 2010; Takata et al. 2011; Navarrete et al. 2012; Wang et al. 2012b; Cao et al. 2013; Jego et al. 2014; Li et al. 2015; Srinivasan et al. 2015; Yang et al. 2016; Rakers and Petzold 2017; Tanaka et al. 2017; Sherwood et al. 2017; Okubo et al. 2019; Pinto-Duarte et al. 2019).

These mice are viable and fertile and display no major alterations in brain cytoarchitecture (Li et al. 2005; Petravicz et al. 2008). However, the constitutive nature of the IP_3R2 deletion might lead to alterations that could influence experimental results obtained during development and adult stages. To address this issue, we performed a detailed examination of somatic parameters and neurological reflexes acquired during development, in male and female IP_3R2 KO mice and respective wild-type (WT) littermates. Moreover, we complemented this analysis by assessing general phenotypical behavior in adult mice through the analysis of motor behavior and exploratory drive. Our results show that IP_3R2 KO mice display a normal somatic and neurological reflex development, as well as unaffected locomotor or exploratory abilities in adulthood. Therefore, they are suitable for functional testing during development and adult stages.

Materials and Methods

Animals

All experimental procedures were conducted in accordance with the guidelines described in Directive 2010/63/EU and were approved by the local ethical committee (SECVS 075/2015) and the national authority for animal experimentation (DGAV 17469/2012). A mouse strain with targeted deletion of *Itpr2* gene was kindly supplied for this project by Prof. Alfonso Araque (U. Minnesota, USA) (Navarrete et al. 2012), under agreement with Prof. Ju Chen (U.C. San Diego, USA) (Li et al. 2005). Mice were backcrossed at least 5 generations to C57BL/6J. All mice had *ad libitum* access to food and water in their home cages and lights were maintained on a 12h light/dark cycle (lights on 8:00 A.M. to 8:00 P.M.) at 22 ± 1°C, 55% humidity. IP_3R2 KO and their respective littermate WT controls were obtained by mating pairs of $IP_3R2^{+/-}$. A total of 19 WT littermates (9 males and 10 females) and 20 IP_3R2 KO mice (10 males and 10 females) were used to perform a neurodevelopmental evaluation. All animals received a toe tag at postnatal day (PND) 5 as described in Castelhano-Carlos et al. (2010), which remained unaltered throughout the experiment and allowed to evaluate each animal response in a blind manner. The collected toe tissue was used for DNA extraction and subsequent genotyping by PCR analysis using WT (forward, ACCCTGATGAGGGAAGGTCT; reverse, ATCGATTCATAGGGCACACC) and mutant allele specific primers (neo - specific primer: forward, AATGGGCTGACCGCTTCCTCGT; reverse, TCTGAGAGTGC CTGG CTTTT) as previously described (Li et al. 2005). For general behavioral assessment, we used male and female WT and IP3R2 KO mice (n=6-8 per group) of 3 to 4-month-old (adults).

Developmental milestones

Neonatal neurodevelopmental milestones were performed according to previously validated protocols in mice (Fox 1965; Santos et al. 2007; Hill et al. 2008; Castelhano-Carlos et al. 2010). It consisted of a daily evaluation for 21 days, since the day of birth. At birth, only the number of pups in the litter was counted without any further examination. From PND1 onwards, newborn animals were inspected for skin appearance, activity, and presence of a milk spot in the stomach, which are indicators for correct maternal care and well-being. Moreover, animals were daily weighted and examined for the acquisition of developmental milestones until weaning (PND21). This daily scoring included the assessment of the acquisition of a mature response regarding several somatic and neurological parameters. Pups were tested every day at the same time, in the same experimental room, by the same experimenters. Throughout the evaluation several parameters were assessed according to the age of the pup (Figure 2.1A), and the score value was registered in an individual table for each animal.

Somatic parameters

Body weight was registered every day from PND1 to PND21 (weight ± 0.01 g), as an indicator of morphological development. Anogenital distance, which corresponds to the distance between the opening of the anus and the opening of the genitalia, is a marker for reproductive development and maturation. This parameter was daily registered starting from PND3 (distance ± 0.05 mm). Eye opening was daily scored according to the state of the eyes. Eye opening was considered when an initial break in the membrane sealing was observed. When one of the eyes was opened, a score of 1 was attributed; when both eyes were opened a score of 2 was achieved. PND of mature response was registered when both eyes were open.

Neurological reflexes

Neurological reflexes were daily assessed from PND1 to PND21. Cages containing the mother and pups were taken from the housing room to an experimental room at the same circadian rhythm hour. To ensure the minimal disturbance of the pups, tests were performed on a smooth foam pad and after the evaluation, pups were immediately returned to the home cage. The daily score was attributed as following: tests that evaluated absence/presence of a mature response were scored as 0/1 (rooting, ear twitch, auditory startle, open field traversal, air righting, wire suspension, postural reflex); parameters where a gradual evolution was observable were scored from 0 to 3 (walking, surface righting, grasping, negative geotaxis, cliff aversion), with 0 representing absence and 3 corresponding to achievement of the mature response. In the end, PND of mature response achievement was registered for each pup. Neurological reflexes were divided into several categories according to the function analyzed and they were assessed as following:

Tactile reflex

Rooting - This test consists in gently stroking a fine filament of cotton three times along the side of the head of the pup. If it turns the head towards the filament, a mature response is considered.

Ear twitch - It consisted in stimulating the ear of the pup by brushing it with the end of a cotton tip three times. If the newborn responded by flattening the ear against the side of the head, a score for a mature response was attributed.

Auditory reflex

Auditory startle - Newborn mice were tested for auditory reflex from PND7 until PND18. The response of the animal to a handclap was observed. If the animal reacted, then a mature response was present and a score of 1 was attributed.

Motor

Open Field Traversal - Newborn mice (PND8-21) were placed in the center of a plastic sheet containing a circle with 13 cm of diameter. The time that the animal took to move out of the circle was recorded. A mature response was considered when the mouse was able to respond in less than 30 s. This test allows the evaluation of locomotion and the extinguishing of pivoting behavior.

Walking - The development of locomotion and coordination was evaluated by observing animals freely moving, since PND5 until PND21. The mature response was considered when pups were able to walk straight with their body completely supported by the four limbs.

Labyrinthine reflex, coordination, and strength

Surface righting reflex - This parameter was evaluated from PND1 until PND13. It consisted in putting the animal on its back, and the mature response was considered when the animal was able to get right. It evaluates spatial, body righting and labyrinthine mechanisms.

Air righting reflex - This parameter was assessed from PND8 until PND21. Mice were turned back and held at approximately 13 cm distance from the soft surface and released. A mature response was observed when the pup developed the reflex to turn his body during the fall and land on its four paws.

Postural reflex - Mice response was assessed from PND5 until weaning. Animals were placed in a small plastic open box and gently shaken vertically and horizontally. If the animal maintained its original position in the box, it was assumed to have acquired a mature postural reflex response. This parameter allows the evaluation of spatial and body righting responses.

Negative geotaxis - This behavioral response was evaluated from PND1 until PND14. Pups were placed in a horizontal grid, tilted 45° to the plane, with its head facing downwards. It was considered a mature

response when the animal was able to turn immediately by 180° and moved towards the top of the slope. It tests spatial, body righting and labyrinthine mechanisms.

Cliff aversion - It evaluates the ability of mice to turn and crawl away when put on the edge of a cliff, with its forepaws and face over the edge (from PND1 until PND14). This parameter allows the assessment of spatial reflex and coordination.

Wire suspension - This parameter evaluates forelimb grasp and was assessed from PND5 until the weaning age. This strength test consists in placing the pup vertically to hold a 2 mm metal bar with its forelimbs. A mature response was achieved when the animal was able to hold its body weight alone, without falling.

Grasping - This is a strength test performed from PND5 until PND21. The forelimb of the pup was stimulated with a thin wire. If the animal held the wire firmly, a mature response was considered.

Locomotor and swimming abilities

Open Field

The Open Field test was used to assess locomotor and exploratory activity (Seibenhener and Wooten 2015). The apparatus consisted of a brightly illuminated Plexiglas box enclosing a white arena (43.2 x 43.2 x 30.5 cm), equipped with infrared beams to detect mice activity (Med Associates Inc, USA). Mice were individually placed in the center of the arena and let to freely explore it for 5 min. This test allowed the assessment of motor (by the distance walked) and exploratory activity (by the number of vertical rearings).

Swimming Performance Test

Swimming performance test was conducted in a dark circular pool with 106 cm diameter filled with water at 23 ± 1°C, under dim light conditions (Sardinha et al. 2017). The water was made opaque using nontoxic titanium dioxide (Sigma-Aldrich, 250 mg/L) to improve mice detection. Mice were placed in the pool and allowed to swim freely during 60 s. The distance swam during this trial was monitored and analyzed by a video-tracking system (Viewpoint, France).

Statistical analysis

Developmental milestones were performed and analyzed by the same researchers, who were blind to the mouse genotype during the protocol. Prism 7 (GraphPad Software Inc., USA) was used to assess normal distributions and further group comparisons. Continuous variables followed a Gaussian distribution (Kolmogorov-Smirnov test) within groups and parametric tests were applied, while non-parametric tests were used for discrete variables. Two-way analysis of variance (ANOVA) with Sidak *post hoc* test was applied to analyze somatic parameters, considering either factors: postnatal day and genotype. For neurological reflexes, Mann-Whitney two-tailed test was used. Multiple t-tests were applied for swimming and locomotor ability experiments. Data are expressed as mean ± SEM (Standard Error of the Mean), except for neurological reflexes in which data are plotted as median. The results were considered statistically significant for a $p < 0.05$.

Results

WT and IP_3R2 KO newborn mice included in this study received correct maternal care and welfare. They were daily evaluated for the acquisition of several somatic and neurological responses, during the first 21 days of life (Figure 2.1A).

IP_3R2 KO mice display a normal somatic development

Somatic parameters assessed during the developmental milestones protocol in WT and IP_3R2 KO mice were body weight, anogenital distance and eye opening (Figure 2.1A, grey).

Results show that male WT and IP_3R2 KO mice display a body weight increase along time (Figure 2.1B; $F_{20, 340} = 329.0$, $p < 0.001$), which was similar between genotypes ($F_{1, 17} = 0.62$, $p = 0.44$). Female mice daily increased their body weight (Figure 2.1B; $F_{20, 360} = 278.4$, $p < 0.001$), and this parameter was also similar between WT and IP_3R2 KO littermates ($F_{1, 18} = 2.001$, $p = 0.170$).

Anogenital distance in male WT and IP_3R2 KO mice equivalently increased along time (Figure 2.1C; $F_{18, 288} = 197.1$, $p < 0.001$) and no differences were observed between genotypes ($F_{1, 16} = 0.04$, $p = 0.84$). Similarly, WT and IP_3R2 KO female mice displayed a daily increase in anogenital distance (Figure 2.1C; $F_{18, 324} = 185.5$, $p < 0.001$), which was not significantly different between genotypes ($F_{1, 18} = 2.54$, $p = 0.13$). Regarding eye opening, WT and IP_3R2 KO mice from both genders acquired the mature response simultaneously (male: $U = 38.0$; $p = 0.60$; female: $U = 40.5$; $p = 0.46$) (Figure 2.2A). Altogether, these results are indicators that the constitutive genetic deletion of IP_3R2 does not interfere with general growth during the development of male and female newborn mice.

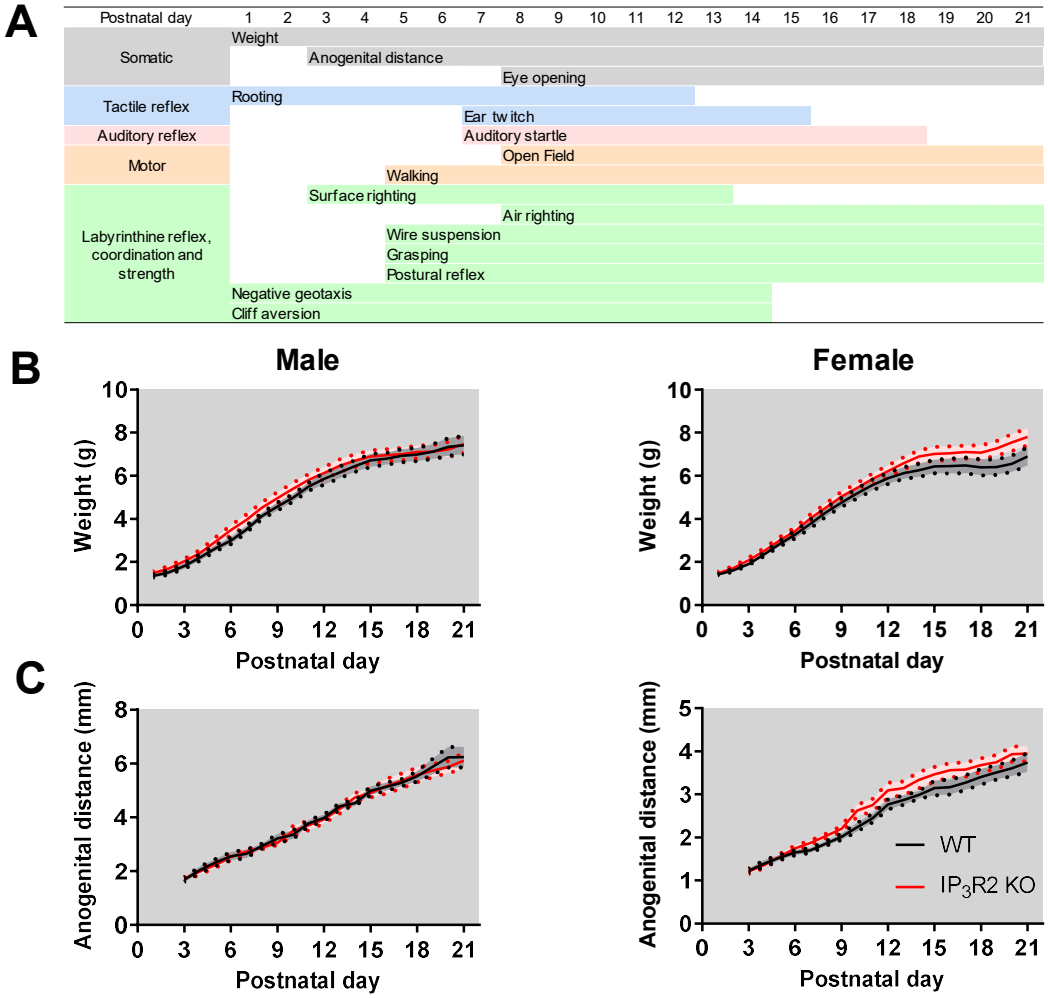

Figure 2.1 - Male and female IP_3R2 KO mice gain weight similarly to controls and display a normal genital development.

(A) Representative scheme of the experimental timeline used, depicting each developmental parameter according to the tested function (grey – somatic parameters, blue – tactile reflex, pink – auditory reflex, orange – motor function, green – labyrinthine reflex, coordination, and strength). (B) Body weight evolution from postnatal day 1 to postnatal day 21 of WT and IP_3R2 KO mice (male and female). (C) Anogenital distance measurement from postnatal day 3 to postnatal day 21 of WT and IP_3R2 KO mice (male and female). Males are represented in left panels and female mice are depicted in right panels (WT – black, IP_3R2 KO – red). Data plotted as mean ± SEM. n=9-10 per group.

IP_3R2 KO mice acquire all neurological milestones normally

Neurodevelopmental evaluation included the examination of several neurological parameters related to sensorial (Figure 2.1A, blue and pink) and motor functions (Figure 2.1A, orange), labyrinthine reflex, coordination and strength (Figure 2.1A, green) in male and female WT and IP_3R2 KO mice. Tactile reflex development was evaluated in rooting and ear twitch tests (Figure 2.2B). Our results show that male WT and IP_3R2 KO mice display a similar mature response in the rooting test ($U = 34.5$; $p = 0.40$), which was equivalently observed for females ($U = 35.5$; $p = 0.29$). More so, ear twitch test revealed no significant differences between WT and IP_3R2 KO mice from both genders (male: $U = 41.5$; $p = 0.78$; female:

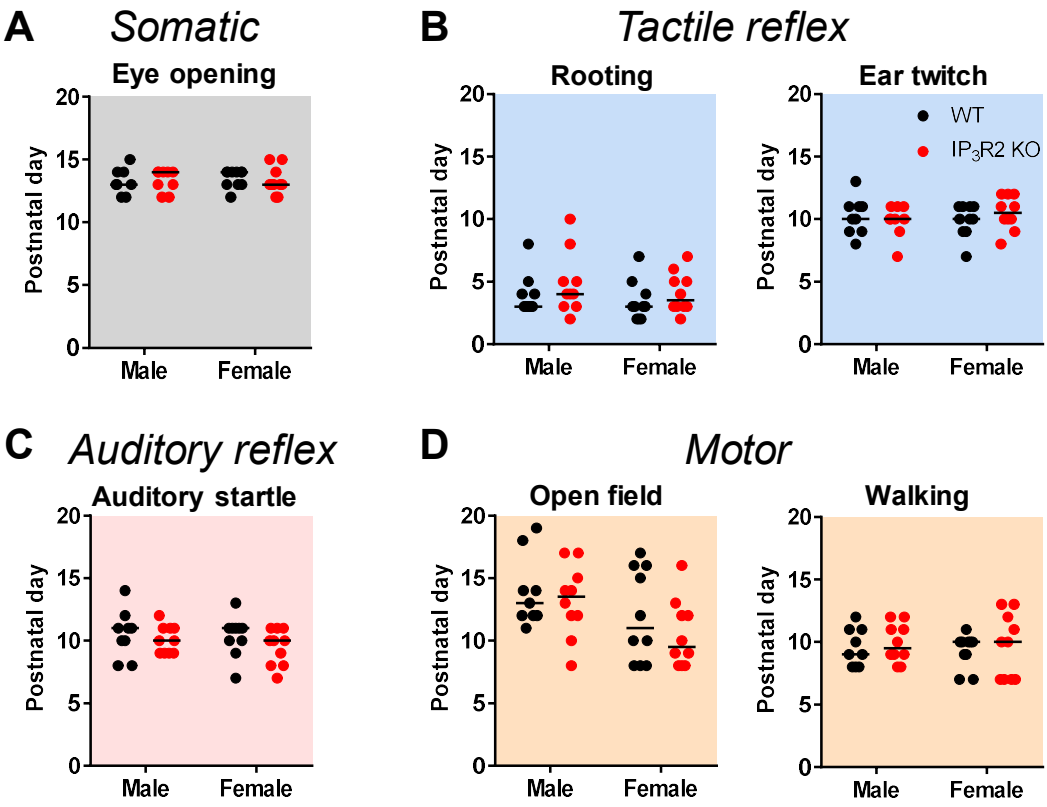

Figure 2.2 - Male and female IP_3R2 KO mice retain a normal acquisition of somatic and sensory-motor parameters.

(A) Postnatal acquisition of a somatic milestone (eye opening, grey background). (B-D) Postnatal acquisition of neurological reflexes related with sensorial (B,C) and motor function (D). (B) Rooting and ear twitch tests were performed to evaluate the developmental acquisition of tactile reflex (blue background). (C) Auditory startle evaluated the acquisition of a mature auditory reflex (pink background). (D) Open Field and Walking are parameters for the assessment of a mature locomotor response (orange background). WT mice are represented in black and IP_3R2 KO mice are represented in red (males, left column; females, right column). Data plotted as median. n=9-10 per group.

$U = 37.5$; $p = 0.36$). Auditory system development was assessed by the auditory startle test. We observed that male WT and IP_3R2 KO

newborn mice equally acquired this milestone (Figure 2.2C; $U = 38.0$; $p = 0.58$), and females from both genotypes displayed a similar mature response ($U = 32.5$; $p = 0.19$). The achievement of motor abilities is a good indicator of neurological development. We evaluated motor function in the open field traversal and walking tests (Figure 2.2D). Our results show an equal acquisition of the mature response in the open field traversal for male ($U = 42.5$; $p = 0.86$) and female ($U = 39.5$; $p = 0.44$) mice from both genotypes. Furthermore, male WT and IP_3R2 KO mice equally acquired a mature walking ability ($U = 38.5$; $p = 0.63$), which was also observed for females from both genotypes ($U = 43.5$; $p = 0.63$).

The neurological milestones also comprise several tests to evaluate the vestibular system formation, namely surface righting, air righting, postural reflex, negative geotaxis and cliff aversion (Figure 2.3). In the surface righting test, we evaluated labyrinthine reflex and coordination. We found no differences between male WT and IP_3R2 KO mice in this test ($U = 40.5$; $p = 0.73$). A similar mature response was also observed for female WT and IP_3R2 KO mice ($U = 33.5$; $p = 0.21$). In the air righting test, male WT and IP_3R2 KO displayed an analogous mature response ($U = 34.0$; $p = 0.38$), which was also observed for females ($U = 49.5$; $p = 0.97$). Moreover, we found that genetic deletion of IP_3R2 did not alter postural reflex acquisition in males ($U = 37.5$; $p = 0.56$) and females ($U = 38.5$; $p = 0.38$). In the negative geotaxis test the mature response of male IP_3R2 KO mice was similar to WT littermates ($U = 42.0$; $p = 0.83$). Female WT and IP_3R2 KO mice also equally acquired this developmental milestone ($U = 43.0$; $p = 0.59$). Lastly, cliff aversion test showed that male WT and IP_3R2 KO mice present a mature response approximately at the same postnatal day ($U = 42.0$; $p = 0.82$), which was also confirmed for female IP_3R2 KO mice ($U = 31.0$; $p = 0.16$). Another important measure of postnatal development is strength. We assessed this parameter by performing wire suspension and grasping test (Figure 2.3). Our results show that male WT and IP_3R2 KO display a similar mature response in wire suspension ($U = 44.5$; $p = 0.98$), which was again confirmed for IP_3R2 KO female mice ($U = 26.0$; $p = 0.06$). Overall, this detailed assessment of neurological parameters shows that IP_3R2 KO mouse model acquires a mature response for sensory-motor functions, vestibular area-dependent tasks, and strength similarly to WT.

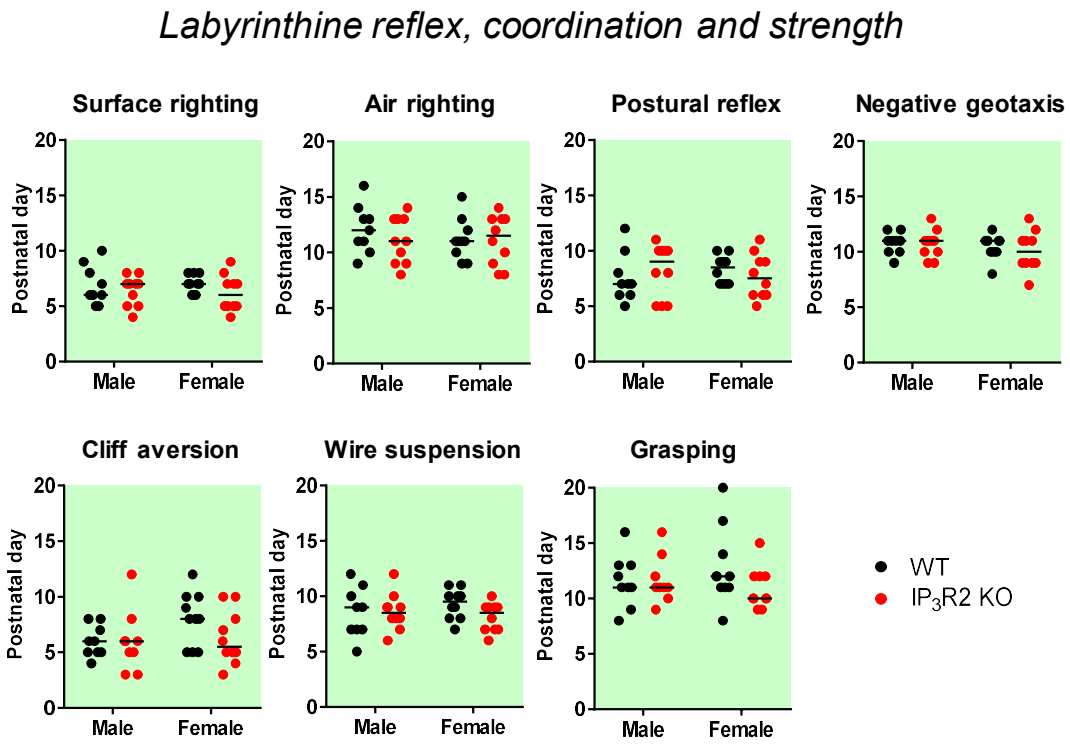

Figure 2.3 - Male and female IP_3R2 KO mice display normal labyrinthine reflex, coordination and strength.

Surface righting, air righting, postural reflex, negative geotaxis, cliff aversion, wire suspension and grasping as measures of vestibular system formation and strength acquisition. WT mice are represented in black and IP_3R2 KO mice are represented in red (males, left column; females, right column). Data plotted as median. n=9-10 per group.

IP_3R2 KO adult mice display normal motor and exploratory behavior

Developmental milestones showed that impairment of IP_3-dependent Ca^{2+} signaling in astrocytes does not interfere with the acquisition of somatic and neurological parameters. Nevertheless, we also aimed to assess locomotor and exploratory function in adult WT and IP_3R2 KO mice, both in males and females. The open field test provided us with measures of ambulatory behavior and motor function, such as distance traveled and number of vertical rearings (Figure 2.4A). Male and female IP_3R2 KO mice traveled similar distances as controls (males: $t_{11} = 0.91$; $p = 0.38$; females: $t_{11} = 2.02$; $p = 0.07$). Regarding exploratory behavior, no differences between male WT and IP_3R2 KO mice were observed for the number of rearings ($t_{11} = 0.63$; $p = 0.54$). Female IP_3R2 KO display a similar number of vertical rearings when compared to WT mice ($t_{11} = 1.32$; $p = 0.21$). Next, we analyzed the distance swam by each mouse during 60 s (Figure 2.4B). Results showed that IP_3R2 KO mice traveled similar distances, as compared with control littermates, for both males ($t_{14} = 1.44$; $p = 0.17$) and females ($t_{14} = 1.35$; $p = 0.20$). These findings support the use of adult IP_3R2 KO mice for general behavior assessment in adulthood.

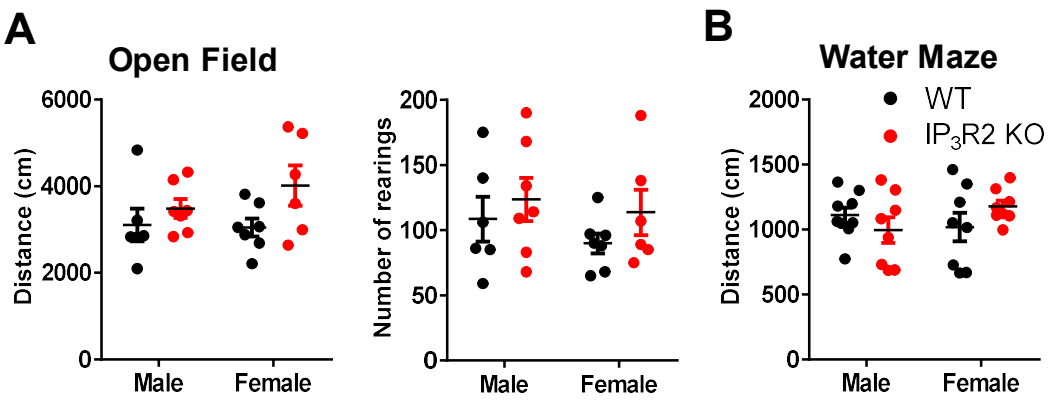

Figure 2.4 – Adult IP_3R2 KO mice display normal locomotor and exploratory functions.

(A) Distance traveled and number of rearings recorded in the Open Field test. (B) Distance freely swam in a swimming pool during 60 s. WT mice are represented in black and IP_3R2 KO mice are represented in red (males, left column; females, right column). Data plotted as mean ± SEM. n=6-8 per group.

Discussion

This comprehensive evaluation of somatic parameters and neurological reflexes shows that the constitutive deletion of IP_3R2 does not interfere with the normal development of these mice. This is an important observation since this approach is being used by multiple laboratories to study the role of astrocytes in health and disease contexts, resulting occasionally in negative or controversial results (Oliveira et al. 2015; Guerra-Gomes et al. 2017). The IP_3R2 KO model described in 2005 (Li et al. 2005) and used by most of the laboratories is a constitutive knockout mouse. Such gene deletions may result in developmental impairments and compensatory mechanisms that could bias experimental results obtained at different ages: development and adulthood. Until now, no study addressed the influence of IP_3R2 genetic deletion during the postnatal period. Therefore, we performed a detailed evaluation of neurodevelopmental milestones that consisted of a thorough examination of the somatic parameters and neurological reflexes.

Our results showed that IP_3R2 KO mice displayed a body weight increase similar to controls, both in males and females. This result is in line with previous studies showing that adult WT and IP_3R2 KO mice display a similar body weight (Li et al. 2015; Pinto-Duarte et al. 2019). More so, anogenital distance is not altered in both IP_3R2 KO males and females, indicating a normal sexual differentiation in this mouse model. This result is in accordance with our normal colony breeding observations and with a previous report indicating that this mouse strain displays normal reproductive behavior (Petravicz et al. 2008). Regarding eye opening, our results are in line with the typical age described for the acquisition of this developmental

milestone, which is on average at PND13 (Heyser 2004). These evidences indicate that IP_3R2 KO mice display a healthy physical maturation.

A neurodevelopmental assessment is fundamental to determine and discard possible alterations that might influence brain function and behavior performance (Sousa et al. 2006). We examined the acquisition of several neurological parameters related to sensory-motor reflexes, locomotion, coordination and strength in both WT and IP_3R2 KO mice (males and females). In our study, we found that WT and IP_3R2 KO mice similarly acquired a mature response for sensory-motor and auditory reflexes. These responses are in accordance with the average age previously described for C57BL/6 mice (Heyser 2004; Kleiber et al. 2011). From these evidences, we expect IP_3R2 KO mice to be able to perform behavioral tests that depend on the tactile, auditory and motor abilities. Another battery of developmental tests covered a progressive maturation of sensory and motor skills depending on the vestibular system maturation (Khan et al. 2004). In these tests, such as surface righting, air righting, postural reflex, negative geotaxis, and cliff aversion, no significant differences were detected between WT and IP_3R2 KO mice from both genders. This reflects a normal acquisition of sensorimotor-related parameters by IP_3R2 KO mice, which discards the existence of possible compensatory mechanisms occurring in vestibular system related functions during postnatal development. Accordingly, in the wire suspension and grasping tests, we found that WT and IP_3R2 KO mice equally performed this test within the typical range for the appearance of these developmental milestones (Heyser 2004; Kleiber et al. 2011). These tests are related to the acquisition of balance control mechanisms, which are intimately dependent on visual afferent information (Mesquita et al. 2007). It is noteworthy that by backcrossing the original mouse (Li et al. 2005) to C57BL/6J, we eliminated the retinal degeneration and associated loss of visual capacity described to mice that carry Black Swiss background. Altogether, these results discarded any alterations that could be occurring during development in IP_3R2 KO mice that could compromise results obtained from these mice. These data provide strong evidence for a normal somatic and neurological development of IP_3R2 KO mice, and they represent the first attempt to assess the influence of the constitutive genetic deletion of IP_3R2.

Finally, we assessed the general motor and exploratory phenotype of adult WT and IP_3R2 KO mice (male and female). Our approach consisted of two behavioral tests that allowed us to obtain several readouts directly related with locomotor and exploratory function measures. In the open field test, we analyzed two motor-related measures: distance traveled and rearings. The first parameter corresponds to a pure measure of motor ability, while the second one is more related with exploratory drive (Seibenhener and Wooten 2015). Next, we evaluated swimming ability of WT and IP_3R2 KO, to explore further their locomotor

capabilities. Our results show that WT and IP_3R2 KO mice of both genders behaved similarly in both tests. Taken together, these findings show that IP_3R2 KO mice display a normal development, which results in regular motor and exploratory behavior in adulthood.

Deletion of IP_3R2 in mice emerged as a promising genetic tool to study astrocytic Ca^{2+} signaling (Petravicz et al. 2008; Takata et al. 2011; Navarrete et al. 2012). Advances in the analysis of astrocytic Ca^{2+} elevations showed that astrocytes display rather complex spatial and temporal properties, whose functional consequences are still far from fully understood (Volterra et al. 2014; Shigetomi et al. 2016). Therefore, the field clearly needs tools to tackle differentially global or focal Ca^{2+} elevations. Functionally, the IP_3R2 KO mouse model is an excellent tool to study the roles of global Ca^{2+} elevations specifically in astrocytes as shown by different labs (Di Castro et al. 2011; Navarrete et al. 2012; Yu et al. 2018; Guerra-Gomes et al. 2018; Mederos et al. 2019). Recently, by employing a viral tool to genetically drive the continuous extrusion of cytosolic Ca^{2+} in astrocytes, Yu et al. (2018) yielded similar levels of impairment of global events, which confirms the functional relevance of the IP_3R2 KO mice. This observation together with our present findings fully supports the use of the IP_3R2 KO mouse for the study of astrocyte involvement in all developmental stages and adulthood.

Author Contributions

SGG designed and performed the experiments, analyzed the data and wrote the manuscript; ELC participated in experimental conception and design; VMS, DSMN, JFV participated in experimental conception and data analysis; NS, LP and JFO supervised the study, secured funding, analyzed the data and wrote the manuscript.

CHAPTER 3

Sónia Guerra-Gomes, Vanessa Morais Sardinha, Gabriela Tavares, Inês Caetano, Diana Sofia Marques Nascimento, João Filipe Viana, Martin Irmler, Mareike Bamberger, Johannes Beckers, Michal Korostynski, Andreia Teixeira-Castro, Nuno Sousa, Luísa Pinto, João Filipe Oliveira

The role of astrocytic calcium signaling in cognitive function

(Manuscript to be submitted)

(2019)

Title

The role of astrocytic calcium signaling in the cognitive function

Authors

Sónia Guerra-Gomes[1,2], Vanessa Morais Sardinha[1,2], Gabriela Tavares[1,2], Inês Caetano[1,2], Diana Sofia Marques Nascimento[1,2], João Filipe Viana[1,2], Martin Irmler[4], Mareike Bamberger[4], Johannes Beckers[4], Michal Korostynski[5], Andreia Teixeira-Castro[1,2], Nuno Sousa[1,2], Luísa Pinto[1,2], João Filipe Oliveira[1,2,3]

Affiliations

1 - Life and Health Sciences Research Institute (ICVS), School of Medicine, University of Minho, 4710-057 Braga, Portugal

2 - ICVS/3B's - PT Government Associate Laboratory, Braga/Guimarães, Portugal

3 - IPCA-EST-2Ai, Polytechnic Institute of Cávado and Ave, Applied Artificial Intelligence Laboratory, Campus of IPCA, Barcelos, Portugal

4 - Institute of Experimental Genetics, Helmholtz Zentrum München, German Research Center for Environmental Health, Neuherberg, Germany;

5 - Department of Molecular Neuropharmacology, Institute of Pharmacology, Polish Academy of Sciences, Kraków, Poland;

Corresponding author:

João Filipe Pedreira de Oliveira (PhD), Life and Health Sciences Research Institute (ICVS), School of Medicine, University of Minho, Campus de Gualtar, 4710-057 Braga, Portugal, Tel: +351-253-604871, Fax: +351-253-604809, joaooliveira@med.uminho.pt

ACKNOWLEDGMENTS

The authors are grateful to Prof. Alfonso Araque and Prof. Ju Chen for sharing the mice line. They acknowledge J. D. Silva for his helpful comments on the statistical analysis. The authors also acknowledge funding from national funds through Foundation for Science and Technology (FCT) fellowships to SGG, VMS, IC, CEEC to DSMN and IF grants to LP (IF/01079/2014) and JFO (IF/00328/2015); Bial Foundation Grants 207/14 and 037/18 to JO, and 427/14 to LP; Northern Portugal Regional Operational Programme (NORTE 2020), under the Portugal 2020 Partnership Agreement, through the European Regional Development Fund (FEDER) (NORTE-01-0145-FEDER-000013); FEDER Funds, through the

Competitiveness Factors Operational Programme (COMPETE), and The National Fund, through the FCT (POCI-01-0145-FEDER-007038).

Abstract

Astrocytes modulate neuronal activity and synaptic transmission, thus contributing to learning and memory processing. These cells sense and respond to neuronal activity by elevating their intracellular calcium (Ca^{2+}) levels. Intracellular Ca^{2+} derives from different sources and displays complex spatio-temporal properties. Here we assessed the role of inositol 1,4,5-triphosphate receptor type 2 (IP_3R2)-dependent Ca^{2+} signaling in cognitive function by testing the performance of a mouse model lacking this receptor in hippocampal-dependent tasks. Our results show that IP_3R2 KO mice display enhanced cognitive performance in tasks associated with spatial reference (MWM) and fear memory (CFC). Moreover, we found that interfering with global astrocytic Ca^{2+} signaling in astrocytes does not affect the morphology of CA1 pyramidal neurons, but promotes an increased percentage of immature spines at apical dendrites. Strikingly, we found an astrocytic structural atrophy that seems to be compensated by an increased density of $GFAP^+$-cells in the same hippocampal sub-region. At the molecular level, we identified the transcription factor *Foxo1* as the transcription factor controlling a higher number of differentially expressed genes in IP_3R2 KO mice, namely the astrocyte-specific syndecan-2 (*Sdc2*) and ezrin (*Ezr*). These genes are related with fine cytoskeleton modulation and dendritic spine formation and might influence synaptic plasticity and cognitive function. To test this hypothesis, we overexpressed FOXO1 specifically in hippocampal astrocytes (GFAP-mCherry-FOXO1) of naïve C57BL/6J mice. We observed that GFAP-mCherry-FOXO1 mice display enhanced fear memory, as previously observed for IP_3R2 KO mice, pointing to a key role of astrocytic FOXO1 regulated-pathways in cognitive modulation.
Altogether, this work provides evidence that interfering with global IP_3R2-dependent Ca^{2+} mechanisms or overexpressing FOXO1 in astrocytes, favors *Foxo1* transcriptional activity towards the expression of relevant genes to support cognitive performance.

Keywords

astrocyte, calcium signaling, IP_3R2, hippocampus, cognitive function, *Foxo1*

Introduction

Astrocytes are the most numerous glial cell type in the central nervous system (CNS), playing an important role in higher brain functions, such as learning and memory (Oberheim et al. 2012; Verkhratsky and Parpura 2014; Oliveira et al. 2015; Verkhratsky and Nedergaard 2016). These glial cells form a network that controls information processing by establishing an orchestrated response specific for each brain region and adapted to a physiological or pathological state (Araque 2008; Wang and Bordey 2008; Guerra-Gomes et al. 2017). Astrocytes sense neuronal activity through the expression of a variety of neurotransmitter receptors, ion channels, and transporters (Pannasch and Rouach 2013; Verkhratsky and Parpura 2014; De Pitta et al. 2016). Astrocytic calcium (Ca^{2+}) signaling is intimately involved in the control of synaptic transmission and closely related to learning and memory processing (Henneberger et al. 2010; Chen et al. 2012; Tanaka et al. 2013). It occurs mainly through a Gq-linked G-protein-coupled receptor (GPCR) signaling pathway, leading to the activation of inositol 1,4,5-triphosphate receptors (IP_3Rs). Astrocyte activation can elicit complex Ca^{2+} events that vary from global (mainly observed in the soma and main processes) to focal (restricted to thin processes and microdomains), whose complexity and functional consequences are still underexplored (Shigetomi et al., 2016; Volterra et al., 2014). Type 2 inositol IP_3Rs (IP_3R2) are selectively expressed in astrocytes and are responsible for global astrocytic Ca^{2+} elevations (Petravicz et al. 2008; Takata et al. 2011; Petravicz et al. 2014). Several studies have added important contributions to the understanding of astrocytic Ca^{2+} signaling in the control of synaptic communication, circuit computation, and behavioral performance. Most authors interfere with astrocytic Ca^{2+} signaling using two main approaches: (1) triggering intracellular Ca^{2+} elevations via chemogenetic activation of the GPCR signaling, and (2) inhibiting IP_3 signaling by IP_3R deletion or IP_3 molecule buffering (Guerra-Gomes et al. 2017). The IP_3R2 knockout (KO) mouse model displays normal neuronal Ca^{2+} activity, but critically impaired global astrocytic Ca^{2+} signals, and therefore it has been extensively used both in health and disease conditions (Petravicz et al. 2008; Agulhon et al. 2010; Takata et al. 2011; Navarrete et al. 2012; Wang et al. 2012b; Wang et al. 2012a; Cao et al. 2013; Jego et al. 2014; Li et al. 2015; Srinivasan et al. 2015; Yang et al. 2016; Rakers and Petzold 2017; Tanaka et al. 2017; Sherwood et al. 2017; Pinto-Duarte et al. 2019; Okubo et al. 2019). This mouse model has been tested under different backgrounds and/or crossed with distinct animal models. Therefore, each manipulation may trigger distinct consequences, which might lead to confounding results. Interestingly, an overall role of neuroprotection against an insult or a pathological state has been observed (Dong et al. 2013a; Kanemaru et al. 2013; Li et al. 2015; Kim et al. 2016; Rakers and Petzold 2017; Reichenbach et al. 2018; Guerra-Gomes et al. 2018; Saito et al. 2018). So far, the impact of IP_3R2 deletion in cognitive function remains

poorly understood. Nevertheless, recent studies revealed that activation of astrocytic Ca^{2+} signaling in a time-controlled manner improved memory acquisition (Adamsky et al. 2018; Mederos et al. 2019). Furthermore, Navarrete et al. (2019) demonstrated that hippocampal NMDAR-dependent LTD is dependent on astrocytic Ca^{2+} elevations and relies on astrocytic p38α MAPK signaling. The specific deletion of p38α MAPK in astrocytes, impaired LTD and enhanced long-term fear memory. These studies support an emerging role of astrocytic Ca^{2+} signaling in relevant molecular signaling pathways acting downstream of the generation of Ca^{2+} elevations.

In this study, we addressed the role of IP_3R2-dependent Ca^{2+} signaling in adult mice behavior, focusing on its importance for the performance of hippocampal-dependent tasks. For that, we performed a cognitive, morphological and molecular characterization in the hippocampus of WT and IP_3R2 KO mice.

Materials and Methods

Animals

All experimental procedures were carried out in accordance with the guidelines described in Directive 2010/63/EU and were approved by the local ethical committee (SECVS 075/2015) and the national authority for animal experimentation (DGAV 17469/2012). Male IP_3R2 KO mice and wild-type (WT) littermates were generated as previously described (Guerra-Gomes et al. 2018), in a C57BL/6J background. These mice were supplied by Prof. Alfonso Araque (U. Minnesota, USA) (Navarrete et al. 2012), under agreement with Prof. Ju Chen (U.C. San Diego, USA) (Li et al. 2005). All mice were maintained according to the guidelines for care and handling of laboratory animals (*ad libitum* access to food and water in their home cages; lights maintained on a 12 h light/dark cycle; 22 ± 1°C, 55% humidity). All animals received an ear tag at weaning age (around P21), which remained unaltered throughout the experiment and allowed to evaluate each animal response in a blind manner. The collected ear tissue was used for DNA extraction and subsequent genotyping by PCR analysis using WT (forward, ACCCTGATGAGGGAAGGTCT; reverse, ATCGATTCATAGGGCACACC) and mutant allele specific primers (neo-specific primer: forward, AATGGGCTGACCGCTTCCTCGT; reverse, TCTGAGAGTGCCTGGCTTTT) as previously described (Li et al., 2005).

Behavioral testing

Behavioral assessment was performed during the light phase. One week prior to behavioral testing, mice were daily handled for 5 min. On the testing day, animals were left in the testing room during 30 min, prior to behavioral assessment, for habituation.

Anxious-like behavior, locomotor and exploratory activity

Elevated Plus Maze

Elevated Plus Maze (EPM) test is a recognized method to assess anxious-like behavior in rodents (Belzung and Griebel 2001; Bourin et al. 2007). This test consists on placing mouse individually in the hub of a plus-like apparatus elevated 72.4 cm above the floor (ENV560; Med Associates Inc, Vermont, USA), containing two open (50.8 cm x 10.2 cm) and two closed arms (50.8 cm x 10.2 cm x 40.6 cm). Mice were allowed to freely explore the maze for 5 min. Time spent in each arm and the number of entries were recorded and analysed using Ethovision XT 13 software (Noldus, Netherlands).

Light/Dark box

The Light/Dark (LD) box test is also a conventional test to assess anxiety in mice. This test is based on the innate aversion of rodents to brighter areas and on its propensity to explore an arena in response to mild stressors as novel environment and light (Bourin and Hascoet 2003). The LDbox apparatus consists of an arena equally divided into light and dark compartments, connected by an opening (Med Associates Inc, Vermont, USA). WT and IP_3R2 KO mice were placed in the middle of the illuminated compartment, facing towards the dark compartment. Mice were let to freely explore the maze during 10 min. Data was extracted using the activity monitor software (Med Associates Inc, Vermont, USA) and the dark/light ratio was used as an index of anxiety-like behavior.

Open Field

The Open Field (OF) test is a behavioral paradigm that allows the evaluation of anxious-like behavior, motor and exploratory activity (Seibenhener and Wooten 2015). In this test, mice are placed in a brightly illuminated open field arena (43.2 x 43.2 x 30.5 cm) that is equipped with a system of two 16-beam infrared arrays connected to a computer. Mice are allowed to freely explore the arena during 5 min. Data was extracted using the activity monitor software (Med Associates Inc, Vermont, USA).

Acoustic Startle

The Acoustic Startle test evaluates the startle response, which consists in a rapid and involuntary movement to a loud, unexpected sound (Koch 1999). This paradigm is a measure of an anxious-like state. This test was performed in a startle response box (SR-LAB, San Diego Instruments, San Diego, CA, USA), which was a ventilated and sound-attenuated chamber, containing a small animal cylinder enclosure inside. Each cylinder was provided with a piezoelectric element that allowed the detection and

measurement of the movements of mice. Mice were presented with randomized startle sounds varying from 70 to 120 dB, each lasting 50 ms. For analysis, a sampling of the startle magnitude every millisecond over a period of 200 ms was performed. The startle response was defined as the peak response obtained during the 200 ms recording. A higher startle amplitude is related with a more anxious-like state of the animal.

Depressive-like behavior

Forced Swim Test

The Forced Swim Test (FST) is used to assess depressive-like behavior in rodents (Castagne et al. 2011). Briefly, mice were individually placed in transparent glass cylinders (diameter approximately 20 cm), filled with water at 24°C during 6 min. Each trial was recorded using a video camera and analyzed using the Ethovision XT 12 software (Noldus, Netherlands). This test is a learned helplessness paradigm based on the ability of mice to learn that there is no escape from that stressful situation. Therefore, latency to immobility and immobility time were analyzed during the last 4 min of testing.

Tail Suspension Test

The Tail Suspension Test (TST) evaluates depressive-like behavior in mice (Steru et al. 1985). This test is based on the principle that mice tend to stay immobile when they cannot escape from a stressful situation. In the TST, mice are suspended by the tail, using adhesive tape, on the edge of a shelf (approximately 80 cm above the floor) during 6 min. Each trial was recorded using a video camera and analyzed using the Ethovision XT 12 software (Noldus, Netherlands). Latency to the first immobility period and total immobility time was analysed during the last 4 min of testing, as a measure of learned helplessness.

Cognitive behavior

Morris Water Maze - Reference memory task

Morris Water Maze (MWM) was used to evaluate spatial reference memory and performed as previously described by Sardinha et al. (2017). This test was conducted in a dark circular pool with 106 cm diameter filled with water at 23 ± 1°C, under dim light conditions. The room was provided with extrinsic cues (cross, square, triangle, horizontal stripes) to allow spatial navigation. The water was made opaque using nontoxic titanium dioxide (Sigma-Aldrich, 250 mg/L) to improve mice detection. A hidden platform was maintained in the same position (horizontal stripes quadrant) during the four days of testing. Every day mice were allowed to find the hidden platform, based on their spatial navigation abilities, during four consecutive trials (with a maximum duration of 60 s and an inter-trial interval of 30 s). If mice failed to reach the platform, they were guided there and left to explore the surrounding for 30 s. On the last day of testing, a probe trial was conducted by allowing animals to freely swim in the pool without any platform. If they correctly remember the place where the platform was hidden during the four days of testing, they will spend more time in that quadrant. Escape latencies and distances swam were obtained using a video-tracking system (Viewpoint, France). Additionally, tracking patterns were extracted and the strategies used to reach the hidden platform during the reference memory task were analyzed. This evaluation was performed by two experimenters, blind to the animal's genotype, according to the strategies categorization described by Graziano et al. (2003).

Contextual Fear Conditioning

Contextual Fear Conditioning (CFC) test was performed in white sound-attenuated chambers (20 cm x 16 cm x 20.5 cm) (SR-LAB, San Diego Instruments, San Diego, CA, USA) containing a light bulb on the ceiling to illuminate the entire box. The chamber where animals received a footshock (Context A) was equipped with an acrylic cylinder containing a stainless steel shock grid at the bottom. Mouse freezing behavior was recorded using a video camera and analyzed using a behavioral scoring program (Observador v0.2.7). CFC was conducted for three consecutive days and was performed according to the following paradigm:

Day 1 - Training session

Mice were placed in a white chamber containing an acrylic cylinder with a shock grid on the floor. They received three consecutive light-shock pairings of 3 min. More specifically, 20 s before the application of a foot shock a light was turned on, and this period co-terminated with a shock of 0.5 mA. During this day, the testing room was only illuminated with a red light. This session lasted 9 min and 30 s. For the analysis

of baseline and post-shock freezing response, the first minute and the last 30 s were analyzed, respectively.

Day 2 - Context phase

Context A: On day 2 (24 h later), mice were re-exposed to the familiar (white) chamber where they had been conditioned and their freezing behavior was evaluated for 3 min. A freezing response was considered when we observed complete immobility of the animal for a minimum of 1 s.

Context B: 2 h later, mice were placed in a novel context (black chamber). In this new context, room conditions changed (room light was turned on, black plastic cardboards covered the whole box, shock grid was removed from the acrylic cylinder and the chamber was scented with a vanilla extract). This session lasted 3 min and freezing behavior was scored during all session time.

Day 3 - Cue probe

On day 3, mice were re-exposed to context B conditions. After 3 min, the light bulb on the ceiling was turned on and their freezing behavior was scored during 1 min.

Morphological analysis

Three dimensional (3D) morphological analysis of neurons and astrocytes was performed on Golgi-Cox stained neurons and GFAP-stained astrocytes, at the CA1 region of the hippocampus. This mouse brain subregion was identified according to the mouse brain atlas (Paxinos and Franklin 2004). Mice were anesthetized with a mixture of ketamine (75 mg/kg, intraperitonealy (i.p.); Imalgene 1000, Merial, United States) and medetomidine (1 mg/kg, i.p.; Dorbene Vet, Pfizer, United States) and were transcardially perfused with 0.9% saline. Tissue processing was performed as described in the following sections.

Golgi-Cox staining and 3D-reconstruction of CA1 hippocampal neurons

All procedures applied to 3D-dendritic morphology were performed as previously described by Guerra-Gomes et al. (2018) and Sardinha et al. (2017). Brains were impregnated in a Golgi-Cox solution (1:1 solution of 5% potassium dichromate and 5% mercuric chloride diluted 4:10 with 5% potassium chromate) for 14 days, following three washes with PBS 1x, they were transferred to a 30% sucrose solution until vibratome sectioning. Coronal sections (200 µm thick) were transferred to a 6% sucrose solution and blotted dry onto gelatin-coated microscope slides. Next, sections were alkalinized in 18.7% ammonia, developed in Dektol (Kodak, USA), fixed in Kodak Rapid Fix, dehydrated and xylene cleared in a dark room. After this histochemical procedure, brain sections were mounted and coverslipped. CA1 hippocampal neurons from WT (n=4 mice; 22 neurons) and IP_3R2 KO mice (n=6 mice; 27 neurons) were

analyzed if they fulfilled the following criteria: 1) presence of a defined soma within the CA1 pyramidal layer; 2) complete impregnation along the entire length of the dendritic arborization; 3) no morphological alterations due to deficient impregnation or truncated branches. For each selected neuron, apical dendritic branches were reconstructed using a motorized microscope controlled by the Neurolucida software (MBF Bioscience, USA) under 100x magnification. This analysis allowed the acquisition of several parameters such as total length, number of endings, nodes, Sholl analysis, and spine number and classification. Dendritic segments of 30 µm, in the proximal and distal portions of the apical dendrite were randomly selected to assess the percentage of each spine category (from more immature to mature: thin, mushroom, thick and ramified) in both WT and IP_3R2 KO mice. Data extraction was performed using the NeuroExplorer software (MBF Bioscience, USA).

Tissue preparation and 3D-reconstruction of astrocytes

The astrocytic main structure was analyzed by performing 3D-reconstructions of GFAP-stained cells using the Simple Neurite Tracer plugin, from the Fiji software (http://fiji.sc/Fiji), as previously described by Tavares et al. (2017). Brains were immersed in 4% paraformaldehyde solution [PFA, 0.1M, pH 7.4, in phosphate saline buffer (PBS)] overnight and then transferred to a 30% sucrose/PBS solution at 4°C. Brains were frozen by immersion in isopentane (BDH Prolabo; cooled in liquid nitrogen) in Neg-50 frozen section medium (Thermo Scientific, USA) and stored at -20°C until cryostat sectioning. Hippocampal sections (20 µm thick) containing the dHIP of WT and IP_3R2 KO mice were incubated with the primary antibody rabbit anti-GFAP (1:200; Dako, Denmark) at 4°C overnight. In the next day, sections were rinsed in PBS and incubated with the respective secondary antibody Alexa Fluor 594 goat anti-rabbit (1:1000; Molecular Probes, Invitrogen, USA). After several washes with PBS, brain sections were incubated with DAPI (1:1000; Invitrogen, USA), for cell nuclei labeling, for 10 min. Coverslips were mounted using Immu-Mount™ (Thermo Scientific, USA) and analyzed in the confocal microscope (FV1000, Olympus, Japan). Each Z-stack image (1 µm z-step interval) was obtained with a resolution of 640 x 640 px under a 60x oil magnification, with a field size of 211.51 x 211.51 µm. The following criteria were taken into account to select astrocytes for reconstruction: i) GFAP-stained structure is located in the region of interest (hippocampal CA1 *stratum radiatum*) and ii) present a clearly identifiable DAPI-stained nucleus with a iii) complete labeled GFAP-structure, without truncated processes. From this analysis we gathered relevant structural features as total process length, number of processes, process thickness, and Sholl analysis.

Assessment of astrocyte density

We determined the number of $GFAP^+$ cells in hippocampal CA1 *stratum radiatum* and *stratum pyramidale* layers brain sections from WT and IP_3R2 KO mice. For that, we performed immunofluorescence staining for GFAP, as previously described. Images were acquired with the Olympus Fluoview FV1000 confocal microscope (Olympus, Hamburg, Germany) using a 20x objective (resolution: 1024x1024 px; field size: 635.28 x 635.28 µm). The number of $GFAP^+$ cells was assessed using the Fiji plugin "Cell counter".

Molecular analysis

To identify molecular signaling pathways and transcription factors altered in our mouse model of global astrocytic Ca^{2+} dysfunction, western blot and microarray analysis were performed in the total hippocampus of IP_3R2 KO mice and WT littermates.

Western blot

Western blot analysis was performed in brain samples from WT and IP_3R2 KO mice. Total hippocampus was lysed using a cold HEPES-buffered sucrose (0.32M sucrose, 4mM HEPES pH 7.4) buffer with 25x protease inhibitors, 1% Nonidet-P40 and 0.5% sodium dodecyl sulfate (SDS). Lysed samples were sonicated and centrifuged at 10.000 rpm during 25 min at 4°C. The collected supernatant was quantified for the total amount of protein using the Bradford protein assay (Bio-Rad, USA). Total lysates were denatured in 2x Laemmli Buffer (Bio-Rad, USA) by heating the samples at 98°C for 5 min. Next, 50 µg of protein were loaded onto an SDS-PAGE gel (10%) and transferred to a nitrocellulose membrane (Trans-blot Turbo Kit, Bio-Rad, USA). Membrane was blocked for 1 h in a 5% non-fat milk/TBS solution, to prevent non-specific background binding of the primary and/or secondary antibodies. Next, the membrane was incubated with the primary antibody rabbit anti-GFAP (1:50.000; Dako, Denmark) overnight. The next day, the membrane was washed with TBS-T, and incubated, at room temperature with agitation during 2 h, with the respective secondary antibody anti-rabbit HRP (1:15.000; BioRad USA). After this period, the membrane was washed again three times in TBS-T, followed by the detection of the chemiluminescent signal using the Clarity Western ECL substrate kit (Bio-Rad, USA) using a gel blotting imaging system (Chemidoc, Bio-Rad, USA). Protein expression quantification was performed using the Image Lab software (Bio-Rad, USA.) All the samples were normalized for a loading control protein (mouse anti-α-tubulin; 1:500, DSHB, USA).

Transcriptome analysis

Microarray analysis was performed in total RNA extracted from the whole hippocampus of WT and IP_3R2 KO mice (n=3 biological replicates/group) that did not perform any behavioral test. A single experienced researcher performed hippocampus macrodissection, in order to avoid variability. After dissection, tissues were immediately frozen in dry ice and stored at -80°C until RNA extraction.

RNA isolation

Total RNA was extracted using QIAzol (Qiagen, Germantown, MD, USA) in combination with the miRNeasy Mini kit (Qiagen, Germantown, MD, USA). The Agilent 2100 Bioanalyzer was used to assess RNA quality and only high quality RNA (RIN > 7) was used for microarray analysis.

Expression profiling

Total RNA (40 ng) was amplified using the Ovation Pico WTA System V2 in combination with the Encore Biotin Module (NuGEN Technologies, Inc, San Carlos, CA, USA). Amplified cDNA was hybridized on a mouse Gene 2.0 ST arrays (Affymetrix, Santa Clara, CA, USA). Staining and scanning (Scanner 3000 7G) was done according to the Affymetrix expression protocol including minor modifications as suggested in the Encore Biotion protocol (NuGEN Technologies, Inc).

cDNA synthesis and real-time quantitative PCR analysis

Total RNA (500 ng) was converted from the samples used for microarray analysis (total hippocampus) using qScript cDNA SuperMix (Quanta Biosciences, Gaithersburg, MD, USA). The primers for the selected genes of interest for microarrays confirmation were designed using PRIMER-BLAST (NCBI, http://www.ncbi.nlm.nih.gov/tools/primer-blast/) (Table 3.1).

Table 3.1 - Forward and reverse sequences of oligonucleotide primers of the selected genes used for microarrays data validation.

Gene	Forward Sequence (5'→3')	Reverse Sequence (5'→3')
F5	CCT GGC AAG CCA AGG CAA ACA	GCC ACA CCC TGG TCA CTG TAC T
Sulf1	TGA GTG CTT GAG GAC GTG TTT C	TGG CCC TCA GCA CCT GAA AAT AC
Clic6	CCT GGG ACG AAC CCT CCT TTC A	AGG GTA CCT CGG GGG AAC TAA CT
Vat1l	GGC CCT GGA GGA GGT AAA AGA	TCT TCC CAG CCA TCC TCC ACT TT
Vamp8	GGA AGC CAC GTC TGA ACA CTT CAA	AGA GGG CTC CTC TTG GCA CAT A
Kl	ACT ACG TTC AAG TGG ACA CTA CTC	GGC CGG ATG GCA GAG AAA TCA
Gper1	AAC GCC ACG GCA CAG ATC A	TGG TGG GTG CAT GGC AGA AAT G
Grik1	ACA TTG AGC AGT GTC TCT CTT TCA	GGG TCA CGC CAC AGT CTC TT
Plcb3	GCC GGG CCA GAT CCA GTA AA	GCG AAT GGA CTC ACT TCG GTT GAA
S100a4	TCT TGG TCT GGT CTC AAC GGT TA	TAG GCA GCT CCC TGG TCA GTA
Cib2	GAC AAC TAC CAG GAC TGC ACT TT	CCT CGG AGA AAG CCT CCA CAA TC
Smad3	GAG GAG AAG TGG TGC GAG AAG	CAG TGA CCT GGG GAT GGT AAT G

Quantifications were performed in a Fast Real-Time PCR System (Applied Biosystems, USA) using the 5x HOT FIREPol® EvaGreen® qPCR Mix Plus, ROX (Solis Biodyne, Estonia). The housekeeping gene 18S rRNA was used as an internal control and the relative expression was calculated using the ΔΔCt method.

Bioinformatic analysis

Functional annotation analysis

We analyzed enriched molecular functions associated with IP_3R2 KO mice differentially expressed targets using PANTHER Classification System (http://www.pantherdb.org/). After importing our list of genes to the PANTHER tool, we selected a functional classification view in pie charts, and selected ontology "Molecular function".

Prediction of transcription regulators

To identify possible regulons from our list of differentially expressed genes, the Cytoscape plugin (https://cytoscape.org/) – iRegulon – was used (Janky et al. 2014). This plugin detects transcription factors (TFs) and its direct regulated targets based on motif discovery from a list of genes. Briefly, we imported the network file containing our gene list into Cytoscape. After selecting all nodes and edges, we

performed an iRegulon analysis using the following ranking options: species and gene nomenclature (Mus musculus, MGI symbols), motif collection [10K (9713 PWMs)], no track collection, putative regulatory region (20kb centered around TSS), motif rankings database [20 kb centered around TSS (7 species)], track rankings database [20 kb centered around TSS (ChIP-seq-derived)]. Regarding recovery, the following parameters were applied: enrichment score threshold ≥ 3.0 and maximum false discovery rate (FDR) on motif similarity = 0.001.

Prediction of functional interactions

Target genes regulated by the most enriched TF from our iRegulon analysis – *Foxo1* – were uploaded at the STRING tool (https://string-db.org/, version 11.0). These genes encode proteins that are involved in several cellular functions. STRING analysis retrieved possible functional associations between our targets. The minimum required interaction score established was 0.4 (medium confidence). We combined these results with a published transcriptome database (https://web.stanford.edu/group/barres_lab/brain_rnaseq.html; http://www.brainrnaseq.org/) (Zhang et al. 2014), in order to identify *Foxo1* targets in IP_3R2 KO mice that have functional similarity and that are astrocyte-enriched genes.

Viral approach to overexpress FOXO1 in hippocampal astrocytes

Stereotaxic virus injection

AAV5-GFAP(0.7)-mCherry-2A-m-FOXO1 was obtained from Vector Biolabs (USA) and its titer corresponds to 3.9 x 10^{12} genome copies (GC)/mL. The GFAP (gfaABC1D) promoter drives the expression of both FOXO1 and mCherry, which have a 2A linker in between for protein co-expression.

Male C57BL/6J mice, 8-12 weeks old were anesthetized with a mixture of ketamine (75 mg/kg, i.p.; Imalgene 1000, Merial, United States) and medetomidine (1 mg/kg, i.p.; Dorbene Vet, Pfizer, United States), injected locally in the head with lidocaine (30 µL/0.5% lidocaine) before incision and submitted to a stereotaxic surgery for the bilateral injection of either saline (Sham group, n=8) or an adeno-associated virus 5 (AAV5) under the control of a GFAP promotor to specifically overexpress FOXO1 in astrocytes (n=13). AAV5-GFAP(0.7)-mCherry-2A-m-FOXO1 (1 µL; 3.9 x 10^{12} GC/mL) was bilaterally injected into the dHIP (coordinates from bregma, according to Paxinos and Franklin (2004): 1.8 mm anteroposterior, 1.3 mm mediolateral, and 1.3 mm dorsoventral). The injection volume and flow rate were established at 100 nL/min. At the end of the procedure, the needle was pulled up 0.1 mm and it was left in place during approximately 5 min to allow proper viral vector diffusion. After this, mice were

removed from the stereotaxic apparatus and sutured. To revert the effect of anesthesia, 1 mg/kg of atipamezole was administered. After surgery, mice received subcutaneous injections of an anti-inflammatory (Carprofeno, 5 mg/kg), an opioid for analgesia (Bupac®, 0.05 mg/kg) and vitamins (Duphalyte/Pfizer, USA). Animals were allowed to recover during 4 weeks prior to behavioral testing.

Immunofluorescence for the confirmation of virus expression

Two and 12 weeks post injection, AAV5-GFAP(0.7)-mCherry-2A-m-FOXO1 mice (2 weeks, n=1; 12 weeks, n=2) were anesthetized with a mixture of ketamine and medetomidine and transcardially perfused with 0.9% saline, followed by perfusion with 4% PFA in PBS. Brain was removed and kept in 4% PFA overnight at 4°C. In the next day, it was washed in PBS 1x and cryoprotected in 30% sucrose/PBS 1x solution. Free-floating sections (50 µm thick) were obtained using a vibrating-blade microtome Leica VT 1000 S. Sections were washed in PBS 1x and PBS-Tx 0.3% and incubated during 1 h with a blocking solution containing PBS 1x/10% FBS/0.25 M glycine. These steps were followed by the incubation with primary antibodies overnight at 4°C: chicken anti-mCherry (1:1000, HenBiotech, Portugal), rabbit anti-NeuN (1:100, Cell Signaling, USA), rabbit anti-FOXO1 (1:100, Cell Signaling, USA), mouse anti-GFAP (1:200, Sigma Aldrich, USA), and rabbit anti-S100β (1:200, DakoCytomation, USA). In the next day, sections were washed in PBS 1x and incubated during 2 h at room temperature with the secondary antibodies: Alexa Fluor 594 goat anti-chicken, Alexa Fluor 488 goat anti-rabbit, Alexa Fluor 647 donkey anti-mouse (1:1000, Thermo Fisher Scientific). Finally, sections were washed again in PBS 1x, incubated during 10 min with DAPI (1:1000), rinsed in PBS 1x twice and were mounted in Immu-Mount™ (Thermo Scientific, USA). Images were acquired in an Olympus Fluoview FV100 confocal microscope (Olympus, Germany) using the 20x objective and 100x oil immersion objective.

Statistical analysis

Statistical significance was considered for $p < 0.05$. All data assumed a Gaussian distribution as revealed by the central limit theorem for samples $n > 30$ (MWM data) or by the Kolmogorov-Smirnov normality test. Two-tailed Student's t-test was applied for comparisons between WT and IP_3R2 KO or Sham and GFAP-mCherry-FOXO1 mice, whereas a Two-way analysis of variance (Two-way ANOVA), followed by Sidak *post hoc* analysis was used for multiple comparisons. For the analysis of different behavioral categories of strategies in the MWM, the two-sided Chi-square test was carried out. All statistical analyses were carried out using SPSS 22.0 or GraphPad Prism 7.04.

For transcriptome analysis, Pearson coefficients were calculated to assess the correlation between microarray and RT-PCR data. Expression console (v.1.4.1.46, Affymetrix) was used for quality control and to obtain annotated normalized SST-RMA gene-level data (standard settings including median polish and sketch-quantile normalization). Statistical analyses were performed with the statistical programming environment R [R Development Core Team (2005)]. Genewise testing for differential expression was done employing the limma t-test and Benjamini-Hochberg multiple testing correction (FDR < 10%). Heatmaps were generated with Genesis (Sturn et al. 2002) and cluster dendrograms with the R script hclust.

Results

A previous neurodevelopmental evaluation of IP_3R2 KO mice showed that male and female IP_3R2 KO mice display normal development. Therefore, the IP_3R2 KO mouse model is reliable to study the functional impact of global IP_3R2-dependent astrocytic Ca^{2+} elevations in adulthood (Chapter 2).

We performed a full behavioral characterization in adult WT and IP_3R2 KO mice by assessing several behavioral dimensions: anxiety, mood, and cognition (Figure S 3.1A-F). Anxious-like behavior was assessed by the Elevated-Plus Maze (EPM), Open Field (OF) and Light-Dark box (LD box). Impulsivity was evaluated by the Acoustic Startle Test. Depressive-like behavior was assessed by the Forced Swim Test (FST) and Tail Suspension Test (TST). Our results show that IP_3R2 KO mice do not present an anxious- or depressive-like phenotype that could bias cognitive performance. Thus, we evaluated the impact of IP_3R2-dependent Ca^{2+} signaling in hippocampal-dependent cognitive tasks.

IP_3R2 KO mice display an enhanced performance in hippocampal-dependent cognitive tasks

We employed the IP_3R2 KO mouse model of global astrocytic Ca^{2+} signaling dysfunction to study its implications for cognitive function, mainly in hippocampal-dependent tasks. The MWM task was used to assess spatial reference memory. In this paradigm, mice had to learn the hidden platform location, which was kept always in the same position, based on their spatial navigation abilities. Results show that both WT and IP_3R2 KO mice learned to find the platform and improved their performance during the four days of testing similarly (Figure 3.1A; escape latency: day, $F_{3,207} = 128.70$; $p < 0.0001$; distance swam: day, $F_{3,207} = 74.58$; $p < 0.0001$), but IP_3R2 KO mice performed better in day 3 ($t_{276} = 3.00$; $p < 0.05$). Moreover, in the probe trial, both genotypes displayed a similar preference for the quadrant where the platform was hidden (Figure 3.1B). Interestingly, the analysis of the strategies used to reach the platform during the acquisition phase revealed that IP_3R2 KO mice employed more hippocampal-dependent strategies as compared with WT mice, indicating an enhanced spatial orientation (Figure 3.1C). In fact, WT and IP_3R2

KO mice display similar percentages of failure to reach the platform, but IP_3R2 KO mice use less random and more directed strategies when compared to control mice (Figure 3.1C; χ^2 (1) = 9.59; $p < 0.01$).

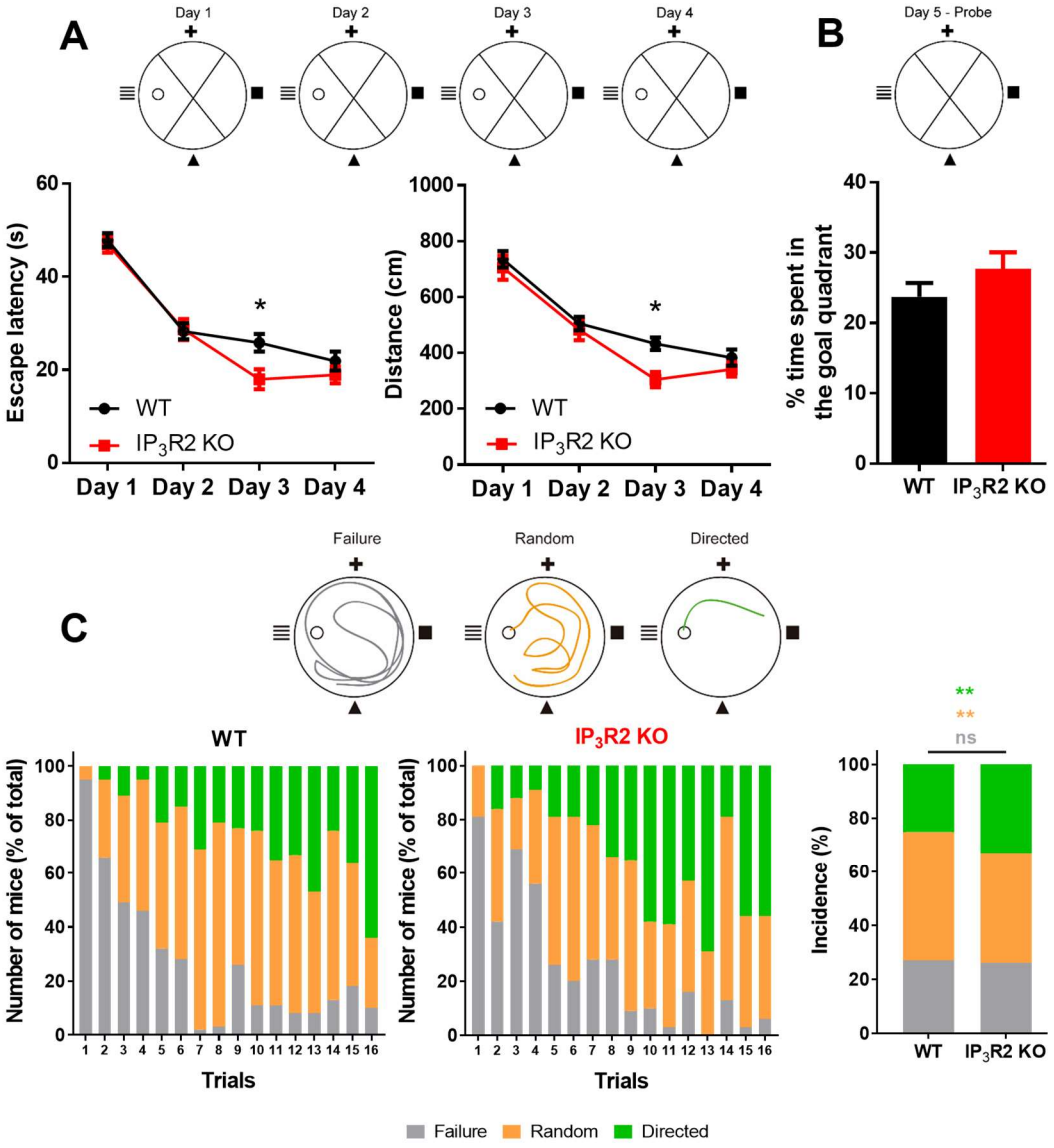

Figure 3.1 – IP_3R2-dependent Ca^{2+} signaling modulates spatial reference memory in the MWM.

(A-C) Spatial reference memory task (RM) of the Morris Water Maze (n=32-39 per group). (A) RM task scheme (top) with the respective learning curves (bottom) depicting escape latencies and distance swam to reach the platform during the 4 days of testing, for WT and IP_3R2 KO mice. (B) Probe trial (top, right) showing the percentage of time spent in the goal quadrant for both genotypes. (A, B) WT mice are represented in black and IP_3R2 KO mice in red bars. Data plotted as mean ± SEM. (C) Representative scheme of the swimming strategies (top) used to reach the platform. Swimming tracks were classified as failure (gray), random scanning (orange) or directed to the platform (green). Search strategy used by WT and IP_3R2 KO mice (bottom, left) over the 16 trials of RM. Graphical representation showing the proportion of failures and strategies used to reach the platform (bottom, right) for WT and IP_3R2 KO mice. ** orange, refers to difference in random strategies used between WT and IP_3R2 KO mice, ** green, refers to difference in directed strategies used between WT and IP_3R2 KO mice. * $p < 0.05$ ** $p < 0.01$.

To explore further the role of global astrocytic Ca^{2+} signaling in a different form of hippocampal-dependent memory, we tested WT and IP_3R2 KO mice in the CFC task. In the training day, we found similar baseline activity and freezing responses, after the application of three footshocks associated with a light cue (Figure 3.2A). These results discarded any genotype-related alterations in baseline activity and similar conditioning for WT and IP_3R2 KO mice. Moreover, we observed that the light-shock pairings triggered a conditioned fear response in both genotypes (session, $F_{1,35} = 433.2$; $p < 0.0001$). In the next day, re-exposure to the same context revealed a significant increase in freezing response by IP_3R2 KO mice, as compared with WT littermates (Figure 3.2B; $t_{35} = 2.22$; $p = 0.03$). In the cue probe phase (day 3), no differences between genotypes were observed after light stimulus presentation (Figure 3.2C).

Overall, these results support an impact of IP_3R2-dependent Ca^{2+} signaling in cognitive functions, specifically enhancing the performance in hippocampal-dependent tasks. These results prompted us to look for histological and molecular correlates to better understand the underpinnings of this cognitive enhancement.

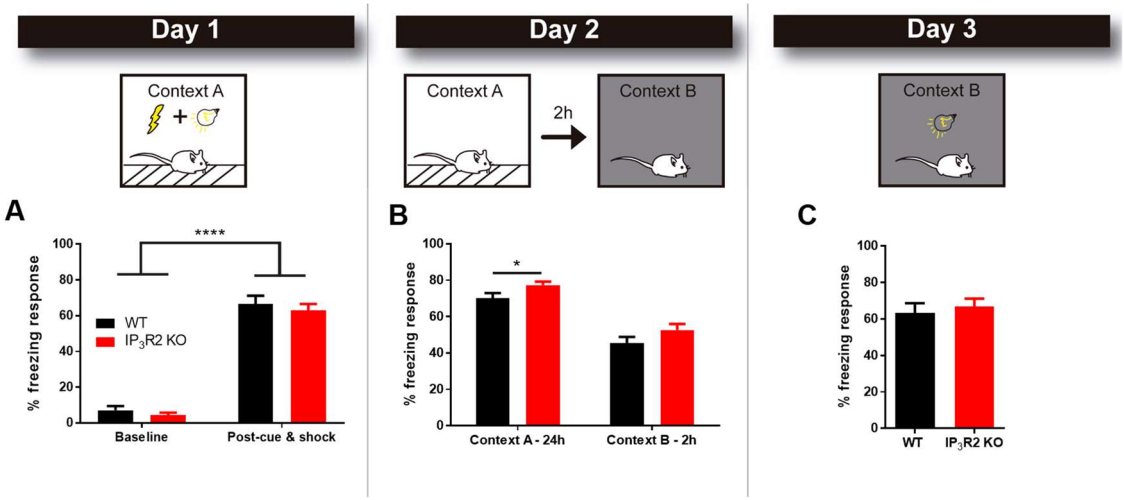

Figure 3.2 – IP_3R2 KO mice display an increased context-dependent fear memory.

(A-C) WT and IP_3R2 KO mice were tested in a contextual fear conditioning paradigm (n=16-21 per group). (A) Training session depicting baseline activity (left) and freezing acquired after light-shock exposure (right) at context A. (B) Re-exposure to context A (left) enhanced freezing response in IP_3R2 KO mice, compared to WT animals, but revealed similar responses after switching to a new context (context B, right). (C) Presentation of a light stimulus in context B led to similar freezing responses between genotypes. WT mice are represented in black and IP_3R2 KO mice in red bars. Data are presented as mean ± SEM. * $p < 0.05$, **** $p < 0.0001$.

IP_3R2 KO mice display intact dendritic morphology, but an increased percentage of immature spines in dorsal CA1 pyramidal neurons

To correlate the behavioral outcomes observed in IP_3R2 KO mice with morphological alterations, we performed a 3D-reconstruction of dorsal CA1 hippocampal pyramidal neurons (Figure 3.3A). These neurons are responsible for the integration of spatial, contextual and emotional information, and are actively involved in the processing of cognitive function (Graves et al. 2012). Our results showed that WT CA1 neurons are morphologicaly similar to IP_3R2 KO neurons for the parameters assessed (Figure 3.3B). Specifically, no differences were found in total dendritic length, number of endings and nodes. Moreover, Sholl analysis revealed unaltered dendritic arbor complexity of IP_3R2 KO neurons as compared with WT neurons (Figure 3.3C). Since dendritic spine structure is crucial for long-term memory, we further analyzed the relative distribution of different spine subtypes to understand their dependence on astrocytic Ca^{2+} signaling (Kasai et al. 2010). For that, we performed a spine categorization (thin, mushroom, thick

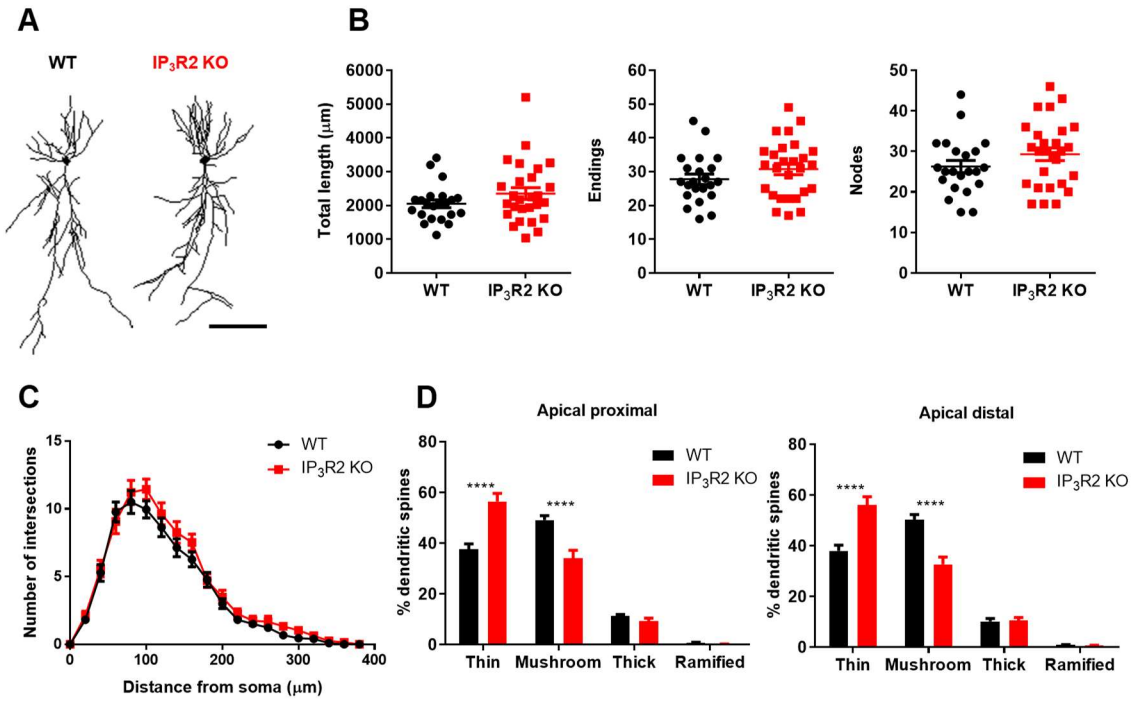

Figure 3.3 – CA1 pyramidal neurons in the dHIP of IP_3R2 KO mice are morphologically similar to those of WT, but display more immature spines.

(A) Representative 3D reconstructions of dHIP CA1 pyramidal neurons from WT and IP_3R2 KO mice (scale bar = 100 µm). (B) Morphological parameters of apical dendrites, namely total length, number of endings and nodes (from left to right) (n=22-27 neurons per group). (C) Sholl analysis for intersections of apical dendrites. (D) Percentage of each spine type at apical proximal and distal dendrites (n=17-19 neurons per group). WT mice are represented in black dots and lines/bars and IP_3R2 KO mice in red dots and lines/bars. Data plotted as mean ± SEM. **** $p < 0.0001$.

and ramified) in apical proximal and distal segments of WT and IP_3R2 KO neurons (Figure 3.3D). Interestingly, CA1 pyramidal neurons of IP_3R2 mice display an increased percentage of thin spines (apical proximal: t_{136} = 6.69; $p < 0.0001$; apical distal: t_{136} = 6.36; $p < 0.0001$) which is accompanied by a decrease in mushroom spines (apical proximal: t_{136} = 5.40; $p < 0.0001$; apical distal: t_{136} = 6.15; $p < 0.0001$), when compared to WT neurons. In summary, although IP_3R2 KO mice count on dorsal CA1 pyramidal neurons with normal morphology, they present a shift to more immature spine types.

Astrocytes of IP_3R2 KO mice exhibit decreased structural complexity and increased density in the dorsal CA1 subregion

Astrocytes exhibit a complex morphology, which is essential for synaptic coverage and modulation. By extending their processes, they stand in close apposition to functional synapses and blood vessels. We observed above that, in the dorsal CA1 hippocampal subregion, IP_3R2 KO neurons are morphologically similar to WT neurons. Thus, we aimed to screen astrocytic structure in the same brain area. For that, we performed a 3D-reconstruction of GFAP-stained structures in the *stratum radiatum* layer of CA1. Results show that IP_3R2 KO astrocytes from this CA1 subregion are less complex as compared with WT astrocytes (Figure 3.4A). This decreased structural complexity was observed for the several parameters analyzed: total length (t_{70}=4.035, $p = 0.001$), number of processes (t_{70} = 2.834, $p = 0.006$) and process thickness (t_{70} = 4.742, $p < 0.0001$). Moreover, Sholl analysis revealed a significant effect of radius, genotype and an interaction between both factors (radius: $F_{16,1120}$ = 300.000, $p < 0.0001$; genotype: $F_{1,70}$ = 11.160, $p = 0.0013$; interaction: $F_{16,1120}$ = 8.082, $p < 0.0001$). Post hoc analysis (Sidak's *post hoc* test, $p < 0.05$) showed a decreased number of intersections between 16-32 μm from the soma in IP_3R2 KO astrocytes, as compared with WT littermates. These results prompted us to evaluate the density of astrocytic ($GFAP^+$) cells in dorsal CA1, namely in the *stratum radiatum* and *stratum pyramidale* layers (Figure 3.4B). Interestingly, we found an increased number of $GFAP^+$-cells in the *stratum radiatum* layer in IP_3R2 KO mice (t_{14} = 2.675, $p = 0.018$), when compared with WT littermates. This increase appears to be specific of the *stratum radiatum* layer since no differences between genotypes were observed for astrocyte densities in the *stratum pyramidale* layer. To verify if these morphological and cellular density changes are accompanied by alterations in GFAP protein expression in the whole hippocampus, relative levels were quantified by Western blot (Figure 3.4C). We observed similar levels of GFAP protein expression in the hippocampus of WT and IP_3R2 KO mice. Altogether, these evidences show that astrocytes from IP_3R2 KO are less complex, but are present in a higher number in CA1 *stratum radiatum*.

These changes are not translated in differential GFAP protein levels in the total hippocampus of IP_3R2 KO mice, as compared with WT controls.

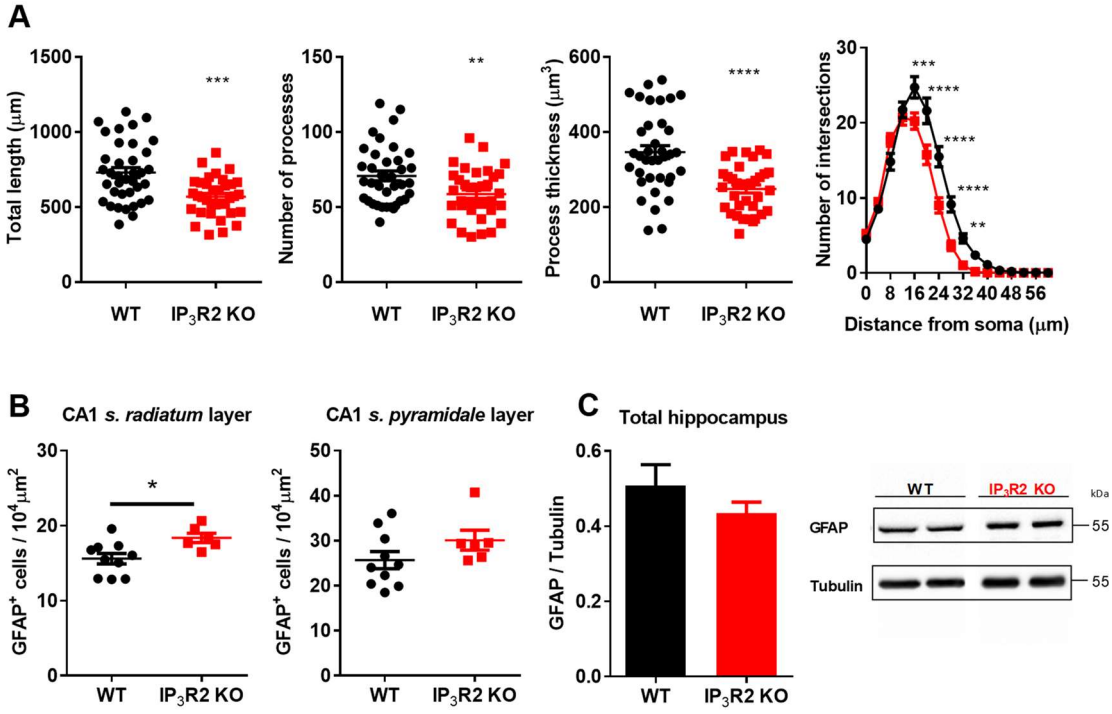

Figure 3.4 – Astrocytes of the dHIP CA1 of IP_3R2 KO mice display a reduced structure.

(A) Morphological parameters to assess the 3D structure of dHIP CA1 astrocytes from WT and IP_3R2 KO mice included: total length, number of processes, process thickness and number of intersections by Sholl analysis (n=35-37 astrocytes per group). (B) Densities of $GFAP^+$ cells in dHIP CA1 *stratum radiatum* and *stratum pyramidale* layers (n=6-10 images per group). (C) WT and IP_3R2 KO mice display similar levels of GFAP expression in the total hippocampus (n=3-5 mice per group). WT mice are represented in black dots and lines/bars and IP_3R2 KO mice in red dots and lines/bars. Data plotted as mean ± SEM. * $p < 0.05$, ** $p < 0.01$, *** $p < 0.001$, **** $p < 0.0001$.

Microarray analysis of hippocampal transcriptome indicates *Foxo1* as an important astrocytic regulator of gene expression

To disclose relevant molecular signaling pathways that could underlie our behavioral and morphological effects, we performed a thorough evaluation that included microarray analysis followed by a bioinformatic approach and a cell-type enrichment analysis (Figure 3.5A). We started by extracting RNA from the total hippocampus of WT and IP_3R2 KO mice. After RNA quality validation, a microarray analysis was performed (Affymetrix, Santa Clara, CA, USA). We obtained 677 differentially expressed genes, among which 349 genes were significantly up-regulated (51.6%) and 328 genes were down-regulated (48.4%) in the hippocampus of IP_3R2 KO mice as compared with WT littermates (Figure 3.5B; Statistical analysis: *Itpr2*

vs Ctrl, limma t-test; fold change (FC) > 1.3x, $p < 0.05$, average expression (Av) > 10, n=3 per group). We started by validating the microarray data, by performing real-time quantitative PCR (RT-qPCR) of selected candidate genes. These genes were chosen according to its functional relevance for cognition and/or astrocytic function or its fold change levels. This RT-qPCR analysis confirmed the differential expression obtained in microarray data, for all up- and down-regulated selected genes (Figure 3.5C). Specifically, a direct correlation between RT-qPCR and microarray fold changes was found (Figure 3.5D, Pearson correlation coefficient r = 0.9768, $R^2 = 0.9541$, $p < 0.0001$). Moreover, PANTHER Classification System for functional annotation analysis revealed that our differentially expressed genes are mainly associated with molecular functions related to binding and catalytic activity (Figure 3.5E).

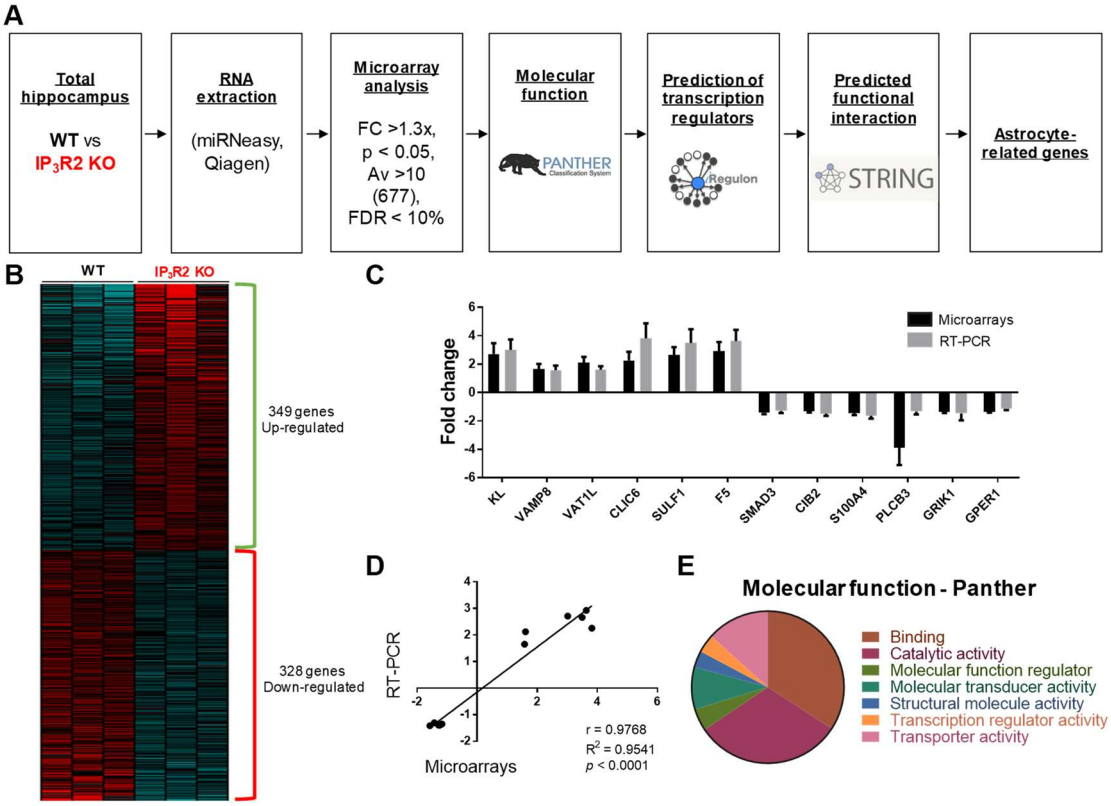

Figure 3.5 – Identification of relevant molecular signaling pathways/targets related with IP_3R2-dependent Ca^{2+} signaling modulation in astrocytes.

(A) Schematic analysis pipeline of relevant molecular targets and/or pathways present in IP_3R2 KO mice involved: RNA extraction from total hippocampus of both genotypes, microarray analysis, functional annotation analysis (PANTHER), prediction of transcription regulators by iRegulon (Cytoscape plugin), prediction of functional interactions among targets (STRING analysis) and search for astrocyte-enriched genes according to a published database by Zhang et al. (2014). (B) Microarray analysis of total hippocampus of WT and IP_3R2 KO mice (n=3 per group) gathered 677 differentially expressed genes in IP_3R2 KO mice as compared with WT littermates: 349 genes (51.6%) were up-regulated, 328 genes (48.4%) were down-regulated. (C) RT-qPCR analysis for selected candidate

genes, to confirm FC levels observed in the microarrays data. Black bars correspond to the observed linear FC from Affymetrix microarrays data, grey bars correspond to the linear FC of mRNA levels calculated after normalization to 18S, for each experimental group. Data presented as mean ± SEM. (D) Pearson's correlation plot between FC from microarrays and RT-PCR for the candidate genes analyzed. Correlation coefficients and respective p-value are depicted. (E) Molecular function identification by PANTHER Classification System in 677 differentially expressed genes from IP_3R2 KO mice. Percentages represented at pie chart correspond to the percentage of gene hit against total number of function hits.

To identify master regulators from our list of 677 differentially expressed genes, we conducted an iRegulon analysis (Table 3.2). This computational method is based on the analysis of the regulatory sequences

Table 3.2 – iRegulon results regarding the most enriched transcription factors from our list of differentially expressed genes.

TF	Name	NES	# TARGETS	CELL TYPE ENRICHMENT (Zhang et al., 2014)
Foxo1	Forkhead box protein O1	**4.033**	**76**	**Astrocytes and endothelial cells**
Vsx1	Visual System Homeobox 1	3.871	77	Very low expression in the mouse brain
Sfpi1	Spi-1 Proto-Oncogene	3.573	19	Microglia/macrophages
Mafk	MAF BZIP Transcription Factor K	3.336	62	Microglia/macrophages and endothelial cells
Stat1	Signal Transducer And Activator Of Transcription 1	3.270	74	OPCs, microglia/macrophages and endothelial cells
Nkx2-1	NK2 homeobox 1	3.164	36	Neurons
Hmga1	High Mobility Group AT-Hook 1	3.160	45	Microglia/Macrophages
Xbp1	X-Box Binding Protein 1	3.089	23	Microglia/Macrophages and endothelial cells
Klf4	Kruppel Like Factor 4	3.043	10	**Astrocytes** and Microglia/Macrophages

associated with each gene to detect enriched TF motifs (Janky et al. 2014). We found nine TFs (*Foxo1*, *Vsx1*, *Sfpi1*, *Mafk*, *Stat1*, *Nkx2*-1, *Hmga1*, *Xbp1*, *Klf4*) significantly enriched in our list of differentially expressed up- and down-regulated genes. Of these, only two – *Foxo1* and *Klf4* – display an astrocyte-enriched expression, as compared to other cell types according to a published transcriptome database (Zhang et al. 2014). Moreover, *Foxo1* presented the highest enrichment score (Enrichment Score threshold (NES) = 4.033), controlling a high number of target genes (76 target genes). In the brain, FOXOs act as pivotal effectors of cell homeostasis, metabolism and response to stress, which ultimately may influence cognitive performance (Kim and Webb 2017).

To explore functional associations between *Foxo1* target genes in IP_3R2 KO mice, we performed a STRING analysis. We obtained an interaction diagram of the analyzed targets containing three functionally related clusters (Figure 3.6). We looked for the genes present in these clusters regarding their cell-type expression in the brain (Zhang et al. 2014) and recognized functions described in the literature. According to microarrays data, we found a cluster (in red) that contained 5 significantly up-regulated genes in IP_3R2 KO mice. Two of these genes, syndecan-2 (*Sdc2*) and ezrin (*Ezr*), are highly expressed in astrocytes, as confirmed by Zhang et al. (2014) transcriptome database (Table 3.3). Functionally, *Sdc2* and *Ezr* are related with spinogenesis and dendritic spine formation (Granes et al. 2000; Lin et al. 2007). Together with our spine distribution analysis, these results point to a role of astrocytic IP_3R2-dependent signaling controlling the expression of genes related with plastic changes occurring in CA1 neuronal dendritic spines, which corresponds to the major neuron-astrocyte interacting domain.

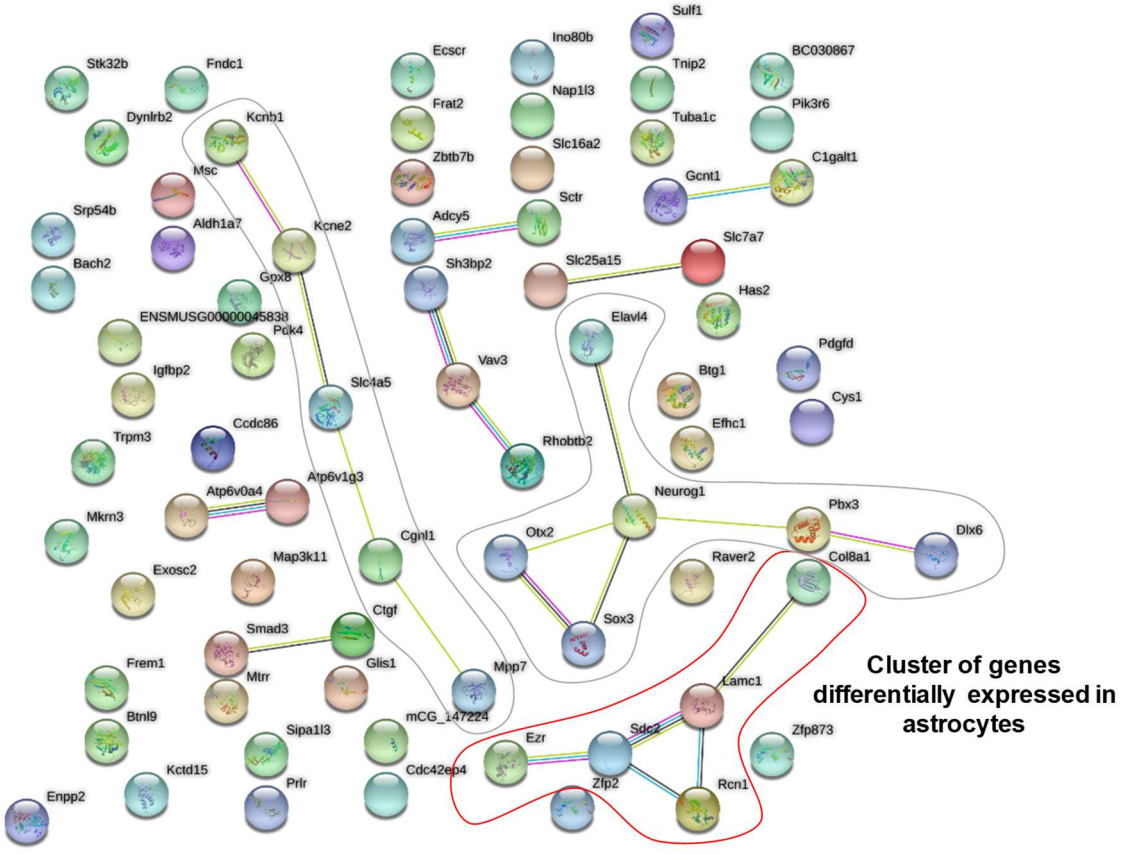

Figure 3.6 – STRING analysis revealed a functional cluster from the list of *Foxo1* target genes that are up-regulated in the hippocampus of IP_3R2 KO mice, and are specific of astrocytes.

Foxo1 target genes (76 differentially expressed genes) were inserted in the STRING tool to look for functional interactions between them. This analysis revealed three clusters of genes with related functions, but only one cluster (in red) displays genes that are specifically enriched in astrocytes.

Table 3.3 – Fold change, cellular specificity and reported functions of genes in the identified cluster.

GENE	FOLD CHANGE (microarrays)	CELL TYPE ENRICHMENT (Zhang et al., 2014)	REPORTED FUNCTIONS
Sdc2 (syndecan-2)	1.37	**Astrocytes** and OPCs	Spinogenesis and dendritic spine formation (Lin et al., 2007)
Ezr (ezrin)	1.41	Highly expressed in **astrocytes**	Involved in perisynaptic astrocyte processes (PAPs) protursions and neuronal filopodia formation (Heller and Rusakov 2015)
Lamc1 (laminin Subunit Gamma 1)	1.36	Endothelial cells	Essential for basement membrane formation (Zhang et al.,2017)
Rcn1 (reticulocalbin 1)	1.38	OPCs	Ca^{2+}-binding protein in the endoplasmic reticulum (ER) (Ding et al., 2015)
Col8a1 (collagen, type VIII, alpha 1)	2.60	Neurons	Extracellular matrix structural component (Li et al., 2018)

Overexpression of FOXO1 in dHIP CA1 astrocytes from C57BL/6 mice drives fear memory enhancement

In this work, we demonstrated that the lack of IP_3R2-dependent astrocytic Ca^{2+} signaling leads to an enhanced hippocampal-dependent cognitive performance, accompanied with a shift to immature spines in CA1 pyramidal neurons. Our molecular evaluation revealed *Foxo1* as a key transcriptional regulator of several genes differentially expressed in IP_3R2 KO mice, including astrocyte-specific genes involved in spinogenesis and dendritic spine formation. Based on the above, we hypothesized that astrocytic FOXO1 could be involved in these changes to enhance cognitive performance. To test this hypothesis, we evaluated whether selective overexpression of FOXO1 in astrocytes would influence contextual hippocampal-associated memory in C57BL/6 mice. To this end, we performed stereotaxic injections of an AAV5 encoding mouse FOXO1 and the mCherry reporter, under the control of a GFAP(0.7) promotor. Mice were bilaterally injected in the dorsal CA1 hippocampal subregion with AAV5-GFAP(0.7)-mCherry-2A-m-FOXO1 virus (Figure 3.7A, GFAP-mCherry-FOXO1 group) or with saline (Sham group). To confirm the viral distribution and cellular specificity of FOXO1 overexpression at the CA1 subregion, we sacrificed GFAP-mCherry-FOXO1 mice at two timepoints: two weeks (n=1) and 12 weeks (n=2) post-injection. We observed that, at both timepoints, $mCherry^+$-cells were distributed along the CA1 hippocampal area, which allowed us to confirm the region-specific infection of AAV5-GFAP(0.7)-mCherry-2A-m-FOXO1 virus (12

weeks; Figure 3.7B). At a higher magnification, we confirmed the well-distributed expression throughout CA1 *stratum oriens* down to the *stratum radiatum* layer (Figure 3.7C).

Specific antibodies were used to double-label mCherry in combination with astrocytic (GFAP and S100β) or neuronal (NeuN) markers (Figure 3.7D-F) in brain tissue collected only 2 weeks after the viral injection. Our results show that mCherry co-localizes with both $S100\beta^+$ (Figure 3.7D) and $GFAP^+$ (Figure 3.7E) cells, which confirms the specificity of the promotor GFAP(0.7) for astrocytes. Additionally, we excluded any neuronal expression of the virus, as shown by the immunostaining for the neuronal-specific nuclear protein marker, NeuN, which does not overlap with mCherry staining (Figure 3.7F).

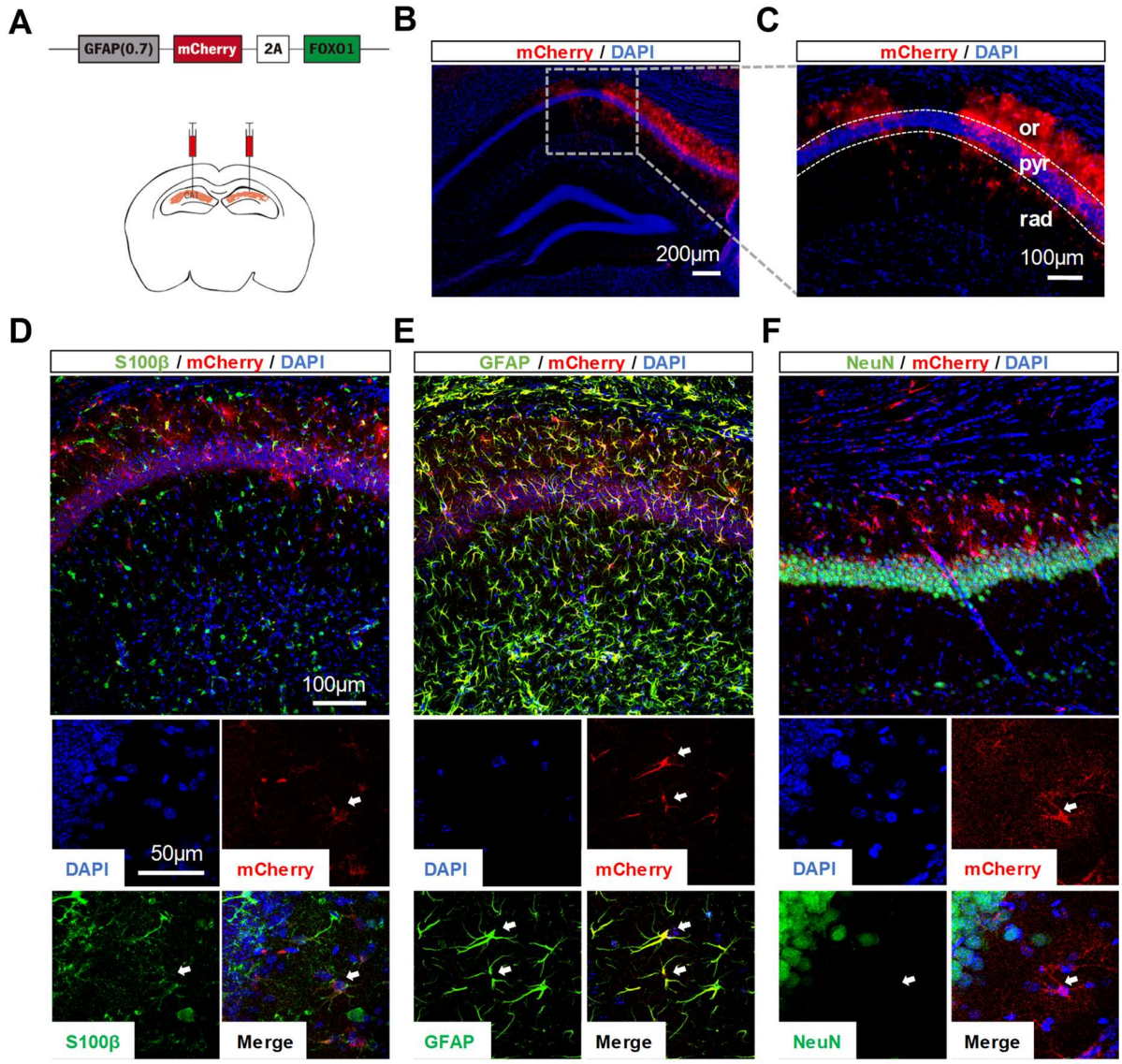

Figure 3.7 – AAV5-GFAP(0.7)-mCherry-2A-m-FOXO1 effectively infected astrocytes of the dHIP CA1 of C57BL/6 mice.

(A) Representative scheme depicting the bilateral stereotaxic injections of AAV5-GFAP(0.7)-mCherry-2A-m-FOXO1 virus in the hippocampal CA1 area of C57BL/6 mice. (B) Anti-mCherry reporter fluorescence (red) and DAPI staining in the hippocampus. (C) 12 weeks post-injection it is possible to observe a clear infection of CA1 *stratum oriens* (or) and a spreading of the virus through the *stratum pyramidale* (pyr) and *stratum radiatum* (rad) layers. (D-F) Confocal micrographs of immuno-histochemistry in brain slices illustrating co-expression of mCherry reporter with astrocytic (S100β and GFAP), but not neuronal (NeuN) markers. (D,E) mCherry (red) reporter gene is co-expressed with S100β (D, green) and GFAP (E, green). (F) mCherry (red) expression is absent in NeuN^{+} neurons (green). White arrows indicate co-localization of (D) mCherry/S100β and (E) mCherry/GFAP and the (F) absence of a co-localization of mCherry with NeuN. DAPI staining, blue. Scale bars depicted in representative images.

Furthermore, we evaluated the co-localization of FOXO1 expression with mCherry (Figure 3.8A) and GFAP (Figure 3.8B) immunostainings. We confirmed that FOXO1 is overexpressed specifically in astrocytes already at two weeks after infection with AAV5-GFAP(0.7)-mCherry-2A-m-FOXO1.

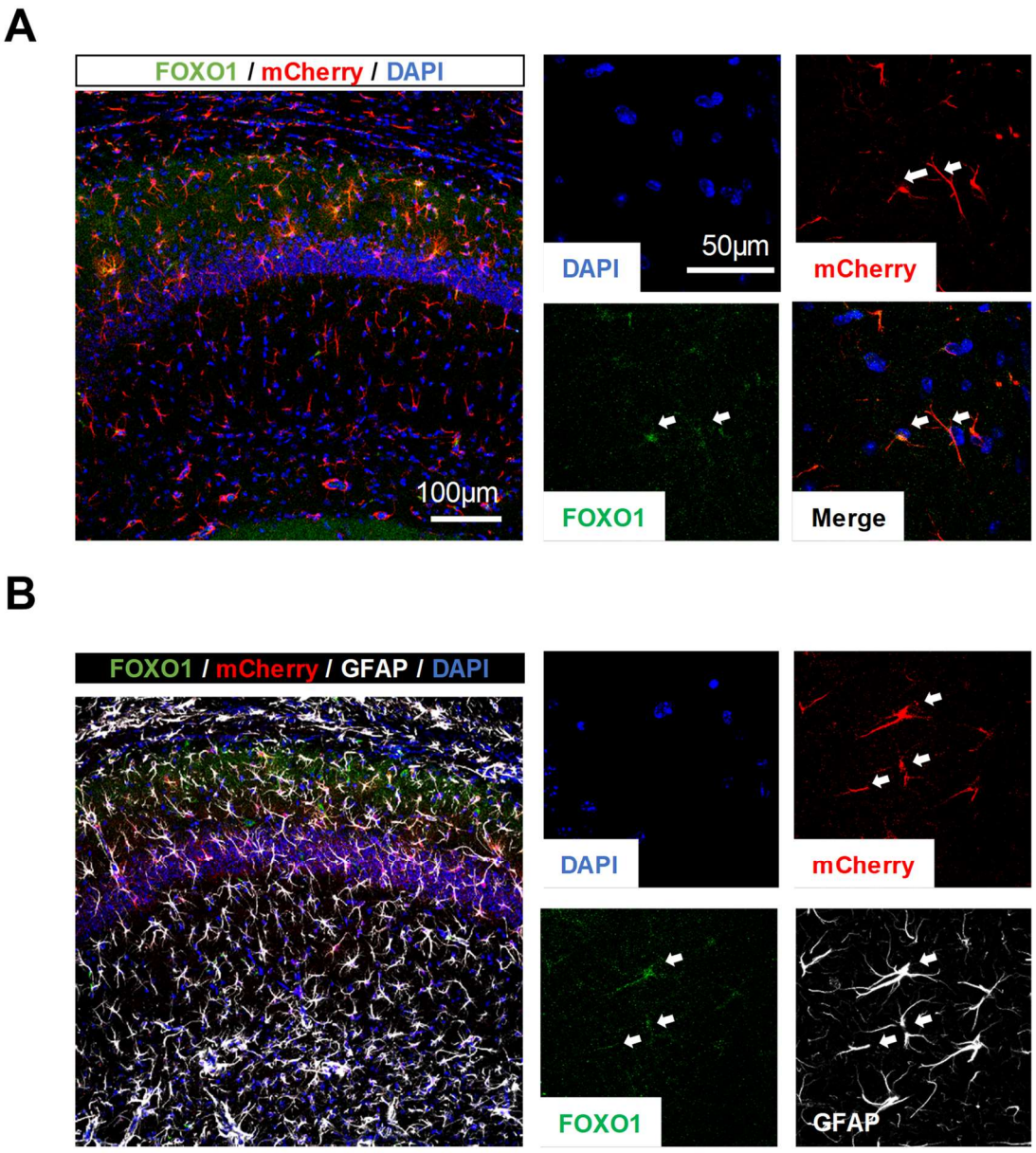

Figure 3.8 – Astrocyte-specific overexpression of FOXO1 in the dHIP CA1 of C57BL/6 mice with AAV5-GFAP(0.7)-mCherry-2A-m-FOXO1.

(A-B) Confocal images of immuno-histochemistry in brain slices showing that FOXO1 (green) is co-expressed with mCherry reporter (red) and the astrocytic marker GFAP (white). (A) FOXO1 (green) expression is detected in mCherry^{+}-cells (red) and (B) co-localizes specifically with the astrocyte marker GFAP. White arrows indicate co-localization of (A) mCherry/FOXO1 and (B) mCherry/FOXO1/GFAP. DAPI staining, blue. Scale bars depicted in representative images.

Based on our previous findings, *Foxo1* regulates the expression of key astrocytic genes that appear to support hippocampal-dependent cognitive function, in IP_3R2 KO mice. Therefore, we tested whether increasing FOXO1 expression in the hippocampus of pure C57BL/6 mice would recapitulate the memory enhancement observed in IP_3R2 KO mice. For that, we started by performing a behavioral characterization of Sham and GFAP-mCherry-FOXO1 mice four weeks after viral injection. We assessed anxious-like behavior, motor, and exploratory functions. We observed that overexpression of FOXO1 specifically in astrocytes induced neither an anxious-like phenotype nor alterations in locomotor activity (Figure S 3.2). Next, we evaluated contextual fear memory in both groups, using exactly the same paradigm and conditions previously described for WT and IP_3R2 KO mice (Figure 3.9). On the first day of testing, both groups displayed a similar freezing response before and after light-shock pairings (Figure 3.9A). From this analysis, we excluded any effect of the injection and concluded that both Sham and GFAP-mCherry-FOXO1 mice had similar freezing responses after the conditioning trials. Furthermore, light-shock pairings triggered a conditioned fear response in both groups (session, $F_{1,17} = 352.2$; $p < 0.0001$). Interestingly, re-exposure to the same context 24 h later revealed an increased freezing response of GFAP-mCherry-FOXO1 mice as compared with Sham (Figure 3.9B; $t_{17} = 2.918$, $p = 0.0096$). This result goes in line with our previous observations using IP_3R2 KO mice regarding contextual memory. Moreover, switching both groups to a new environment 2 h later, decreased freezing response percentages in both groups, but GFAP-mCherry-FOXO1 mice still presented an increased freezing response, as compared with Sham animals (Figure 3.9B; $t_{17} = 3.221$, $p = 0.005$). Nevertheless, in the cue probe, when the light stimulus was presented in a new context, similar freezing responses were observed for both groups. Altogether, these results support the role of astrocytic FOXO1 in the control of cognitive function, namely by enhancing hippocampal contextual memory.

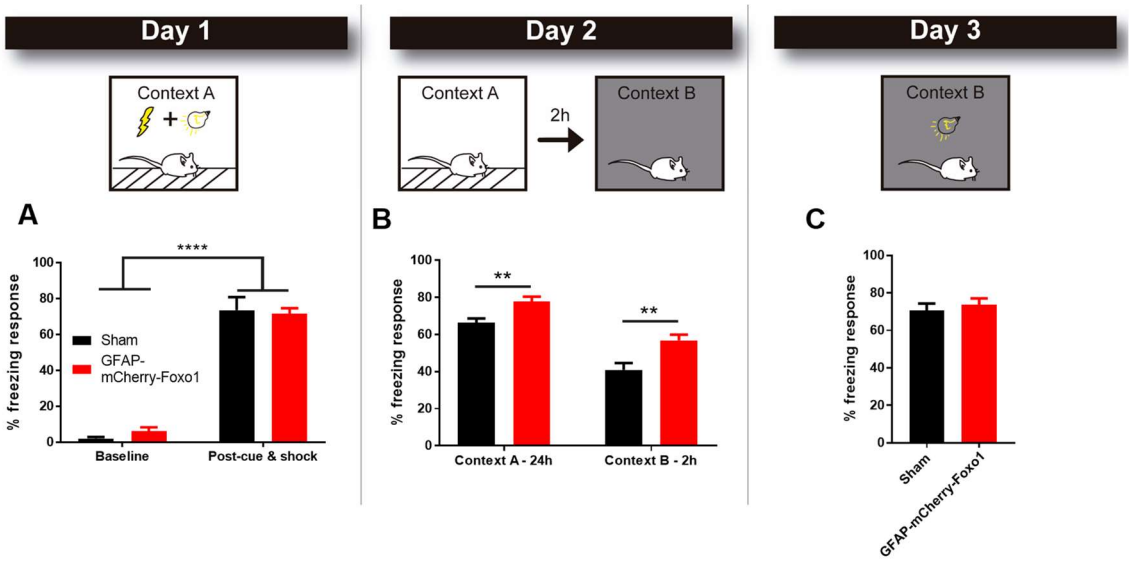

Figure 3.9 – GFAP-mCherry-FOXO1 mice present an increased contextual fear memory.

(A-C) Sham and GFAP-mCherry-FOXO1 mice were tested in a contextual fear conditioning paradigm (n= 7-12 per group). (A) Training session depicting baseline activity (left) and freezing acquired after light-shock exposure (right) at context A. (B) Re-exposure (24 h later) to context A (left) enhanced freezing response in GFAP-mCherry-FOXO1 mice. After switching to a new context, GFAP-mCherry-FOX01 mice still displayed a higher freezing response, as compared with Sham mice (context B, right). (C) Presentation of a light stimulus in the new context led to similar freezing responses between groups. Sham mice are represented in black and GFAP-mCherry-FOXO1 mice in red bars. Data are presented as mean ± SEM. ** $p < 0.01$, **** $p < 0.0001$.

Discussion

In this work, we observed that the deletion of IP_3R2-dependent astrocytic Ca^{2+} signaling regulates cognitive performance. Particularly, we demonstrated that this regulation is mostly observed in hippocampal-dependent tasks. In this region, CA1 pyramidal neurons that are crucial for this performance, display an intact dendritic tree, but have more immature spines. We also showed that IP_3R2 KO astrocytes display a shrinkage of its main structure, which appears to be compensated by an increased number of $GFAP^+$ cells. At a molecular level, we identified the transcription factor *Foxo1* as a key regulator of 76 differentially expressed genes in the IP_3R2 KO mouse model. Looking deeper into the functional interactions between *Foxo1* target genes and its cell-type enrichment from a widely accepted database, we found two genes, *Sdc2* and *Ezr,* which are mainly transcribed in astrocytes. They are described to regulate spine structure, with impact to synaptic function and therefore expected to play an important role in behavior dependent on the hippocampus of IP_3R2 KO mice. We will discuss these results in light of the existing literature, following the hypothesis depicted in Figure 3.10.

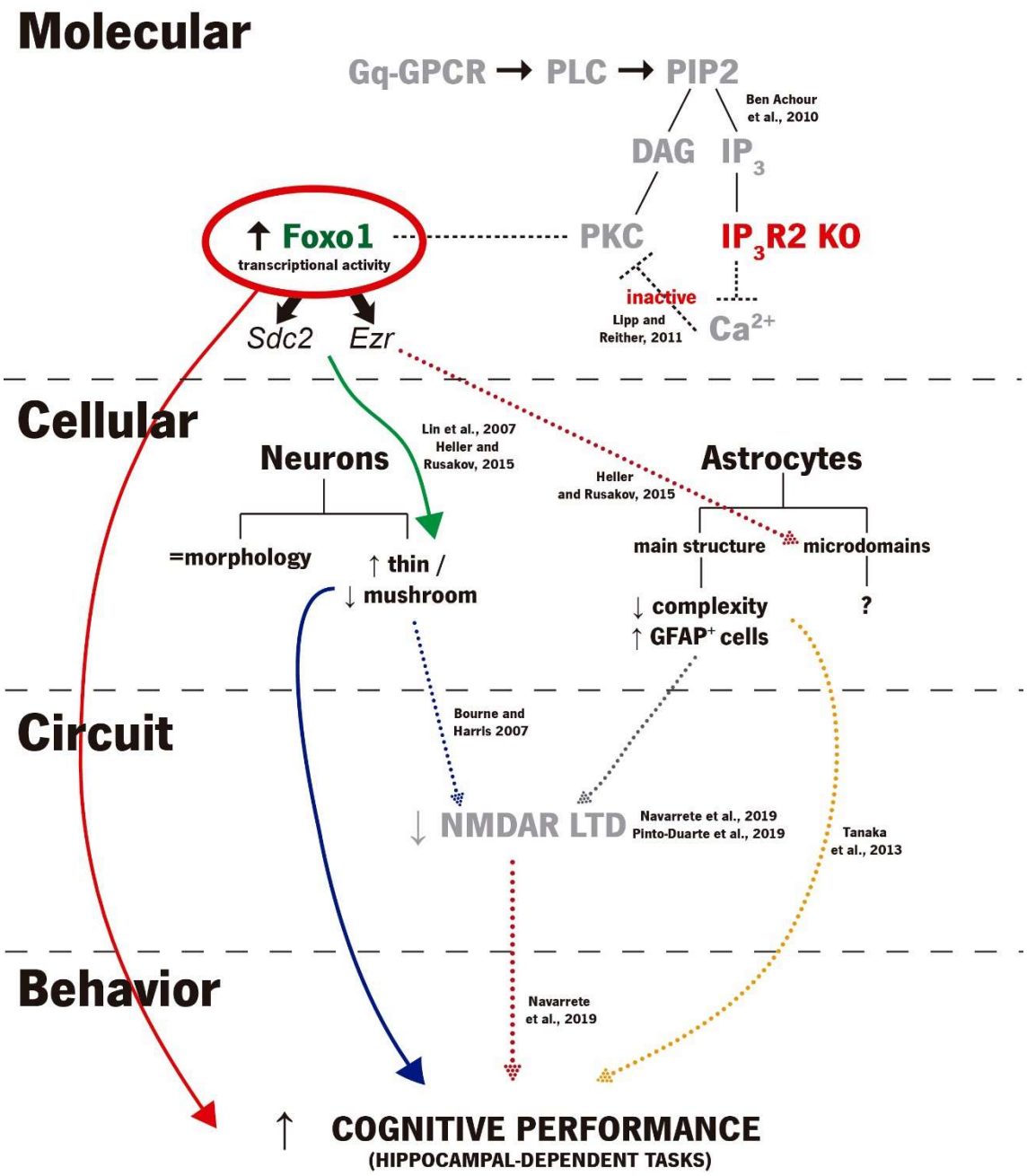

Figure 3.10 – Schematic representation of the hypothesis linking our molecular, structural and behavioral observations.

We studied the IP_3R2 KO mouse model, since it is a widely used model of astrocyte signaling dysfunction described in the literature. Besides, IP_3R2 KO mice are reported to maintain intact Ca^{2+} levels in CA1 pyramidal neurons, whereas intracellular Ca^{2+} elevations in the soma and main astrocytic processes are abolished (Petravicz et al. 2008; Navarrete et al. 2012). Astrocytes from this model still present "focal" astrocytic Ca^{2+} elevations in far distant microdomains (Srinivasan et al. 2015), mainly arising from the mitochondria (Agarwal et al. 2017), which are expected to play a role in the control of specific synapses

or micro-circuits. Recently, the Bal Khakh's laboratory used a viral approach to express Ca^{2+} pumps under the control of a GfaABC1D promoter to continuously extrude this ion in striatal astrocytes (Yu et al. 2018). In this study, authors found that this approach mimics the decreased frequency of spontaneous Ca^{2+} signals and reduced Ca^{2+} signal amplitude in astrocyte branches, as observed in IP_3R2 KO mice. Both models responded similarly to phenylephrine, although IP_3R2 KO mice displayed a larger reduction of Ca^{2+} responses. Together with the available Ca^{2+} imaging observations (Navarrete et al. 2012), these data confirm that IP_3R2 KO astrocytes are not able to use reticular Ca^{2+} to drive Ca^{2+}-dependent pathways.

The forkhead box O (FOXO) family of transcription factors is responsible for the regulation of several genes involved in distinct cellular processes, with possible roles in the modulation of cognitive function (Eijkelenboom and Burgering 2013; Kim and Webb 2017). Four members compose the FOXO family: FOXO1, FOXO3, FOXO4, and FOXO6. It is accepted that FOXOs are regulated via two main conserved signaling pathways: the insulin/insulin-like growth factor/protein kinase B (AKT) signaling, in response to growth factors; and the Jun N-terminal kinase signaling, upon stress conditions. These pathways regulate FOXO transcriptional activity through post-translational modifications (PTM), namely phosphorylation. However, it is known that a higher complexity of signaling pathways and PTMs regulate FOXOs activity (Eijkelenboom and Burgering 2013). For instance, FOXOs can be ubiquitylated, methylated and acetylated, affecting both its subcellular location and its activation state (Calnan and Brunet 2008; Eijkelenboom and Burgering 2013). However, to the best of our knowledge the mechanisms underlying FOXOs regulation in astrocytes are unknown. According to a widely used transcriptomic database (Zhang et al. 2014), *Foxo1* is highly expressed in astrocytes, as compared with the remaining family members. Interestingly, the available literature reports that in different cell types (Kawakami et al. 2004; Barragan et al. 2006; Wu et al. 2009) protein kinase C (PKC) controls AKT activation, which in turn is responsible for the negative regulation of *Foxo1* activity (Biggs et al. 1999; Kim and Webb 2017). Since PKC is tightly regulated both by DAG and cytosolic Ca^{2+}, in the absence of Ca^{2+}, *Foxo1* activity is disinhibited. Our results showed that in the hippocampus of IP_3R2 KO mice, *Foxo1* induces the expression of a large number of targets. Among these targets, we found astrocyte-enriched genes such as *Sdc2* and *Ezr* (Zhang et al. 2014), which play a role in perisynaptic astrocyte processes (PAPs) morphology and dendritic spine formation (Lin et al. 2007; Lavialle et al. 2011; Molotkov et al. 2013; Hu et al. 2016) and might contribute to the observed shift to more immature spines, leading to changes in synaptic function with impact to cognitive behavior. Besides the spine modulation, *Ezr* is found at PAPs and is involved in morphological plasticity during synaptic communication (Derouiche and Frotscher 2001; Lavialle et al. 2011; Heller and Rusakov 2015). It is described that PAPs correspond to areas of proximity between dendritic spines and

astrocytic processes and display structural plasticity that is fundamental for learning and memory. Moreover, activity-related structural remodeling of PAPs was shown to be dependent on astrocytic Ca^{2+}-elevations (Perez-Alvarez et al. 2014). One should not rule out that, at least partially, by displaying IP_3R2-independent Ca^{2+} events in the microdomains, IP_3R2 KO astrocytes might circumvent the lack of global Ca^{2+} signals in the soma and main processes. The CA1 *stratum radiatum* of IP_3R2 KO present a higher density of astrocytes with simpler $GFAP^+$ arbor complexity. By evaluating the GFAP-stained structure of astrocytes, we targeted its main structure, which corresponds to around 15% of astrocytes total volume (Bernardinelli et al. 2014). The astrocytic atrophy observed seems to be a result of global Ca^{2+} signaling interference. In fact, a study using the IP_3 "sponge" mouse model reported a reduction in the astrocytic coverage in hippocampal CA1 *stratum radiatum* (Tanaka et al. 2013). However, our observations show that an increased cellular density of $GFAP^+$ in the *stratum radiatum* layer circumvents astrocytic atrophy. This screening of astrocyte structure lacks however, the detail required to disentangle the fine astrocyte morphology, which could provide additional cues on further morphological consequences. To assess the detailed astrocytic morphology, including its microdomains, it would require much more powerful and time-consuming monitoring methods (Heller and Rusakov 2015). Altogether, these data suggest that the individual or combinatory effects of (1) a higher density of less complex astrocytes at the CA1 *stratum radiatum*, (2) *Sdc2* and *Ezr* modulation of PAPs and vicinal spines shall have an influence on synaptic plasticity.

Synaptic plasticity is frequently observed in mouse models of cognitive enhancement (Lee and Silva 2009). Our data shows that interfering with IP_3R2-dependent Ca^{2+} signaling contributes to a shift to more immature (thin) spines in apical dendrites of CA1 pyramidal neurons, critical for cognitive processing. Thin spines are recognized as "learning spines", whereas mushroom spines are called "memory spines" (Bourne and Harris 2007) mainly due to their intrinsic features. Thin spines display a more plastic and transient structure and retain biochemical signals such as Ca^{2+}, which favors learning mechanisms (Bourne and Harris 2007). Moreover, glia interacts closer to thin spines associated with the learning process (Medvedev et al. 2014). A dendritic spine simplification, from large "memory" spines to thinner "learning" spines, is associated with LTD induction (Bourne and Harris 2007). Evidences point to an important role of hippocampal LTD in memory formation and consolidation (Nicholls et al. 2008; Ge et al. 2010; Dong et al. 2013b). Chen et al. (2013) described that astrocytes contribute to heterosynaptic long-term depression (hLTD) in the hippocampus. However, interfering with astrocytic Ca^{2+} signaling impairs this phenomenon. Recently, Navarrete et al. (2019) found that astrocytes control NMDAR-dependent LTD, supporting memory enhancement. Specifically, these authors show that the deletion of

p38α MAPK from hippocampal astrocytes impairs LTD, which has an enhancing effect in hippocampal-associated fear memory. Moreover, a recent work provided new insights into NMDAR-dependent LTD in IP_3R2 KO mice under a C57BL/6 background (Pinto-Duarte et al. 2019). This study shows that IP_3R2 KO mice present an impaired hippocampal LTD. This observation, together with the Navarrete et al. (2019), supports the hypothesis that LTD impairment in IP_3R2 KO mice could underlie the cognitive enhancement observed in our experiments.

The influence of global IP_3R2-dependent Ca^{2+} signaling in behavior is still poorly understood. We performed a full behavioral characterization of adult IP_3R2 KO mice on a C57BL/6J background. For a behavioral analysis, it is important to take into consideration the mouse strain and the targeted mechanism since it could easily mislead data interpretation (Oliveira et al. 2015; Guerra-Gomes et al. 2017). In accordance with other studies, we found that IP_3R2 KO mice do not display an anxious phenotype (Cao et al. 2013; Tanaka et al. 2013; Petravicz et al. 2014; Pinto-Duarte et al. 2019). However, in what concerns depressive-like behavior results are contradictory. IP_3R2 KO mice generated on a Black Swiss background display increased learned helplessness (Cao et al. 2013), in opposition to an IP_3Rs knocking-down approach, which leads to an antidepressant phenotype (Galeotti et al. 2008). Moreover, the specific deletion of IP_3R2 in astrocytes neither affects depressive-like behavior nor impulsivity (Petravicz et al. 2014), as we have observed, suggesting that the previously described anxious- or depressive-like phenotypes may be dependent on the mouse genetic background. Regarding the normal motor function and coordination, our observations are in agreement with other reports targeting IP_3R2-dependent Ca^{2+} signaling (Cao et al. 2013; Tanaka et al. 2013; Petravicz et al. 2014; Kim et al. 2016; Pinto-Duarte et al. 2019).

We observed a cognitive enhancement in the performance of hippocampal-dependent tasks by IP_3R2 KO mice. Interestingly, an enhanced cognitive performance was previously described in other mouse models targeting Ca^{2+}-related mechanisms (Lee and Silva 2009). For instance, the ryanodine receptor 3 KO mice display an increased spatial learning performance (Futatsugi et al. 1999). Authors claim that this effect might be the result of smaller intracellular Ca^{2+} increases in neurons that are sufficient to induce LTP and modulate cognitive performance. In a different study, a mouse model knockout for S100B, a Ca^{2+} binding protein and highly expressed in astrocytes (Wang and Bordey 2008), presents a cognitive performance similar to what we have observed in the IP_3R2 KO mice. S100B KO mice display an increased spatial reference memory in the MWM and increased fear memory (Nishiyama et al. 2002). Moreover, Jeon et al. (2003) reported that genetic deletion of plasma membrane Na^+/Ca^{2+} exchanger 2 increased the time required for neuronal-induced intracellular Ca^{2+} clearance and resulted in enhanced performance on tasks

engaging the hippocampus. Ca^{2+} signals play a pivotal role in functional neuron-astrocyte interactions (Losi et al. 2017). Together, these observations indicate that cytosolic Ca^{2+}, and its downstream pathways, are critical for cognitive function.

Overall, our findings show that interfering with global Ca^{2+} signaling in astrocytes favors cognitive performance in hippocampal-dependent tasks. We found that *Foxo1* is particularly active leading to the increased expression of astrocyte-specific *Sdc2* and *Ezr*. These might contribute to alterations in fine cytoskeleton and dendritic spine formation in the hippocampus, with impact in synaptic plasticity, leading to a cognitive enhancement. To test this hypothesis, we used a viral approach to specifically overexpress FOXO1 in hippocampal astrocytes of naïve C57BL/6 mice. This specific modulation was enough to recapitulate the enhanced fear memory previously observed in IP_3R2 KO mice, confirming an astrocyte role in cognitive modulation through FOXO1 regulated-pathways. Our results suggest that astrocytic Ca^{2+} regulates *Foxo1* transcriptional activity, which ultimately controls cognitive function via morphological changes and synaptic plasticity. The identified gene candidates should be further tested as therapeutic targets for cognitive disabilities, for instance in aging, neurodegenerative disorders or stress-related pathologies.

Author Contributions

SGG designed the study, performed and analyzed the experiments and wrote the manuscript; VMS, GT, IC, JFV participated in behavioral tests and morphological analysis; DSMN performed the viral injections and helped with molecular and morphological analysis; ATC helped with molecular biology experiments; MI, MB, JB and MK performed the microarray analysis; NS, LP and JFO supervised the study, secured funding, analyzed the data and wrote the manuscript.

Supplementary figures

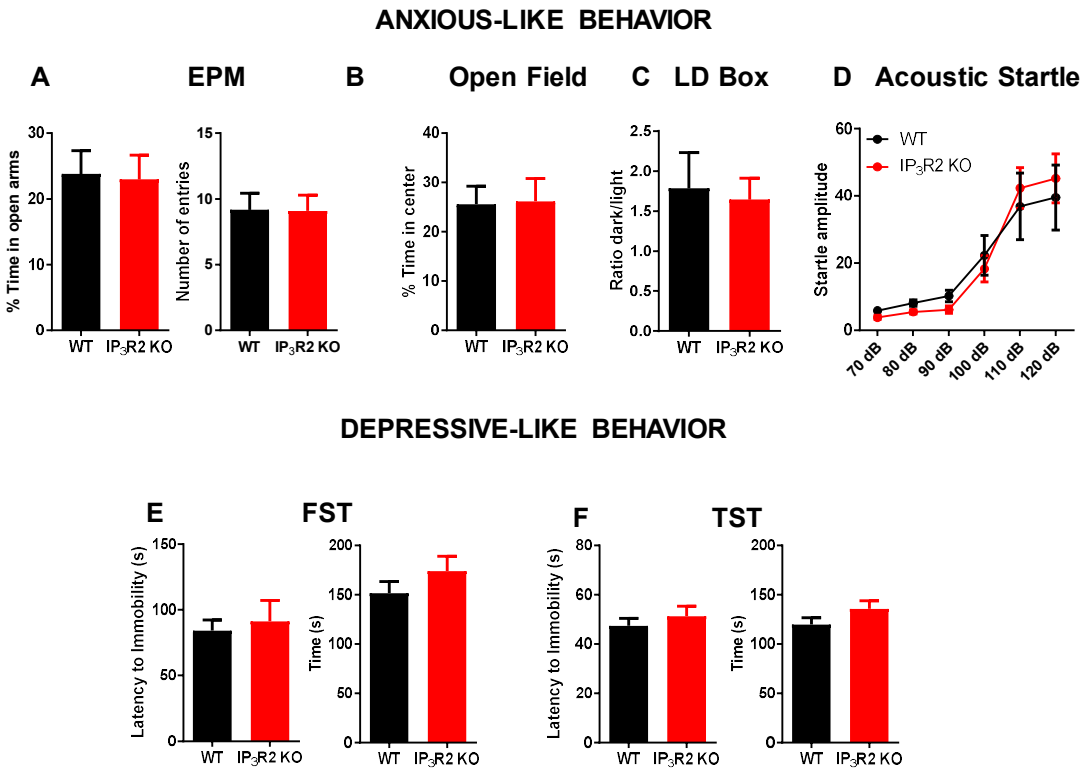

Figure S 3.1 - IP_3R2 KO mice display neither anxious- nor depressive-like behavior.

(A) Elevated Plus Maze (EPM) reveals a similar percentage of time in open arms and number of entries between genotypes (n=10-11 per group). (B) Open Field test display no differences between genotypes regarding time in center (n=11 per group). (C) Light/Dark (LD) box showing an equal exploration time of dark/light of WT and IP_3R2 KO mice (n=6-7 per group). (D) Acoustic Startle reveal similar responsiveness to an increased sound stimulus between genotypes (n=9-12 per group). (E) Forced Swim Test (FST) and (F) Tail Suspension test (TST) allow us to evaluate latency to immobility and total immobility time for each paradigm (n=6-11 per group). Data plotted as mean ± SEM. WT mice are plotted in black bars/lines and IP_3R2 KO mice are plotted in red bars/lines.

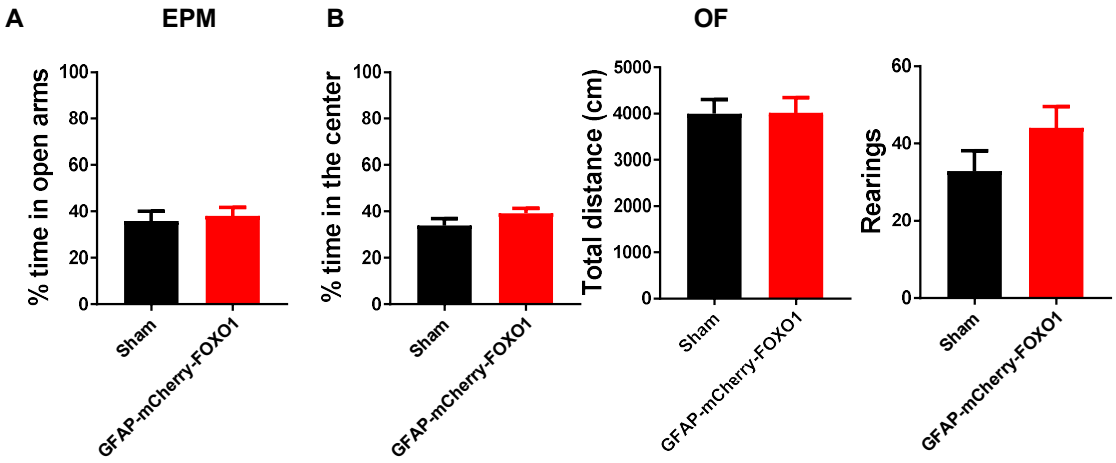

Figure S 3.2 – GFAP-mCherry-FOXO1 mice do not display an anxious-like phenotype and present normal locomotor and exploratory abilities.

(A) Elevated Plus Maze (EPM) reveals a similar percentage of time in open arms between groups (n=8-13 per group). (B) Open Field (OF) test display no differences between groups regarding total distance traveled and number of rearings (n=8-13 per group). Data plotted as mean ± SEM. Sham mice are plotted in black bars and GFAP-mCherry-FOXO1 mice are plotted in red bars.

CHAPTER 4

Sónia Guerra-Gomes, Ana Rita Machado-Santos, Nuno Dinis Alves, Eduardo Loureiro-Campos, Nuno Sousa, Luísa Pinto, João Filipe Oliveira

The impact of uCMS in a mouse model of astrocytic calcium dysfunction

(Manuscript in preparation)

(2019)

Title

The impact of uCMS in a mouse model of astrocytic calcium dysfunction

Authors

Sónia Guerra-Gomes[1,2], Ana Rita Machado-Santos[1,2], Nuno Dinis Alves[1,2], Eduardo Loureiro-Campos[1,2], Nuno Sousa[1,2], Luísa Pinto[1,2], João Filipe Oliveira[1,2,3].

Affiliations

1 - Life and Health Sciences Research Institute (ICVS), School of Medicine, University of Minho, 4710-057 Braga, Portugal

2 - ICVS/3B's - PT Government Associate Laboratory, Braga/Guimarães, Portugal

3 - IPCA-EST-2Ai, Polytechnic Institute of Cávado and Ave, Applied Artificial Intelligence Laboratory, Campus of IPCA, Barcelos, Portugal

Corresponding author:

João Filipe Pedreira de Oliveira (PhD), Life and Health Sciences Research Institute (ICVS), School of Medicine, University of Minho, Campus de Gualtar, 4710-057 Braga, Portugal, Tel: +351-253-604871, Fax: +351-253-604809, joaooliveira@med.uminho.pt

ACKNOWLEDGMENTS

The authors are grateful to Prof. Alfonso Araque and Prof. Ju Chen for sharing the mice line. The authors also acknowledge funding from national funds through Foundation for Science and Technology (FCT) fellowships to SGG, ARMS, NDA, ELC,and IF grants to LP (IF/01079/2014) and JFO (IF/00328/2015); Bial Foundation Grants 207/14 and 037/18 to JO, and 427/14 to LP; Northern Portugal Regional Operational Programme (NORTE 2020), under the Portugal 2020 Partnership Agreement, through the European Regional Development Fund (FEDER) (NORTE-01-0145-FEDER-000013); FEDER Funds, through the Competitiveness Factors Operational Programme (COMPETE), and The National Fund, through the FCT (POCI-01-0145-FEDER-007038).

Abstract

Depression is a multidimensional disorder characterized by a maladaptive response in cortico-limbic regions critical for mood and cognition, such as the hippocampus and the prefrontal cortex. Neuron-astrocyte interactions support neuronal function and structure in these brain circuits, yet little is known about the role of astrocytes in the context of depression. Emerging data suggest interesting molecular and structural alterations of astrocytes in patients and rodent models of disease. In particular, we and others have demonstrated that astrocytic calcium (Ca^{2+}) signaling modulates the behavioral response, namely by enhancing cognitive function of adult mice and providing cognitive resilience during aging. Therefore, we used the IP_3R2 KO mouse model of global astrocytic Ca^{2+} impairment to test the potential of this mechanism in the context of disease, namely to prevent the deleterious effects induced by exposure to unpredictable chronic mild stress (uCMS). Our results show that IP_3R2 KO mice display a resilience to physical and anxiety alterations, typically caused by chronic stress exposure. More specifically, we found that WT mice exposed to uCMS lost weight, willingness to self-care and displayed an anxious-like phenotype, while IP_3R2 KO mice exposed to uCMS behaved similarly to its non-stressed counterparts. This behavioral characterization pointed to an important role of IP_3R2-dependent Ca^{2+} signaling in the modulation of a response to chronic stress exposure. The disclosure of molecular targets involved the resilience observed in IP_3R2 KO mice will certainly create new windows of opportunity for the development of novel therapeutics for depression.

Keywords

Unpredictable chronic mild stress, astrocyte, calcium signaling, IP_3R2, behavior, resilience

Introduction

Depression is a neurobiological, multidimensional disorder that affects approximately 16% of the population worldwide (Hollon et al. 2006; WHO 2017). Remarkably, over 75% of affected patients suffer recurrent episodes of depression, despite their treatment with currently available antidepressants (Hollon et al. 2006; Baldessarini et al. 2015). Therefore, there is an urgent need to understand the pathophysiology underlying this disease. Several studies have demonstrated that chronic stress exposure triggers detrimental effects in several brain systems that leads, among others, to a condition of persistent mood impairment in patients and animal models of depression (Bessa et al. 2009b; Mateus-Pinheiro et al. 2013; Patricio et al. 2015; Alves et al. 2017). These brain systems include cortico-limbic areas such as hippocampus (Hip), amygdala (Amy) and prefrontal cortex (PFC) (McEwen et al. 2016). Depression is a recognized neural circuit disorder and antidepressant' actions rely on neuronal structural remodeling and signaling modulation to recover mood deficits (Pittenger and Duman 2008; Bessa et al. 2009a). Astrocytes, the major glial cell type in the brain, have been increasingly associated with the etiology of this disorder (Rial et al. 2015). A disruption of the neuron-astrocyte signaling could lead to circuit malfunction and behavioral impairments. Changes in the expression of astrocytic markers were reported in cortico-limbic regions in rodent models of depression (Musholt et al. 2009; Gosselin et al. 2009) or human patients (Cotter et al. 2002; Gittins and Harrison 2011). Moreover, analysis of cortical astrocytes revealed morphological alterations in samples from depressed suicidal patients (Torres-Platas et al. 2011). We and others have shown that specific ablation of astrocytes in the PFC, one of the brain regions affected in depression, leads to cognitive deficits in a working memory task and induced an anhedonic phenotype, major hallmarks of depression (Banasr and Duman 2008; Banasr et al. 2010; Lima et al. 2014). We also showed that interfering with astrocytic exocytosis led to a Hip-PFC theta rhythm desynchronization (Sardinha et al. 2017) similar to previous observations in a rat model of depression (Oliveira et al. 2013). However, the putative role of astrocytes in depression remains unclear, mostly due to their heterogeneity and functional complexity. After identifying a global Ca^{2+} and FOXO1-dependent signaling with a positive modulation on cognitive behavior (Chapter 3), we designed an approach to address the role of global astrocytic Ca^{2+} signaling in depression. For that, we used the same IP_3R2 KO mouse model (Li et al. 2005) that lacks global astrocytic Ca^{2+} signaling (Navarrete et al. 2012), to assess the relevance of this mechanism for the development of the deleterious effects induced by exposure to an unpredictable chronic mild stress (uCMS) protocol. We carried out a battery of tests covering several behavioral domains, namely anxiety, mood and cognition. This characterization revealed a surprising

resilience of IP_3R2 KO mice to the installation of an anxious-like phenotype induced by stress exposure, which suggests an important therapeutic potential.

Materials and Methods

Animals

3 to 5-month old WT and IP_3R2 KO mice maintained on C57BL/6J background (Guerra-Gomes et al. 2018) were bred according to the guidelines for care and handling of laboratory animals (*ad libitum* access to food and water in their home cages; lights maintained on a 12h light/dark cycle; 22 ± 1°C, 55% humidity). These mice were kindly supplied by Prof. Alfonso Araque (U. Minnesota, USA) (Navarrete et al. 2012), under agreement with Prof. Ju Chen (U.C. San Diego, USA) (Li et al. 2005). IP_3R2 KO and WT littermate mice were obtained from crossing heterozygous animals, and their genotype was confirmed by polymerase chain reaction (PCR). Age and gender-matched sets of WT and IP_3R2KO mice were divided into two experimental groups (n=7 WT + 6 IP_3R2 KO per group): control (gently handled for 6 weeks) and uCMS-exposed mice. All experimental procedures were performed in accordance with the guidelines described in Directive 2010/63/EU and were approved by the local ethical committee (SECVS 075/2015) and national authority for animal experimentation (DGAV 17469/2012).

unpredictable Chronic Mild Stress (uCMS) protocol

Male WT and IP_3R2 KO mice were exposed to a validated unpredictable Chronic Mild Stress (uCMS) protocol as previously described (Bessa et al. 2009a; Mateus-Pinheiro et al. 2013). Briefly, the uCMS paradigm consisted of a random exposure to mild stressors in an unpredictable fashion for six weeks. The applied stressors were as follows: shake – mice placed in an orbital shaker for 1 h at 150 rpm; strobe lights – light flashes exposure for 2 h; tilted cage – homecage tilted in a 45° angle overnight; damp bed – homecage with damp sawdust overnight; confinement – mice were limited to a restricted space for 1 h; overcrowding and noise – mice were placed in a restricted space and exposed to noise for 1 h; inverted lights – reversed light/dark cycle during the weekend.

Biometric parameters assessment: body weight and coat state

Stress efficacy was controlled through weekly body weight and fur state (coat score) monitoring. This assessment was performed on the same weekday and same time period. Coat score evaluation is a readout for an anhedonic phenotype, as previously described (Nollet et al. 2013). Stressed mice display a worse coat state as compared to control non-stressed animals. The coat score was attributed according

to the fur state in seven different body areas: head, neck, dorsal coat, ventral coat, tail, forepaws, and hindpaws. This classification was 0 (bad) if the fur was unkempt and 1 (good) if the coat presented a well-groomed state. The sum of the scores for the seven body parts reached a maximal score of seven, whenever mice were motivated for self-care. Since some stressors, as damp bed and confinement, may influence coat state we assessed this biometric parameter in a period distanced from the exposure to these stressors.

Corticosterone levels

We assessed corticosterone levels in WT and IP_3R2 KO mice from both groups. This assessment was performed in the blood serum using a Corticosterone ELISA kit (ab108821, Abcam, UK), following the manufacturer's instructions. Blood sampling by tail venipuncture was performed within a maximum of 120 s after the mouse was removed from its homecage. Next, each sample was centrifuged at 13.000 rpm during 5 min and the supernatant (blood serum) was collected and stored at -80°C. Blood serum corticosterone levels were assessed in the last week of the uCMS protocol at the diurnal nadir (8-9 a.m) and diurnal zenith (8-9 p.m).

Behavioral analysis

After chronic stress exposure for 6 weeks, we performed behavioral experiments to assess emotional and cognitive phenotypes. Emotional states are the result of both physical and psychological alterations in response to internal or external stimuli that influence behavior (Fox 2008). Anxious-like behavior was assessed by the Elevated Plus Maze, depressive-like behavior was tested in the Tail Suspension Test and cognition was evaluated in the Novel Object Recognition test.

Elevated-plus maze

The Elevated-plus maze (EPM) is a gold standard method to assess anxious-like behavior in rodents (Belzung and Griebel 2001; Bourin et al. 2007). EPM test relies on propensity of mice to explore secure enclosed spaces and an intrinsic fear of heights/open zones (Walf and Frye 2007; Arabo et al. 2014). WT and IP_3R2 KO mice, both control and exposed to the uCMS paradigm, were placed in the hub of a plus-like apparatus elevated 72.4 cm above the floor (ENV560; Med Associates Inc, Vermont, USA), containing two open arms (50.8 cm x 10.2 cm) and two closed arms (50.8 cm x 10.2 cm x 40.6 cm). Mice were let freely explore the maze for 5 min. Time spent in each arm and the number of entries were recorded and analyzed using Ethovision XT 13 software (Noldus, Netherlands).

Tail Suspension Test

The Tail Suspension Test (TST) evaluates learned helplessness. In this test, a mouse suspended by its tail tends to develop an immobile state in a situation of behavior despair. During the total duration of the test (6 min), periods of mobility vs. immobility are analyzed (Steru et al. 1985). WT and IP_3R2 KO mice (control and uCMS-exposed) were suspended by the tip of their tails using adhesive tape (approximately 80 cm above the floor). The activity of each mouse was recorded using a video camera. Mobility vs. immobility periods were analyzed using Ethovision XT 13 software (Noldus, Netherlands). Since this test evaluates learned helplessness, mice had to learn that there is no possible escape. Thus, only the final 4 min of testing were considered for analysis, for each animal. Regarding the latency to immobility, one animal was not included in the analysis due to an initial failure of the video-recording system.

Novel Object Recognition Test

The Novel Object Recognition Test (NOR) test was performed in white boxes (30 x 30 x 30 cm) under dim white-light room illumination. Boxes contained two visual cues (two stripes) on one side of the arena wall, as spatial reference. During the first three days, mice were let to explore the empty boxes during 20 min for habituation. The next day, a training session consisted of exposing mice to two equal objects during 10 min. After one hour, spatial recognition memory was assessed. One of the familiar objects was displaced to the opposite side of the box and mice were allowed to explore it during 10 min. After 24 h mice were tested for long-term memory. A novel object replaced a previously explored familiar object and mice were allowed to explore it during 10 min. The arena was cleaned between trials with 10% ethanol. This test was recorded with a video camera and analyzed using Ethovision XT 13 software (Noldus, Netherlands). Total object exploration time was extracted to calculate the percentage of exploration for the novel or displaced objects. Two mice were removed from the analysis because they did not perform the test (no exploration of the objects).

Statistical analysis

GraphPad Prism 7 (GraphPad Software Inc., USA) was used to assess normal distributions and further group comparisons. Parametric tests were applied to continuous variables following a Gaussian distribution (Kolmogorov-Smirnov), while non-parametric tests were used for discrete variables. Two-way analysis of variance (ANOVA) with Sidak *post hoc* test was applied to body weight gain, corticosterone levels, EPM, TST, and NOR parameters, considering either factors: control vs. uCMS or genotype. For coat score, a discrete variable, Kruskal-Wallis test was used, followed by Dunn's multiple comparisons

test. Data are expressed as mean ± SEM, except for coat score, which is represented as a scatter dot plot and median. The results were considered statistically significant for a $p < 0.05$.

Results

IP_3R2 KO mice display resilience to uCMS exposure induced alterations in body weight and coat score

WT and IP_3R2 KO uCMS mice were exposed to several stressors in a random and unpredictable fashion (Figure 4.1A). To evaluate the efficiency of the uCMS protocol, we performed a weekly monitoring of body weight gain and coat score for all tested groups. In the last week of uCMS exposure, serum corticosterone levels were measured. Afterwards, a behavioral assessment covering distinct behavioral dimensions (anxiety-like behavior, depressive-like behavior, and cognition) was performed (Figure 4.1B).

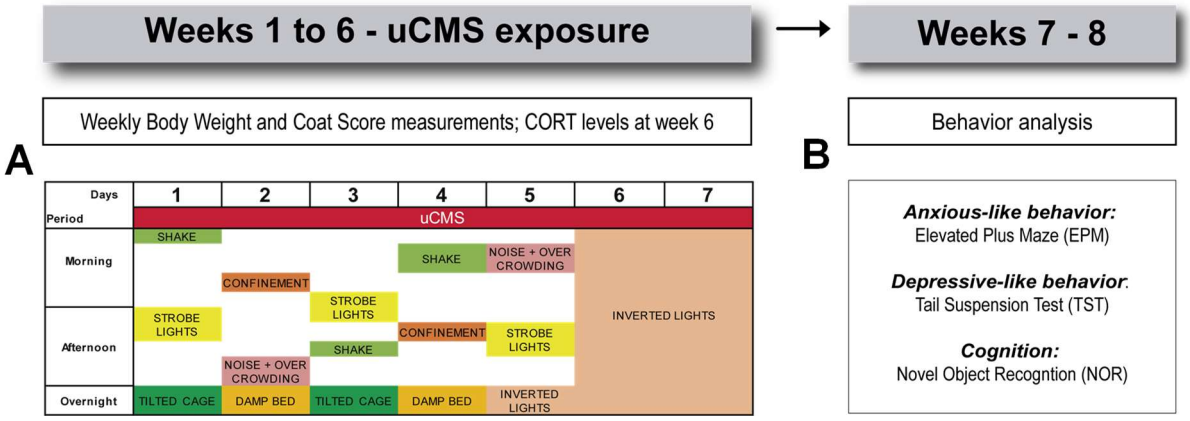

Figure 4.1 – Experimental design for the uCMS protocol and behavioral characterization.

(A) Schematic example of weekly stressors exposure. Once a week, the body weight was measured, and coat score was assessed. Blood collection was performed at the 6th week for corticosterone levels determination. (B) The behavioral assessment was performed in the weeks following uCMS exposure and covered three dimensions: anxious-like behavior tested in Elevated Plus Maze (EPM), mood assessed in the Tail Suspension Test (TST) and cognition evaluated in the Novel Object Recognition (NOR).

The biometrical assessment showed a significant impact of stress on body weight gain at week 6 of the uCMS protocol (Figure 4.2A; $F_{1, 22} = 24.02$, $p < 0.0001$). Moreover, an interaction between stress exposure and genotype was found ($F_{1, 22}=4.464$, $p = 0.046$), which was related to a smaller body weight gain in uCMS-exposed mice. Surprisingly, Sidak's *post hoc* comparison revealed that WT-uCMS mice significantly lost weight after 6 weeks of uCMS exposure ($t_{22} = 5.162$, $p < 0.0001$), while IP_3R2 KO-uCMS mice did not. Regarding self-care, our results showed that exposure to stress significantly impacted WT-uCMS coat

state, at week 6, (Figure 4.2B, $t_{22} = 3.666$, $p = 0.003$), but the same was not observed for IP_3R2 KO-uCMS mice. Serum corticosterone measurements, a proxy of hypothalamic-pituitary-adrenal (HPA) function, revealed a significant effect of uCMS exposure during 6 weeks (Figure 4.2C, $F_{1, 22} = 7.465$, $p = 0.012$). However, *post hoc* analysis shows no differences between groups, pointing to a similar stress impact on corticosterone levels in WT and IP_3R2 KO-uCMS mice. Altogether, our results show that both WT and IP_3R2 KO mice exposed to uCMS present a dysregulation in corticosterone levels, reflecting the efficacy of chronic stress protocols. In sum, mice that lack IP_3-dependent astrocytic Ca^{2+} signaling display a remarkable resilience to the establishment of the depressive phenotype, as shown by body weight maintenance and an increased self-care, even in the presence of a HPA-axis dysregulation.

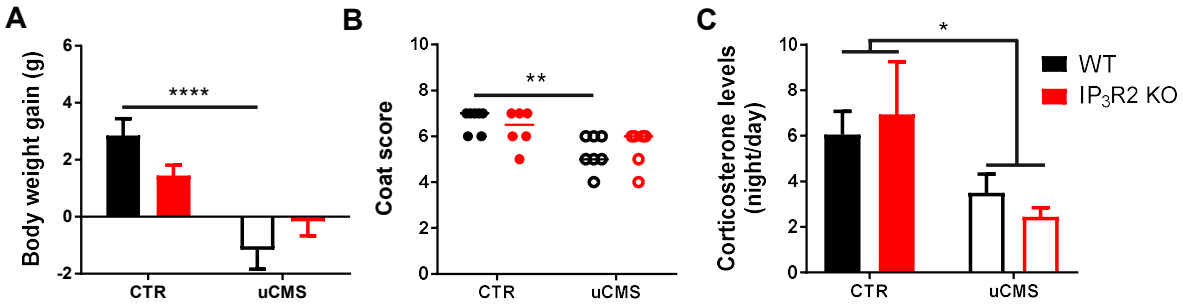

Figure 4.2 – Exposure to uCMS induces reduction of body weight and deteriorates self-care in WT, but not IP_3R2 KO mice.

(A) Body weight gain in WT and IP_3R2 KO mice from control and uCMS-exposed groups after 6 weeks of uCMS exposure. (B) Coat score assessment in WT and IP_3R2 KO mice from control and uCMS-exposed groups after 6 weeks of uCMS exposure. (C) Night/day ratio of corticosterone levels in the serum of WT and IP_3R2 KO mice from control and uCMS-exposed groups after 6 weeks of uCMS exposure. WT mice represented in black and IP_3R2 KO mice in red dots and bars. CTR group is represented in filled and uCMS group is represented in empty dots/bars. Body weight gain and corticosterone levels are plotted as mean ± SEM. Coat score is plotted as median. n=6–7 per group. * $p < 0.05$, ** $p < 0.01$, **** $p < 0.0001$

Lack of IP_3R2-dependent astrocytic calcium signaling prevents an anxious-like phenotype after uCMS exposure

Stress is associated with complex interactions between distinct behavioral domains as anxiety, mood, and cognition (Bessa et al. 2009b). We assessed anxiety-like behavior in the EPM (Figure 4.3A). Our results show a similar performance for both groups regarding the percentage of entries in open arms. However, a significant effect of genotype was found in the percentage of time spent in open arms ($F_{1, 22} = 7.204$, $p = 0.014$), which may be accounted by a pronounced decrease in the percentage of time spent in open arms observed in WT-uCMS exposed animals as compared with WT-CTR littermates ($t_{22} = 2.747$, $p = 0.023$). On the contrary, IP_3R2 KO-uCMS mice spent a similar time in open arms when compared with their IP_3R2 KO-CTR counterparts. Next, we performed a behavioral assessment for a depressive-like phenotype in the TST (Figure 4.3B). In this test, we analyzed the latency to immobility and the percentage of immobility as a measure of learned helplessness. We observed no differences between groups neither for latency to immobility, nor for immobility percentage. These results indicate that the

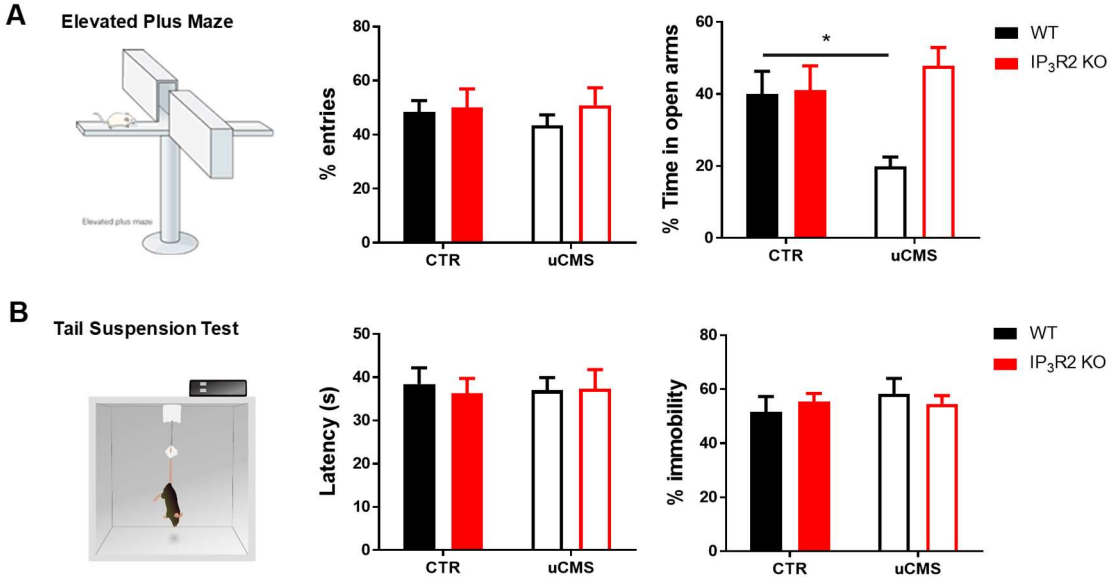

Figure 4.3 – Assessment of anxious- and depressive-like behavior in WT and IP_3R2 KO mice exposed to uCMS and respective non-stressed controls.

(A) Elevated Plus Maze (EPM) test shows the percentage of entries and time spent in the open arms of the maze; (B) Tail Suspension Test (TST) evaluates latency to immobility and the percentage of time immobile in the last 4 min of testing. WT mice are represented in black bars and IP_3R2 KO mice in red bars. CTR mice are represented in filled bars; uCMS-exposed mice are represented in empty bars. n=6–7 per group. Data plotted as mean ± SEM, * $p < 0.05$. Representative images obtained from https://neurology.mhmedical.com/data/books/1049/kan_ch63_f010.png (EPM) and https://www.creative-biolabs.com/drug-discovery/therapeutics/tail-suspension-test.htm (TST).

protocol used for uCMS exposure during 6 weeks was unable to induce a depressive-like state in WT, and thus we cannot conclude any effect on this dimension regarding IP_3R2 KO mice.

Next, we aimed at evaluating the impact of uCMS protocol in the cognitive dimension. For that, we performed the NOR test to assess spatial recognition (Figure S 4.1A) and long-term memory (Figure S 4.1B). Spatial recognition was evaluated by displacing one of the familiar objects, presented 1 hbefore, to the opposite side of the box. We found no differences in the performance of this task between WT and IP_3R2 KO mice from both groups. In accordance, when a familiar object was replaced by a novel one 24 h later both groups performed similarly.

In summary, our results show that uCMS exposure was able to induce an anxious-like phenotype in WT mice, but not in IP_3R2 KO mice. However, exposing mice to an uCMS protocol during 6 weeks was unable to affect or indicate genotype-related effects in depressive-like behavior and cognition, at least for the behavioral paradigms tested.

Discussion

In this work, we addressed the influence of IP_3R2-dependent astrocytic Ca^{2+} signaling in the context of depression. Growing evidence has shown that astrocytes undergo morphological and cell number alterations in depressive patients and in animal models of depression (Gosselin et al. 2009; Rajkowska and Stockmeier 2013; Rial et al. 2015; Wang et al. 2017). Astrocytes are actively involved in the modulation of synaptic function in brain regions affected by depression. While previous observations have suggested roles for astrocytic Ca^{2+} signaling in neurological and psychiatric diseases (Nedergaard et al. 2010), it is still missing to what extent astrocytic Ca^{2+} signals contribute to the installation and/or propagation of such pathologies (Shigetomi et al. 2016). Interestingly, recent studies reported a beneficial effect of IP_3R2 genetic deletion in cases of brain insult or neurodegeneration (Li et al. 2015; Reichenbach et al. 2018). These results, together with our observations of cognitive enhancement in adulthood (Chapter 3), prompted us to test a putative protective role of IP_3R2-dependent Ca^{2+} signaling in a chronic stress model that mimics anxious-like and depressive-like behavior of humans.

Firstly, we applied an already validated protocol that mimics the biological correlates of depression – the uCMS protocol (Bessa et al. 2009a; Surget et al. 2011; Nollet et al. 2013; Gosselin et al. 2017). Our results indicate that we were able to induce a stress-response in WT mice on a C57BL/6J background, characterized by alterations in the anxious-state of these animals. However, the exposure of IP_3R2 KO mice to uCMS revealed a surprising resilience to the deleterious effects of chronic stress. More

specifically, this resilience consisted of less body weight loss, more self-care behavior and reduced anxious-like phenotype, as observed in non-stressed IP_3R2 KO mice.

The available literature concerning the emotional consequences of the IP_3R2 gene deletion are rather controversial. A previous study reported that control IP_3R2 KO mice displayed a depressive-like behavior. The authors claim that this phenotype was due to decreased levels of astrocytic ATP release (Cao et al. 2013). Although we have not addressed the levels of gliotransmitters release from IP_3R2 KO astrocytes, we observed that IP_3R2 KO mice on a C57BL/6J background do not display a depressive-like phenotype (Chapter 3). In concomitance, the conditional deletion of IP_3R2 specifically in astrocytes did not induce a depressive phenotype (Petravicz et al. 2014). In their study, Cao et al. (2013) employed several mouse models generated under distinct backgrounds. Therefore, the generation of mouse models with consistent genetic background and cellular specificity might help to clarify these observations (Oliveira et al. 2015). Another study reported that IP_3R2 KO mice display increased learned helplessness after exposure to a chronic restraint stress (CRS) protocol (Monai et al. 2016). The CRS protocol consists of a repeated exposure to the same stressor. Protocols related to this paradigm display a high variability concerning its duration and extension (Moreira et al. 2016), which is critical for the impact of chronic stress. The CRS protocol might lead to distinct readouts as compared with the uCMS protocol. Beery and Kaufer (2015) discussed that stress response is influenced by a myriad of factors such as the time, nature and severity of the stressor. The protocol applied by Monai and co-workers (2016) subjected mice to an extensive period out of their homecages with no access to food or water, which is much more aggressive for mice. We believe that, by employing unpredictability of the presentation of distinct psychological and physical stressors we are testing a condition closer to daily life stress faced by humans.

Body weight variations and coat state score are commonly used measures of stress efficacy in rodents (Nollet et al. 2013). We observed that, after 6 weeks of stress exposure, WT mice presented a significant body weight loss and coat state deterioration. Contrarily, IP_3R2 KO-uCMS mice presented resilience to body weight variations and a better coat state. This result should not be due to metabolic alterations occurring in IP_3R2 KO mice that could influence its body weight *a priori*, since our group and other studies confirmed that healthy IP_3R2 KO mice gain weight similarly to WT littermates (Li et al. 2015; Pinto-Duarte et al. 2019). Body weight analysis should be considered as a measure for uCMS effectiveness, and not as a predictor of a certain behavioral response to it. For instance, Tau-KO mice display a reduction in body weight similar to the WT when exposed to stress. Even so, these mice display a protected response to stress in several behavioral domains, while WT mice reveal the deleterious stress effects (Lopes et al. 2016).

A stressful event, either with low or high intensity, influences self-grooming behavior in rodents (Kalueff and Tuohimaa 2005). Our results demonstrate that IP_3R2 KO mice still display an interest for taking care of its fur state, whether WT littermates exposed to uCMS do not. The decreased coat score in WT mice goes in line with previous descriptions of a significant deterioration of the fur state after uCMS exposure (Ibarguen-Vargas et al. 2008). Here, we observed that interfering with IP_3R2-dependent Ca^{2+} signaling prevented the deterioration of the coat state after uCMS exposure. A similar observation was found in stressed mice treated with an antidepressant, fluoxetine, which reversed the uCMS detrimental effect on coat state (Nollet et al. 2013).

Chronic stress may affect distinct behavioral domains and dysregulate the HPA axis (de Kloet et al. 2005). As a result, disturbed corticosterone (CORT) levels are observed in mouse and rat models of depression (Monteiro et al. 2015; Patricio et al. 2015; Silva et al. 2018). Our results show that both genotypes presented a disruption in the healthy night/day ratio of CORT production in response to uCMS. These evidences suggest that the observed resilience to stress in IP_3R2 KO mice is not due to preservation of the HPA axis rather it should appear downstream. CORT could act, at least partilly via astrocyte activation, and by silencing the global astrocyte Ca^{2+} signaling we could be blocking the deleterious pathways. Indeed, several studies showed that astrocytes express functional glucocorticoid receptors and might be key players in the development of the anxious-like phenotype (Tertil et al. 2018).

Exposure to the 6-week uCMS protocol influenced anxious-like behavior in WT-uCMS mice, but IP_3R2 KO-uCMS mice were able to cope with it. Specifically, WT-uCMS mice spent less time in the open arms of the EPM, as compared with their control counterparts. Contrarily, IP_3R2 KO mice exposed to uCMS display a similar exploration time of the open arms as compared to control IP_3R2 KO mice. Different mouse models lacking IP_3R2-dependent signaling were reported by several labs to be devoided of a basal anxious-like phenotype (Tanaka et al. 2013; Petravicz et al. 2014; Pinto-Duarte et al. 2019). Therefore, the observed prevention of an uCMS-triggered anxious-like phenotype should be related with an IP_3R2-dependent response to stress.

Despite having found a resilient response to anxiety-like behavior in IP_3R2 KO mice, we were unable to observe a depressive-like phenotype or cognitive impairments in stressed mice from both genotypes. Depressive-like behavior was evaluated by TST. Both Forced Swimming Test and TST were considered pivotal tests to assess the validity of novel antidepressants. However, the relevance of immobility time in the context of depression is still under debate (Cryan and Holmes 2005). Therefore, coat state assessment emerged as a good measure for depressive-like behavior, and further demonstrated a

reversal effect following antidepressant treatment in uCMS mice (Santarelli et al. 2003; Nollet et al. 2013). In the future, this evaluation should be combined with a behavioral paradigm to assess anhedonia, such as the sucrose preference test, since both behavioral domains were shown to be correlated in depression (Bessa et al. 2009b).

Regarding cognition, our results suggest that the chronic stress exposure failed to induce a phenotype of cognitive decline (Monteiro et al. 2015). Further studies, using different chronic stress protocols should be used to assess the relevance of astrocytic Ca^{2+}-dependent signiling to support cognitive function.

Overall, our results show that exposure to uCMS for 6 weeks was able to induce physiological and behavioral changes in WT mice. Surprisingly, IP_3R2 KO-uCMS mice show less anxious-like behavior, maintain their weight and display more self-care, similarly to their non-stressed counterparts. This behavioral screening gathered relevant information on the role of astrocytic Ca^{2+} signaling in the function of healthy and stressed animals. These findings suggest that IP_3R2-dependent Ca^{2+} signaling is required for the cellular mechanisms underlying the depressive pathology and that identifying key modulators for astrocytic function may afford for new therapeutic opportunities in the context of depression.

Author Contributions

SGG designed the study, performed and analyzed the experiments and wrote the manuscript; ARMS designed the study and performed the experiments; NDA and ELC helped with the uCMS protocol and behavioral tests; NS, LP and JFO supervised the study, secured funding, analyzed the data and wrote the manuscript.

Supplementary figure

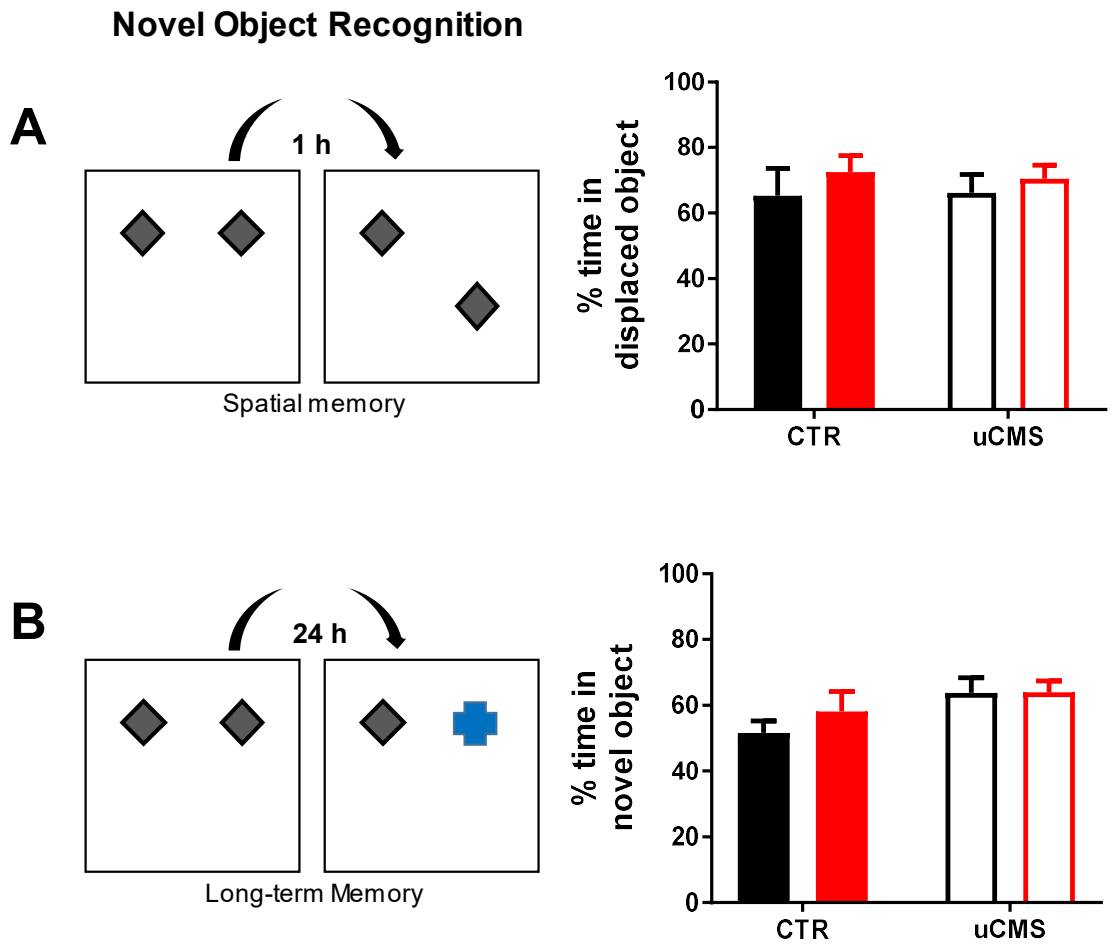

Figure S 4.1 - Exposing WT and IP_3R2 KO mice to an uCMS protocol do not have an impact in cognitive performance assessed by the Novel Object Recognition test.

(A) Spatial recognition memory was evaluated by assessing the percentage of time spent exploring the displaced object. (B) Long-term memory was evaluated by assessing the percentage of time spent exploring the novel object. WT mice are represented in black bars and IP_3R2 KO mice in red bars. CTR mice are represented in filled bars; uCMS-exposed mice are represented in unfilled bars. n=5–7 per group. Data plotted as mean ± SEM.

CHAPTER 5

Sónia Guerra-Gomes, João Filipe Viana, Diana Sofia Marques Nascimento, Joana Sofia Correia, Vanessa Morais Sardinha, Inês Caetano, Nuno Sousa, Luísa Pinto, João Filipe Oliveira

The role of astrocytic calcium signaling in the aged prefrontal cortex

Frontiers in Cellular Neuroscience 12(379). doi: 10.3389/fncel.2018.00379

(2018)

Title

The Role of Astrocytic Calcium Signaling in the Aged Prefrontal Cortex

Authors

Sónia Guerra-Gomes[1,2], João Filipe Viana[1,2], Diana Sofia Marques Nascimento[1,2], Joana Sofia Correia[1,2], Vanessa Morais Sardinha[1,2], Inês Caetano[1,2], Nuno Sousa[1,2], Luísa Pinto[1,2], João Filipe Oliveira[1,2,3]

Affiliations

1 - Life and Health Sciences Research Institute (ICVS), School of Medicine, University of Minho, 4710-057 Braga, Portugal

2 - ICVS/3B's - PT Government Associate Laboratory, Braga/Guimarães, Portugal

3 - IPCA-EST-2Ai, Applied Artificial Intelligence Laboratory, Polytechnic Institute of Cávado and Ave, Campus of IPCA, Barcelos, Portugal

Corresponding author:

João Filipe Pedreira de Oliveira (PhD), Life and Health Sciences Research Institute (ICVS), School of Medicine, University of Minho, Campus de Gualtar, 4710-057 Braga, Portugal, Tel: +351-253-604871, Fax: +351-253-604809, joaooliveira@med.uminho.pt

ACKNOWLEDGMENTS

The authors acknowledge J. D. Silva for helpful comments on the manuscript. They are grateful to Prof. Alfonso Araque and Prof. Ju Chen for sharing the mice line. The authors acknowledge funding from national funds through Foundation for Science and Technology (FCT) fellowships (SFRH/BPD/97281/2013 to JO, SFRH/BD/101298/2014 to SG, IF/00328/2015 to JO, IF/01079/2014 to LP, and SFRH/BD/133006/2017 to IC); Marie Curie Fellowship FP7- PEOPLE-2010-IEF 273936 and BIAL Foundation Grants 207/14 to JO and 427/14 to LP; Northern Portugal Regional Operational Programme (NORTE 2020), under the Portugal 2020 Partnership Agreement, through the European Regional Development Fund (FEDER) (NORTE-01-0145-FEDER-000013); FEDER Funds, through the Competitiveness Factors Operational Programme (COMPETE) and The National Fund, through the FCT (POCI-01-0145-FEDER-007038).

Abstract

Aging is a lifelong process characterized by cognitive decline putatively due to structural and functional changes of neural circuits of the brain. Neuron-glial signaling is a fundamental component of structure and function of circuits of the brain, and yet its possible role in aging remains elusive. Significantly, neuron-glial networks of the prefrontal cortex undergo age-related alterations that can affect cognitive function, and disruption of glial calcium signaling has been linked with cognitive performance. Motivated by these observations, we explored the possible role of glia in cognition during aging, considering a mouse model where astrocytes lacked IP_3R2 - dependent Ca^{2+} signaling. Contrarily to aged wild-type animals that showed significant impairment in a two-trial place recognition task, aged IP_3R2 KO mice did not. Consideration of neuronal and astrocytic cell densities in the prefrontal cortex, revealed that aged IP_3R2 KO mice present decreased densities of $NeuN^+$ neurons and increased densities of $S100\beta^+$ astrocytes. Moreover, aged IP_3R2 KO mice display refined dendritic trees in this region. These findings suggest a novel role for astrocytes in the aged brain. Further evaluation of the neuron-glial interactions in the aged brain will disclose novel strategies to handle healthy cognitive aging in humans.

Keywords

aging, astrocyte, calcium signaling, IP_3R2, prefrontal cortex, spatial recognition, dendritic morphology

Introduction

Aging associates cognitive decline involving decrease of attention, working memory capacity, inhibitory control, and speed processing (Rajah and D'Esposito 2005; Grady 2008; Bizon et al. 2012). Several factors may contribute to the installation of selective cognitive impairments. Recent literature suggests that changes in cellular morphology, signaling, and gene expression may disrupt the network dynamics of aged prefrontal circuits, leading to cognitive dysfunction (Burke and Barnes 2006). While the available literature agrees that changes in neuronal structure are tightly linked to cognitive alterations, there is still controversy in the field regarding the type of morphological changes that occur (Konsolaki and Skaliora 2015). This controversy may be partially justified by the biological variability of subjects and brain populations across the long-lasting aging process, as well as the variety of experimental approaches used for the analysis (Engle and Barnes 2012; Lemaitre et al. 2012; Jagust 2013). Moreover, recent reports highlight age-dependent changes in glial signaling that could modulate network computation with impact in cognitive performance (Soreq et al. 2017; Boisvert et al. 2018). Being the most abundant type of glial cell in the central nervous system, astrocytes can sense, process and respond to incoming signals, modulating the extracellular milieu and transmission of neural signals (Araque et al. 2014). Significantly, astrocytes seem crucially involved in structural and functional integrity of neural circuits of the prefrontal cortex (PFC) – a brain area chiefly involved in cognition – related tasks that are affected by aging. Ablation of PFC astrocytes for example, results in detrimental effects in different behavior domains. Specifically, astrocyte ablation in this region induces an anxious and depressive phenotype (Banasr and Duman 2008) and is responsible for impairments in spatial working memory, attention, and behavioral flexibility (Lima et al. 2014). Although astrocytic features during both development and adulthood are well studied, its implications for the aging brain are still poorly understood. Together with microglia, astrocytes may exert beneficial or detrimental influence onto neuronal circuits and therefore impact the aging process (Lynch et al. 2010). Recently, it was shown that neuron-glia signaling remains conserved during brain aging and that astrocytic intracellular calcium (Ca^{2+}) elevations are maintained during lifetime (Gomez-Gonzalo et al. 2017). This is important since astrocytes respond to synaptic activity by increasing their intracellular Ca^{2+} levels within a spatio-temporal scale (Araque et al. 2014; Volterra et al. 2014). This physiological hallmark of the astrocytic response has a functional impact in several brain regions, specifically in synapses, circuits, and behavior (Oliveira et al. 2015; Guerra-Gomes et al. 2017). Astrocytic Ca^{2+} signaling (and Ca^{2+}-dependent pathways) is intimately involved in the control of synaptic transmission and plasticity in brain regions responsible for learning and memory processing (Henneberger et al. 2010; Tanaka et al. 2013), however, the direct cognitive consequences are still poorly understood (Guerra-Gomes et al. 2017). Ca^{2+}

elevations in astrocytes range from global Ca^{2+} elevations in the soma to focal Ca^{2+} events at thinner processes (Kanemaru et al. 2014; Srinivasan et al. 2015; Agarwal et al. 2017; Bindocci et al. 2017; Stobart et al. 2018; Yu et al. 2018). A predominant component of this signaling is by the Ca^{2+} release from the endoplasmic reticulum via IP_3 receptor channels (IP_3Rs) (Volterra et al. 2014; Bazargani and Attwell 2016). With this regard, immunohistochemistry and transcriptomic analysis revealed that type 2 IP_3Rs (IP_3R2) are mainly expressed in astrocytes (Sharp et al. 1999; Hertle and Yeckel 2007; Takata et al. 2011; Zhang et al. 2014; Li et al. 2015). They are the major source of ER-dependent global astrocyte Ca^{2+} , and mice lacking IP_3R2 display "silent" astrocytes with minimal Ca^{2+} elevations in the soma and main processes (Petravicz et al. 2008; Takata et al. 2011; Navarrete et al. 2012). Leveraging on these findings, we study cognitive performance of IP_3R2 KO mice to explore on the importance of IP_3R2-dependent Ca^{2+} signaling in astrocytes during aging. Our results show that aged IP_3R2 KO mice display a preserved cognitive performance in a PFC dependent task, along with neuronal dendritic refinement and reduced neuron- to-astrocyte ratios in this brain region.

Materials and Methods

Animals

All experimental procedures were conducted in accordance with the guidelines described in Directive 2010/63/EU and were approved by the local ethical committee (SECVS 075/2015) and Portugal national authority for animal experimentation (DGAV 17469/2012). IP_3R2 KO mice were kindly supplied by Prof. Alfonso Araque (University of Minnesota, United States) (Navarrete et al. 2012), under agreement with Prof. Ju Chen (University of San Diego, United States) (Li et al. 2005). Mice were backcrossed to C57BL/6J for at least five generations in our lab. IP_3R2 KO and their respective littermate wild-type (WT) controls were obtained by mating $IP3R^{2+/-}$ mice. Male WT and IP_3R2 KO mice of 2- to 3-month-old (adults) and 18- to 19-month-old (aged) were used for the experiments. They received an individual tag, which remained unaltered throughout the experiment and allowed to perform the behavioral and histological evaluation in a blind manner. All mice had ad libitum access to food and water in their home cages and lights were maintained on a 12 h light/dark cycle (lights on 8:00 A.M. to 8:00 P.M.) at 22 ± 1◦ C, 55% humidity.

Two-Trial Place Recognition Task

The Y-maze two-trial place recognition (2TPR) task evaluates spatial recognition memory, a form of episodic-like memory, by taking advantage of the innate propensity of rodents to explore novel

environments, as previously described (Sardinha et al. 2017). The maze was composed by three equal arms (33.2 L × 7 W × 15 cm H), made of white Plexiglas. To increase spatial recognition and navigation, the end of each arm contained a visual cue. Each mouse was initially placed at the end of the Start (S) arm and it was allowed to freely explore this arm and an additional arm (Familiar arm, F) for 5 min. In the second trial, a divider was removed allowing the exploration of a novel (N) arm, and each mouse was allowed to explore the three arms for 2 min for memory retrieval. The test was performed in dim light conditions and the maze was cleaned with 10% ethanol between subjects. All trials were acquired and analyzed using a video-tracking system (Videotrack; Viewpoint) and the EthoVision XT 12 software (Noldus, Netherlands). Data was expressed as a discrimination index (D.I.) of time and distance, calculated for the distal third of each arm using the following equation (1):

$$D.I. = \frac{Novel - \frac{Start + Familiar}{2}}{Novel + \frac{Start + Familiar}{2}} \quad (1)$$

A positive D.I. indicates preference for the novel arm, meaning that mice retained a memory of the arms previously explored (start and familiar), and therefore display a better spatial recognition performance.

Tissue Processing and Immunohistochemical Analysis

Mice were anesthetized with a mixture of ketamine (75 mg/kg, i.p.; Imalgene 1000, Merial, United States) and medetomidine (1 mg/kg, i.p.; Dorbene Vet, Pfizer, United States), and transcardially perfused with 0.9% saline. Brains were carefully removed, fixed overnight with 4% paraformaldehyde and immunofluorescence experiments were performed in cryostat coronal brain sections (20 μm thick). Sections were incubated overnight with the primary antibodies: rabbit anti-S100β (1:200, DakoCytomation; AB_2315306) and rabbit anti-NeuN (1:100, Cell Signaling Technology; AB_2651140). In the next day, incubation with the secondary antibody Alexa Fluor® 594 donkey anti-rabbit (1:1000, Thermo Fisher Scientific; AB_2556543) was carried out. Images were acquired in an Olympus Fluoview FV1000 confocal microscope (Olympus, Hamburg, Germany), and the number of $S100\beta^+$ and $NeuN^+$ cells was calculated using the ImageJ plugin – "Cell counter[1]".

Three Dimensional-Reconstruction of mPFC Layer V Pyramidal Neurons

Three dimensional (3D) dendritic morphology was assessed in Golgi-Cox stained material as previously described (Lima et al. 2014). mPFC layer V pyramidal neurons were analyzed for the following dendritic

[1] http://fiji.sc/Fiji

features: length, arborization, Sholl analysis and spine number and classification. Briefly, at least five neurons were analyzed for each animal by using a motorized microscope controlled by the Neurolucida software (MBF Bioscience, United States) under 100× magnification. Dendritic spine densities were assessed in randomly selected dendritic segments of 30 µm, in the proximal and distal portions of the apical dendrite and in the proximal portion of the basal dendrite. Moreover, spines were classified into four categories: thin, mushroom, thick, and ramified. The extraction of data for both reconstructed neurons and spines was performed by using NeuroExplorer software (MBF Bioscience, United States).

Statistical Analysis

Statistical analysis was performed using the GraphPad Prism 6.01 (GraphPad Software Inc., United States). All data analyzed passed the D'Agostino and Pearson normality test for Gaussian distributions. Two-way analysis of variance (ANOVA) with Sidak *post hoc* test was applied to analyze the performance in the Y-maze 2TPR, cell densities, neuronal length, and endings, considering either factor: genotype or age. Two-way ANOVA with Tukey's multiple comparisons test was used to analyze Sholl analysis data for neuronal 3D reconstructions. Data are presented throughout the manuscript as mean ± SEM (Standard Error of the Mean) and results were considered significant for $p < 0.05$.

Results

Lack of IP_3R2-Dependent Astrocytic Calcium Prevents Age-Related Cognitive Decline

We tested the performance of both WT and IP_3R2 KO mice (adult and aged) in a PFC-dependent task. We performed the 2TPR task which evaluates spatial recognition memory in mice, based on their natural drive to explore novelty (Figure 5.1). This test has the advantage of being physically less demanding, and therefore more suitable to assess cognition in aged mice (Pistell et al. 2012; Dolgin 2013). Our results show that aged WT mice display a deficit in recognition memory, since they retain less memory of the familiar arms and fail to discriminate the novel arm when compared to their adult WT littermates (Figure 5.1A,B; Sidak *post hoc* test; $p < 0.05$). Surprisingly, this deficit in spatial recognition memory is not observed in aged IP_3R2 KO mice, as those animals explored the novel arm longer, similarly to their adult counterparts (Figure 5.1A,B). In accordance, aged WT mice walk less distance in the novel area than their adult WT littermates (Figure 5.1A,C; Sidak *post hoc* test; $p < 0.05$), a deficit not observed in aged IP_3R2 KO mice. The Sidak *post hoc* comparison between genotypes discarded any significant difference for both measures (time or distance), excluding an effect of IP_3R2 KO in the performance between adult or aged mice in this experimental setup. Importantly, tested mice equally explored the maze during the

task, as given by their total distance traveled (Figure 5.1D) and number of arm entries (Figure 5.1E), regardless of their genotype or age, hence excluding any age-related loss of their natural exploratory drive.

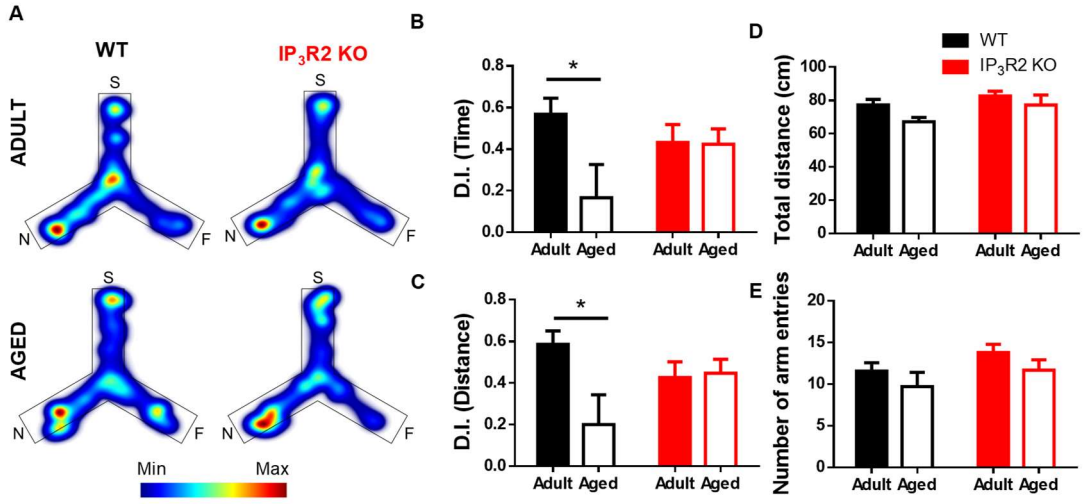

Figure 5.1 - Lack of IP_3R2-dependent astrocytic calcium prevents age-related cognitive decline in a PFC-dependent task.

(A) Representative heatmaps of cumulative time exploration of start (S), familiar (F), and novel (N) arms of the Y-maze for WT (left, black) and IP_3R2 KO (right, red) mice (warm colors, more time; cold colors, less time); Discrimination index (D.I.) for time (B) and distance (C), representative of the spatial preference for the novel arm in the retrieval trial. (D) Total distance traveled in the maze; (E) Total number of entries in the three arms. Adult mice are represented in filled bars; aged mice are represented in unfilled bars. n= 9–13 per group, two-way ANOVA, Sidak's multiple comparisons test; data plotted as mean ± SEM. $^*p < 0.05$.

Together, these results point out an unpredicted maintenance of PFC-dependent cognitive performance in aged mice that lack IP_3-dependent astrocytic Ca^{2+} signaling.

Aging Leads to a Decrease in Neuronal but Not Glial Densities in IP_3R2 KO Mice

To correlate the observed behavioral phenotype with possible alterations in the populations of neurons and astrocytes, we estimated the density of cells, respectively, stained for $NeuN^+$ and $S100\beta^+$ markers. NeuN is a well-known marker for post-mitotic neurons (Mullen et al. 1992), whereas S100β is a recognized marker for astrocytes (Wang and Bordey 2008). We assessed these cellular densities in layer V of the medial PFC (Figure 5.2A), which is the main prefrontal output to other cortical and subcortical regions involved in cognitive behavior (Opris and Casanova 2014; Naka and Adesnik 2016), and receives a main hippocampal input involved in episodic memory with a strong spatial component (Hoover and Vertes 2007; Barker et al. 2017) required for the performance in the 2TPR task. $S100\beta^+$ cells were

previously shown to colocalize with IP_3R2 in the rodent brain (Sharp et al. 1999; Takata et al. 2011; Li et al. 2015). Our analysis indicated an effect of aging on $NeuN^+$ cell density (Figure 5.2B,D; age: $F_{1,33}$ = 6.192, p = 0.018), which may be accounted by a pronounced decrease of $NeuN^+$ cells observed in aged IP_3R2 KO mice when compared with their aged WT littermates (Figure 5.2D; Sidak *post hoc* test; p < 0.05). Moreover, this reduction in the number of neuronal cells in IP_3R2 KO mice is also significantly different from their adult IP_3R2 KO mice (Sidak *post hoc* test; p < 0.01), that maintain similar cellular densities to WT mice. On the contrary, we found an overall increase of $S100\beta^+$ astrocytes in IP_3R2 KO mice (Figure 5.2C,E; genotype: $F_{1,40}$ = 16.19, p < 0.05). Contrarily to what we observed for neurons, we found an increase in $S100\beta^+$ cells in aged IP_3R2 KO when compared to aged WT mice (Sidak *post hoc* test; p < 0.01). Altogether, these results suggest that lack of age-related cognitive impairment in the absence of IP_3R2-mediated Ca^{2+} signaling in astrocytes, correlates with a different neuron-to-glia ratio in the PFC which could ultimately result either in different neuron-glial circuits, or functional neuron-glia interactions or both.

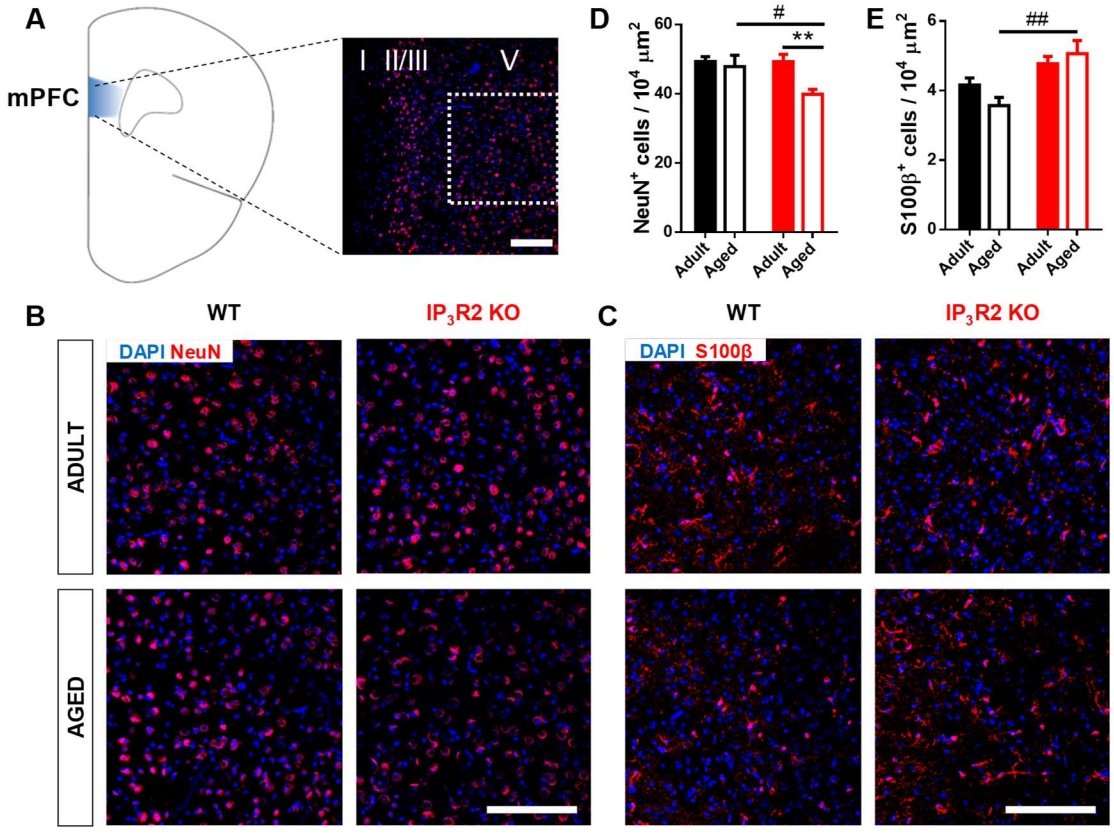

Figure 5.2 - Aged IP_3R2 KO mice display decreased $NeuN^+$ neuron densities and increased $S100\beta^+$ astrocyte densities.

(A) Scheme of the prelimbic subregion of the medial prefrontal cortex (mPFC, blue) and respective layers I, II/III, and V. mPFC layer V (white dash line) corresponds to the area considered for cell counting. (B) Representative mPFC layer V confocal images of DAPI/NeuN labeling for WT and IP_3R2 KO mice (adult and aged). (C)

Representative mPFC layer V confocal images of DAPI/S100β labeling for WT and IP_3R2 KO mice (adult and aged); (A–C) scale bars = 200 μm. (D,E) Densities of $NeuN^+$ (D) and $S100\beta^+$ (E) cells in mPFC layer V of WT and IP_3R2 KO mice (adult and aged; n=8–15 images per group; two-way ANOVA, Sidak's multiple comparisons test). WT (adults and aged) mice are represented in filled/unfilled black bars, whilst IP_3R2 KO (adults and aged) are represented in filled/unfilled red bars. Data plotted as mean ± SEM. $^{\#}$ $p < 0.05$ and $^{\#\#}$ $p < 0.01$ between genotypes and ** $p < 0.01$ between ages.

Aging Leads to a Dendritic Refinement of mPFC Layer V Pyramidal Neurons in IP_3R2 KO Mice

An important component underpinning neuron-glial interaction, is the neuropil morphology to the extent that it may define structural and functional constraints of such interaction (Volterra et al. 2014; De Pitta et al. 2016). With this regard, we considered dendrite morphology for WT vs. IP_3R2 KO and adult vs. aged mice (Figure 5.3A). Significantly, both age and lack of IP_3R2 lead to a decrease in apical dendrite length of 3D-reconstructed Golgi-impregnated neurons (Figure 5.3B; age: $F_{1,42} = 6.340$, $p = 0.016$; genotype: $F_{1,42} = 5.168$, $p = 0.028$), which was accompanied by a reduction of apical endings in mice that lack IP_3R2 ($F_{1,42} = 6.259$, $p = 0.016$). In line with neuronal density data, these effects were caused by the marked reductions of apical dendrites of layer V pyramidal neurons observed in aged IP_3R2 KO mice. Specifically, aged IP_3R2 KO pyramidal neurons display a shorter and less ramified morphology, as compared with aged WT mice (Sidak *post hoc* test; $p < 0.05$). Furthermore, when compared with their adult IP_3R2 KO littermates, aged IP_3R2 KO mice also revealed significantly reduced apical dendritic length (Sidak *post hoc* test; $p < 0.05$). These alterations are detailed by the Sholl analysis data, which revealed an overall effect of radius, genotype and an interaction between these two factors (radius: $F_{22,924} = 41.86$, $p < 0.0001$; genotype: $F_{3,42} = 4.089$, $p = 0.012$; interaction: $F_{66,924} = 1.821$, $p = 0.0001$). Post hoc analysis showed that aged IP_3R2 KO mice display fewer intersections, as compared with aged WT and their adult genotype matches (Tukey *post hoc* test; $p < 0.05$). The analysis of basal dendritic morphology in neurons from the same layer V revealed that although they seem to be also reduced in aged IP_3R2 KO mice, this is only significant in the overall comparison by age and in the detailed Sholl analysis. Specifically, aging seems to lead to dendritic shortening (Figure 5.3C; $F_{1,42} = 7.230$, $p = 0.010$). Moreover, the Sholl analysis revealed a significant effect of radius, genotype and an interaction between factors (radius: $F_{17,714} = 160.4$, $p < 0.0001$; genotype: $F_{3,42} = 3.532$, $p = 0.023$; interaction: $F_{51,714} = 2.055$, $p < 0.0001$). Additional analysis showed a decreased number of intersections around 40–100 μm from the soma in aged IP_3R2 KO, as compared with aged WT and adult IP_3R2 KO mice (Tukey *post hoc* test; $p < 0.05$). Since dendritic remodeling frequently has consequences for spine stability, we further analyzed the implication of IP_3R2-

dependent signaling to spine integrity upon aging. For that, we performed dendritic spine categorization at the apical proximal, apical distal, and basal segments of these neurons (Figure 5.3D,E). We observed the typical distribution of spines in the three dendritic segments, being the thin and mushroom types much more abundant than thick or ramified types: apical proximal ($F_{3,99}$ = 386.1, p < 0.0001); apical distal ($F_{3,99}$ = 312.6, p < 0.0001); basal ($F_{3,99}$ = 250.9, p < 0.0001). Besides this expected spine distribution, aging led to an increase in the mushroom type specifically in the basal dendrites in mice of both genotypes, which was accompanied by a decrease in the densities of thick spines (Tukey *post hoc* test; p < 0.05). This observation was also described previously (Burke and Barnes 2006) and was independent of the lack of IP_3R2.

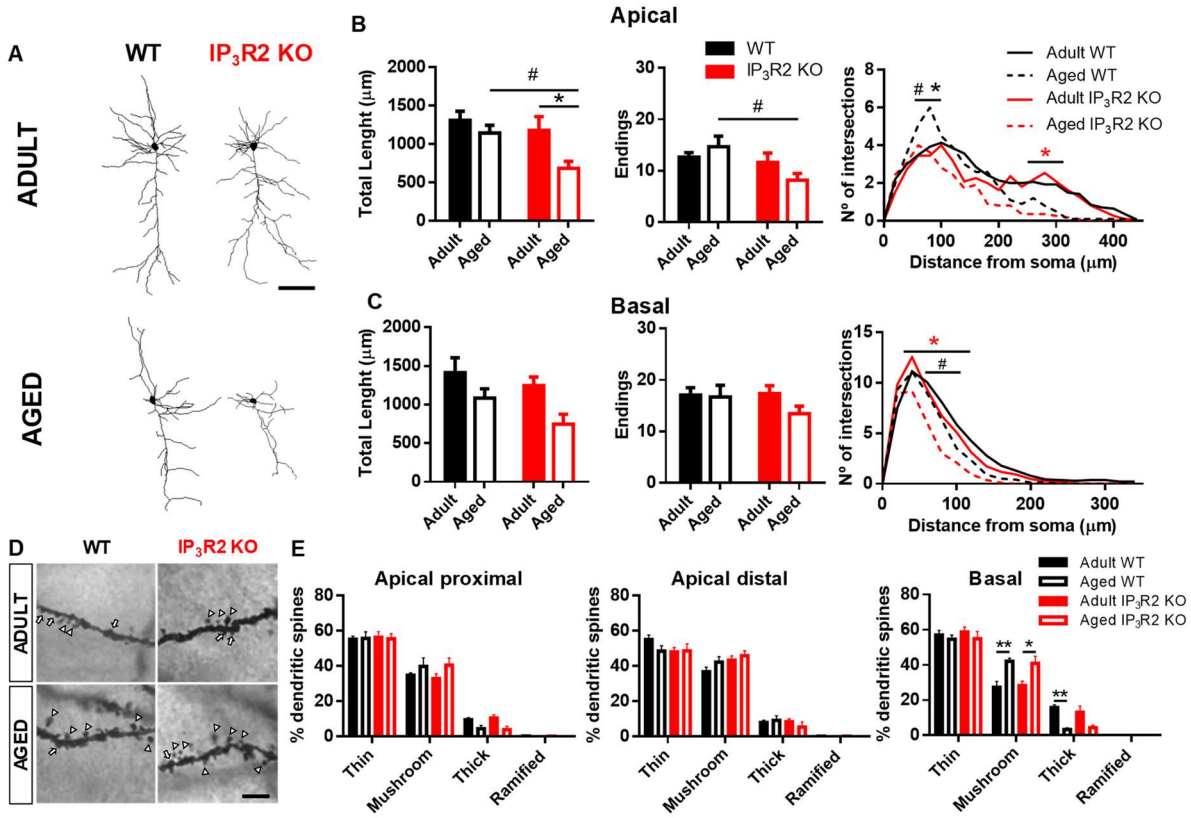

Figure 5.3 - Aging leads to a dendritic refinement of mPFC layer V pyramidal neurons in IP_3R2 KO mice.

(A) Representative 3D reconstructions of layer V mPFC neurons from WT and IP_3R2 KO mice (adults or aged; scale bar = 100 µm). (B,C) Morphological parameters of apical (B) and basal (C) dendrites by assessing total dendritic length, number of endings and Sholl intersections (n=10–14 neurons per group; two-way ANOVA, Sidak's multiple comparisons test). (D) Representative images of basal dendritic segments of each experimental group; scale bar = 5 µm; arrowheads, mushroom-type; arrow, thick-type. (E) Percentage of each spine type at proximal and distal segments of apical dendrites, and basal dendrites (n=6–14 neurons per group; two-way ANOVA, Tukey's multiple

comparisons test). WT (adults and aged) mice are represented either by filled/unfilled black bars or black line/dashed line, while IP_3R2 KO (adults and aged) are represented either by filled/unfilled red bars or red line/dashed line. Data plotted as mean ± SEM. * Denotes the effect of age; # denotes the effect of genotype. Sholl analysis: black * ,refers to difference between WT; red * , refers to difference between IP_3R2 KO; #, * $p < 0.05$; ** $p < 0.01$.

Discussion

In the present study we applied behavioral and morphological approaches to untangle the influence of IP_3R2-dependent astrocytic Ca^{2+} in the aged PFC. We found memory impairment in aged WT mice, which is in accordance with several evidences pointing to a cognitive decline during aging (Rajah and D'Esposito 2005; Grady 2008; Weber et al. 2015). Surprisingly, aged mice that lack astrocyte Ca^{2+} elevations (IP_3R2 KO) perform similarly to WT mice in the same PFC-dependent task, suggesting that astrocytes are involved in the age-related cognitive decline.

Regarding the behavioral observations, the cognitive conservation of aged IP_3R2 KO mice is in line with previous studies using the same mouse model that show a putative role for IP_3R2-dependent Ca^{2+} signaling in neuroprotection and behavior conservation after brain damage (Li et al. 2015; Rakers and Petzold 2017). More importantly, a recent study shows that the deletion of IP_3R2 in a AD model (typically associated with cognitive decline) leads to the retention of spatial learning and memory (Reichenbach et al. 2018). This suggests that astrocyte activity mediated by reticular Ca^{2+} elevations may influence the network structure and function along the aging process. Indeed, Boisvert et al. (2018) demonstrated that in spite of maintaining homeostatic and neurotransmission-regulating genes, aged astrocytes in the cortex partially resemble reactive astrocytes creating an environment permissive to synapse elimination and neuronal damage, possibly contributing to aging-associated cognitive decline.

The available literature appears to agree that normal aging does not lead to major neuronal loss in most cortical regions (Burke and Barnes 2006; Bishop et al. 2010). Besides, the neuron-glia signaling seems to remain conserved during lifespan (Gomez-Gonzalo et al. 2017). Our data are in agreement with these evidences, since both neuronal ($NeuN^+$) and astrocyte ($S100\beta^+$) densities remain unchanged in aged WT mice. Curiously, aged IP_3R2 KO mice – that retain the cognitive ability in a PFC-dependent task – display a reduction in neuronal densities, while astrocyte densities display an inverse tendency in the same region, when compared to the observations of us and others at the adult stage (Li et al. 2015). These findings may be linked since overexpression of astrocyte markers in aged mice has been associated with its detrimental effects to neuronal networks in several cortical areas, namely through astrogliosis (Lynch

et al. 2010; Orre et al. 2014; Rodriguez et al. 2014; Rogers et al. 2017; Boisvert et al. 2018). While healthy aging is linked with mild or subtle morphological changes, pathological aging is rather linked to drastic reductions of neuronal structures (Hof and Morrison 2004; Dickstein et al. 2007; Konsolaki and Skaliora 2015). In this work, aged IP_3R2 KO mice display a marked reduction of dendritic tree complexity, namely in apical dendrites, which appears to be related with the retention of their cognitive abilities as they age. Although our data does not provide a causal link between structural changes (dendritic simplification and different cell densities) and "silenced" age-related astrocyte signals, we believe that the preserved cognitive performance is rather a result of both. These neuronal alterations may result from changes in activation and signaling of a larger number of astrocytes (similarly to a mild astrogliosis), additional glial involvement (i.e., microglia, that play an extensive role in brain aging) (Lynch et al. 2010; Lalo et al. 2014; Das and Svendsen 2015; Verkhratsky et al. 2016b), and homeostatic regulatory mechanisms at the neuron network level (Wefelmeyer et al. 2016). It is noteworthy that our data indicate a great degree of spine stability in aged mice, namely at apical dendrites. Spine distribution and number in the PFC is tightly related with cognitive performance and evolves along the aging process (Burke and Barnes 2006; Holtmaat and Svoboda 2009; Bloss et al. 2011). In basal dendrites, aging triggers a shift to the mushroom type, which refers to a need for synaptic stability and complexity in aged layer V synapses. Nevertheless, this effect was visible in tissue of both WT and IP_3R2 KO mice, which suggests that spine remodeling may not play a relevant role in the observed cognitive maintenance.

Conclusion

In conclusion, the present study demonstrates that silencing the main source of global astrocytic Ca^{2+} leads to a conservation of the cognitive ability along aging. This cognitive resilience appears to be a product of gross neuronal structure refinement, together with an addition of astrocytes to the network. Whether other cell types and/or circuits might be involved in this cognitive maintenance is a matter that should be addressed in the future. Either way, disclosing further the astrocyte roles in the aging brain should be pivotal to provide alternative solutions to prevent or treat cognitive decline in humans.

Author Contributions

SGG, JV, DSMN, JC, VS, and IC designed, performed, and analyzed the experiments; composed the figures; and wrote the manuscript. NS, LP, and JO supervised the study, wrote the manuscript, and secured funding.

CHAPTER 6

General Discussion and Conclusions

Astrocytes respond to excitatory or inhibitory receptor activation with intracellular Ca^{2+} elevations, that may lead to downstream effects, such as release of gliotransmitters with impact in synaptic function. These Ca^{2+} elevations display complex and specific spatio-temporal properties that control synapses, circuits and behavior (Volterra et al. 2014; Guerra-Gomes et al. 2017). Since the emergence of the tripartite synapse concept (Araque et al. 1999), several efforts have been made in the field to develop tools to study the role of astrocytes in the control of higher brain functions, namely by assessing its Ca^{2+} dynamics. From the initial studies using Ca^{2+} dyes in cell culture (Cornell-Bell et al. 1990; Charles et al. 1991), to the development of genetically encoded Ca^{2+} indicators (Shigetomi et al. 2016) a long way has been traveled. However, there is still a longer way to go. For instance, it remains unexplored how different astrocytic Ca^{2+} signals in distinct brain areas could affect brain functioning. Moreover, the association of a diversity of Ca^{2+} sources with the astrocytic response to synaptic modulation is unknown. Until now, the contribution of a Gq-GPCR signaling pathway triggering Ca^{2+} elevations in astrocytes is widely recognized. The activation of this pathway results in the production of the IP_3 molecule, which binds to the IP_3Rs present in the ER and leads to Ca^{2+} release from this intracellular store. In the CNS, the IP_3R2 was proven to be mainly expressed in astrocytes (Sharp et al. 1999; Hertle and Yeckel 2007; Takata et al. 2011; Zhang et al. 2014; Li et al. 2015). It corresponds to the major source of ER-dependent global astrocytic Ca^{2+} and mice lacking this receptor display an impairment in Ca^{2+} elevations mainly in the soma and main processes (Petravicz et al. 2008; Takata et al. 2011; Navarrete et al. 2012).

In this thesis, our main goal was to explore the role of IP_3R2-dependent Ca^{2+} signaling in cortico-limbic function and behavior. Our main findings are summarized in Figure 6.1.

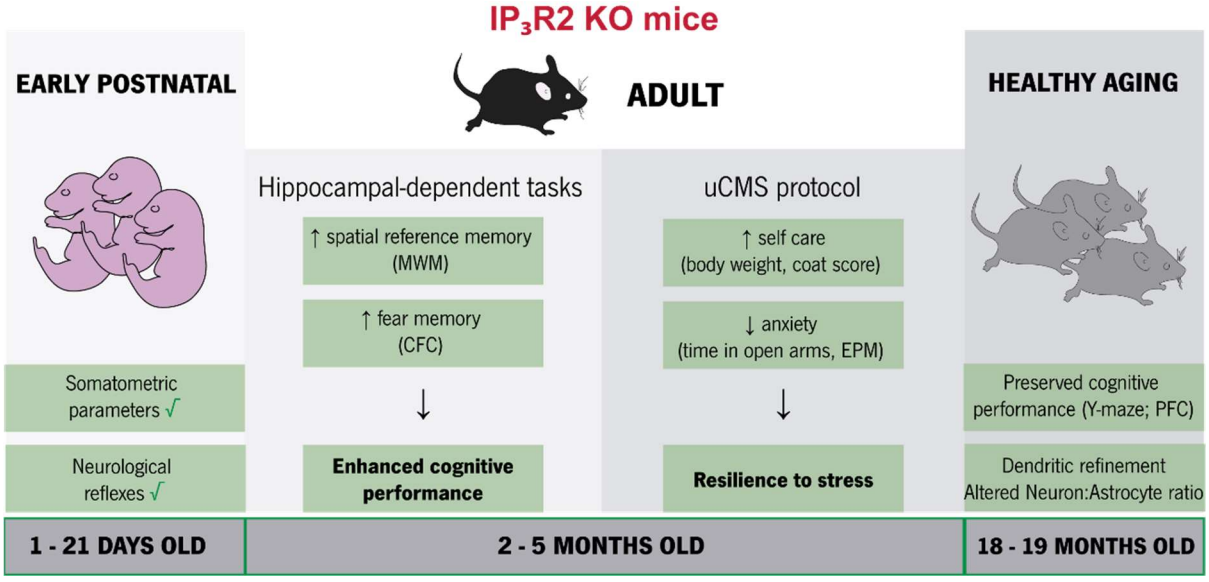

Figure 6.1 – Scheme depicting the behavior characterization performed in IP_3R2 KO mice throughout the lifespan.

We performed a thorough analysis to dissect the impact of global Ca^{2+} signaling in astrocytes during development, adulthood (healthy and in a depression context) and aging. For that, we took advantage of the IP_3R2 KO mouse model that lacks global astrocytic Ca^{2+} signaling. A recent report demonstrated that, by employing a viral tool to genetically drive the continuous extrusion of cytosolic Ca^{2+} in astrocytes, it yielded similar levels of impairment of global Ca^{2+} events, which confirms the functional relevance of the IP_3R2 KO mice (Yu et al. 2018). We backcrossed the IP_3R2 KO mice initially generated by Li et al. (2005) to C57BL/6J for at least five generations, to prevent retinal degeneration associated with the initial Black Swiss background (Clapcote et al. 2005). Moreover, some studies raised the question of possible developmental adaptations occurring in IP_3R2 KO mice, since this model is a constitutive knockout (Petravicz et al. 2014; Yu et al. 2018). This thesis work provided for the first time a demonstration that male and female IP_3R2 KO mice display a normal development, as compared with WT mice (Chapter 2). Therefore, the IP_3R2 KO mouse model is reliable to study the functional impact of global IP_3R2-dependent astrocytic Ca^{2+} elevations in adulthood.

Next, we aimed at evaluating the influence of global Ca^{2+} signaling in astrocytes on brain circuits associated with cognitive function. Astrocytes are recognized partners of neurons in learning and memory processing (Santello et al. 2019). Recent studies have shown that chemogenetic activation of astrocytes on important brain circuits modulates memory performance (Martin-Fernandez et al. 2017; Adamsky et al. 2018; Mederos et al. 2019). However, these studies do not explore the mechanistical contribution of astrocytes during learning and memory processing. Recently, Navarrete et al. (2019) proved that hippocampal NMDAR-dependent LTD depends on astrocytic Ca^{2+} elevations and pointed astrocytic p38α MAPK signaling as an important pathway controlling this phenomenon. There is a clear link between astrocyte Ca^{2+} events and synaptic and brain circuits functioning. However, its involvement in cognitive behavior (e.g. hippocampal-dependent tasks) is still poorly understood (Guerra-Gomes et al. 2017). Therefore, we carried out a battery of cognitive tests and morphological/molecular correlates to confirm the involvement of astrocytic Ca^{2+} signaling in cognitive performance. Our results point to an enhanced cognitive performance of IP_3R2 KO mice that relies on the expression of astrocytic genes related with cytoskeletal organization and dendritic spine formation, and whose expression is being controlled by the transcription factor *Foxo1* (Chapter 3). These observations prompted us to test the potential of global IP_3R2-dependent Ca^{2+} in different contexts characterized by cortico-limbic deficits: stress-related pathologies (Chapter 4) and aging (Chapter 5).

In Chapter 4, we applied the gold-standard uCMS protocol, which is described to impact multidimensional behavioral domains that mimics the human disease. In fact, rats exposed to this stress paradigm display

a strong negative correlation between sucrose consumption and immobility time in the FST, which recapitulates an important link between anhedonia and learned helplessness, both symptoms of depression (Bessa et al. 2009b). We exposed WT and IP_3R2 KO mice to the uCMS paradigm during 6 weeks. Our observations support an important role of IP_3R2-dependent Ca^{2+} signaling in the installation of an anxious-like phenotype after chronic stress exposure.

Finally, we explored the influence of global astrocytic Ca^{2+} signaling in aging (Chapter 5). Although a putative role for IP_3R2-dependent Ca^{2+} signaling in neuroprotection and behavior conservation after brain damage was already described (Li et al. 2015; Rakers and Petzold 2017), little is known about the influence of this astrocytic mechanism in healthy cognitive aging. Recent transcriptomic data demonstrated that aged astrocytes shift their molecular profile to express more inflammatory and synapse elimination-related genes, which could contribute to aging-associated cognitive decline (Boisvert et al. 2018). The PFC is a brain area highly related with cognitive function, and astrocytic dysfunction in this brain area was shown to impact anxious- and depressive-like behavior (Banasr and Duman 2008) and cognitive function (Lima et al. 2014). Our behavioral and morphological analysis revealed that aged IP_3R2 KO mice display a preserved cognitive performance in a PFC-dependent task, which is accompanied by a neuronal dendritic refinement and reduced neuron/astrocyte ratios (Guerra-Gomes et al. 2018).

This thesis provides further insights into the role of IP_3R2-dependent Ca^{2+} signaling in brain function under health and disease conditions. Therefore, we will now discuss specifically the main findings of the present work from early postnatal development, through adult behavior in health and disease, to aging in IP_3R2 KO mice.

IP_3R2 KO mouse model of global astrocytic Ca^{2+} signaling dysfunction displays a normal postnatal development, normal locomotion and exploratory drive in adulthood

In Chapter 2, we performed a developmental evaluation of somatic parameters and neurological reflexes in male and female WT and IP_3R2 KO mice. As far as we know, this is the first attempt to characterize the impact of the constitutive deletion of IP_3R2 during postnatal development. This is an important observation since the reliability of this model was called into question due to negative or controversial results (Oliveira et al. 2015; Guerra-Gomes et al. 2017). We found that IP_3R2 KO mice displayed a similar acquisition of a mature response for all the neurological parameters analyzed, as compared with WT littermates and according to the typical ages described for the appearance of developmental milestones (Heyser 2004). Moreover, IP_3R2 KO mice display a healthy physical maturation. These observations were fundamental to discard any possible developmental alterations that could influence brain function and

behavior performance (Sousa et al. 2006). In this chapter, we also performed a characterization of general motor and exploratory phenotype of adult WT and IP_3R2 KO mice (male and female) in the open field test and in the swimming ability test of the MWM. Our results show that WT and IP_3R2 KO mice of both genders behaved similarly in both tests. These findings support the previous developmental response observed for motor tests and coordination (e.g. open field traversal, walking, negative geotaxis), excluding the implication of motor or exploratory problems in the behavioral analysis and providing the first behavioral observation for IP_3R2 KO female mice.

The IP_3R2 KO mouse model emerged as a promising tool in the field because it lacks spontaneous and agonist-evoked IP_3R2-dependent Ca^{2+} elevations in astrocytes, without interfering with Ca^{2+} signaling in neurons (Petravicz et al. 2008; Navarrete et al. 2012). In the meantime, some studies using this model failed to detect alterations regarding synaptic transmission and plasticity (Petravicz et al. 2008; Agulhon et al. 2010). Moreover, advances in Ca^{2+} imaging techniques revealed that astrocytes display complex spatio-temporal Ca^{2+} properties (Volterra et al. 2014). This complexity is translated into more "global" Ca^{2+} responses (IP_3R2-dependent) or more "focal" [IP_3R2-independent, Ca^{2+} from the mitochondria (Agarwal et al. 2017)], which should be taken into account when drawing conclusions on the results obtained. Functionally, the IP_3R2 KO mouse model is an excellent tool to study the roles of global Ca^{2+} elevations specifically in astrocytes as shown by different labs (Di Castro et al. 2011; Navarrete et al. 2012; Yu et al. 2018; Guerra-Gomes et al. 2018; Mederos et al. 2019; Pinto-Duarte et al. 2019). Now, we showed that blocking astrocytic IP_3R2-dependent Ca^{2+} in development leads to a normal acquisition of age-specific neurological functions. Therefore, the IP_3R2 KO mouse model is suitable for the study of global astrocyte Ca^{2+} in all developmental stages and throughout life.

IP_3R2-dependent Ca^{2+} signaling modulates the performance in hippocampal-dependent tasks through the expression of *Foxo1* downstream targets

In Chapter 2, we found that IP_3R2 KO mice display a normal postnatal development. This made us move forward to assess the functional impact of global astrocytic Ca^{2+} signaling in the healthy brain.

A thorough behavioral characterization revealed that IP_3R2 KO mice on a C57BL/6J background present neither an anxious-, depressive-like phenotype, nor alterations in motor function and coordination, which is in accordance with studies using this mouse model on the same genetic background (Petravicz et al. 2014; Pinto-Duarte et al. 2019). This is a relevant observation on the importance of the mouse strain and the targeted mechanism in behavioral analysis, since it could easily mislead data interpretation (Sousa et al. 2006; Oliveira et al. 2015; Guerra-Gomes et al. 2017).

Our results show that IP_3R2-dependent astrocytic Ca^{2+} signaling modulates cognitive performance, namely in hippocampal-dependent tasks. At the CA1 region, IP_3R2 KO neurons, which are tightly linked to these forms of memory, display an intact dendritic morphology, but an increased thin-to-mushroom spine ratio. Moreover, we found an atrophy of the GFAP-stained structure in IP_3R2 KO astrocytes from the CA1 *stratum radiatum*, which was compensated by an increased number of astrocytes in the same layer. It is known that astrocytes surround synapses by extending their fine protrusions called PAPs. These close connections are pivotal for synaptic remodeling and neural network rewiring (Heller and Rusakov 2015; Zorec et al. 2016). Our molecular analysis revealed two up-regulated genes, *Sdc2* and *Ezr*, which are related with spinogenesis and PAPs morphology (Lin et al. 2007; Heller and Rusakov 2015), mainly expressed in astrocytes (Zhang et al. 2014), and controlled by the most enriched transcription factor *Foxo1* (iRegulon analysis). The IP_3R2 KO mouse model allowed us to explore the influence of Ca^{2+}-related pathways specifically in astrocytes. Our results demonstrated that *Foxo1* was controlling a high number of targets in the hippocampus of IP_3R2 KO mice. However, the mechanism underlying *Foxo1* transcriptional activity in astrocytes remains elusive. The available published data point to a connection between PKC and the regulation of *Foxo1* transcriptional activity. PKC is a Gq-GPCR downstream target and a Ca^{2+}-dependent kinase. Our hypothesis is that in the absence of Ca^{2+}, PKC is not able to activate AKT, allowing *Foxo1* to increase its activity (Kawakami et al. 2004; Barragan et al. 2006; Wu et al. 2009; Kim and Webb 2017) favoring the expression of key target genes, such as *Sdc2* and *Ezr* with impact in spinogenesis and astrocyte process coverage of synapses (Lin et al. 2007; Heller and Rusakov 2015). Based on our molecular data, a detailed assessment of astrocytic morphology in fine processes would be pivotal to provide additional cues on further morphological consequences of IP_3R2-dependent Ca^{2+} signaling in astrocytes.

Dendritic spine remodeling occurs in response to synaptic activity (Bibb et al. 2010; Bosch and Hayashi 2012). In fact, LTP and LTD phenomena influence spine enlargement and shrinkage, respectively (Bourne and Harris 2007; Bosch and Hayashi 2012). Two recent studies explored the role of astrocytes in NMDAR-dependent hippocampal LTD (Pinto-Duarte et al. 2019; Navarrete et al. 2019). Both groups demonstrated that IP_3R2 KO mice display an impaired hippocampal LTD. Specifically, Navarrete et al. (2019) showed that the deletion of p38α MAPK from hippocampal astrocytes impairs LTD, which has an enhancing effect in hippocampal-associated contextual memory. In this thesis, by tackling a distinct signaling pathway, in which FOXO1 was specifically overexpressed in C57BL/6 astrocytes, we were able to mimetize the enhanced fear memory previously observed in IP_3R2 KO mice, confirming an astrocyte role in cognitive modulation through FOXO1 regulated-pathways. However, it remains to explore whether astrocytic FOXO1

overexpression modulates LTD *in vivo*. Wiegert and Oertner (2013) demonstrated that LTD induction in hippocampal CA1 eliminates weaker synapses and those with a higher probability to release are more likely to survive. The LTD mechanism relies on the internalization of AMPA receptors triggered by NMDA receptor activation. It was further demonstrated that interfering with this endocytic process after long-term memory formation prevents the normal forgetting of these memories (Migues et al. 2016). These observations support the hypothesis that LTD impairment in IP_3R2 KO mice could underlie the cognitive enhancement observed in our experiments. It remains to explore the role of astrocytic FOXO1 in synaptic plasticity, since the present study identified it as a key regulator of hippocampal cognitive performance.

Altogether these findings led us to postulate the following hypothesis: 1) IP_3R2-dependent Ca^{2+} signaling regulates *Foxo1* transcriptional activity, which consequently controls the expression of astrocyte-enriched genes, as *Sdc2* and *Ezr*; 2) IP_3R2 KO pyramidal neurons display an intact morphology, but an increased percentage of thin spines, which could be related to the up-regulation of *Sdc2* and *Ezr* function; 3) a higher number of less complex CA1 *stratum radiatum* astrocytes may favor a close proximity between dendritic spines and astrocytic processes; 4) alterations in dendritic spines are related with an altered LTD induction in IP3R2 KO mice; 5) "silencing" IP_3R2-dependent mechanisms favors its transcriptional activity towards the expression of relevant genes and molecular remodeling, which are important events supporting cognitive performance.

To test this hypothesis, we used a viral approach to specifically overexpress FOXO1 in hippocampal astrocytes of naïve C57BL/6 mice. This specific modulation was enough to recapitulate the enhanced fear memory previously observed in IP_3R2 KO mice, confirming an astrocyte role in cognitive modulation through FOXO1 regulated-pathways. Our results suggest that astrocytic Ca^{2+} regulates *Foxo1* transcriptional activity, which ultimately controls cognitive function via morphological changes and synaptic plasticity. The identified gene candidates should be further tested as therapeutic targets for cognitive disabilities, for instance in aging, neurodegenerative disorders or stress-related pathologies.

IP_3R2-dependent Ca^{2+} signaling modulates the stress-response related with self-care and anxiety, but not depressive-like or cognitive behavior

Following our observations that IP_3R2-dependent astrocytic Ca^{2+} signaling is regulating cognitive function in the healthy brain (Chapter 3), we next explored its role upon chronic stress exposure (Chapter 4), which is known to affect, several behavioral domains, namely cognitive and emotional (Bessa et al. 2009b). For that, we took advantage of an already validated protocol that mimics the biological correlates of the

disease – the uCMS protocol (Bessa et al. 2009a; Surget et al. 2011; Nollet et al. 2013; Gosselin et al. 2017). Exposing WT mice to a 6-week uCMS protocol led to several physical, endocrine and behavioral alterations consistent with the induction of a stress response. Surprisingly, exposing IP_3R2 KO mice to uCMS resulted in a resilient response, namely translated by less body weight loss, more self-care and reduced levels of anxiety. It was interesting to observe though, that when exposed to uCMS both genotypes displayed a dysregulated HPA axis response, a typical hallmark of the stress-response (de Kloet et al. 2005). This result suggests that the underlying protective effect of IP_3R2-dependent astrocytic Ca^{2+} signaling on behavior appears downstream of the endocrine dysregulation to stress in WT and IP_3R2 KO mice. Indeed, several studies showed that astrocytes express functional glucocorticoid receptors, whose activation could trigger a Ca^{2+}-dependent pathway that could justify the anxious-like phenotype caused by stress exposure (Tertil et al. 2018).

Still puzzling was the inability to observe alterations in depressive or cognitive behavior either in one or both genotypes after chronic stress exposure. The behavioral test used to assess depressive-like behavior in this study - the TST - is more sensitive to evaluate response to antidepressants (Cryan and Holmes 2005). Therefore, in the future we should consider to perform a behavioral test to evaluate anhedonia (e.g. sucrose preference test), since both behavioral dimensions were shown to be highly correlated with a rodent model of uCMS (Bessa et al. 2009b). On the other hand, we scored the physical state of the fur, which accounts as a good measure for depressive-like behavior (Griebel et al. 2002; Santarelli et al. 2003). In fact, this evaluation revealed that WT mice exposed to uCMS displayed a deterioration of its coat state, but IP_3R2 KO mice did not. The absence of cognitive impairments after 6-weeks of exposure to uCMS in rodents was also previously observed by other studies from our lab (Bessa et al. 2009b; Monteiro et al. 2015). This might indicate that the stressors used in our stress paradigm had no effect on spatial recognition and long-term memory. Therefore, in future experiments we should consider an occasional exposure to a high-impact stressor (e.g. social defeat), which may emphasize depressive and cognitive impairments (Yu et al. 2011). One should bear in mind, that a severer set of stressors might cause a pronounced induction of emotional and cognitive deficits and difficult the reappraisal of the potential of Ca^{2+}-dependent astrocyte signaling to modulate them.

Overall, this behavioral screening gathered relevant information on the role of IP_3R2-dependent astrocytic Ca^{2+} signaling after chronic stress exposure. Our data suggests that astrocytes are an important player in the mediation of stress-induced effects as biometrical alterations and an anxiety-like behavior, which appears to have therapeutic potential and should be further addressed.

Aged mice lacking astrocytic reticular Ca^{2+} display preserved cognitive performance in a PFC-dependent task

The differential cognitive phenotype observed in adult mice led us to assess the evolution of cognitive performance along healthy aging. This work was published in Frontiers in Cellular Neuroscience (Guerra-Gomes et al. 2018). We performed the Y-Maze 2TPR task, which has the advantage of being less physically demanding, and consequently more adjusted to evaluate cognitive function in aged mice (Pistell et al. 2012; Dolgin 2013). Similar to previous observations in aged humans and rodents (Rajah and D'Esposito 2005; Grady 2008; Weber et al. 2015), we found an impaired PFC-dependent cognitive performance in aged WT mice. In opposition, aged IP_3R2 KO mice performed similarly to their adult counterparts, showing a surprising resilience to age-related cognitive decline in this test. This result goes in line with a recent study using an AD mouse model lacking IP_3R2 ($Appps1^{+/-} \times Ip3r2^{-/-}$), which displayed a protected cognitive performance in a spatial reference memory task (Reichenbach et al. 2018).

This striking result led us to address morphological and cellular correlates of network function in the mPFC layer V. This layer contains the major excitatory neurons, responsible for cortical-cortical and cortical-subcortical projections (Tang et al. 2014). This cellular characterization provided evidences for conserved neuronal and astrocyte cell numbers in aged WT mice, as previously described (Burke and Barnes 2006; Bishop et al. 2010; Gomez-Gonzalo et al. 2017). Such result is supported by observations, in both humans and rodents, describing that cognitive decline is more associated with synaptic changes rather than neuronal loss (Berchtold and Cotman 2009). We observed that adult IP_3R2 KO mice have similar neuronal and astrocytic densities in mPFC layer V, as compared with WT littermates, as previously reported (Li et al. 2015). Absence of global astrocytic Ca^{2+} signaling leads to a decreased density of $NeuN^+$ cells in aged mice, which is compensated by an increased number of $S100\beta^+$ cells, and may account for the preserved cognitive performance observed in aged IP_3R2 KO mice.

In Chapter 3, we have performed a morphological characterization of CA1 pyramidal neurons in WT and IP_3R2 KO mice. Here, we took advantage of the same strategy to evaluate mPFC layer V pyramidal neurons, in adult and aged mice. Similar to CA1 pyramidal neurons morphology, we observed no differences between adult WT and IP_3R2 KO mPFC layer V neurons. In opposition, we found no alterations regarding the percentage of dendritic spines in WT and IP_3R2 KO mice. This result is interesting since it points to a region-specific effect of IP_3R2-dependent Ca^{2+} signaling in the mPFC and the hippocampus: while the former display no alterations, the latter has apical dendrites with a higher percentage of immature spines. The present study revealed that aged IP_3R2 KO mice presented a neuronal dendritic refinement in the PFC. This result is in accordance with a recent work from our lab, stating a better

performance in aged rats presenting a shorter dendritic arborization. In fact, animals that were classified as “bad performers” in PFC- and hippocampal-dependent tasks displayed increased dendritic arborization and impaired autophagy (Mota et al. 2019). Curiously, a link between astrocytic function and autophagy was described in cultures of cerebellar cells from a mouse model of a neurodegenerative disease (Kanner et al. 2018). Thus, it would be interesting to look for autophagy markers in the PFC of aged WT and IP_3R2 KO, to correlate possible alterations with dendritic morphology and behavioral results.

Taken together, our results demonstrated an IP_3R2-related maintenance of PFC-dependent behavioral phenotype during aging, which is supported by altered densities of $NeuN^+$ and $S100\beta^+$ cells and a neuronal dendritic refinement in the PFC of aged IP_3R2 KO mice. Considering the results of Chapter 3, FOXO1-related mechanisms could also play a role in the morphology of the aged prefrontal circuits influencing synaptic coverage and signaling, with impact in behavior.

Conclusion and Future Perspectives

The work developed during this PhD thesis demonstrates, for the first time, that interfering with the major source of global Ca^{2+} signaling in astrocytes does not influence postnatal development. Therefore, the IP_3R2 KO mouse model is suitable to study astrocyte involvement in the behavioral response, in all developmental stages and adulthood. Our results highlight an important role of IP_3R2-dependent Ca^{2+} signaling in astrocytes in the regulation of cognitive behavior in the adult and aged brain. In the adult age, we found that IP_3R2 KO mice display an enhanced cognitive performance at hippocampal-dependent tasks. Our results provided the first evidence of a transcription factor, *Foxo1*, which is highly enriched in astrocytes and whose activity seems to be controlled by global Ca^{2+} signaling in astrocytes. *Foxo1* is regulating the expression of relevant astrocytic-related genes in the hippocampus - *Sdc2* and *Ezr* - that have an important role in PAP morphology and spinogenesis (Heller and Rusakov 2015; Hu et al. 2016), which in turn should control synaptic plasticity phenomena to enhance cognitive performance. Moreover, we have provided evidence for the role of astrocytic IP_3R2-dependent Ca^{2+} signaling in the stressed brain. Specifically, we observed that IP_3R2 KO mice display a resilience to physical and anxious-like alterations, typically caused by chronic stress exposure. The disclosure of astrocytic molecular pathways involved in this resilience may add therapeutical advances to improve behavioral deficits related to depression. Finally, in healthy aging, we found that cognitive function dependent on another cortico-limbic area, the PFC, was preserved in mice lacking IP_3R2-dependent Ca^{2+} signaling in astrocytes. These results open a new window in the search for therapeutic targets/mechanisms, specifically in astrocytes, to treat aged-related cognitive loss.

In this thesis, we showed that long-lasting, slower Ca^{2+} events that rely on reticular Ca^{2+} influence cortico-limbic function and behavior. We performed a multifactorial assessment of its implications in brain functioning throgout life (from postnatal development to aging; health vs disease context). These results open several windows of research that should be further studied to target specific spatio-temporal dynamics of Ca^{2+} signaling in astrocytes:

1) This thesis work pointed *Foxo1* and its regulated transcription genes (*Sdc2* and *Ezr*) as potential astrocytic mediators to control cognitive performance in the hippocampus. Therefore, it is important to assess the expression levels of *Foxo1* target genes, *Sdc2* and *Ezr*, (and others identified in the STRING analysis, even if they are not astrocyte-specific) in astrocyte-enriched samples, not only in the adult mouse, but also in the aged mouse and in the chronically stressed

mouse. This complete analsyis will elucidate us regarding the therapeutic potential of global Ca^{2+}-*Foxo1* pathway modulation.

2) The molecular dissection of the global Ca^{2+}-*Foxo1* pathway modulation in these 3 conditions, should be correlated with a behavior analysis of mice that locally overexpress FOXO1 in the hippocampus or PFC, to confirm behavior recovery or protection.

3) We found that IP_3R2 KO-dependent Ca^{2+} signaling regulates cognitive performance in hippocampal-dependent tasks. Therefore, it is pivotal to perform electrophysiological recordings to obtain a functional readout of cortico-limbic structures, namely related with hip-PFC regional activity and temporal synchronization, to better understand the link between molecular alterations and cognitve enhancement or resilience.

4) The IP_3R2 KO mouse model has a similar reduction in global Ca^{2+} signaling as the recently generated viral tool to genetically drive the continuous extrusion of cytosolic Ca^{2+} in astrocytes (Yu et al. 2018). Therefore, this tool should be used to control Ca^{2+} signals locally in physiological processes to fully understand the implications of IP_3R2-dependent Ca^{2+} signaling in distinct brain regions and under different levels of activation.

References

Adamsky A, Kol A, Kreisel T, Doron A, Ozeri-Engelhard N, Melcer T, Refaeli R, Horn H, Regev L, Groysman M, London M, Goshen I. 2018. Astrocytic Activation Generates De Novo Neuronal Potentiation and Memory Enhancement. Cell 174:59-71 e14.

Agarwal A, Wu PH, Hughes EG, Fukaya M, Tischfield MA, Langseth AJ, Wirtz D, Bergles DE. 2017. Transient Opening of the Mitochondrial Permeability Transition Pore Induces Microdomain Calcium Transients in Astrocyte Processes. Neuron 93:587-605 e7.

Aguado F, Espinosa-Parrilla JF, Carmona MA, Soriano E. 2002. Neuronal activity regulates correlated network properties of spontaneous calcium transients in astrocytes in situ. J Neurosci 22:9430-44.

Agulhon C, Boyt KM, Xie AX, Friocourt F, Roth BL, McCarthy KD. 2013. Modulation of the autonomic nervous system and behaviour by acute glial cell Gq protein-coupled receptor activation in vivo. J Physiol 591:5599-609.

Agulhon C, Fiacco TA, McCarthy KD. 2010. Hippocampal short- and long-term plasticity are not modulated by astrocyte Ca2+ signaling. Science 327:1250-4.

Agulhon C, Petravicz J, McMullen AB, Sweger EJ, Minton SK, Taves SR, Casper KB, Fiacco TA, McCarthy KD. 2008. What is the role of astrocyte calcium in neurophysiology? Neuron 59:932-46.

Agulhon C, Sun MY, Murphy T, Myers T, Lauderdale K, Fiacco TA. 2012. Calcium Signaling and Gliotransmission in Normal vs. Reactive Astrocytes. Front Pharmacol 3:139.

Allen NJ. 2014. Astrocyte regulation of synaptic behavior. Annu Rev Cell Dev Biol 30:439-63.

Allen NJ, Barres BA. 2009. Neuroscience: Glia - more than just brain glue. Nature 457:675-7.

Allen NJ, Lyons DA. 2018. Glia as architects of central nervous system formation and function. Science 362:181-185.

Alvarez JI, Katayama T, Prat A. 2013. Glial influence on the blood brain barrier. Glia 61:1939-58.

Alves ND, Correia JS, Patricio P, Mateus-Pinheiro A, Machado-Santos AR, Loureiro-Campos E, Morais M, Bessa JM, Sousa N, Pinto L. 2017. Adult hippocampal neuroplasticity triggers susceptibility to recurrent depression. Transl Psychiatry 7:e1058.

Amorim L, Magalhaes R, Coelho A, Moreira PS, Portugal-Nunes C, Castanho TC, Marques P, Sousa N, Santos NC. 2018. Poor Sleep Quality Associates With Decreased Functional and Structural Brain Connectivity in Normative Aging: A MRI Multimodal Approach. Front Aging Neurosci 10:375.

Arabo A, Potier C, Ollivier G, Lorivel T, Roy V. 2014. Temporal analysis of free exploration of an elevated plus-maze in mice. J Exp Psychol Anim Learn Cogn 40:457-66.

Araque A. 2008. Astrocytes process synaptic information. Neuron Glia Biol 4:3-10.

Araque A, Carmignoto G, Haydon PG, Oliet SH, Robitaille R, Volterra A. 2014. Gliotransmitters travel in time and space. Neuron 81:728-39.

Araque A, Navarrete M. 2010. Glial cells in neuronal network function. Philos Trans R Soc Lond B Biol Sci 365:2375-81.

Araque A, Parpura V, Sanzgiri RP, Haydon PG. 1999. Tripartite synapses: glia, the unacknowledged partner. Trends Neurosci 22:208-15.

Bailey C, Barco A, Hawkins R, Kandel E. 2008. 4.02 - Molecular studies of learning and memory in Aplysia and the hippocampus: a comparative analysis of implicit and explicit memory storage. In: Byrne J, editor. Learning and memory: a comprehensive reference Oxford, UK: Elsevier Press.

Baldessarini RJ, Lau WK, Sim J, Sum MY, Sim K. 2015. Duration of initial antidepressant treatment and subsequent relapse of major depression. J Clin Psychopharmacol 35:75-6.

Banasr M, Chowdhury GM, Terwilliger R, Newton SS, Duman RS, Behar KL, Sanacora G. 2010. Glial pathology in an animal model of depression: reversal of stress-induced cellular, metabolic and behavioral deficits by the glutamate-modulating drug riluzole. Mol Psychiatry 15:501-11.

Banasr M, Duman RS. 2008. Glial loss in the prefrontal cortex is sufficient to induce depressive-like behaviors. Biol Psychiatry 64:863-70.

Barker GR, Banks PJ, Scott H, Ralph GS, Mitrophanous KA, Wong LF, Bashir ZI, Uney JB, Warburton EC. 2017. Separate elements of episodic memory subserved by distinct hippocampal-prefrontal connections. Nat Neurosci 20:242-250.

Barragan M, de Frias M, Iglesias-Serret D, Campas C, Castano E, Santidrian AF, Coll-Mulet L, Cosialls AM, Domingo A, Pons G, Gil J. 2006. Regulation of Akt/PKB by phosphatidylinositol 3-kinase-dependent and -independent pathways in B-cell chronic lymphocytic leukemia cells: role of protein kinase C{beta}. J Leukoc Biol 80:1473-9.

Bayraktar OA, Fuentealba LC, Alvarez-Buylla A, Rowitch DH. 2014. Astrocyte development and heterogeneity. Cold Spring Harb Perspect Biol 7:a020362.

Bazargani N, Attwell D. 2016. Astrocyte calcium signaling: the third wave. Nat Neurosci 19:182-9.

Bechtholt-Gompf AJ, Walther HV, Adams MA, Carlezon WA, Jr., Ongur D, Cohen BM. 2010. Blockade of astrocytic glutamate uptake in rats induces signs of anhedonia and impaired spatial memory. Neuropsychopharmacology 35:2049-59.

Beery AK, Kaufer D. 2015. Stress, social behavior, and resilience: insights from rodents. Neurobiol Stress 1:116-127.

Belzung C, Griebel G. 2001. Measuring normal and pathological anxiety-like behaviour in mice: a review. Behav Brain Res 125:141-9.

Ben Haim L, Rowitch DH. 2017. Functional diversity of astrocytes in neural circuit regulation. Nat Rev Neurosci 18:31-41.

Benediktsson AM, Marrs GS, Tu JC, Worley PF, Rothstein JD, Bergles DE, Dailey ME. 2012. Neuronal activity regulates glutamate transporter dynamics in developing astrocytes. Glia 60:175-88.

Berchtold NC, Cotman CW. 2009. Normal and Pathological Aging: From Animals to Humans. In: Bizon JL, Woods A, editors. Animal Models of Human Cognitive Aging. Totowa, NJ: Humana Press. p 1-28.

Bernardinelli Y, Muller D, Nikonenko I. 2014. Astrocyte-synapse structural plasticity. Neural Plast 2014:232105.

Bessa JM, Ferreira D, Melo I, Marques F, Cerqueira JJ, Palha JA, Almeida OF, Sousa N. 2009a. The mood-improving actions of antidepressants do not depend on neurogenesis but are associated with neuronal remodeling. Mol Psychiatry 14:764-73, 739.

Bessa JM, Mesquita AR, Oliveira M, Pego JM, Cerqueira JJ, Palha JA, Almeida OF, Sousa N. 2009b. A trans-dimensional approach to the behavioral aspects of depression. Front Behav Neurosci 3:1.

Bibb JA, Mayford MR, Tsien JZ, Alberini CM. 2010. Cognition enhancement strategies. J Neurosci 30:14987-92.

Biesecker KR, Srienc AI, Shimoda AM, Agarwal A, Bergles DE, Kofuji P, Newman EA. 2016. Glial Cell Calcium Signaling Mediates Capillary Regulation of Blood Flow in the Retina. J Neurosci 36:9435-45.

Biggs WH, 3rd, Meisenhelder J, Hunter T, Cavenee WK, Arden KC. 1999. Protein kinase B/Akt-mediated phosphorylation promotes nuclear exclusion of the winged helix transcription factor FKHR1. Proc Natl Acad Sci U S A 96:7421-6.

Bindocci E, Savtchouk I, Liaudet N, Becker D, Carriero G, Volterra A. 2017. Three-dimensional Ca2+ imaging advances understanding of astrocyte biology. Science 356.

Bishop NA, Lu T, Yankner BA. 2010. Neural mechanisms of ageing and cognitive decline. Nature 464:529-35.

Bissonette GB, Martins GJ, Franz TM, Harper ES, Schoenbaum G, Powell EM. 2008. Double dissociation of the effects of medial and orbital prefrontal cortical lesions on attentional and affective shifts in mice. J Neurosci 28:11124-30.

Bizon JL, Foster TC, Alexander GE, Glisky EL. 2012. Characterizing cognitive aging of working memory and executive function in animal models. Front Aging Neurosci 4:19.

Bliss TV, Lomo T. 1973. Long-lasting potentiation of synaptic transmission in the dentate area of the anaesthetized rabbit following stimulation of the perforant path. J Physiol 232:331-56.

Bloss EB, Janssen WG, Ohm DT, Yuk FJ, Wadsworth S, Saardi KM, McEwen BS, Morrison JH. 2011. Evidence for reduced experience-dependent dendritic spine plasticity in the aging prefrontal cortex. J Neurosci 31:7831-9.

Boisvert MM, Erikson GA, Shokhirev MN, Allen NJ. 2018. The Aging Astrocyte Transcriptome from Multiple Regions of the Mouse Brain. Cell Rep 22:269-285.

Bonder DE, McCarthy KD. 2014. Astrocytic Gq-GPCR-linked IP3R-dependent Ca2+ signaling does not mediate neurovascular coupling in mouse visual cortex in vivo. J Neurosci 34:13139-50.

Bosch M, Hayashi Y. 2012. Structural plasticity of dendritic spines. Curr Opin Neurobiol 22:383-8.

Bourin M, Hascoet M. 2003. The mouse light/dark box test. Eur J Pharmacol 463:55-65.

Bourin M, Petit-Demouliere B, Dhonnchadha BN, Hascoet M. 2007. Animal models of anxiety in mice. Fundam Clin Pharmacol 21:567-74.

Bourne J, Harris KM. 2007. Do thin spines learn to be mushroom spines that remember? Curr Opin Neurobiol 17:381-6.

Bowser DN, Khakh BS. 2007. Vesicular ATP is the predominant cause of intercellular calcium waves in astrocytes. J Gen Physiol 129:485-91.

Burke SN, Barnes CA. 2006. Neural plasticity in the ageing brain. Nat Rev Neurosci 7:30-40.

Bushong EA, Martone ME, Jones YZ, Ellisman MH. 2002. Protoplasmic astrocytes in CA1 stratum radiatum occupy separate anatomical domains. J Neurosci 22:183-92.

Cabezas R, Avila-Rodriguez M, Vega-Vela NE, Echeverria V, Gonzalez J, Hidalgo OA, Santos AB, Aliev G, Barreto GE. 2016. Growth Factors and Astrocytes Metabolism: Possible Roles for Platelet Derived Growth Factor. Med Chem 12:204-10.

Cahoy JD, Emery B, Kaushal A, Foo LC, Zamanian JL, Christopherson KS, Xing Y, Lubischer JL, Krieg PA, Krupenko SA, Thompson WJ, Barres BA. 2008. A transcriptome database for astrocytes, neurons, and oligodendrocytes: a new resource for understanding brain development and function. J Neurosci 28:264-78.

Cai J, Chen Y, Cai WH, Hurlock EC, Wu H, Kernie SG, Parada LF, Lu QR. 2007. A crucial role for Olig2 in white matter astrocyte development. Development 134:1887-99.

Calnan DR, Brunet A. 2008. The FoxO code. Oncogene 27:2276-88.

Cao X, Li LP, Wang Q, Wu Q, Hu HH, Zhang M, Fang YY, Zhang J, Li SJ, Xiong WC, Yan HC, Gao YB, Liu JH, Li XW, Sun LR, Zeng YN, Zhu XH, Gao TM. 2013. Astrocyte-derived ATP modulates depressive-like behaviors. Nat Med 19:773-7.

Castagne V, Moser P, Roux S, Porsolt RD. 2011. Rodent models of depression: forced swim and tail suspension behavioral despair tests in rats and mice. Curr Protoc Neurosci Chapter 8:Unit 8 10A.

Castelhano-Carlos MJ, Sousa N, Ohl F, Baumans V. 2010. Identification methods in newborn C57BL/6 mice: a developmental and behavioural evaluation. Lab Anim 44:88-103.

Cenquizca LA, Swanson LW. 2007. Spatial organization of direct hippocampal field CA1 axonal projections to the rest of the cerebral cortex. Brain Res Rev 56:1-26.

Cerqueira JJ, Pego JM, Taipa R, Bessa JM, Almeida OF, Sousa N. 2005. Morphological correlates of corticosteroid-induced changes in prefrontal cortex-dependent behaviors. J Neurosci 25:7792-800.

Chai H, Diaz-Castro B, Shigetomi E, Monte E, Octeau JC, Yu X, Cohn W, Rajendran PS, Vondriska TM, Whitelegge JP, Coppola G, Khakh BS. 2017. Neural Circuit-Specialized Astrocytes: Transcriptomic, Proteomic, Morphological, and Functional Evidence. Neuron 95:531-549 e9.

Charles AC, Merrill JE, Dirksen ER, Sanderson MJ. 1991. Intercellular signaling in glial cells: calcium waves and oscillations in response to mechanical stimulation and glutamate. Neuron 6:983-92.
Chen J, Tan Z, Zeng L, Zhang X, He Y, Gao W, Wu X, Li Y, Bu B, Wang W, Duan S. 2013. Heterosynaptic long-term depression mediated by ATP released from astrocytes. Glia 61:178-91.
Chen N, Sugihara H, Sharma J, Perea G, Petravicz J, Le C, Sur M. 2012. Nucleus basalis-enabled stimulus-specific plasticity in the visual cortex is mediated by astrocytes. Proc Natl Acad Sci U S A 109:E2832-41.
Ciocchi S, Passecker J, Malagon-Vina H, Mikus N, Klausberger T. 2015. Brain computation. Selective information routing by ventral hippocampal CA1 projection neurons. Science 348:560-3.
Clapcote SJ, Lazar NL, Bechard AR, Wood GA, Roder JC. 2005. NIH Swiss and Black Swiss mice have retinal degeneration and performance deficits in cognitive tests. Comp Med 55:310-6.
Clarke LE, Liddelow SA, Chakraborty C, Munch AE, Heiman M, Barres BA. 2018. Normal aging induces A1-like astrocyte reactivity. Proc Natl Acad Sci U S A 115:E1896-E1905.
Copeland CS, Wall TM, Sims RE, Neale SA, Nisenbaum E, Parri HR, Salt TE. 2017. Astrocytes modulate thalamic sensory processing via mGlu2 receptor activation. Neuropharmacology 121:100-110.
Cornell-Bell AH, Finkbeiner SM, Cooper MS, Smith SJ. 1990. Glutamate induces calcium waves in cultured astrocytes: long-range glial signaling. Science 247:470-3.
Cotrina ML, Nedergaard M. 2002. Astrocytes in the aging brain. J Neurosci Res 67:1-10.
Cotter D, Mackay D, Chana G, Beasley C, Landau S, Everall IP. 2002. Reduced neuronal size and glial cell density in area 9 of the dorsolateral prefrontal cortex in subjects with major depressive disorder. Cereb Cortex 12:386-94.
Covelo A, Araque A. 2016. Lateral regulation of synaptic transmission by astrocytes. Neuroscience 323:62-6.
Cryan JF, Holmes A. 2005. The ascent of mouse: advances in modelling human depression and anxiety. Nat Rev Drug Discov 4:775-90.
Dallerac G, Rouach N. 2016. Astrocytes as new targets to improve cognitive functions. Prog Neurobiol 144:48-67.
Das MM, Svendsen CN. 2015. Astrocytes show reduced support of motor neurons with aging that is accelerated in a rodent model of ALS. Neurobiol Aging 36:1130-9.
de Kloet ER, Joels M, Holsboer F. 2005. Stress and the brain: from adaptation to disease. Nat Rev Neurosci 6:463-75.
De Pitta M, Brunel N, Volterra A. 2016. Astrocytes: Orchestrating synaptic plasticity? Neuroscience 323:43-61.
Derouiche A, Frotscher M. 2001. Peripheral astrocyte processes: monitoring by selective immunostaining for the actin-binding ERM proteins. Glia 36:330-41.
Di Castro MA, Chuquet J, Liaudet N, Bhaukaurally K, Santello M, Bouvier D, Tiret P, Volterra A. 2011. Local Ca2+ detection and modulation of synaptic release by astrocytes. Nat Neurosci 14:1276-84.
Dias-Ferreira E, Sousa JC, Melo I, Morgado P, Mesquita AR, Cerqueira JJ, Costa RM, Sousa N. 2009. Chronic stress causes frontostriatal reorganization and affects decision-making. Science 325:621-5.
Dickstein DL, Kabaso D, Rocher AB, Luebke JI, Wearne SL, Hof PR. 2007. Changes in the structural complexity of the aged brain. Aging Cell 6:275-84.
Dimou L, Gotz M. 2014. Glial cells as progenitors and stem cells: new roles in the healthy and diseased brain. Physiol Rev 94:709-37.
Djukic B, Casper KB, Philpot BD, Chin LS, McCarthy KD. 2007. Conditional knock-out of Kir4.1 leads to glial membrane depolarization, inhibition of potassium and glutamate uptake, and enhanced short-term synaptic potentiation. J Neurosci 27:11354-65.

Dolgin E. 2013. Old mice require new experimental tricks to study aging process. Nat Med 19:518-9.
Dong QP, He JQ, Chai Z. 2013a. Astrocytic Ca(2+) waves mediate activation of extrasynaptic NMDA receptors in hippocampal neurons to aggravate brain damage during ischemia. Neurobiol Dis 58:68-75.
Dong Z, Bai Y, Wu X, Li H, Gong B, Howland JG, Huang Y, He W, Li T, Wang YT. 2013b. Hippocampal long-term depression mediates spatial reversal learning in the Morris water maze. Neuropharmacology 64:65-73.
Durkee CA, Araque A. 2019. Diversity and Specificity of Astrocyte-neuron Communication. Neuroscience 396:73-78.
Edlund T, Jessell TM. 1999. Progression from extrinsic to intrinsic signaling in cell fate specification: a view from the nervous system. Cell 96:211-24.
Eijkelenboom A, Burgering BM. 2013. FOXOs: signalling integrators for homeostasis maintenance. Nat Rev Mol Cell Biol 14:83-97.
Emsley JG, Macklis JD. 2006. Astroglial heterogeneity closely reflects the neuronal-defined anatomy of the adult murine CNS. Neuron Glia Biol 2:175-86.
Engle JR, Barnes CA. 2012. Characterizing cognitive aging of associative memory in animal models. Front Aging Neurosci 4:10.
Fanselow MS, Dong HW. 2010. Are the dorsal and ventral hippocampus functionally distinct structures? Neuron 65:7-19.
Farmer WT, Murai K. 2017. Resolving Astrocyte Heterogeneity in the CNS. Front Cell Neurosci 11:300.
Feriod CN, Nguyen L, Jurczak MJ, Kruglov EA, Nathanson MH, Shulman GI, Bennett AM, Ehrlich BE. 2014. Inositol 1,4,5-trisphosphate receptor type II (InsP3R-II) is reduced in obese mice, but metabolic homeostasis is preserved in mice lacking InsP3R-II. Am J Physiol Endocrinol Metab 307:E1057-64.
Fiacco TA, McCarthy KD. 2018. Multiple Lines of Evidence Indicate That Gliotransmission Does Not Occur under Physiological Conditions. J Neurosci 38:3-13.
Fields RD, Araque A, Johansen-Berg H, Lim SS, Lynch G, Nave KA, Nedergaard M, Perez R, Sejnowski T, Wake H. 2014. Glial biology in learning and cognition. Neuroscientist 20:426-31.
Foley J, Blutstein T, Lee S, Erneux C, Halassa MM, Haydon P. 2017. Astrocytic IP3/Ca2+ Signaling Modulates Theta Rhythm and REM Sleep. Front Neural Circuits 11:3.
Fox E. 2008. Emotion Science: Cognitive and Neuroscientific Approaches to Understanding Human Emotions: Palgrave Macmillan.
Fox WM. 1965. Reflex-ontogeny and behavioural development of the mouse. Anim Behav 13:234-41.
Freeman SH, Kandel R, Cruz L, Rozkalne A, Newell K, Frosch MP, Hedley-Whyte ET, Locascio JJ, Lipsitz LA, Hyman BT. 2008. Preservation of neuronal number despite age-related cortical brain atrophy in elderly subjects without Alzheimer disease. J Neuropathol Exp Neurol 67:1205-12.
Futatsugi A, Kato K, Ogura H, Li ST, Nagata E, Kuwajima G, Tanaka K, Itohara S, Mikoshiba K. 1999. Facilitation of NMDAR-independent LTP and spatial learning in mutant mice lacking ryanodine receptor type 3. Neuron 24:701-13.
Futatsugi A, Nakamura T, Yamada MK, Ebisui E, Nakamura K, Uchida K, Kitaguchi T, Takahashi-Iwanaga H, Noda T, Aruga J, Mikoshiba K. 2005. IP3 receptor types 2 and 3 mediate exocrine secretion underlying energy metabolism. Science 309:2232-4.
Galeotti N, Vivoli E, Norcini M, Bartolini A, Ghelardini C. 2008. An antidepressant behaviour in mice carrying a gene-specific InsP3R1, InsP3R2 and InsP3R3 protein knockdown. Neuropharmacology 55:1156-64.
Ge Y, Dong Z, Bagot RC, Howland JG, Phillips AG, Wong TP, Wang YT. 2010. Hippocampal long-term depression is required for the consolidation of spatial memory. Proc Natl Acad Sci U S A 107:16697-702.

Giaume C, Koulakoff A, Roux L, Holcman D, Rouach N. 2010. Astroglial networks: a step further in neuroglial and gliovascular interactions. Nat Rev Neurosci 11:87-99.

Gibbs ME, Hutchinson D, Hertz L. 2008. Astrocytic involvement in learning and memory consolidation. Neurosci Biobehav Rev 32:927-44.

Gittins RA, Harrison PJ. 2011. A morphometric study of glia and neurons in the anterior cingulate cortex in mood disorder. J Affect Disord 133:328-32.

Gomez-Gonzalo M, Martin-Fernandez M, Martinez-Murillo R, Mederos S, Hernandez-Vivanco A, Jamison S, Fernandez AP, Serrano J, Calero P, Futch HS, Corpas R, Sanfeliu C, Perea G, Araque A. 2017. Neuron-astrocyte signaling is preserved in the aging brain. Glia 65:569-580.

Gomez-Gonzalo M, Navarrete M, Perea G, Covelo A, Martin-Fernandez M, Shigemoto R, Lujan R, Araque A. 2015. Endocannabinoids Induce Lateral Long-Term Potentiation of Transmitter Release by Stimulation of Gliotransmission. Cereb Cortex 25:3699-712.

Gosselin RD, Gibney S, O'Malley D, Dinan TG, Cryan JF. 2009. Region specific decrease in glial fibrillary acidic protein immunoreactivity in the brain of a rat model of depression. Neuroscience 159:915-25.

Gosselin T, Le Guisquet AM, Brizard B, Hommet C, Minier F, Belzung C. 2017. Fluoxetine induces paradoxical effects in C57BL6/J mice: comparison with BALB/c mice. Behav Pharmacol 28:466-476.

Gourine AV, Kasymov V, Marina N, Tang F, Figueiredo MF, Lane S, Teschemacher AG, Spyer KM, Deisseroth K, Kasparov S. 2010. Astrocytes control breathing through pH-dependent release of ATP. Science 329:571-5.

Grady CL. 2008. Cognitive neuroscience of aging. Ann N Y Acad Sci 1124:127-44.

Granes F, Urena JM, Rocamora N, Vilaro S. 2000. Ezrin links syndecan-2 to the cytoskeleton. J Cell Sci 113 (Pt 7):1267-76.

Graves AR, Moore SJ, Bloss EB, Mensh BD, Kath WL, Spruston N. 2012. Hippocampal pyramidal neurons comprise two distinct cell types that are countermodulated by metabotropic receptors. Neuron 76:776-89.

Graziano A, Petrosini L, Bartoletti A. 2003. Automatic recognition of explorative strategies in the Morris water maze. J Neurosci Methods 130:33-44.

Griebel G, Simiand J, Serradeil-Le Gal C, Wagnon J, Pascal M, Scatton B, Maffrand JP, Soubrie P. 2002. Anxiolytic- and antidepressant-like effects of the non-peptide vasopressin V1b receptor antagonist, SSR149415, suggest an innovative approach for the treatment of stress-related disorders. Proc Natl Acad Sci U S A 99:6370-5.

Gu Y, Arruda-Carvalho M, Wang J, Janoschka SR, Josselyn SA, Frankland PW, Ge S. 2012. Optical controlling reveals time-dependent roles for adult-born dentate granule cells. Nat Neurosci 15:1700-6.

Guerra-Gomes S, Sousa N, Pinto L, Oliveira JF. 2017. Functional Roles of Astrocyte Calcium Elevations: From Synapses to Behavior. Front Cell Neurosci 11:427.

Guerra-Gomes S, Viana JF, Nascimento DSM, Correia JS, Sardinha VM, Caetano I, Sousa N, Pinto L, Oliveira JF. 2018. The Role of Astrocytic Calcium Signaling in the Aged Prefrontal Cortex. Frontiers in Cellular Neuroscience 12.

Gutierrez Y, Garcia-Marques J, Liu X, Fortes-Marco L, Sanchez-Gonzalez R, Giaume C, Lopez-Mascaraque L. 2019. Sibling astrocytes share preferential coupling via gap junctions. Glia 67:1852-1858.

Habbas S, Santello M, Becker D, Stubbe H, Zappia G, Liaudet N, Klaus FR, Kollias G, Fontana A, Pryce CR, Suter T, Volterra A. 2015. Neuroinflammatory TNFalpha Impairs Memory via Astrocyte Signaling. Cell 163:1730-41.

Heidbreder CA, Groenewegen HJ. 2003. The medial prefrontal cortex in the rat: evidence for a dorso-ventral distinction based upon functional and anatomical characteristics. Neurosci Biobehav Rev 27:555-79.

Heller JP, Rusakov DA. 2015. Morphological plasticity of astroglia: Understanding synaptic microenvironment. Glia 63:2133-51.

Henneberger C, Papouin T, Oliet SH, Rusakov DA. 2010. Long-term potentiation depends on release of D-serine from astrocytes. Nature 463:232-6.

Hertle DN, Yeckel MF. 2007. Distribution of inositol-1,4,5-trisphosphate receptor isotypes and ryanodine receptor isotypes during maturation of the rat hippocampus. Neuroscience 150:625-38.

Heuser K, Nome CG, Pettersen KH, Abjorsbraten KS, Jensen V, Tang W, Sprengel R, Tauboll E, Nagelhus EA, Enger R. 2018. Ca2+ Signals in Astrocytes Facilitate Spread of Epileptiform Activity. Cereb Cortex 28:4036-4048.

Heyser CJ. 2004. Assessment of developmental milestones in rodents. Curr Protoc Neurosci Chapter 8:Unit 8.18.

Hill JM, Lim MA, Stone MM. 2008. Developmental Milestones in the Newborn Mouse,39: Neuromethods, Humana Press.

Hirase H, Qian L, Bartho P, Buzsaki G. 2004. Calcium dynamics of cortical astrocytic networks in vivo. PLoS Biol 2:E96.

Hof PR, Morrison JH. 2004. The aging brain: morphomolecular senescence of cortical circuits. Trends Neurosci 27:607-13.

Hol EM, Pekny M. 2015. Glial fibrillary acidic protein (GFAP) and the astrocyte intermediate filament system in diseases of the central nervous system. Curr Opin Cell Biol 32:121-30.

Hollon SD, Shelton RC, Wisniewski S, Warden D, Biggs MM, Friedman ES, Husain M, Kupfer DJ, Nierenberg AA, Petersen TJ, Shores-Wilson K, Rush AJ. 2006. Presenting characteristics of depressed outpatients as a function of recurrence: preliminary findings from the STAR*D clinical trial. J Psychiatr Res 40:59-69.

Holter SM, Garrett L, Einicke J, Sperling B, Dirscherl P, Zimprich A, Fuchs H, Gailus-Durner V, Hrabe de Angelis M, Wurst W. 2015. Assessing Cognition in Mice. Curr Protoc Mouse Biol 5:331-58.

Holtmaat A, Svoboda K. 2009. Experience-dependent structural synaptic plasticity in the mammalian brain. Nat Rev Neurosci 10:647-58.

Hoover WB, Vertes RP. 2007. Anatomical analysis of afferent projections to the medial prefrontal cortex in the rat. Brain Struct Funct 212:149-79.

Hu HT, Umemori H, Hsueh YP. 2016. Postsynaptic SDC2 induces transsynaptic signaling via FGF22 for bidirectional synaptic formation. Sci Rep 6:33592.

Ibarguen-Vargas Y, Surget A, Touma C, Palme R, Belzung C. 2008. Multifaceted strain-specific effects in a mouse model of depression and of antidepressant reversal. Psychoneuroendocrinology 33:1357-68.

Ishii T, Takanashi Y, Sugita K, Miyazawa M, Yanagihara R, Yasuda K, Onouchi H, Kawabe N, Nakata M, Yamamoto Y, Hartman PS, Ishii N. 2017. Endogenous reactive oxygen species cause astrocyte defects and neuronal dysfunctions in the hippocampus: a new model for aging brain. Aging Cell 16:39-51.

Jagust W. 2013. Vulnerable neural systems and the borderland of brain aging and neurodegeneration. Neuron 77:219-34.

Jakel S, Dimou L. 2017. Glial Cells and Their Function in the Adult Brain: A Journey through the History of Their Ablation. Front Cell Neurosci 11:24.

Janky R, Verfaillie A, Imrichova H, Van de Sande B, Standaert L, Christiaens V, Hulselmans G, Herten K, Naval Sanchez M, Potier D, Svetlichnyy D, Kalender Atak Z, Fiers M, Marine JC, Aerts S. 2014.

iRegulon: from a gene list to a gene regulatory network using large motif and track collections. PLoS Comput Biol 10:e1003731.
Jego P, Pacheco-Torres J, Araque A, Canals S. 2014. Functional MRI in mice lacking IP3-dependent calcium signaling in astrocytes. J Cereb Blood Flow Metab 34:1599-603.
Jeon D, Yang YM, Jeong MJ, Philipson KD, Rhim H, Shin HS. 2003. Enhanced learning and memory in mice lacking Na+/Ca2+ exchanger 2. Neuron 38:965-76.
John CS, Smith KL, Van't Veer A, Gompf HS, Carlezon WA, Jr., Cohen BM, Ongur D, Bechtholt-Gompf AJ. 2012. Blockade of astrocytic glutamate uptake in the prefrontal cortex induces anhedonia. Neuropsychopharmacology 37:2467-75.
Kalueff AV, Tuohimaa P. 2005. The grooming analysis algorithm discriminates between different levels of anxiety in rats: potential utility for neurobehavioural stress research. J Neurosci Methods 143:169-77.
Kamphuis W, Mamber C, Moeton M, Kooijman L, Sluijs JA, Jansen AH, Verveer M, de Groot LR, Smith VD, Rangarajan S, Rodriguez JJ, Orre M, Hol EM. 2012. GFAP isoforms in adult mouse brain with a focus on neurogenic astrocytes and reactive astrogliosis in mouse models of Alzheimer disease. PLoS One 7:e42823.
Kandel ER, Dudai Y, Mayford MR. 2014. The molecular and systems biology of memory. Cell 157:163-86.
Kandel ER, Jessell TM, Schwartz JH, Siegelbaum SA, Hudspeth AJ. 2013. Principles of Neural Science, Fifth Edition: McGraw-Hill Education.
Kanemaru K, Kubota J, Sekiya H, Hirose K, Okubo Y, Iino M. 2013. Calcium-dependent N-cadherin up-regulation mediates reactive astrogliosis and neuroprotection after brain injury. Proc Natl Acad Sci U S A 110:11612-7.
Kanemaru K, Sekiya H, Xu M, Satoh K, Kitajima N, Yoshida K, Okubo Y, Sasaki T, Moritoh S, Hasuwa H, Mimura M, Horikawa K, Matsui K, Nagai T, Iino M, Tanaka KF. 2014. In vivo visualization of subtle, transient, and local activity of astrocytes using an ultrasensitive Ca(2+) indicator. Cell Rep 8:311-8.
Kanner S, Goldin M, Galron R, Ben Jacob E, Bonifazi P, Barzilai A. 2018. Astrocytes restore connectivity and synchronization in dysfunctional cerebellar networks. Proc Natl Acad Sci U S A 115:8025-8030.
Kasai H, Fukuda M, Watanabe S, Hayashi-Takagi A, Noguchi J. 2010. Structural dynamics of dendritic spines in memory and cognition. Trends Neurosci 33:121-9.
Kawakami Y, Nishimoto H, Kitaura J, Maeda-Yamamoto M, Kato RM, Littman DR, Leitges M, Rawlings DJ, Kawakami T. 2004. Protein kinase C betaII regulates Akt phosphorylation on Ser-473 in a cell type- and stimulus-specific fashion. J Biol Chem 279:47720-5.
Kessaris N, Pringle N, Richardson WD. 2008. Specification of CNS glia from neural stem cells in the embryonic neuroepithelium. Philos Trans R Soc Lond B Biol Sci 363:71-85.
Kettenmann H, Ransom BR. 2005. Neuroglia. New York: Oxford University Press Inc.
Kettenmann H, Verkhratsky A. 2008. Neuroglia: the 150 years after. Trends Neurosci 31:653-9.
Khakh BS, McCarthy KD. 2015. Astrocyte calcium signaling: from observations to functions and the challenges therein. Cold Spring Harb Perspect Biol 7:a020404.
Khakh BS, Sofroniew MV. 2015. Diversity of astrocyte functions and phenotypes in neural circuits. Nat Neurosci 18:942-52.
Khan Z, Carey J, Park HJ, Lehar M, Lasker D, Jinnah HA. 2004. Abnormal motor behavior and vestibular dysfunction in the stargazer mouse mutant. Neuroscience 127:785-96.
Kim SK, Hayashi H, Ishikawa T, Shibata K, Shigetomi E, Shinozaki Y, Inada H, Roh SE, Kim SJ, Lee G, Bae H, Moorhouse AJ, Mikoshiba K, Fukazawa Y, Koizumi S, Nabekura J. 2016. Cortical

astrocytes rewire somatosensory cortical circuits for peripheral neuropathic pain. J Clin Invest 126:1983-97.
Kim SY, Webb AE. 2017. Neuronal functions of FOXO/DAF-16. Nutr Healthy Aging 4:113-126.
Kleiber ML, Wright E, Singh SM. 2011. Maternal voluntary drinking in C57BL/6J mice: advancing a model for fetal alcohol spectrum disorders. Behav Brain Res 223:376-87.
Knierim J. 2010. Synaptic Plasticity and Place Cell Formation: Elsevier Ltd.
Koch M. 1999. The neurobiology of startle. Prog Neurobiol 59:107-28.
Konsolaki E, Skaliora I. 2015. Premature Aging Phenotype in Mice Lacking High-Affinity Nicotinic Receptors: Region-Specific Changes in Layer V Pyramidal Cell Morphology. Cereb Cortex 25:2138-48.
Kreft M, Potokar M, Stenovec M, Pangrsic T, Zorec R. 2009. Regulated exocytosis and vesicle trafficking in astrocytes. Ann N Y Acad Sci 1152:30-42.
Kuga N, Sasaki T, Takahara Y, Matsuki N, Ikegaya Y. 2011. Large-scale calcium waves traveling through astrocytic networks in vivo. J Neurosci 31:2607-14.
Lalo U, Bogdanov A, Pankratov Y. 2018. Diversity of Astroglial Effects on Aging- and Experience-Related Cortical Metaplasticity. Front Mol Neurosci 11:239.
Lalo U, Rasooli-Nejad S, Pankratov Y. 2014. Exocytosis of gliotransmitters from cortical astrocytes: implications for synaptic plasticity and aging. Biochem Soc Trans 42:1275-81.
Lavialle M, Aumann G, Anlauf E, Prols F, Arpin M, Derouiche A. 2011. Structural plasticity of perisynaptic astrocyte processes involves ezrin and metabotropic glutamate receptors. Proc Natl Acad Sci U S A 108:12915-9.
Lee HS, Ghetti A, Pinto-Duarte A, Wang X, Dziewczapolski G, Galimi F, Huitron-Resendiz S, Pina-Crespo JC, Roberts AJ, Verma IM, Sejnowski TJ, Heinemann SF. 2014. Astrocytes contribute to gamma oscillations and recognition memory. Proc Natl Acad Sci U S A 111:E3343-52.
Lee Y, Gaskins D, Anand A, Shekhar A. 2007. Glia mechanisms in mood regulation: a novel model of mood disorders. Psychopharmacology (Berl) 191:55-65.
Lee YS, Silva AJ. 2009. The molecular and cellular biology of enhanced cognition. Nat Rev Neurosci 10:126-40.
Leger M, Quiedeville A, Bouet V, Haelewyn B, Boulouard M, Schumann-Bard P, Freret T. 2013. Object recognition test in mice. Nat Protoc 8:2531-7.
Lemaitre H, Goldman AL, Sambataro F, Verchinski BA, Meyer-Lindenberg A, Weinberger DR, Mattay VS. 2012. Normal age-related brain morphometric changes: nonuniformity across cortical thickness, surface area and gray matter volume? Neurobiol Aging 33:617 e1-9.
Leybaert L, Sanderson MJ. 2012. Intercellular Ca(2+) waves: mechanisms and function. Physiol Rev 92:1359-92.
Li H, Xie Y, Zhang N, Yu Y, Zhang Q, Ding S. 2015. Disruption of IP(3)R2-mediated Ca(2)(+) signaling pathway in astrocytes ameliorates neuronal death and brain damage while reducing behavioral deficits after focal ischemic stroke. Cell Calcium 58:565-76.
Li X, Zima AV, Sheikh F, Blatter LA, Chen J. 2005. Endothelin-1-induced arrhythmogenic Ca2+ signaling is abolished in atrial myocytes of inositol-1,4,5-trisphosphate(IP3)-receptor type 2-deficient mice. Circ Res 96:1274-81.
Liddelow SA, Guttenplan KA, Clarke LE, Bennett FC, Bohlen CJ, Schirmer L, Bennett ML, Munch AE, Chung WS, Peterson TC, Wilton DK, Frouin A, Napier BA, Panicker N, Kumar M, Buckwalter MS, Rowitch DH, Dawson VL, Dawson TM, Stevens B, Barres BA. 2017. Neurotoxic reactive astrocytes are induced by activated microglia. Nature 541:481-487.
Lima A, Sardinha VM, Oliveira AF, Reis M, Mota C, Silva MA, Marques F, Cerqueira JJ, Pinto L, Sousa N, Oliveira JF. 2014. Astrocyte pathology in the prefrontal cortex impairs the cognitive function of rats. Mol Psychiatry 19:834-41.

Lin YL, Lei YT, Hong CJ, Hsueh YP. 2007. Syndecan-2 induces filopodia and dendritic spine formation via the neurofibromin-PKA-Ena/VASP pathway. J Cell Biol 177:829-41.

Lopes S, Vaz-Silva J, Pinto V, Dalla C, Kokras N, Bedenk B, Mack N, Czisch M, Almeida OF, Sousa N, Sotiropoulos I. 2016. Tau protein is essential for stress-induced brain pathology. Proc Natl Acad Sci U S A 113:E3755-63.

Losi G, Mariotti L, Sessolo M, Carmignoto G. 2017. New Tools to Study Astrocyte Ca(2+) Signal Dynamics in Brain Networks In Vivo. Front Cell Neurosci 11:134.

Lynch AM, Murphy KJ, Deighan BF, O'Reilly JA, Gun'ko YK, Cowley TR, Gonzalez-Reyes RE, Lynch MA. 2010. The impact of glial activation in the aging brain. Aging Dis 1:262-78.

Magalhaes R, Barriere DA, Novais A, Marques F, Marques P, Cerqueira J, Sousa JC, Cachia A, Boumezbeur F, Bottlaender M, Jay TM, Meriaux S, Sousa N. 2018. The dynamics of stress: a longitudinal MRI study of rat brain structure and connectome. Mol Psychiatry 23:1998-2006.

Magistretti PJ, Allaman I. 2018. Lactate in the brain: from metabolic end-product to signalling molecule. Nat Rev Neurosci 19:235-249.

Mariotti L, Losi G, Sessolo M, Marcon I, Carmignoto G. 2016. The inhibitory neurotransmitter GABA evokes long-lasting Ca(2+) oscillations in cortical astrocytes. Glia 64:363-73.

Martin-Fernandez M, Jamison S, Robin LM, Zhao Z, Martin ED, Aguilar J, Benneyworth MA, Marsicano G, Araque A. 2017. Synapse-specific astrocyte gating of amygdala-related behavior. Nat Neurosci 20:1540-1548.

Martin R, Bajo-Graneras R, Moratalla R, Perea G, Araque A. 2015. Circuit-specific signaling in astrocyte-neuron networks in basal ganglia pathways. Science 349:730-4.

Martineau M. 2013. Gliotransmission: focus on exocytotic release of L-glutamate and D-serine from astrocytes. Biochem Soc Trans 41:1557-61.

Mateus-Pinheiro A, Pinto L, Bessa JM, Morais M, Alves ND, Monteiro S, Patricio P, Almeida OF, Sousa N. 2013. Sustained remission from depressive-like behavior depends on hippocampal neurogenesis. Transl Psychiatry 3:e210.

Matyash V, Kettenmann H. 2010. Heterogeneity in astrocyte morphology and physiology. Brain Res Rev 63:2-10.

Mayford M, Siegelbaum SA, Kandel ER. 2012. Synapses and memory storage. Cold Spring Harb Perspect Biol 4.

McEwen BS, Nasca C, Gray JD. 2016. Stress Effects on Neuronal Structure: Hippocampus, Amygdala, and Prefrontal Cortex. Neuropsychopharmacology 41:3-23.

McIver SR, Faideau M, Haydon PG. 2013. Astrocyte-Neuron Communications. In: Cui C, Grandison L, Noronha A, editors. Neural-Immune Interactions in Brain Function and Alcohol Related Disorders. Boston, MA: Springer US. p 31-64.

Mederos S, González-Arias C, Perea G. 2018. Astrocyte–Neuron Networks: A Multilane Highway of Signaling for Homeostatic Brain Function. Frontiers in Synaptic Neuroscience 10.

Mederos S, Hernandez-Vivanco A, Ramirez-Franco J, Martin-Fernandez M, Navarrete M, Yang A, Boyden ES, Perea G. 2019. Melanopsin for precise optogenetic activation of astrocyte-neuron networks. Glia 67:915-934.

Medvedev N, Popov V, Henneberger C, Kraev I, Rusakov DA, Stewart MG. 2014. Glia selectively approach synapses on thin dendritic spines. Philos Trans R Soc Lond B Biol Sci 369:20140047.

Mesquita AR, Pego JM, Summavielle T, Maciel P, Almeida OF, Sousa N. 2007. Neurodevelopment milestone abnormalities in rats exposed to stress in early life. Neuroscience 147:1022-33.

Miguel-Hidalgo JJ, Baucom C, Dilley G, Overholser JC, Meltzer HY, Stockmeier CA, Rajkowska G. 2000. Glial fibrillary acidic protein immunoreactivity in the prefrontal cortex distinguishes younger from older adults in major depressive disorder. Biol Psychiatry 48:861-73.

Migues PV, Liu L, Archbold GE, Einarsson EO, Wong J, Bonasia K, Ko SH, Wang YT, Hardt O. 2016. Blocking Synaptic Removal of GluA2-Containing AMPA Receptors Prevents the Natural Forgetting of Long-Term Memories. J Neurosci 36:3481-94.

Miller EK, Cohen JD. 2001. An integrative theory of prefrontal cortex function. Annu Rev Neurosci 24:167-202.

Miller FD, Gauthier AS. 2007. Timing is everything: making neurons versus glia in the developing cortex. Neuron 54:357-69.

Mineur YS, Picciotto MR, Sanacora G. 2007. Antidepressant-like effects of ceftriaxone in male C57BL/6J mice. Biol Psychiatry 61:250-2.

Molofsky AV, Krencik R, Ullian EM, Tsai HH, Deneen B, Richardson WD, Barres BA, Rowitch DH. 2012. Astrocytes and disease: a neurodevelopmental perspective. Genes Dev 26:891-907.

Molotkov D, Zobova S, Arcas JM, Khiroug L. 2013. Calcium-induced outgrowth of astrocytic peripheral processes requires actin binding by Profilin-1. Cell Calcium 53:338-48.

Monai H, Ohkura M, Tanaka M, Oe Y, Konno A, Hirai H, Mikoshiba K, Itohara S, Nakai J, Iwai Y, Hirase H. 2016. Calcium imaging reveals glial involvement in transcranial direct current stimulation-induced plasticity in mouse brain. Nat Commun 7:11100.

Monteiro S, Roque S, de Sa-Calcada D, Sousa N, Correia-Neves M, Cerqueira JJ. 2015. An efficient chronic unpredictable stress protocol to induce stress-related responses in C57BL/6 mice. Front Psychiatry 6:6.

Moreira PS, Almeida PR, Leite-Almeida H, Sousa N, Costa P. 2016. Impact of Chronic Stress Protocols in Learning and Memory in Rodents: Systematic Review and Meta-Analysis. PLoS One 11:e0163245.

Morquette P, Verdier D, Kadala A, Fethiere J, Philippe AG, Robitaille R, Kolta A. 2015. An astrocyte-dependent mechanism for neuronal rhythmogenesis. Nat Neurosci 18:844-54.

Mota C, Taipa R, das Neves SP, Monteiro-Martins S, Monteiro S, Palha JA, Sousa N, Sousa JC, Cerqueira JJ. 2019. Structural and molecular correlates of cognitive aging in the rat. Sci Rep 9:2005.

Mullen RJ, Buck CR, Smith AM. 1992. NeuN, a neuronal specific nuclear protein in vertebrates. Development 116:201-11.

Musholt K, Cirillo G, Cavaliere C, Rosaria Bianco M, Bock J, Helmeke C, Braun K, Papa M. 2009. Neonatal separation stress reduces glial fibrillary acidic protein- and S100beta-immunoreactive astrocytes in the rat medial precentral cortex. Dev Neurobiol 69:203-11.

Nagy JI, Patel D, Ochalski PA, Stelmack GL. 1999. Connexin30 in rodent, cat and human brain: selective expression in gray matter astrocytes, co-localization with connexin43 at gap junctions and late developmental appearance. Neuroscience 88:447-68.

Naka A, Adesnik H. 2016. Inhibitory Circuits in Cortical Layer 5. Front Neural Circuits 10:35.

Navarrete M, Araque A. 2008. Endocannabinoids mediate neuron-astrocyte communication. Neuron 57:883-93.

Navarrete M, Cuartero MI, Palenzuela R, Draffin JE, Konomi A, Serra I, Colie S, Castano-Castano S, Hasan MT, Nebreda AR, Esteban JA. 2019. Astrocytic p38alpha MAPK drives NMDA receptor-dependent long-term depression and modulates long-term memory. Nat Commun 10:2968.

Navarrete M, Perea G, Fernandez de Sevilla D, Gomez-Gonzalo M, Nunez A, Martin ED, Araque A. 2012. Astrocytes mediate in vivo cholinergic-induced synaptic plasticity. PLoS Biol 10:e1001259.

Navarrete M, Perea G, Maglio L, Pastor J, Garcia de Sola R, Araque A. 2013. Astrocyte calcium signal and gliotransmission in human brain tissue. Cereb Cortex 23:1240-6.

Nedergaard M. 1994. Direct signaling from astrocytes to neurons in cultures of mammalian brain cells. Science 263:1768-71.

Nedergaard M, Rodriguez JJ, Verkhratsky A. 2010. Glial calcium and diseases of the nervous system. Cell Calcium 47:140-9.

Nett WJ, Oloff SH, McCarthy KD. 2002. Hippocampal astrocytes in situ exhibit calcium oscillations that occur independent of neuronal activity. J Neurophysiol 87:528-37.

Nicholls RE, Alarcon JM, Malleret G, Carroll RC, Grody M, Vronskaya S, Kandel ER. 2008. Transgenic mice lacking NMDAR-dependent LTD exhibit deficits in behavioral flexibility. Neuron 58:104-17.

Nimmerjahn A, Mukamel EA, Schnitzer MJ. 2009. Motor behavior activates Bergmann glial networks. Neuron 62:400-12.

Nishiyama H, Knopfel T, Endo S, Itohara S. 2002. Glial protein S100B modulates long-term neuronal synaptic plasticity. Proc Natl Acad Sci U S A 99:4037-42.

Nizar K, Uhlirova H, Tian P, Saisan PA, Cheng Q, Reznichenko L, Weldy KL, Steed TC, Sridhar VB, MacDonald CL, Cui J, Gratiy SL, Sakadzic S, Boas DA, Beka TI, Einevoll GT, Chen J, Masliah E, Dale AM, Silva GA, Devor A. 2013. In vivo stimulus-induced vasodilation occurs without IP3 receptor activation and may precede astrocytic calcium increase. J Neurosci 33:8411-22.

Nollet M, Le Guisquet AM, Belzung C. 2013. Models of depression: unpredictable chronic mild stress in mice. Curr Protoc Pharmacol Chapter 5:Unit 5.65.

O'Keefe J, Dostrovsky J. 1971. The hippocampus as a spatial map. Preliminary evidence from unit activity in the freely-moving rat. Brain Res 34:171-5.

Oberheim NA, Goldman SA, Nedergaard M. 2012. Heterogeneity of astrocytic form and function. Methods Mol Biol 814:23-45.

Ojo JO, Rezaie P, Gabbott PL, Stewart MG. 2015. Impact of age-related neuroglial cell responses on hippocampal deterioration. Front Aging Neurosci 7:57.

Okubo Y, Kanemaru K, Suzuki J, Kobayashi K, Hirose K, Iino M. 2019. Inositol 1,4,5-trisphosphate receptor type 2-independent Ca(2+) release from the endoplasmic reticulum in astrocytes. Glia 67:113-124.

Oliveira JF, Dias NS, Correia M, Gama-Pereira F, Sardinha VM, Lima A, Oliveira AF, Jacinto LR, Ferreira DS, Silva AM, Reis JS, Cerqueira JJ, Sousa N. 2013. Chronic stress disrupts neural coherence between cortico-limbic structures. Front Neural Circuits 7:10.

Oliveira JF, Sardinha VM, Guerra-Gomes S, Araque A, Sousa N. 2015. Do stars govern our actions? Astrocyte involvement in rodent behavior. Trends Neurosci 38:535-49.

Opris I, Casanova MF. 2014. Prefrontal cortical minicolumn: from executive control to disrupted cognitive processing. Brain 137:1863-75.

Orr AG, Hsiao EC, Wang MM, Ho K, Kim DH, Wang X, Guo W, Kang J, Yu GQ, Adame A, Devidze N, Dubal DB, Masliah E, Conklin BR, Mucke L. 2015. Astrocytic adenosine receptor A2A and Gs-coupled signaling regulate memory. Nat Neurosci 18:423-34.

Orre M, Kamphuis W, Osborn LM, Melief J, Kooijman L, Huitinga I, Klooster J, Bossers K, Hol EM. 2014. Acute isolation and transcriptome characterization of cortical astrocytes and microglia from young and aged mice. Neurobiol Aging 35:1-14.

Pabst M, Braganza O, Dannenberg H, Hu W, Pothmann L, Rosen J, Mody I, van Loo K, Deisseroth K, Becker AJ, Schoch S, Beck H. 2016. Astrocyte Intermediaries of Septal Cholinergic Modulation in the Hippocampus. Neuron 90:853-65.

Padmashri R, Suresh A, Boska MD, Dunaevsky A. 2015. Motor-Skill Learning Is Dependent on Astrocytic Activity. Neural Plast 2015:938023.

Palmer AL, Ousman SS. 2018. Astrocytes and Aging. Front Aging Neurosci 10:337.

Panatier A, Vallee J, Haber M, Murai KK, Lacaille JC, Robitaille R. 2011. Astrocytes are endogenous regulators of basal transmission at central synapses. Cell 146:785-98.

Pannasch U, Rouach N. 2013. Emerging role for astroglial networks in information processing: from synapse to behavior. Trends Neurosci 36:405-17.

Pannasch U, Vargova L, Reingruber J, Ezan P, Holcman D, Giaume C, Sykova E, Rouach N. 2011. Astroglial networks scale synaptic activity and plasticity. Proc Natl Acad Sci U S A 108:8467-72.

Papouin T, Dunphy JM, Tolman M, Dineley KT, Haydon PG. 2017. Septal Cholinergic Neuromodulation Tunes the Astrocyte-Dependent Gating of Hippocampal NMDA Receptors to Wakefulness. Neuron 94:840-854 e7.
Parpura V, Basarsky TA, Liu F, Jeftinija K, Jeftinija S, Haydon PG. 1994. Glutamate-mediated astrocyte-neuron signalling. Nature 369:744-7.
Parpura V, Grubisic V, Verkhratsky A. 2011. Ca(2+) sources for the exocytotic release of glutamate from astrocytes. Biochim Biophys Acta 1813:984-91.
Parpura V, Verkhratsky A. 2012. Homeostatic function of astrocytes: Ca(2+) and Na(+) signalling. Transl Neurosci 3:334-344.
Parpura V, Zorec R. 2010. Gliotransmission: Exocytotic release from astrocytes. Brain Res Rev 63:83-92.
Patricio P, Mateus-Pinheiro A, Irmler M, Alves ND, Machado-Santos AR, Morais M, Correia JS, Korostynski M, Piechota M, Stoffel R, Beckers J, Bessa JM, Almeida OF, Sousa N, Pinto L. 2015. Differential and converging molecular mechanisms of antidepressants' action in the hippocampal dentate gyrus. Neuropsychopharmacology 40:338-49.
Paxinos G, Franklin KBJ. 2004. The Mouse Brain in Stereotaxic Coordinates: Gulf Professional Publishing.
Perea G, Araque A. 2005. Properties of synaptically evoked astrocyte calcium signal reveal synaptic information processing by astrocytes. J Neurosci 25:2192-203.
Perea G, Araque A. 2007. Astrocytes potentiate transmitter release at single hippocampal synapses. Science 317:1083-6.
Perea G, Gomez R, Mederos S, Covelo A, Ballesteros JJ, Schlosser L, Hernandez-Vivanco A, Martin-Fernandez M, Quintana R, Rayan A, Diez A, Fuenzalida M, Agarwal A, Bergles DE, Bettler B, Manahan-Vaughan D, Martin ED, Kirchhoff F, Araque A. 2016. Activity-dependent switch of GABAergic inhibition into glutamatergic excitation in astrocyte-neuron networks. Elife 5.
Perea G, Navarrete M, Araque A. 2009. Tripartite synapses: astrocytes process and control synaptic information. Trends Neurosci 32:421-31.
Perea G, Sur M, Araque A. 2014. Neuron-glia networks: integral gear of brain function. Front Cell Neurosci 8:378.
Perez-Alvarez A, Navarrete M, Covelo A, Martin ED, Araque A. 2014. Structural and functional plasticity of astrocyte processes and dendritic spine interactions. J Neurosci 34:12738-44.
Peters R. 2006. Ageing and the brain. Postgrad Med J 82:84-8.
Petravicz J, Boyt KM, McCarthy KD. 2014. Astrocyte IP3R2-dependent Ca(2+) signaling is not a major modulator of neuronal pathways governing behavior. Front Behav Neurosci 8:384.
Petravicz J, Fiacco TA, McCarthy KD. 2008. Loss of IP3 receptor-dependent Ca2+ increases in hippocampal astrocytes does not affect baseline CA1 pyramidal neuron synaptic activity. J Neurosci 28:4967-73.
Petrelli F, Bezzi P. 2016. Novel insights into gliotransmitters. Curr Opin Pharmacol 26:138-45.
Petzold GC, Murthy VN. 2011. Role of astrocytes in neurovascular coupling. Neuron 71:782-97.
Pinto-Duarte A, Roberts AJ, Ouyang K, Sejnowski TJ. 2019. Impairments in remote memory caused by the lack of Type 2 IP3 receptors. Glia 67:1976-1989.
Pistell PJ, Spangler EL, Kelly-Bell B, Miller MG, de Cabo R, Ingram DK. 2012. Age-associated learning and memory deficits in two mouse versions of the Stone T-maze. Neurobiol Aging 33:2431-9.
Pittenger C, Duman RS. 2008. Stress, depression, and neuroplasticity: a convergence of mechanisms. Neuropsychopharmacology 33:88-109.
Poskanzer KE, Yuste R. 2011. Astrocytic regulation of cortical UP states. Proc Natl Acad Sci U S A 108:18453-8.
Poskanzer KE, Yuste R. 2016. Astrocytes regulate cortical state switching in vivo. Proc Natl Acad Sci U S A 113:E2675-84.

Rajah MN, D'Esposito M. 2005. Region-specific changes in prefrontal function with age: a review of PET and fMRI studies on working and episodic memory. Brain 128:1964-83.

Rajkowska G, Stockmeier CA. 2013. Astrocyte pathology in major depressive disorder: insights from human postmortem brain tissue. Curr Drug Targets 14:1225-36.

Rakers C, Petzold GC. 2017. Astrocytic calcium release mediates peri-infarct depolarizations in a rodent stroke model. J Clin Invest 127:511-516.

Reichenbach N, Delekate A, Breithausen B, Keppler K, Poll S, Schulte T, Peter J, Plescher M, Hansen JN, Blank N, Keller A, Fuhrmann M, Henneberger C, Halle A, Petzold GC. 2018. P2Y1 receptor blockade normalizes network dysfunction and cognition in an Alzheimer's disease model. J Exp Med 215:1649-1663.

Reyes RC, Verkhratsky A, Parpura V. 2013. TRPC1-mediated Ca2+ and Na+ signalling in astroglia: differential filtering of extracellular cations. Cell Calcium 54:120-5.

Rial D, Lemos C, Pinheiro H, Duarte JM, Goncalves FQ, Real JI, Prediger RD, Goncalves N, Gomes CA, Canas PM, Agostinho P, Cunha RA. 2015. Depression as a Glial-Based Synaptic Dysfunction. Front Cell Neurosci 9:521.

Rivera-Pagan AF, Rivera-Aponte DE, Melnik-Martinez KV, Zayas-Santiago A, Kucheryavykh LY, Martins AH, Cubano LA, Skatchkov SN, Eaton MJ. 2015. Up-regulation of TREK-2 potassium channels in cultured astrocytes requires de novo protein synthesis: relevance to localization of TREK-2 channels in astrocytes after transient cerebral ischemia. PLoS One 10:e0125195.

Robin LM, Oliveira da Cruz JF, Langlais VC, Martin-Fernandez M, Metna-Laurent M, Busquets-Garcia A, Bellocchio L, Soria-Gomez E, Papouin T, Varilh M, Sherwood MW, Belluomo I, Balcells G, Matias I, Bosier B, Drago F, Van Eeckhaut A, Smolders I, Georges F, Araque A, Panatier A, Oliet SHR, Marsicano G. 2018. Astroglial CB1 Receptors Determine Synaptic D-Serine Availability to Enable Recognition Memory. Neuron 98:935-944 e5.

Rodriguez JJ, Yeh CY, Terzieva S, Olabarria M, Kulijewicz-Nawrot M, Verkhratsky A. 2014. Complex and region-specific changes in astroglial markers in the aging brain. Neurobiol Aging 35:15-23.

Rogers JT, Liu CC, Zhao N, Wang J, Putzke T, Yang L, Shinohara M, Fryer JD, Kanekiyo T, Bu G. 2017. Subacute ibuprofen treatment rescues the synaptic and cognitive deficits in advanced-aged mice. Neurobiol Aging 53:112-121.

Rungta RL, Bernier LP, Dissing-Olesen L, Groten CJ, LeDue JM, Ko R, Drissler S, MacVicar BA. 2016. Ca(2+) transients in astrocyte fine processes occur via Ca(2+) influx in the adult mouse hippocampus. Glia 64:2093-2103.

Rusakov DA. 2015. Disentangling calcium-driven astrocyte physiology. Nat Rev Neurosci 16:226-33.

Rusakov DA, Bard L, Stewart MG, Henneberger C. 2014. Diversity of astroglial functions alludes to subcellular specialisation. Trends Neurosci 37:228-42.

Saito K, Shigetomi E, Yasuda R, Sato R, Nakano M, Tashiro K, Tanaka KF, Ikenaka K, Mikoshiba K, Mizuta I, Yoshida T, Nakagawa M, Mizuno T, Koizumi S. 2018. Aberrant astrocyte Ca(2+) signals "AxCa signals" exacerbate pathological alterations in an Alexander disease model. Glia 66:1053-1067.

Santarelli L, Saxe M, Gross C, Surget A, Battaglia F, Dulawa S, Weisstaub N, Lee J, Duman R, Arancio O, Belzung C, Hen R. 2003. Requirement of hippocampal neurogenesis for the behavioral effects of antidepressants. Science 301:805-9.

Santello M, Cali C, Bezzi P. 2012. Gliotransmission and the tripartite synapse. Adv Exp Med Biol 970:307-31.

Santello M, Toni N, Volterra A. 2019. Astrocyte function from information processing to cognition and cognitive impairment. Nat Neurosci 22:154-166.

Santos M, Silva-Fernandes A, Oliveira P, Sousa N, Maciel P. 2007. Evidence for abnormal early development in a mouse model of Rett syndrome. Genes Brain Behav 6:277-86.

Sardinha VM, Guerra-Gomes S, Caetano I, Tavares G, Martins M, Reis JS, Correia JS, Teixeira-Castro A, Pinto L, Sousa N, Oliveira JF. 2017. Astrocytic signaling supports hippocampal-prefrontal theta synchronization and cognitive function. Glia 65:1944-1960.

Sasaki T, Ishikawa T, Abe R, Nakayama R, Asada A, Matsuki N, Ikegaya Y. 2014. Astrocyte calcium signalling orchestrates neuronal synchronization in organotypic hippocampal slices. J Physiol 592:2771-83.

Savtchouk I, Volterra A. 2018. Gliotransmission: Beyond Black-and-White. J Neurosci 38:14-25.

Scemes E, Giaume C. 2006. Astrocyte calcium waves: what they are and what they do. Glia 54:716-25.

Seibenhener ML, Wooten MC. 2015. Use of the Open Field Maze to measure locomotor and anxiety-like behavior in mice. J Vis Exp:e52434.

Seifert G, Henneberger C, Steinhauser C. 2018. Diversity of astrocyte potassium channels: An update. Brain Res Bull 136:26-36.

Serrano A, Haddjeri N, Lacaille JC, Robitaille R. 2006. GABAergic network activation of glial cells underlies hippocampal heterosynaptic depression. J Neurosci 26:5370-82.

Sharp AH, Nucifora FC, Jr., Blondel O, Sheppard CA, Zhang C, Snyder SH, Russell JT, Ryugo DK, Ross CA. 1999. Differential cellular expression of isoforms of inositol 1,4,5-triphosphate receptors in neurons and glia in brain. J Comp Neurol 406:207-20.

Sherwood MW, Arizono M, Hisatsune C, Bannai H, Ebisui E, Sherwood JL, Panatier A, Oliet SH, Mikoshiba K. 2017. Astrocytic IP3 Rs: Contribution to Ca(2+) signalling and hippocampal LTP. Glia 65:502-513.

Shigetomi E, Jackson-Weaver O, Huckstepp RT, O'Dell TJ, Khakh BS. 2013. TRPA1 channels are regulators of astrocyte basal calcium levels and long-term potentiation via constitutive D-serine release. J Neurosci 33:10143-53.

Shigetomi E, Patel S, Khakh BS. 2016. Probing the Complexities of Astrocyte Calcium Signaling. Trends Cell Biol 26:300-312.

Shigetomi E, Tong X, Kwan KY, Corey DP, Khakh BS. 2011. TRPA1 channels regulate astrocyte resting calcium and inhibitory synapse efficacy through GAT-3. Nat Neurosci 15:70-80.

Silva JM, Rodrigues S, Sampaio-Marques B, Gomes P, Neves-Carvalho A, Dioli C, Soares-Cunha C, Mazuik BF, Takashima A, Ludovico P, Wolozin B, Sousa N, Sotiropoulos I. 2018. Dysregulation of autophagy and stress granule-related proteins in stress-driven Tau pathology. Cell Death Differ 26:1411-1427.

Sofroniew MV. 2014. Astrogliosis. Cold Spring Harb Perspect Biol 7:a020420.

Sofroniew MV, Vinters HV. 2010. Astrocytes: biology and pathology. Acta Neuropathol 119:7-35.

Soreq L, Consortium UKBE, North American Brain Expression C, Rose J, Soreq E, Hardy J, Trabzuni D, Cookson MR, Smith C, Ryten M, Patani R, Ule J. 2017. Major Shifts in Glial Regional Identity Are a Transcriptional Hallmark of Human Brain Aging. Cell Rep 18:557-570.

Sousa N, Almeida OF, Wotjak CT. 2006. A hitchhiker's guide to behavioral analysis in laboratory rodents. Genes Brain Behav 5 Suppl 2:5-24.

Spitzer M. 2006. Chapter 3: Brain Research and Learning over the Life Cycle: Organization for Economic Co-operation and Development.

Srinivasan R, Huang BS, Venugopal S, Johnston AD, Chai H, Zeng H, Golshani P, Khakh BS. 2015. Ca(2+) signaling in astrocytes from Ip3r2(-/-) mice in brain slices and during startle responses in vivo. Nat Neurosci 18:708-17.

Srinivasan R, Lu TY, Chai H, Xu J, Huang BS, Golshani P, Coppola G, Khakh BS. 2016. New Transgenic Mouse Lines for Selectively Targeting Astrocytes and Studying Calcium Signals in Astrocyte Processes In Situ and In Vivo. Neuron 92:1181-1195.

Steru L, Chermat R, Thierry B, Simon P. 1985. The tail suspension test: a new method for screening antidepressants in mice. Psychopharmacology (Berl) 85:367-70.

Stobart JL, Ferrari KD, Barrett MJP, Gluck C, Stobart MJ, Zuend M, Weber B. 2018. Cortical Circuit Activity Evokes Rapid Astrocyte Calcium Signals on a Similar Timescale to Neurons. Neuron 98:726-735 e4.

Stranahan AM, Jiam NT, Spiegel AM, Gallagher M. 2012. Aging reduces total neuron number in the dorsal component of the rodent prefrontal cortex. J Comp Neurol 520:1318-26.

Sturn A, Quackenbush J, Trajanoski Z. 2002. Genesis: cluster analysis of microarray data. Bioinformatics 18:207-8.

Surget A, Tanti A, Leonardo ED, Laugeray A, Rainer Q, Touma C, Palme R, Griebel G, Ibarguen-Vargas Y, Hen R, Belzung C. 2011. Antidepressants recruit new neurons to improve stress response regulation. Mol Psychiatry 16:1177-88.

Suzuki A, Stern SA, Bozdagi O, Huntley GW, Walker RH, Magistretti PJ, Alberini CM. 2011. Astrocyte-neuron lactate transport is required for long-term memory formation. Cell 144:810-23.

Takata N, Hirase H. 2008. Cortical layer 1 and layer 2/3 astrocytes exhibit distinct calcium dynamics in vivo. PLoS One 3:e2525.

Takata N, Mishima T, Hisatsune C, Nagai T, Ebisui E, Mikoshiba K, Hirase H. 2011. Astrocyte calcium signaling transforms cholinergic modulation to cortical plasticity in vivo. J Neurosci 31:18155-65.

Takata N, Nagai T, Ozawa K, Oe Y, Mikoshiba K, Hirase H. 2013. Cerebral blood flow modulation by Basal forebrain or whisker stimulation can occur independently of large cytosolic Ca2+ signaling in astrocytes. PLoS One 8:e66525.

Tanaka K, Watase K, Manabe T, Yamada K, Watanabe M, Takahashi K, Iwama H, Nishikawa T, Ichihara N, Kikuchi T, Okuyama S, Kawashima N, Hori S, Takimoto M, Wada K. 1997. Epilepsy and exacerbation of brain injury in mice lacking the glutamate transporter GLT-1. Science 276:1699-702.

Tanaka M, Shih PY, Gomi H, Yoshida T, Nakai J, Ando R, Furuichi T, Mikoshiba K, Semyanov A, Itohara S. 2013. Astrocytic Ca2+ signals are required for the functional integrity of tripartite synapses. Mol Brain 6:6.

Tanaka M, Wang X, Mikoshiba K, Hirase H, Shinohara Y. 2017. Rearing-environment-dependent hippocampal local field potential differences in wild-type and inositol trisphosphate receptor type 2 knockout mice. J Physiol 595:6557-6568.

Tang G, Gudsnuk K, Kuo SH, Cotrina ML, Rosoklija G, Sosunov A, Sonders MS, Kanter E, Castagna C, Yamamoto A, Yue Z, Arancio O, Peterson BS, Champagne F, Dwork AJ, Goldman J, Sulzer D. 2014. Loss of mTOR-dependent macroautophagy causes autistic-like synaptic pruning deficits. Neuron 83:1131-43.

Tavares G, Martins M, Correia JS, Sardinha VM, Guerra-Gomes S, das Neves SP, Marques F, Sousa N, Oliveira JF. 2017. Employing an open-source tool to assess astrocyte tridimensional structure. Brain Struct Funct 222:1989-1999.

team RDc. 2005. r: A language and environment for statistical computing. Vienna, Austria: r foundation for statistical computing.

Tertil M, Skupio U, Barut J, Dubovyk V, Wawrzczak-Bargiela A, Soltys Z, Golda S, Kudla L, Wiktorowska L, Szklarczyk K, Korostynski M, Przewlocki R, Slezak M. 2018. Glucocorticoid receptor signaling in astrocytes is required for aversive memory formation. Transl Psychiatry 8:255.

Torres-Platas SG, Hercher C, Davoli MA, Maussion G, Labonte B, Turecki G, Mechawar N. 2011. Astrocytic hypertrophy in anterior cingulate white matter of depressed suicides. Neuropsychopharmacology 36:2650-8.

Tosato M, Zamboni V, Ferrini A, Cesari M. 2007. The aging process and potential interventions to extend life expectancy. Clin Interv Aging 2:401-12.

Vardjan N, Verkhratsky A, Zorec R. 2017. Astrocytic Pathological Calcium Homeostasis and Impaired Vesicle Trafficking in Neurodegeneration. Int J Mol Sci 18.
Verkhratsky A. 2006. Glial calcium signaling in physiology and pathophysiology. Acta Pharmacol Sin 27:773-80.
Verkhratsky A. 2009. Neurotransmitter Receptors in Astrocytes. In: Parpura V, Haydon PG, editors. Astrocytes in (Patho)Physiology of the Nervous System: Springer Science + Business Media.
Verkhratsky A, Matteoli M, Parpura V, Mothet JP, Zorec R. 2016a. Astrocytes as secretory cells of the central nervous system: idiosyncrasies of vesicular secretion. EMBO J 35:239-57.
Verkhratsky A, Nedergaard M. 2016. The homeostatic astroglia emerges from evolutionary specialization of neural cells. Philos Trans R Soc Lond B Biol Sci 371.
Verkhratsky A, Nedergaard M. 2018. Physiology of Astroglia. Physiol Rev 98:239-389.
Verkhratsky A, Parpura V. 2014. Introduction to Neuroglia: Morgan & Claypool Life Sciences.
Verkhratsky A, Reyes RC, Parpura V. 2014. TRP channels coordinate ion signalling in astroglia. Rev Physiol Biochem Pharmacol 166:1-22.
Verkhratsky A, Zorec R, Rodriguez JJ, Parpura V. 2016b. Astroglia dynamics in ageing and Alzheimer's disease. Curr Opin Pharmacol 26:74-9.
Volterra A, Liaudet N, Savtchouk I. 2014. Astrocyte Ca(2)(+) signalling: an unexpected complexity. Nat Rev Neurosci 15:327-35.
Vorhees CV, Williams MT. 2006. Morris water maze: procedures for assessing spatial and related forms of learning and memory. Nat Protoc 1:848-58.
Walf AA, Frye CA. 2007. The use of the elevated plus maze as an assay of anxiety-related behavior in rodents. Nat Protoc 2:322-8.
Wang DD, Bordey A. 2008. The astrocyte odyssey. Prog Neurobiol 86:342-67.
Wang F, Smith NA, Xu Q, Fujita T, Baba A, Matsuda T, Takano T, Bekar L, Nedergaard M. 2012a. Astrocytes modulate neural network activity by Ca(2)+-dependent uptake of extracellular K+. Sci Signal 5:ra26.
Wang F, Xu Q, Wang W, Takano T, Nedergaard M. 2012b. Bergmann glia modulate cerebellar Purkinje cell bistability via Ca2+-dependent K+ uptake. Proc Natl Acad Sci U S A 109:7911-6.
Wang Q, Jie W, Liu JH, Yang JM, Gao TM. 2017. An astroglial basis of major depressive disorder? An overview. Glia 65:1227-1250.
Wang TF, Zhou C, Tang AH, Wang SQ, Chai Z. 2006a. Cellular mechanism for spontaneous calcium oscillations in astrocytes. Acta Pharmacol Sin 27:861-8.
Wang X, Lou N, Xu Q, Tian GF, Peng WG, Han X, Kang J, Takano T, Nedergaard M. 2006b. Astrocytic Ca2+ signaling evoked by sensory stimulation in vivo. Nat Neurosci 9:816-23.
Weber B, Barros LF. 2015. The Astrocyte: Powerhouse and Recycling Center. Cold Spring Harb Perspect Biol 7.
Weber M, Wu T, Hanson JE, Alam NM, Solanoy H, Ngu H, Lauffer BE, Lin HH, Dominguez SL, Reeder J, Tom J, Steiner P, Foreman O, Prusky GT, Scearce-Levie K. 2015. Cognitive Deficits, Changes in Synaptic Function, and Brain Pathology in a Mouse Model of Normal Aging. eNeuro 2.
Wefelmeyer W, Puhl CJ, Burrone J. 2016. Homeostatic Plasticity of Subcellular Neuronal Structures: From Inputs to Outputs. Trends Neurosci 39:656-667.
WHO. 2017. Depression and other common mental disorders: global health estimates.
Wiegert JS, Oertner TG. 2013. Long-term depression triggers the selective elimination of weakly integrated synapses. Proc Natl Acad Sci U S A 110:E4510-9.
Willner P, Towell A, Sampson D, Sophokleous S, Muscat R. 1987. Reduction of sucrose preference by chronic unpredictable mild stress, and its restoration by a tricyclic antidepressant. Psychopharmacology (Berl) 93:358-64.

Wilson CR, Gaffan D, Browning PG, Baxter MG. 2010. Functional localization within the prefrontal cortex: missing the forest for the trees? Trends Neurosci 33:533-40.

Wu D, Peng F, Zhang B, Ingram AJ, Kelly DJ, Gilbert RE, Gao B, Krepinsky JC. 2009. PKC-beta1 mediates glucose-induced Akt activation and TGF-beta1 upregulation in mesangial cells. J Am Soc Nephrol 20:554-66.

Yang J, Yang H, Liu Y, Li X, Qin L, Lou H, Duan S, Wang H. 2016. Astrocytes contribute to synapse elimination via type 2 inositol 1,4,5-trisphosphate receptor-dependent release of ATP. Elife 5:e15043.

Yang Z, Wang KK. 2015. Glial fibrillary acidic protein: from intermediate filament assembly and gliosis to neurobiomarker. Trends Neurosci 38:364-74.

Yates MA, Markham JA, Anderson SE, Morris JR, Juraska JM. 2008. Regional variability in age-related loss of neurons from the primary visual cortex and medial prefrontal cortex of male and female rats. Brain Res 1218:1-12.

Yu T, Guo M, Garza J, Rendon S, Sun XL, Zhang W, Lu XY. 2011. Cognitive and neural correlates of depression-like behaviour in socially defeated mice: an animal model of depression with cognitive dysfunction. Int J Neuropsychopharmacol 14:303-17.

Yu X, Taylor AMW, Nagai J, Golshani P, Evans CJ, Coppola G, Khakh BS. 2018. Reducing Astrocyte Calcium Signaling In Vivo Alters Striatal Microcircuits and Causes Repetitive Behavior. Neuron 99:1170-1187 e9.

Zamanian JL, Xu L, Foo LC, Nouri N, Zhou L, Giffard RG, Barres BA. 2012. Genomic analysis of reactive astrogliosis. J Neurosci 32:6391-410.

Zhang Y, Chen K, Sloan SA, Bennett ML, Scholze AR, O'Keeffe S, Phatnani HP, Guarnieri P, Caneda C, Ruderisch N, Deng S, Liddelow SA, Zhang C, Daneman R, Maniatis T, Barres BA, Wu JQ. 2014. An RNA-sequencing transcriptome and splicing database of glia, neurons, and vascular cells of the cerebral cortex. J Neurosci 34:11929-47.

Zhang Z, Ma Z, Zou W, Guo H, Liu M, Ma Y, Zhang L. 2019. The Appropriate Marker for Astrocytes: Comparing the Distribution and Expression of Three Astrocytic Markers in Different Mouse Cerebral Regions. Biomed Res Int 2019:9605265.

Zorec R, Araque A, Carmignoto G, Haydon PG, Verkhratsky A, Parpura V. 2012. Astroglial excitability and gliotransmission: an appraisal of Ca2+ as a signalling route. ASN Neuro 4.

Zorec R, Verkhratsky A, Rodriguez JJ, Parpura V. 2016. Astrocytic vesicles and gliotransmitters: Slowness of vesicular release and synaptobrevin2-laden vesicle nanoarchitecture. Neuroscience 323:67-75.

ANNEXES

frontiers in Cellular Neuroscience

MINI REVIEW
published: 17 January 2018
doi: 10.3389/fncel.2017.00427

Functional Roles of Astrocyte Calcium Elevations: From Synapses to Behavior

*Sónia Guerra-Gomes[1,2], Nuno Sousa[1,2], Luísa Pinto[1,2] and João F. Oliveira[1,2,3]**

[1] Life and Health Sciences Research Institute (ICVS), School of Medicine, University of Minho, Braga, Portugal, [2] ICVS/3B's – PT Government Associate Laboratory, Braga, Portugal, [3] DIGARC, Polytechnic Institute of Cávado and Ave, Barcelos, Portugal

Astrocytes are fundamental players in the regulation of synaptic transmission and plasticity. They display unique morphological and phenotypical features that allow to monitor and to dynamically respond to changes. One of the hallmarks of the astrocytic response is the generation of calcium elevations, which further affect downstream cellular processes. Technical advances in the field have allowed to spatially and to temporally quantify and qualify these elevations. However, the impact on brain function remains poorly understood. In this review, we discuss evidences of the functional impact of heterogeneous astrocytic calcium events in several brain regions, and their consequences in synapses, circuits, and behavior.

Keywords: astrocyte, calcium, synapse, neural circuit, behavior

OPEN ACCESS

Edited by:
Kira Poskanzer,
University of California,
San Francisco, United States

Reviewed by:
Hajime Hirase,
RIKEN Brain Science Institute, Japan
Vladislav Volman,
L-3 Communications, United States
Alfonso Araque,
University of Minnesota, United States

***Correspondence:**
João F. Oliveira
joaooliveira@med.uminho.pt

Received: *10 August 2017*
Accepted: *20 December 2017*
Published: *17 January 2018*

Citation:
Guerra-Gomes S, Sousa N, Pinto L and Oliveira JF (2018) Functional Roles of Astrocyte Calcium Elevations: From Synapses to Behavior. Front. Cell. Neurosci. 11:427. doi: 10.3389/fncel.2017.00427

DIFFERENT FORMS OF CALCIUM ELEVATIONS IN ASTROCYTES: THE COMPLEXITY OF SIMPLICITY

Astrocytes have emerged as key players in the regulation of synaptic physiology. They display complex and heterogeneous morphological structures and are able to sense and respond to environmental signals, modulate neuronal activity, synaptic transmission, and vascular function (Araque et al., 2014; Perea et al., 2014; Petrelli and Bezzi, 2016); for review (Petzold and Murthy, 2011; Zorec et al., 2012). Synaptic activity is integrated by astrocytes (Perea and Araque, 2005) and might result in intracellular calcium (Ca^{2+}) elevations with specific spatial and temporal properties. These might appear as "global" and/or "focal" responses within the astrocytic complex morphology. It is yet unclear if global Ca^{2+} elevations are more representative of an integrative response or if they are the result of a linear summation of Ca^{2+} fluctuations or inositol 1,4,5-trisphosphate (IP_3) levels; nevertheless, these have been used for over two decades as a readout of astrocytic function (Khakh and McCarthy, 2015); for review (Rusakov et al., 2014; Volterra et al., 2014). Ca^{2+} elevations may appear spontaneously or may be triggered by endogenous or exogenous stimuli. Traditionally, the use of Ca^{2+} indicator dyes allowed for the detection of Ca^{2+} elevations within astrocyte somata, but failed to efficiently track them in the fine processes (Wang et al., 2006; Takata and Hirase, 2008; Nizar et al., 2013). This hindered the complete interpretation of Ca^{2+} dynamics. More refined methods to image astrocyte Ca^{2+} signals have been recently described (Kanemaru et al., 2014; Srinivasan et al., 2016; Bindocci et al., 2017); for review (Shigetomi et al., 2016).

There are several mechanisms that trigger the elevation of astrocyte intracellular Ca^{2+} levels. The activation of G_q-protein-coupled receptors (GPCR) triggers the IP_3 signaling cascade and

results in robust intracellular Ca^{2+} elevations, mainly via the IP_3 receptor type 2 activation (IP_3R2) (Petravicz et al., 2008; Takata et al., 2011; Navarrete et al., 2012); for review (Parpura et al., 2011). Curiously, $GABA_B$ receptor (G_i-coupled GPCRs) activation was also shown to trigger intracellular Ca^{2+} elevations in astrocytes (Serrano et al., 2006; Mariotti et al., 2016; Perea et al., 2016). Moreover, astrocytes express several types of transient receptor potential (TRP) channels (Verkhratsky et al., 2013). The spontaneous opening of TRPA1 channels was shown to contribute to basal Ca^{2+} levels and to a fraction of intrinsic fluctuations (Shigetomi et al., 2012, 2013), and their blockade contributes to a slight decrease in resting Ca^{2+} levels (Agarwal et al., 2017). Additionally, TRPC channels modulate Ca^{2+}-dependent vesicular glutamate release in cortical astrocytes by contributing to the generation of store-operated Ca^{2+} entry (SOCE) (Reyes et al., 2013). More recently, Agarwal et al. (2017) reported that mitochondria, which are abundant in astrocytic processes, are the main active source of Ca^{2+} for localized events in far distant microdomains.

While our understanding of the origin and features of astrocytic Ca^{2+} signaling is steadily growing, its functional consequences to the surrounding cellular circuits remain poorly understood. Therefore, this review will focus on the available data showing functional outputs of astrocytic Ca^{2+} elevations. The reader may find useful reviews and discussions elsewhere on the origin and features of astrocyte Ca^{2+} elevations (Scemes and Giaume, 2006; Agulhon et al., 2008; Leybaert and Sanderson, 2012; Volterra et al., 2014; Khakh and McCarthy, 2015; Bazargani and Attwell, 2016; Shigetomi et al., 2016), and on the role of astrocyte Ca^{2+} in pathology (Nedergaard et al., 2010; Agulhon et al., 2012; Vardjan et al., 2017).

FUNCTIONAL ROLES OF ASTROCYTE CALCIUM ELEVATIONS

The advent of novel techniques and approaches allowed for the quantification of astrocytic Ca^{2+} elevations and the characterization of their spatiotemporal dynamics in several brain regions. Below, we will discuss relevant studies that report on the functional influence of astrocytic Ca^{2+} elevations on synapses, circuits, and behavior.

Astrocyte Calcium and Synapses

The studies reviewed in this section describe experiments performed in rat and mouse brain slices. Several pieces of evidence indicate that astrocytic Ca^{2+} elevations precede the release of gliotransmitters, which may ultimately modulate synaptic transmission (**Figure 1**). Different levels of neuronal activity appear to scale astrocytic Ca^{2+} levels, leading to orchestrated (multi)synaptic responses (for review, Araque et al., 2014). In the hippocampus, ATP-evoked astrocyte Ca^{2+} was shown to promote glutamate release, which consequently facilitates synaptic transmission through the activation of mGluRs (Perea and Araque, 2007). Although further attempts to control astrocytic Ca^{2+} signaling failed either to affect general readouts of synaptic transmission and plasticity in the hippocampus [using MrgA1 and IP_3R2 KO mouse models (Petravicz et al., 2008; Agulhon et al., 2010)] or to detect glutamate release in the hippocampus or striatum [upon Designer Receptor Exclusively Activated by Designer Drugs (DREADD) activation (Chai et al., 2017)], a series of studies have supported this hypothesis. In fact, the tight modulation of astrocytic intracellular Ca^{2+} is crucial for D-serine-dependent long-term potentiation (LTP) of hippocampal CA1 pyramidal cells (Henneberger et al., 2010). Accordingly, a recent study has showed that acute blockade of Ca^{2+}-dependent IP_3 mechanisms impairs LTP, but that this can be rescued by exogenous D-serine (Sherwood et al., 2017).

Astrocytic Ca^{2+} elevations appear to also promote alternative forms of plasticity in the brain. In the hippocampus, cholinergic afferents from the medial septum modulate CA1 synaptic plasticity via an astrocytic Ca^{2+}-dependent mechanism that triggers glutamate release and consequent activation of mGluRs in neurons (Navarrete et al., 2012). This mechanism of synaptic modulation is not restricted to the hippocampus since astrocytic Ca^{2+} elevations also mediate muscarinic acetylcholine receptor-dependent plasticity in the somatosensory cortex (Takata et al., 2011), as it will be discussed in the next chapter. Moreover, a recent study showed that the cholinergic input to astrocytes, driven by active/sleep phases, controls Ca^{2+}-dependent D-serine release, ultimately gearing up NMDA receptor activation at CA1 synapses (Papouin et al., 2017). In a different hippocampal sub-field, the cholinergic activation of hilar astrocytes triggers intracellular Ca^{2+} elevations that precede the activation of hilar inhibitory interneurons, causing a long-lasting GABAergic inhibition of dentate granule cells (Pabst et al., 2016). Further evidences point out that astrocytic Ca^{2+} mediates endocannabinoid-dependent plasticity. Navarrete and Araque (2008) reported that the activation of astrocytic cannabinoid type 1 (CB1) receptors leads to intracellular Ca^{2+} elevations, triggering glutamate release and slow inward currents (SICs) in vicinal pyramidal neurons. Furthermore, endocannabinoid-triggered elevation of astrocytic Ca^{2+} levels contributes to heteroneuronal LTP (Gómez-Gonzalo et al., 2015). In the striatum, a circuit-specific astrocyte-neuron signaling takes place in which the release of endocannabinoids promotes Ca^{2+} elevations in a specific population of astrocytes, triggering the release of glutamate that modulates excitability and synaptic transmission (Martín et al., 2015). Finally, in the medial central amygdala (CeM), astrocytes receive endocannabinoid signaling to release ATP and depress excitatory synapses from basolateral amygdala via A_1 adenosine receptor activation, and enhance inhibitory synapses from the lateral subdivision of the central amygdala via A_{2A} receptor activation. This redundancy system results in CeM neuronal inhibition with impact in animal behavior (Martin-Fernandez et al., 2017).

Interestingly, astrocytic Ca^{2+} elevations are not exclusive to the action of classic excitatory transmitters. Activation of GABA receptors in astrocytes was shown by different research groups to trigger Ca^{2+} elevations with functional synaptic consequences. Specifically, GABAergic heterosynaptic depression in the hippocampal CA1 subfield requires astrocytic Ca^{2+}

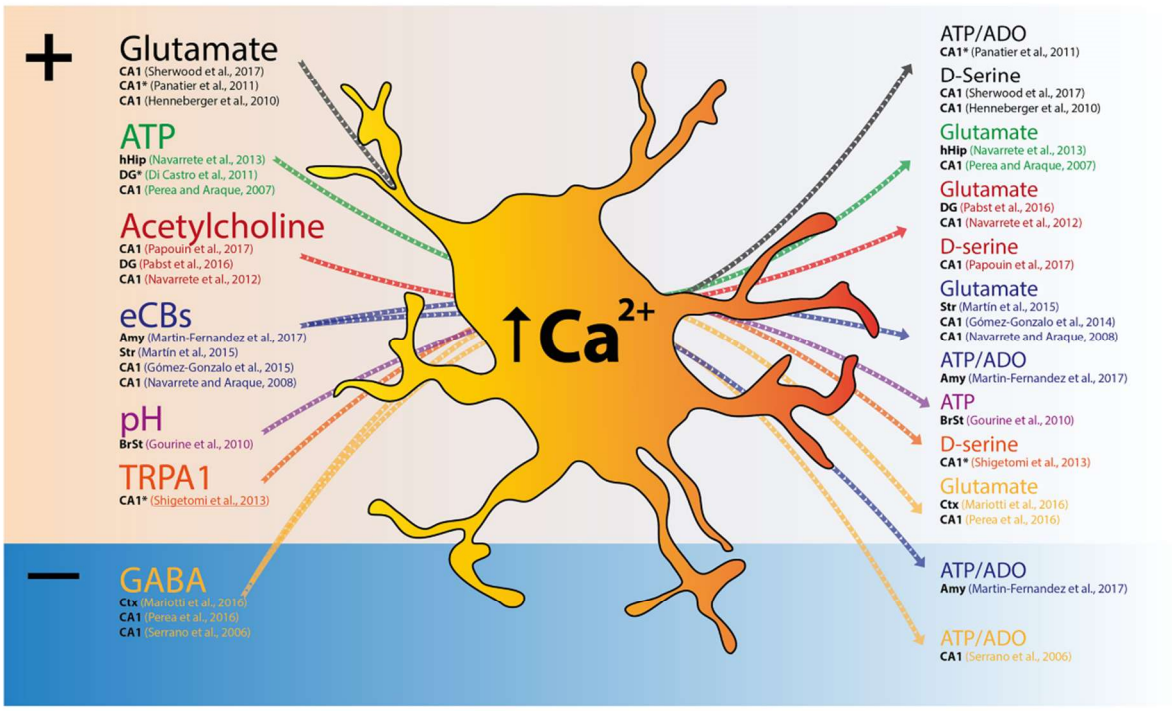

FIGURE 1 | Excitatory and/or inhibitory signals trigger Ca^{2+} elevations in astrocytes and lead to gliotransmitter release. Scheme depicting input signals that trigger astrocyte Ca^{2+} elevations and respective transmitter release. Both excitatory (+) and inhibitory (–) signals cause global or focal Ca^{2+} elevations in astrocytes (Left), and precede gliotransmitter release that might exert excitation or inhibition of neighboring synapses (Right). For each reference, the region studied is indicated in black (Amy, Amygdala; BrSt, brainstem; CA1, CA1 subfield of the hippocampus; Ctx, cortex; DG, dentate gyrus; hHip, human hippocampus; Str, Striatum). *Indicates the studies that described functional consequences to focal Ca^{2+}, rather than global Ca^{2+} responses.

elevations and ATP release, whose metabolite adenosine will activate A_1 receptors (Serrano et al., 2006). More recently, Mariotti et al. (2016) showed that the activation of $GABA_B$ receptors evoked somatic Ca^{2+} elevations, consequently leading to the occurrence of SICs in cortical pyramidal neurons. Curiously, these effects were absent in IP_3R2 KO mice suggesting a relationship between G_i-coupled GPCRs and IP_3 signaling in astrocytes. Moreover, the activation of astrocytic $GABA_B$ receptors triggered intracellular Ca^{2+} elevations in hippocampal CA1 astrocytes, which led to synaptic potentiation via glutamate release and modulation of presynaptic group I mGluRs (Perea et al., 2016).

Astrocytic Ca^{2+} signaling also plays a role in structural integrity of synapses. It was reported that the IP_3 "sponge" mouse model, whose astrocytic IP_3 signaling is impaired, has a reduced astrocytic coverage of asymmetric synapses leading to modulation of glutamatergic transmission (Tanaka et al., 2013). In accordance, activity-related structural remodeling of astrocytic processes in the vicinity of synapses was shown to depend on presynaptic activity and to require G-protein-mediated Ca^{2+} elevations in astrocytes, both in the hippocampus and in the cortex (Perez-Alvarez et al., 2014).

Finally, Navarrete et al. (2013) studied cortical and hippocampal human brain samples and showed that increases in intracellular Ca^{2+} levels of both cortical and hippocampal astrocytes are accompanied by an increase in SICs frequency. These observations confirm that, partially at least, astrocyte Ca^{2+} elevations are also required to modulate synapses in the human brain.

Most of the studies mentioned above regarding synaptic modulation reported consequences of somatic (or in major processes) Ca^{2+} elevations. Recently, several elegant studies suggested that Ca^{2+} signals occurring only at astrocyte microdomains are sufficient to modulate synaptic events. Specifically, Ca^{2+} signals in astrocyte processes of the hippocampal dentate gyrus are relevant for basal synaptic function, since the application of a Ca^{2+} chelator or an antagonist for a GPCR predominantly expressed in astrocyte processes decreased synaptic efficacy (Di Castro et al., 2011). Similarly, mGluR-dependent astrocytic Ca^{2+} signaling was shown to mediate the regulation of basal transmission in CA1 pyramidal neuron synapses (Panatier et al., 2011). The Ca^{2+} signaling that occurs at the distant processes appears to originate from distinct sources, other than the endoplasmic reticulum. For instance, TRPA1 channels mediate a transmembrane Ca^{2+} flux pathway with contributions to basal Ca^{2+} levels and regulation of interneuron inhibitory synapse efficacy via GAT-3 (Shigetomi et al., 2012). In addition, the same group showed that TRPA1 activation contributes to the release of D-serine into the extracellular space, which consequently influences NMDA-dependent hippocampal plasticity (Shigetomi et al., 2013).

Most of the available data resulted from experimental approaches that block general astrocyte Ca^{2+} elevations, namely by using Ca^{2+} chelators or genetic IP_3R2 deletion. This may explain the current bias toward effects of global (soma and main processes) Ca^{2+} signals rather than that of focal events (restricted to cellular microdomains). Nevertheless, it is now clear that global and focal signals coexist in specific spatio-temporal maps. Despite the 10- to 100-fold scale that distinguishes global and focal signals, both have been shown to precede transmitter release and modulate different forms of synaptic transmission (for review, Volterra et al., 2014). Future studies are needed to further discriminate their functional consequences.

Altogether, these sets of data suggest that astrocytes integrate brain circuits following two physiological mechanisms (**Figure 1**). First, the activation of astrocytes appears to represent a novel integration mechanism. Astrocyte Ca^{2+} elevations not only occur upon activation through various excitatory transmitters (e.g., glutamate, ATP, or acetylcholine), but can also be triggered by the inhibitory transmitter GABA. This means that, independently of the nature of the transmitter, astrocytes will be excited/activated (**Figure 1**, left), suggesting they integrate some brain circuits as a redundant layer that reads excitatory and inhibitory neuronal inputs similarly. This concept may add up to the mechanisms of coincidence detection proposed a decade ago by Perea and Araque (2005, 2007). Second, upon activation and Ca^{2+} elevation, astrocytes release gliotransmitters that ultimately cause either neuronal excitation (e.g., glutamate or D-serine) or inhibition (e.g., ATP degraded to adenosine). Curiously, the available literature indicates that astrocytes provide, in most cases, an excitatory output. Nevertheless, astrocytes also release ATP, which is readily degraded to adenosine and in turn activates A_1 receptor leading to synaptic inhibition (Serrano et al., 2006; Martin-Fernandez et al., 2017). This suggests that the type of modulation performed by astrocytes relies not only on the type of transmitter released (which is an intrinsic specificity of the astrocyte), but also on the nature of the receptors expressed by the neighboring cells (which depends on the nature of the neural circuit). In accordance, Martin-Fernandez et al. (2017) also showed that astrocyte-derived ATP results ultimately in excitation or inhibition, depending on the type of receptors found by adenosine. Whether brain circuits are endowed with exclusively excitatory and/or exclusively inhibitory astrocytes, or if these cells play both roles simultaneously (i.e., express machinery to produce, load, and release different transmitters), is still unknown. The first case would not be surprising, since it is the reality for the different neuronal cells (e.g., excitatory glutamatergic vs. inhibitory GABAergic). While recent technical advances have provided fruitful reports of unexpected physiological processes, future studies are needed to confirm their relevance for circuit function.

Astrocyte Calcium and Neural Circuits

The difficulty to measure and/or manipulate intracellular astrocytic Ca^{2+} in the intact brain may explain the lack of studies that report on its functional consequences for circuit and behavior computation. Still, recent reports indicate that the Ca^{2+}-dependent modulation of single synapses (as reviewed above) also have an expected impact on brain circuits.

Regarding the control of cortical synchronization, it was observed that astrocyte Ca^{2+} elevations *in vivo* regulate extracellular glutamate levels, which consequently triggers a slow neuronal rhythm in the brain. This event is characterized by synchronized neuronal firing across different behavioral states, and points to an important regulatory role of astrocytes in cortical circuits (Poskanzer and Yuste, 2016). This observation is in line with previous studies performed in brain slices of the cortex and hippocampus that showed reduced neural synchrony upon disruption of astrocytic Ca^{2+} elevations (Poskanzer and Yuste, 2011; Sasaki et al., 2014). Neural rhythmicity in these regions is essential for several behavioral functions such as attention, learning, memory, and control of sleep/wake cycles (for review, Oliveira et al., 2015). IP_3R2-dependent signaling appears to support ripple-type events that occur during non-theta periods in the CA1 of rodents, a mechanism that might be related to the emotional consequences of social isolation (Tanaka et al., 2017).

In the rat trigeminal sensorimotor circuit for mastication, neural rhythmicity arises after sensory encoding. In this circuit, astrocytes actively respond to sensory stimuli by elevating their intracellular Ca^{2+} levels and, thus, regulating neuronal rhythmic activity, in brainstem slices (Morquette et al., 2015). Furthermore, in thalamo-cortical circuits, astrocytic Ca^{2+} elevations contributed to the modulation of sensory transmission. More specifically, the activation of mGluR2 triggers intracellular Ca^{2+} elevations in astrocytes, which are blocked by the astrocyte-specific toxin fluorocitrate. This effect described *in vivo* and in brain slices is linked to sensory inhibition in the rodent thalamus (Copeland et al., 2017). Furthermore, simultaneous stimulation of whiskers and the nucleus basalis of Meynert revealed that astrocytic Ca^{2+} elevations precede muscarinic acetylcholine receptor (mAChR)-dependent plasticity in the somatosensory cortex *in vivo*. This process is dependent on IP_3R2 signaling and extracellular D-serine (Takata et al., 2011). In the visual cortex, IP_3R2-mediated astrocytic Ca^{2+} elevations are also critical for the integration of visual sensory inputs with the nucleus basalis afferent information (Chen et al., 2012). Moreover, transcranial direct current stimulation (tDCS) was shown to enhance sensory-evoked cortical responses, through elevation of astrocytic intracellular Ca^{2+} via IP_3R2 (Monai et al., 2016). Thus, the authors propose that astrocytic Ca^{2+} elevations might mediate, at least in part, the recognized improvements obtained by tDCS in neuropsychiatric and neurological conditions. Finally, astrocyte Ca^{2+} elevation appears to also be involved in the maintenance of homeostatic mechanisms. Astrocytes in brainstem chemoreceptor areas respond to physiological decreases in pH with vigorous elevations in intracellular Ca^{2+}. These were shown to trigger the release of ATP, inducing adaptive increases in breathing (Gourine et al., 2010).

Astrocyte Ca^{2+} elevations appear to control the function of brain circuits at least in two different forms. On one hand,

astrocytes appear to control plasticity in synapses occurring between neurons projecting to long distances, similarly to the control of local synapses within one brain region, as discussed above. On the other hand, astrocytes of a specific region appear to support local neural synchronization states, controlling the circuit output, most likely in a multi-synaptic process. Whether the two forms of modulation use similar mechanisms, i.e., whether regional integration is a product of 10 to 1000 of synapses being similarly integrated, is still unknown. However, it seems that both temporal and spatial properties of Ca^{2+} signals are important for this modulation to occur.

Astrocyte Calcium Effects on Behavior

The study of rodent models that display altered astrocyte function indicated that astrocytes play important roles in the production of behavior outputs in different dimensions (cognition, emotion, motor, and sensory processing) (for review, Oliveira et al., 2015). As reviewed above, astrocytic Ca^{2+} signaling is reported to mediate synaptic modulation in different brain circuits. Genetic interference in this astrocytic hallmark has been the main strategy used to assess the role played by astrocyte Ca^{2+} elevations in behavior, with different laboratories using mostly two approaches: (1) triggering intracellular Ca^{2+} elevations via chemogenetic activation of GPCR signaling, and (2) inhibiting IP_3 signaling by deletion of IP_3 receptors or by buffering IP_3.

The genetic deletion of IP_3R2, specifically in about 80% of glial fibrillary acidic protein (GFAP)-positive cells (at least in the cortex, hippocampus, and substantia nigra), does not appear to influence spatial memory (Petravicz et al., 2014). However, the attenuation of IP_3 signaling in GLT1-positive cells led to partial cognitive impairment (Tanaka et al., 2013). Despite the extensive evidence showing a clear influence of astrocyte Ca^{2+} events on synapses and circuits involved in cognitive behavior (e.g., hippocampus), these two studies provided only modest evidence to support it. We believe that further studies using more specific tools to modulate astrocyte Ca^{2+} will reveal additional links to cognition. Indeed, we recently showed that spatial learning and memory rely on astrocyte exocytosis, which is a Ca^{2+}-dependent mechanism, and therefore might be dependent on astrocyte integration of surrounding activity (Sardinha et al., 2017).

IP_3-dependent astrocytic Ca^{2+} signaling does not seem to be related to anxiety-like behavior as indicated by studies using a constitutive (Cao et al., 2013; Tanaka et al., 2013) or conditional (Petravicz et al., 2014) IP_3R2 deletion. Regarding the depressive-like behavior, the available data is not consistent. While the constitutive deletion of IP_3R2 was shown to trigger some forms of a depressive phenotype (Cao et al., 2013), these are completely absent in the model with conditional deletion (Petravicz et al., 2014). Curiously, the GFAP-MrgA1 model that allows stimulation of astrocyte Ca^{2+} displayed decreased learned helplessness in the forced swim test (Cao et al., 2013). Further experimentation is required to clarify these apparently contradictory results. Finally, a recent study indicated that the astrocytic control of excitatory/inhibitory inputs to the central amygdala is crucial for fear-related behavior (Martin-Fernandez et al., 2017).

Regarding motor function, the activation of IP_3 "sponge" or deletion of IP_3R2 does not seem to interfere with exploratory behavior (Cao et al., 2013; Tanaka et al., 2013; Petravicz et al., 2014). Interestingly, the chemogenetic activation of astrocyte G_q-coupled signaling led to an impairment in motor coordination in an IP_3R2-independent manner (Agulhon et al., 2013). The specific ablation of IP_3R2 in GLAST-positive cells resulted in an impairment in motor-skill learning of a forelimb reaching task (Padmashri et al., 2015). More so, the attenuation of IP_3/Ca^{2+} signaling in astrocytes resulted in modulation of the rodent sleep, by increasing the time spent in the rapid eye movement (REM) phase and the frequency of REM periods (Foley et al., 2017).

While the research carried out so far has provided us with critical knowledge of the influence of astrocytic Ca^{2+} in synaptic or circuit function, further research should be performed to complement the rather sparse evidence on the influence of astrocytes on behavior. Moreover, further evidence will help clarify the discrepant results and reconcile the existent observations. For instance, the different observed cognitive outcomes might be related to the different mechanism used to target intracellular Ca^{2+} (full deletion of IP_3R2 vs. IP_3 "sponge"), or by the promotor used to drive astrocyte specificity (GFAP vs. GLT1) that could result in differential regional expression. Moreover, there are at least five different IP_3R2 KO strains with different genetic backgrounds (Oliveira et al., 2015); this might not be critically relevant for studies of synaptic plasticity in brain slices, but it may easily lead to distinct observations in behavior tests. Additionally, the different studies should be conducted in a standardized form to allow the linear comparison of the results.

All rodent models reported above result on drastic modulation of global Ca^{2+} elevations. Intracellular Ca^{2+} rises may trigger a multitude of signaling pathways. Thus, it must always be considered that the interference with global Ca^{2+} events may trigger several simultaneous consequences, which might lead to confounding results. Although these models might be very useful when carefully assessed, the research field requires the development of more specific models to allow temporal and, more importantly, local control of Ca^{2+} signals in physiological processes.

CONCLUSION

Intracellular Ca^{2+} elevations are the mechanism by which astrocytes decode afferent information and generate functional outputs. Here, we discussed relevant information showing that astrocytic Ca^{2+} elevations have a direct impact on synapses (gliotransmitters release, synaptic plasticity, and integrity) and influence circuit outputs (sensory plasticity and network synchronization). However, the behavior readouts of rodents whose global astrocytic Ca^{2+} was manipulated remain inconsistent.

Astrocytic Ca^{2+} signals exhibit critical spatio-temporal features that need to be fully understood to allow for the

careful assessment of their functional implications. Among them: spontaneous vs. evoked events; fast vs. slow elevations; synchronous vs. asynchronous; global (soma and main processes) vs. focal (microdomain); single vs. multiple astrocyte; local vs. across brain regions; IP_3-dependent vs. IP_3-independent mechanisms. The complementary application of existing tools, as well as the development of accurate models to tackle its unique and heterogeneous features, will provide us with novel insights on its actions and consequences.

AUTHOR CONTRIBUTIONS

All authors listed have made a substantial, direct and intellectual contribution to the work, and approved it for publication.

ACKNOWLEDGMENTS

The authors acknowledge N. C. Santos and J. D. Silva for their helpful comments on the manuscript. This work was supported by National Funds through Foundation for Science and Technology (FCT) fellowships (SFRH/BPD/97281/2013 to JO, SFRH/BD/101298/2014 to SG-G, IF/00328/2015 to JO, IF/01079/2014 to LP); Marie Curie Fellowship FP7-PEOPLE-2010-IEF 273936 and BIAL Foundation Grant 207/14 to JO and 427/14 to LP; Northern Portugal Regional Operational Programme (NORTE 2020), under the Portugal 2020 Partnership Agreement, through the European Regional Development Fund (FEDER; NORTE-01-0145-FEDER-000013); FEDER funds, through the Competitiveness Factors Operational Programme (COMPETE), and National Funds, through the FCT (POCI-01-0145-FEDER-007038).

REFERENCES

Agarwal, A., Wu, P.-H., Hughes, E. G., Fukaya, M., Tischfield, M. A., Langseth, A. J., et al. (2017). Transient opening of the mitochondrial permeability transition pore induces microdomain calcium transients in astrocyte processes. *Neuron* 93, 587.e7–605.e7. doi: 10.1016/j.neuron.2016.12.034

Agulhon, C., Boyt, K. M., Xie, A. X., Friocourt, F., Roth, B. L., and McCarthy, K. D. (2013). Modulation of the autonomic nervous system and behaviour by acute glial cell G_q protein-coupled receptor activation *in vivo*. *J. Physiol.* 591, 5599–5609. doi: 10.1113/jphysiol.2013.261289

Agulhon, C., Fiacco, T. A., and McCarthy, K. D. (2010). Hippocampal short- and long-term plasticity are not modulated by astrocyte Ca^{2+} signaling. *Science* 327, 1250–1254. doi: 10.1126/science.1184821

Agulhon, C., Petravicz, J., McMullen, A. B., Sweger, E. J., Minton, S. K., Taves, S. R., et al. (2008). What is the role of astrocyte calcium in neurophysiology? *Neuron* 59, 932–946. doi: 10.1016/j.neuron.2008.09.004

Agulhon, C., Sun, M.-Y., Murphy, T., Myers, T., Lauderdale, K., and Fiacco, T. A. (2012). Calcium signaling and gliotransmission in normal vs. reactive astrocytes. *Front. Pharmacol.* 3:139. doi: 10.3389/fphar.2012.00139

Araque, A., Carmignoto, G., Haydon, P. G., Oliet, S. H. R., Robitaille, R., and Volterra, A. (2014). Gliotransmitters travel in time and space. *Neuron* 81, 728–739. doi: 10.1016/j.neuron.2014.02.007

Bazargani, N., and Attwell, D. (2016). Astrocyte calcium signaling: the third wave. *Nat. Neurosci.* 19, 182–189. doi: 10.1038/nn.4201

Bindocci, E., Savtchouk, I., Liaudet, N., Becker, D., Carriero, G., and Volterra, A. (2017). Three-dimensional Ca^{2+} imaging advances understanding of astrocyte biology. *Science* 356:eaai8185. doi: 10.1126/science.aai8185

Cao, X., Li, L.-P., Wang, Q., Wu, Q., Hu, H.-H., Zhang, M., et al. (2013). Astrocyte-derived ATP modulates depressive-like behaviors. *Nat. Med.* 19, 773–777. doi: 10.1038/nm.3162

Chai, H., Diaz-Castro, B., Shigetomi, E., Monte, E., Octeau, J. C., Yu, X., et al. (2017). Neural circuit-specialized astrocytes: transcriptomic, proteomic, morphological, and functional evidence. *Neuron* 95, 531.e9–549.e9. doi: 10.1016/j.neuron.2017.06.029

Chen, N., Sugihara, H., Sharma, J., Perea, G., Petravicz, J., Le, C., et al. (2012). Nucleus basalis-enabled stimulus-specific plasticity in the visual cortex is mediated by astrocytes. *Proc. Natl. Acad. Sci. U.S.A.* 109, E2832–E2841. doi: 10.1073/pnas.1206557109

Copeland, C. S., Wall, T. M., Sims, R. E., Neale, S. A., Nisenbaum, E., Parri, H. R., et al. (2017). Astrocytes modulate thalamic sensory processing via mGlu2 receptor activation. *Neuropharmacology* 121, 100–110. doi: 10.1016/j.neuropharm.2017.04.019

Di Castro, M. A., Chuquet, J., Liaudet, N., Bhaukaurally, K., Santello, M., Bouvier, D., et al. (2011). Local Ca^{2+} detection and modulation of synaptic release by astrocytes. *Nat. Neurosci.* 14, 1276–1284. doi: 10.1038/nn.2929

Foley, J., Blutstein, T., Lee, S., Erneux, C., Halassa, M. M., and Haydon, P. (2017). Astrocytic IP_3/Ca^{2+} signaling modulates theta rhythm and REM sleep. *Front. Neural Circuits* 11:3. doi: 10.3389/fncir.2017.00003

Gómez-Gonzalo, M., Navarrete, M., Perea, G., Covelo, A., Martín-Fernández, M., Shigemoto, R., et al. (2015). Endocannabinoids Induce lateral long-term potentiation of transmitter release by stimulation of gliotransmission. *Cereb. Cortex* 25, 3699–3712. doi: 10.1093/cercor/bhu231

Gourine, A. V., Kasymov, V., Marina, N., Tang, F., Figueiredo, M. F., Lane, S., et al. (2010). Astrocytes control breathing through ph-dependent release of ATP. *Science* 329, 571–575. doi: 10.1126/science.1190721

Henneberger, C., Papouin, T., Oliet, S. H. R., and Rusakov, D. A. (2010). Long-term potentiation depends on release of D-serine from astrocytes. *Nature* 463, 232–236. doi: 10.1038/nature08673

Kanemaru, K., Sekiya, H., Xu, M., Satoh, K., Kitajima, N., Yoshida, K., et al. (2014). In vivo visualization of subtle, transient, and local activity of astrocytes using an ultrasensitive Ca^{2+} indicator. *Cell Rep.* 8, 311–318. doi: 10.1016/j.celrep.2014.05.056

Khakh, B. S., and McCarthy, K. D. (2015). Astrocyte calcium signaling: from observations to functions and the challenges therein. *Cold Spring Harb. Perspect. Biol.* 7:a020404. doi: 10.1101/cshperspect.a020404

Leybaert, L., and Sanderson, M. J. (2012). Intercellular Ca^{2+} waves: mechanisms and function. *Physiol. Rev.* 92, 1359–1392. doi: 10.1152/physrev.00029.2011

Mariotti, L., Losi, G., Sessolo, M., Marcon, I., and Carmignoto, G. (2016). The inhibitory neurotransmitter GABA evokes long-lasting Ca^{2+} oscillations in cortical astrocytes. *Glia* 64, 363–373. doi: 10.1002/glia.22933

Martín, R., Bajo-Grañeras, R., Moratalla, R., Perea, G., and Araque, A. (2015). Circuit-specific signaling in astrocyte-neuron networks in basal ganglia pathways. *Science* 349, 730–734. doi: 10.1126/science.aaa7945

Martin-Fernandez, M., Jamison, S., Robin, L. M., Zhao, Z., Martin, E. D., Aguilar, J., et al. (2017). Synapse-specific astrocyte gating of amygdala-related behavior. *Nat. Neurosci.* 20, 1540–1548. doi: 10.1038/nn.4649

Monai, H., Ohkura, M., Tanaka, M., Oe, Y., Konno, A., Hirai, H., et al. (2016). Calcium imaging reveals glial involvement in transcranial direct current stimulation-induced plasticity in mouse brain. *Nat. Commun.* 7:11100. doi: 10.1038/ncomms11100

Morquette, P., Verdier, D., Kadala, A., Féthière, J., Philippe, A. G., Robitaille, R., et al. (2015). An astrocyte-dependent mechanism for neuronal rhythmogenesis. *Nat. Neurosci.* 18, 844–854. doi: 10.1038/nn.4013

Navarrete, M., and Araque, A. (2008). Endocannabinoids mediate neuron-astrocyte communication. *Neuron* 57, 883–893. doi: 10.1016/j.neuron.2008.01.029

Navarrete, M., Perea, G., de Sevilla, D. F., Gómez-Gonzalo, M., Núñez, A., Martín, E. D., et al. (2012). Astrocytes mediate in vivo cholinergic-induced synaptic plasticity. *PLOS Biol.* 10:e1001259. doi: 10.1371/journal.pbio.1001259

Navarrete, M., Perea, G., Maglio, L., Pastor, J., García de Sola, R., and Araque, A. (2013). Astrocyte calcium signal and gliotransmission in human brain tissue. *Cereb. Cortex* 23, 1240–1246. doi: 10.1093/cercor/bhs122

Nedergaard, M., Rodríguez, J. J., and Verkhratsky, A. (2010). Glial calcium and diseases of the nervous system. *Cell Calcium* 47, 140–149. doi: 10.1016/j.ceca.2009.11.010

Nizar, K., Uhlirova, H., Tian, P., Saisan, P. A., Cheng, Q., Reznichenko, L., et al. (2013). *In vivo* stimulus-induced vasodilation occurs without IP_3 receptor activation and may precede astrocytic calcium increase. *J. Neurosci.* 33, 8411–8422. doi: 10.1523/JNEUROSCI.3285-12.2013

Oliveira, J. F., Sardinha, V. M., Guerra-Gomes, S., Araque, A., and Sousa, N. (2015). Do stars govern our actions? Astrocyte involvement in rodent behavior. *Trends Neurosci.* 38, 535–549. doi: 10.1016/j.tins.2015.07.006

Pabst, M., Braganza, O., Dannenberg, H., Hu, W., Pothmann, L., Rosen, J., et al. (2016). Astrocyte intermediaries of septal cholinergic modulation in the hippocampus. *Neuron* 90, 853–865. doi: 10.1016/j.neuron.2016.04.003

Padmashri, R., Suresh, A., Boska, M. D., and Dunaevsky, A. (2015). Motor-skill learning is dependent on astrocytic activity. *Neural Plast.* 2015:11. doi: 10.1155/2015/938023

Panatier, A., Vallée, J., Haber, M., Murai, K. K., Lacaille, J.-C., and Robitaille, R. (2011). Astrocytes are endogenous regulators of basal transmission at central synapses. *Cell* 146, 785–798. doi: 10.1016/j.cell.2011.07.022

Papouin, T., Dunphy, J. M., Tolman, M., Dineley, K. T., and Haydon, P. G. (2017). Septal cholinergic neuromodulation tunes the astrocyte-dependent gating of hippocampal NMDA receptors to wakefulness. *Neuron* 94, 840.e7–854.e7. doi: 10.1016/j.neuron.2017.04.021

Parpura, V., Grubišić, V., and Verkhratsky, A. (2011). Ca^{2+} sources for the exocytotic release of glutamate from astrocytes. *Biochim. Biophys. Acta BBA Mol. Cell Res.* 1813, 984–991. doi: 10.1016/j.bbamcr.2010.11.006

Perea, G., and Araque, A. (2005). Properties of synaptically evoked astrocyte calcium signal reveal synaptic information processing by astrocytes. *J. Neurosci.* 25, 2192–2203. doi: 10.1523/JNEUROSCI.3965-04.2005

Perea, G., and Araque, A. (2007). Astrocytes potentiate transmitter release at single hippocampal synapses. *Science* 317, 1083–1086. doi: 10.1126/science.1144640

Perea, G., Gómez, R., Mederos, S., Covelo, A., Ballesteros, J. J., Schlosser, L., et al. (2016). Activity-dependent switch of GABAergic inhibition into glutamatergic excitation in astrocyte-neuron networks. *eLife* 5:e20362. doi: 10.7554/eLife.20362

Perea, G., Sur, M., and Araque, A. (2014). Neuron-glia networks: integral gear of brain function. *Front. Cell. Neurosci.* 8:378. doi: 10.3389/fncel.2014.00378

Perez-Alvarez, A., Navarrete, M., Covelo, A., Martin, E. D., and Araque, A. (2014). Structural and functional plasticity of astrocyte processes and dendritic spine interactions. *J. Neurosci.* 34, 12738–12744. doi: 10.1523/JNEUROSCI.2401-14.2014

Petravicz, J., Boyt, K. M., and McCarthy, K. D. (2014). Astrocyte IP3R2-dependent Ca^{2+} signaling is not a major modulator of neuronal pathways governing behavior. *Front. Behav. Neurosci.* 8:384. doi: 10.3389/fnbeh.2014.00384

Petravicz, J., Fiacco, T. A., and McCarthy, K. D. (2008). Loss of IP_3 receptor-dependent Ca^{2+} increases in hippocampal astrocytes does not affect baseline CA1 pyramidal neuron synaptic activity. *J. Neurosci.* 28, 4967–4973. doi: 10.1523/JNEUROSCI.5572-07.2008

Petrelli, F., and Bezzi, P. (2016). Novel insights into gliotransmitters. *Curr. Opin. Pharmacol.* 26, 138–145. doi: 10.1016/j.coph.2015.11.010

Petzold, G. C., and Murthy, V. N. (2011). Role of astrocytes in neurovascular coupling. *Neuron* 71, 782–797. doi: 10.1016/j.neuron.2011.08.009

Poskanzer, K. E., and Yuste, R. (2011). Astrocytic regulation of cortical UP states. *Proc. Natl. Acad. Sci. U.S.A.* 108, 18453–18458. doi: 10.1073/pnas.1112378108

Poskanzer, K. E., and Yuste, R. (2016). Astrocytes regulate cortical state switching in vivo. *Proc. Natl. Acad. Sci. U.S.A.* 113, E2675–E2684. doi: 10.1073/pnas.1520759113

Reyes, R. C., Verkhratsky, A., and Parpura, V. (2013). TRPC1-mediated Ca^{2+} and Na^{+} signalling in astroglia: differential filtering of extracellular cations. *Cell Calcium* 54, 120–125. doi: 10.1016/j.ceca.2013.05.005

Rusakov, D. A., Bard, L., Stewart, M. G., and Henneberger, C. (2014). Diversity of astroglial functions alludes to subcellular specialisation. *Trends Neurosci.* 37, 228–242. doi: 10.1016/j.tins.2014.02.008

Sardinha, V. M., Guerra-Gomes, S., Caetano, I., Tavares, G., Martins, M., Reis, J. S., et al. (2017). Astrocytic signaling supports hippocampal–prefrontal theta synchronization and cognitive function. *Glia* 65, 1944–1960. doi: 10.1002/glia.23205

Sasaki, T., Ishikawa, T., Abe, R., Nakayama, R., Asada, A., Matsuki, N., et al. (2014). Astrocyte calcium signalling orchestrates neuronal synchronization in organotypic hippocampal slices. *J. Physiol.* 592, 2771–2783. doi: 10.1113/jphysiol.2014.272864

Scemes, E., and Giaume, C. (2006). Astrocyte calcium waves: what they are and what they do. *Glia* 54, 716–725. doi: 10.1002/glia.20374

Serrano, A., Haddjeri, N., Lacaille, J.-C., and Robitaille, R. (2006). GABAergic network activation of glial cells underlies hippocampal heterosynaptic depression. *J. Neurosci.* 26, 5370–5382. doi: 10.1523/JNEUROSCI.5255-05.2006

Sherwood, M. W., Arizono, M., Hisatsune, C., Bannai, H., Ebisui, E., Sherwood, J. L., et al. (2017). Astrocytic IP3Rs: contribution to Ca^{2+} signalling and hippocampal LTP. *Glia* 65, 502–513. doi: 10.1002/glia.23107

Shigetomi, E., Jackson-Weaver, O., Huckstepp, R. T., O'Dell, T. J., and Khakh, B. S. (2013). TRPA1 channels are regulators of astrocyte basal calcium levels and long-term potentiation via constitutive D-serine release. *J. Neurosci.* 33, 10143–10153. doi: 10.1523/JNEUROSCI.5779-12.2013

Shigetomi, E., Patel, S., and Khakh, B. S. (2016). Probing the complexities of astrocyte calcium signaling. *Trends Cell Biol.* 26, 300–312. doi: 10.1016/j.tcb.2016.01.003

Shigetomi, E., Tong, X., Kwan, K. Y., Corey, D. P., and Khakh, B. S. (2012). TRPA1 channels regulate astrocyte resting calcium and inhibitory synapse efficacy through GAT-3. *Nat. Neurosci.* 15, 70–80. doi: 10.1038/nn.3000

Srinivasan, R., Lu, T.-Y., Chai, H., Xu, J., Huang, B. S., Golshani, P., et al. (2016). New transgenic mouse lines for selectively targeting astrocytes and studying calcium signals in astrocyte processes in situ and in vivo. *Neuron* 92, 1181–1195. doi: 10.1016/j.neuron.2016.11.030

Takata, N., and Hirase, H. (2008). Cortical layer 1 and layer 2/3 astrocytes exhibit distinct calcium dynamics *in vivo*. *PLOS ONE* 3:e2525. doi: 10.1371/journal.pone.0002525

Takata, N., Mishima, T., Hisatsune, C., Nagai, T., Ebisui, E., Mikoshiba, K., et al. (2011). Astrocyte calcium signaling transforms cholinergic modulation to cortical plasticity *in vivo*. *J. Neurosci.* 31, 18155–18165. doi: 10.1523/JNEUROSCI.5289-11.2011

Tanaka, M., Shih, P.-Y., Gomi, H., Yoshida, T., Nakai, J., Ando, R., et al. (2013). Astrocytic Ca^{2+} signals are required for the functional integrity of tripartite synapses. *Mol. Brain* 6:6. doi: 10.1186/1756-6606-6-6

Tanaka, M., Wang, X., Mikoshiba, K., Hirase, H., and Shinohara, Y. (2017). Rearing-environment-dependent hippocampal local field potential differences in wild-type and inositol trisphosphate receptor type 2 knockout mice. *J. Physiol.* 595, 6557–6568. doi: 10.1113/JP274573

Vardjan, N., Verkhratsky, A., and Zorec, R. (2017). Astrocytic pathological calcium homeostasis and impaired vesicle trafficking in neurodegeneration. *Int. J. Mol. Sci.* 18:358. doi: 10.3390/ijms18020358

Verkhratsky, A., Reyes, R. C., and Parpura, V. (2013). "TRP channels coordinate ion signalling in astroglia," in *Reviews of Physiology, Biochemistry and Pharmacology 166. Reviews of Physiology, Biochemistry and Pharmacology*, Vol. 166, eds B. Nilius, T. Gudermann, R. Jahn, R. Lill, S. Offermanns, and O. H. Petersen (Cham: Springer), 1–22.

Volterra, A., Liaudet, N., and Savtchouk, I. (2014). Astrocyte Ca^{2+} signalling: an unexpected complexity. *Nat. Rev. Neurosci.* 15, 327–335. doi: 10.1038/nrn3725

Wang, X., Lou, N., Xu, Q., Tian, G.-F., Peng, W. G., Han, X., et al. (2006). Astrocytic Ca^{2+} signaling evoked by sensory stimulation *in vivo*. *Nat. Neurosci.* 9, 816–823. doi: 10.1038/nn1703

Zorec, R., Araque, A., Carmignoto, G., Haydon, P. G., Verkhratsky, A., and Parpura, V. (2012). Astroglial excitability and gliotransmission: an appraisal of Ca^{2+} as a signalling route. *ASN Neuro* 4:e00080. doi: 10.1042/AN20110061

Conflict of Interest Statement: The authors declare that the research was conducted in the absence of any commercial or financial relationships that could be construed as a potential conflict of interest.

Table Annex 1 - List of differentially expressed genes in total hippocampus of IP_3R2 KO mice

Microarray analysis, Affimetrix GeneChip: up-regulated genes in green; down-regulated genes in orange.

Symbol or ID	Gene Title (677)	FC>1.3x p<0.05 Av>10
1500015O10Rik	RIKEN cDNA 1500015O10 gene	3,52
Defb11	defensin beta 11	3,31
Mir1912	microRNA 1912 /// microRNA 1912	3,18
Kcnj13	potassium inwardly-rectifying channel, subfamily J, member 13	3,11
Calml4	calmodulin-like 4	2,98
F5	coagulation factor V	2,93
Kl	klotho	2,71
Sulf1	sulfatase 1 /// sulfatase 1	2,66
Col8a1	collagen, type VIII, alpha 1	2,60
Gm11084	predicted gene 11084	2,60
Ace	angiotensin I converting enzyme (peptidyl-dipeptidase A) 1 /// angiotensin I converting enzyme (peptidyl-dipeptidase A) 1	2,56
Lbp	lipopolysaccharide binding protein	2,45
Clic6	chloride intracellular channel 6 /// chloride intracellular channel 6	2,26
Otx2	orthodenticle homolog 2	2,26
17321481		2,19
17513273		2,14
Tmem72	transmembrane protein 72	2,13
Vat1l	vesicle amine transport protein 1 homolog-like (T. californica)	2,12
Gm24445	predicted gene, 24445	2,08
Gm22005	predicted gene, 22005	2,07
Gm6665	predicted gene 6665	2,04
Gm23633	predicted gene, 23633	2,03
Enpp2	ectonucleotide pyrophosphatase/phosphodiesterase 2 /// ectonucleotide pyrophosphatase/phosphodiesterase 2	2,02
Sostdc1	sclerostin domain containing 1	1,98
Gm5136	predicted gene 5136	1,97
Pon3	paraoxonase 3	1,96
17493310		1,96
Pin1	protein (peptidyl-prolyl cis/trans isomerase) NIMA-interacting 1	1,95
Pla2g10os	phospholipase A2, group X, opposite strand /// phospholipase A2, group X, opposite strand	1,94
Slc4a5	solute carrier family 4, sodium bicarbonate cotransporter, member 5	1,94
Gm25014	predicted gene, 25014	1,93
Gm25987	predicted gene, 25987	1,91
Speer4a	spermatogenesis associated glutamate (E)-rich protein 4a	1,90
Folr1	folate receptor 1 (adult)	1,90
Mir493	microRNA 493 /// microRNA 493 /// mmu-mir-493	1,86
Tuba1c	tubulin, alpha 1C	1,85
Snord14e	small nucleolar RNA, C/D box 14E /// heat shock protein 8 /// small nucleolar RNA, C/D box 14E	1,85
Abca4	ATP-binding cassette, sub-family A (ABC1), member 4	1,85
Gm22067	predicted gene, 22067	1,81
Perp	PERP, TP53 apoptosis effector	1,80
Cd59a	CD59a antigen	1,80
Gm20444	predicted gene 20444	1,80
Gm25160	predicted gene, 25160	1,79
Gm3227	predicted gene 3227	1,78
Ccdc135	coiled-coil domain containing 135	1,77
Trim43c	tripartite motif-containing 43C	1,76
Rdh5	retinol dehydrogenase 5 /// retinol dehydrogenase 5	1,76
Gm25552	predicted gene, 25552	1,74
n-R5s1	nuclear encoded rRNA 5S 1	1,74
Aldh3b1	aldehyde dehydrogenase 3 family, member B1	1,73
Smim22	small integral membrane protein 22	1,73
Lrg1	leucine-rich alpha-2-glycoprotein 1	1,73
Gm11651	predicted gene 11651 /// predicted gene 11651	1,71
Trav10d	T cell receptor alpha variable 10D	1,71
Gm26011	predicted gene, 26011	1,71
Steap1	six transmembrane epithelial antigen of the prostate 1	1,71
Igfbp2	insulin-like growth factor binding protein 2 /// insulin-like growth factor binding protein 2	1,70
Kcne2	potassium voltage-gated channel, Isk-related subfamily, gene 2	1,70
Pdgfd	platelet-derived growth factor, D polypeptide	1,69
Prlr	prolactin receptor /// prolactin receptor	1,69
Tmem181b-ps	transmembrane protein 181B, pseudogene	1,68
Trpm3	transient receptor potential cation channel, subfamily M, member 3	1,68
Slc31a1	solute carrier family 31, member 1	1,66
Mir138-2	microRNA 138-2 /// microRNA 138-2	1,66
Snora75	small nucleolar RNA, H/ACA box 75 /// small nucleolar RNA, H/ACA box 75	1,65
Vamp8	vesicle-associated membrane protein 8	1,65
Gm24399	predicted gene, 24399	1,65
Cldn1	claudin 1	1,65
Plbd2	phospholipase B domain containing 2	1,65
Numb	numb gene homolog (Drosophila) /// numb gene homolog (Drosophila)	1,64
Mir3070b	microRNA 3070b /// microRNA 3070b /// mmu-mir-3070b	1,64
Mpp7	membrane protein, palmitoylated 7 (MAGUK p55 subfamily member 7)	1,63
Cgnl1	cingulin-like 1	1,63
Krt18	keratin 18	1,63
Cpq	carboxypeptidase Q	1,63
Gm22720	predicted gene, 22720	1,62
Mok	MOK protein kinase /// MOK protein kinase	1,62
Dynlrb2	dynein light chain roadblock-type 2	1,62
Gpx8	glutathione peroxidase 8 (putative)	1,62
Pcolce2	procollagen C-endopeptidase enhancer 2	1,62
Sag	S-antigen, retina and pineal gland (arrestin) /// S-antigen, retina and pineal gland (arrestin)	1,62
Slc13a4	solute carrier family 13 (sodium/sulfate symporters), member 4	1,62
Gm26446	predicted gene, 26446	1,62
Fbxl12	F-box and leucine-rich repeat protein 12 /// predicted gene, 26521	1,61
Gm24082	predicted gene, 24082	1,61
17274405		1,61
Gm22519	predicted gene, 22519	1,60
17480237		1,59
Gm26404	predicted gene, 26404	1,59
Serpinb1b	serine (or cysteine) peptidase inhibitor, clade B, member 1b	1,59
Gm26353	predicted gene, 26353	1,59
Rexo1	REX1, RNA exonuclease 1 homolog (S. cerevisiae)	1,58

Trpv4	transient receptor potential cation channel, subfamily V, member 4	1,57
Sft2d2	SFT2 domain containing 2	1,57
Gm5639	predicted pseudogene 5639	1,56
Slc2a12	solute carrier family 2 (facilitated glucose transporter), member 12	1,56
Gm24292	predicted gene, 24292	1,55
Mia	melanoma inhibitory activity /// predicted gene 21983	1,55
Cab39l	calcium binding protein 39-like	1,55
Gm24787	predicted gene, 24787	1,55
Emcn	endomucin	1,54
Ighd6-2	immunoglobulin heavy diversity 6-2	1,54
Sox2ot	SOX2 overlapping transcript (non-protein coding) /// SOX2 overlapping transcript (non-protein coding)	1,54
Npm3	nucleoplasmin 3	1,54
Gm22650	predicted gene, 22650	1,54
Gm15409	predicted gene 15409	1,54
Nme5	NME/NM23 family member 5	1,53
17518543		1,53
Gm17250	predicted gene, 17250 /// predicted gene, 17250	1,53
17491644		1,52
Sall3	sal-like 3 (Drosophila)	1,52
Gm14967	predicted gene 14967	1,52
Emb	embigin	1,51
1700016P03Rik	RIKEN cDNA 1700016P03 gene /// RIKEN cDNA 1700016P03 gene	1,51
Car12	carbonic anyhydrase 12	1,51
Gm22027	predicted gene, 22027	1,51
Gm23527	predicted gene, 23527	1,50
Gm24920	predicted gene, 24920	1,50
Ccdc19	coiled-coil domain containing 19 /// coiled-coil domain containing 19	1,50
2310058D17Rik	RIKEN cDNA 2310058D17 gene /// RIKEN cDNA 2310058D17 gene /// RIKEN cDNA 2310058D17 gene	1,50
Gm24165	predicted gene, 24165	1,50
Rps11-ps1	ribosomal protein S11, pseudogene 1 /// ribosomal protein S11, pseudogene 1	1,50
Zfp780b	zinc finger protein 780B	1,50
Gm22098	predicted gene, 22098	1,49
Tppp3	tubulin polymerization-promoting protein family member 3	1,49
Efhc1	EF-hand domain (C-terminal) containing 1	1,49
17465037		1,49
Gm26091	predicted gene, 26091	1,49
Gm16552	predicted gene 16552	1,48
Gm25486	predicted gene, 25486 /// predicted gene, 24487	1,48
17527164		1,48
Pbx3	pre B cell leukemia homeobox 3	1,48
Gm23102	predicted gene, 23102	1,48
LOC102642160	uncharacterized LOC102642160 /// predicted gene, 24966	1,47
Prr5	proline rich 5 (renal)	1,47
Gm10723	predicted gene 10723	1,47
Gm25375	predicted gene, 25375	1,46
LOC102632388	uncharacterized LOC102632388 /// ring finger protein 26	1,46
Sipa1l3	signal-induced proliferation-associated 1 like 3 /// signal-induced proliferation-associated 1 like 3	1,46
Htr2c	5-hydroxytryptamine (serotonin) receptor 2C	1,46
Acot2	acyl-CoA thioesterase 2	1,46
Mir3475	microRNA 3475 /// microRNA 3475	1,45
17483889		1,45
Snap23	synaptosomal-associated protein 23	1,45
Snord42a	small nucleolar RNA, C/D box 42A /// small nucleolar RNA, C/D box 42A	1,45
BC049635	cDNA sequence BC049635	1,45
1810013A23Rik	RIKEN cDNA 1810013A23 gene /// peroxisome proliferator activator receptor delta	1,45
Gm25169	predicted gene, 25169	1,45
Gm24806	predicted gene, 24806	1,45
Nek5	NIMA (never in mitosis gene a)-related expressed kinase 5	1,45
Tfam	transcription factor A, mitochondrial	1,45
1700047M11Rik	RIKEN cDNA 1700047M11 gene /// RIKEN cDNA 1700047M11 gene	1,45
Gm26139	predicted gene, 26139	1,44
Gm26700	predicted gene, 26700	1,44
LOC102635756	uncharacterized LOC102635756 /// predicted gene 15689	1,44
Kdm5d	lysine (K)-specific demethylase 5D	1,44
9530034E10Rik	RIKEN cDNA 9530034E10 gene /// RIKEN cDNA 9530034E10 gene	1,44
Ephb2	Eph receptor B2	1,44
Csnk1g3	casein kinase 1, gamma 3	1,43
NONMMUT012257		1,43
17368096		1,43
Gm15841	predicted gene 15841	1,43
17312603		1,43
Abhd14b	abhydrolase domain containing 14b	1,43
Bglap3	bone gamma-carboxyglutamate protein 3 /// bone gamma-carboxyglutamate protein 2 /// bone gamma carboxyglutamate protein	1,43
Gm22500	predicted gene, 22500	1,43
Gm19359	predicted gene, 19359	1,43
Krtap4-13	keratin associated protein 4-13	1,43
Golga4	golgi autoantigen, golgin subfamily a, 4	1,42
Gm15655	predicted gene 15655	1,42
Acot4	acyl-CoA thioesterase 4	1,42
Igkv9-124	immunoglobulin kappa chain variable 9-124 /// immunoglobulin kappa chain complex /// immunoglobulin kappa chain variable 4-70 /// immunoglobulin kappa chain variable 28 (V28) /// Ig kappa chain V-IV region B17 precursor-like /// V(kappa) gene product /// immunoglobulin kappa-chain VK-1 /// immunoglobulin kappa chain variable 19-93 /// immunoglobulin kappa joining 1	1,42
Gulp1	GULP, engulfment adaptor PTB domain containing 1 /// GULP, engulfment adaptor PTB domain containing 1	1,42
Raver2	ribonucleoprotein, PTB-binding 2	1,42
LOC102635422	5E5 antigen-like /// leucine rich repeat containing 8 family, member C	1,42
Ptges	prostaglandin E synthase	1,42
Mvd	mevalonate (diphospho) decarboxylase	1,42
Slc16a2	solute carrier family 16 (monocarboxylic acid transporters), member 2	1,42
Frem1	Fras1 related extracellular matrix protein 1	1,42
Pifo	primary cilia formation	1,41
Gm17066	predicted gene 17066 /// predicted gene 17066 /// predicted gene 17066	1,41
Gm6921	predicted pseudogene 6921 /// predicted pseudogene 6921	1,41
Gm22578	predicted gene, 22578	1,41
Gm25549	predicted gene, 25549	1,41
Ezr	ezrin	1,41
Taf1d	TATA box binding protein (Tbp)-associated factor, RNA polymerase I, D /// topoisomerase (DNA) II alpha /// 3-	1,40

	hydroxyisobutyrate dehydrogenase /// predicted gene, 22358 /// predicted gene, 24355 /// predicted gene, 23451 /// predicted gene, 22303 /// predicted gene, 25188 /// predicted gene, 23455 /// predicted gene, 24610	
Gm22716	predicted gene, 22716	1,40
Gm4984	predicted pseudogene 4984	1,40
17548070		1,40
17520422		1,40
Arhgef7	Rho guanine nucleotide exchange factor (GEF7)	1,40
Gm25321	predicted gene, 25321	1,40
Mthfd1	methylenetetrahydrofolate dehydrogenase (NADP+ dependent), methenyltetrahydrofolate cyclohydrolase, formyltetrahydrofolate synthase	1,40
4930517O19Rik	RIKEN cDNA 4930517O19 gene /// RIKEN cDNA 4930517O19 gene	1,40
Gorasp1	golgi reassembly stacking protein 1	1,40
Btnl9	butyrophilin-like 9 /// butyrophilin-like 9	1,40
Gpr161	G protein-coupled receptor 161 /// G protein-coupled receptor 161	1,40
Aqp1	aquaporin 1	1,40
Zfp763	zinc finger protein 763	1,40
Slc12a4	solute carrier family 12, member 4	1,40
Dap	death-associated protein	1,40
LOC102641333	uncharacterized LOC102641333 /// predicted gene 15675	1,40
Apoc1	apolipoprotein C-I	1,39
Pla2g15	phospholipase A2, group XV	1,39
Gm24646	predicted gene, 24646	1,39
B130006D01Rik	RIKEN cDNA B130006D01 gene /// RIKEN cDNA B130006D01 gene	1,39
Fndc1	fibronectin type III domain containing 1	1,39
Sh3glb2	SH3-domain GRB2-like endophilin B2	1,39
Kcnb1	potassium voltage gated channel, Shab-related subfamily, member 1	1,39
Tsc22d1	TSC22 domain family, member 1 /// TSC22 domain family, member 1	1,39
Mir15a	microRNA 15a /// microRNA 15a	1,39
Gm15713	predicted gene 15713 /// predicted gene 15713	1,39
NONMMUT001338		1,39
Gm7609	predicted pseudogene 7609 /// predicted pseudogene 7609 /// uncharacterized LOC102638355 /// nuclear autoantigen Sp-100-like	1,38
6820426E19Rik	RIKEN cDNA 6820426E19 gene	1,38
Gm10406	predicted gene 10406 /// predicted gene 2897 /// predicted gene 3264 /// predicted gene, 3488 /// alpha takusan-like /// predicted gene 3591 /// predicted gene 3239 /// predicted gene 3173 /// uncharacterized LOC101055754 /// predicted gene 10340 /// predicted gene 3317 /// predicted gene 3500 /// predicted gene 3558 /// predicted gene 3696 /// predicted gene 5796 /// alpha-takusan pseudogene /// predicted pseudogene 8348 /// predicted gene 3383 /// predicted gene 3373 /// RIKEN cDNA 2610042L04 gene /// predicted gene, 8281 /// predicted gene 3667 /// predicted gene 3095 /// RIKEN cDNA 2610042L04 gene /// predicted gene 8237 /// predicted pseudogene 8348 /// predicted gene 10340 /// predicted gene 3629 /// predicted gene 2237 /// predicted gene 3636 /// predicted gene 3739 /// predicted gene 3005 /// predicted gene 3252 /// predicted gene 2974 /// predicted gene 3164 /// predicted gene 3002 /// predicted gene 3317 /// predicted gene 3642 /// predicted gene 3591 /// predicted gene 3239 /// predicted gene 3558 /// predicted gene 3696 /// predicted gene 5796 /// RIKEN cDNA 2610042L04 gene /// predicted gene, 3488 /// predicted gene 3005 /// predicted gene 10340 /// predicted gene 3317	1,38
C330013J21Rik	RIKEN cDNA C330013J21 gene	1,38
17284694		1,38
Chad	chondroadherin	1,38
Tmem43	transmembrane protein 43	1,38
Fancm	Fanconi anemia, complementation group M /// Fanconi anemia, complementation group M	1,38
Rbm14	RNA binding motif protein 14	1,38
Slc30a4	solute carrier family 30 (zinc transporter), member 4	1,38
17534197		1,38
Man1c1	mannosidase, alpha, class 1C, member 1	1,38
Mrpl27	mitochondrial ribosomal protein L27	1,38
Gas6	growth arrest specific 6	1,38
Rcn1	reticulocalbin 1	1,38
Rpl7l1	ribosomal protein L7-like 1	1,38
Mb	myoglobin	1,37
Gm25804	predicted gene, 25804	1,37
Wasf2	WAS protein family, member 2	1,37
Cdc34	cell division cycle 34 /// cell division cycle 34	1,37
Wdr13	WD repeat domain 13	1,37
A330021E22Rik	RIKEN cDNA A330021E22 gene	1,37
17317949		1,37
Gm24689	predicted gene, 24689	1,37
4930466F19Rik	RIKEN cDNA 4930466F19 gene	1,37
Tulp3	tubby-like protein 3	1,37
Gm25109	predicted gene, 25109	1,37
Slc12a2	solute carrier family 12, member 2	1,37
Tgfbi	transforming growth factor, beta induced	1,37
Sdc2	syndecan 2	1,37
Gpr18	G protein-coupled receptor 18	1,36
Ap5s1	adaptor-related protein 5 complex, sigma 1 subunit	1,36
17550142		1,36
Srp54c	signal recognition particle 54C /// signal recognition particle 54C	1,36
Fam160b1	family with sequence similarity 160, member B1	1,36
Tmem220	transmembrane protein 220	1,36
Gm22906	predicted gene, 22906	1,36
Mfap1b	microfibrillar-associated protein 1B /// microfibrillar-associated protein 1A	1,36
LOC102638849	uncharacterized LOC102638849 /// predicted gene 15764	1,36
Lamc1	laminin, gamma 1	1,36
Slc29a4	solute carrier family 29 (nucleoside transporters), member 4	1,36
Pdpn	podoplanin	1,36
B230325K18Rik	RIKEN cDNA B230325K18 gene /// RIKEN cDNA B230325K18 gene	1,36
Snora21	small nucleolar RNA, H/ACA box 21 /// small nucleolar RNA, H/ACA box 21	1,36

Cabin1	calcineurin binding protein 1 /// calcineurin binding protein 1	1,36
Dhdds	dehydrodolichyl diphosphate synthase	1,36
Srsf12	serine/arginine-rich splicing factor 12	1,36
Gtf3c2	general transcription factor IIIC, polypeptide 2, beta	1,36
1810026B05Rik	RIKEN cDNA 1810026B05 gene /// RIKEN cDNA 1810026B05 gene	1,36
17547666		1,35
4930518I15Rik	RIKEN cDNA 4930518I15 gene /// RIKEN cDNA 4930518I15 gene	1,35
Zfp952	zinc finger protein 952	1,35
Rsph1	radial spoke head 1 homolog (Chlamydomonas)	1,35
Ranbp17	RAN binding protein 17 /// RAN binding protein 17	1,35
Gm23474	predicted gene, 23474 /// RNA imprinted and accumulated in nucleus	1,35
Gm3558	predicted gene 3558 /// RIKEN cDNA 4930555G01 gene /// predicted gene 16440 /// predicted gene 3043 /// RIKEN cDNA D830030K20 gene /// predicted gene 10408 /// predicted gene 8050 /// predicted gene 8271 /// predicted gene 3755 /// predicted gene 2244 /// predicted gene 10408 /// predicted gene 3532 /// predicted gene 3033 /// predicted gene 3278 /// predicted gene 16440	1,35
Mtrr	5-methyltetrahydrofolate-homocysteine methyltransferase reductase /// 5-methyltetrahydrofolate-homocysteine methyltransferase reductase	1,35
Gm26514	predicted gene, 26514	1,35
Gm22596	predicted gene, 22596	1,35
Gm15935	predicted gene 15935	1,35
Gm13528	predicted gene 13528	1,35
Gm23458	predicted gene, 23458	1,35
Acaa2	acetyl-Coenzyme A acyltransferase 2 (mitochondrial 3-oxoacyl-Coenzyme A thiolase)	1,35
Pcdhb22	protocadherin beta 22	1,35
Gm13545	predicted gene 13545	1,35
Ano4	anoctamin 4	1,35
Terf2	telomeric repeat binding factor 2	1,35
2210416O15Rik	RIKEN cDNA 2210416O15 gene /// CUE domain containing 1	1,35
Gm17103	predicted gene 17103	1,35
Mpc1	mitochondrial pyruvate carrier 1	1,35
Hdac4	histone deacetylase 4 /// histone deacetylase 4	1,35
Gm23122	predicted gene, 23122	1,34
Tbc1d22bos	TBC1 domain family, member 22B, opposite strand /// TBC1 domain family, member 22B, opposite strand /// TBC1 domain family, member 22B, opposite strand	1,34
Cnih3	cornichon homolog 3 (Drosophila)	1,34
Pprc1	peroxisome proliferative activated receptor, gamma, coactivator-related 1	1,34
Gm26338	predicted gene, 26338	1,34
Txnip	thioredoxin interacting protein	1,34
Gm22778	predicted gene, 22778	1,34
Efcab1	EF hand calcium binding domain 1 /// EF hand calcium binding domain 1	1,34
Gal3st3	galactose-3-O-sulfotransferase 3	1,34
Mpc1	mitochondrial pyruvate carrier 1 /// mitochondrial pyruvate carrier 1, pseudogene	1,34
Fxyd1	FXYD domain-containing ion transport regulator 1	1,34
Dhrs7	dehydrogenase/reductase (SDR family) member 7	1,34
Pdk4	pyruvate dehydrogenase kinase, isoenzyme 4	1,34
Sfrp1	secreted frizzled-related protein 1	1,34
Pid1	phosphotyrosine interaction domain containing 1 /// phosphotyrosine interaction domain containing 1	1,34
Rpl21-ps7	ribosomal protein L21, pseudogene 7	1,33
LOC101056250	sp110 nuclear body protein-like /// Sp110 nuclear body protein /// predicted gene 15753 /// sp110 nuclear body protein-like /// Sp110 nuclear body protein-like /// sp110 nuclear body protein-like /// sp110 nuclear body protein-like /// sp110 nuclear body protein-like /// sp110 nuclear body protein-like /// uncharacterized LOC102639428 /// RIKEN cDNA A530040E14 gene /// Sp110 nuclear body protein /// predicted gene 15753 /// predicted pseudogene 16026	1,33
Ptbp1	polypyrimidine tract binding protein 1	1,33
D830031N03Rik	RIKEN cDNA D830031N03 gene	1,33
AA474331	expressed sequence AA474331 /// expressed sequence AA474331 /// expressed sequence AA474331	1,33
Ifi27	interferon, alpha-inducible protein 27 /// interferon, alpha-inducible protein 27	1,33
Dgat2	diacylglycerol O-acyltransferase 2	1,33
Gm15632	predicted gene 15632	1,33
17423802		1,33
Dlx6	distal-less homeobox 6	1,33
Fam161a	family with sequence similarity 161, member A /// family with sequence similarity 161, member A	1,33
Zfp185	zinc finger protein 185	1,33
Zfp182	zinc finger protein 182	1,33
Usp50	ubiquitin specific peptidase 50 /// predicted pseudogene 10774	1,33
Exosc2	exosome component 2	1,33
Gm24284	predicted gene, 24284	1,33
Nkd2	naked cuticle 2 homolog (Drosophila) /// naked cuticle 2 homolog (Drosophila)	1,32
Gm2178	predicted gene 2178	1,32
17392520		1,32
17548195		1,32
Zfp648	zinc finger protein 648	1,32
D630041G03Rik	RIKEN cDNA D630041G03 gene	1,32
Spaca4	sperm acrosome associated 4	1,32
Gm24150	predicted gene, 24150	1,32
Gm19500	predicted gene, 19500	1,32
Rhbdl3	rhomboid, veinlet-like 3 (Drosophila)	1,32
Gm13363	predicted gene 13363	1,32
Slc7a7	solute carrier family 7 (cationic amino acid transporter, y+ system), member 7 /// solute carrier family 7 (cationic amino acid transporter, y+ system), member 7	1,32
6030408B16Rik	RIKEN cDNA 6030408B16 gene /// RIKEN cDNA 6030408B16 gene	1,32
Lrrc23	leucine rich repeat containing 23	1,32
Fam50a	family with sequence similarity 50, member A	1,32
17548581		1,32
Gm8619	predicted gene 8619 /// uncharacterized LOC102642832	1,32

Slc23a2	solute carrier family 23 (nucleobase transporters), member 2	1,31
Gnpnat1	glucosamine-phosphate N-acetyltransferase 1	1,31
Tnip2	TNFAIP3 interacting protein 2	1,31
Olfr509	olfactory receptor 509	1,31
Gm13199	predicted gene 13199 /// predicted gene 13199	1,31
C330018A13Rik	RIKEN cDNA C330018A13 gene /// RIKEN cDNA C330018A13 gene	1,31
Lsm14b	LSM14 homolog B (SCD6, S. cerevisiae)	1,31
Zbed4	zinc finger, BED domain containing 4 /// predicted gene 15583	1,31
Olfr539	olfactory receptor 539	1,31
Gm25706	predicted gene, 25706	1,31
Scgb1b3	secretoglobin, family 1B, member 3 /// secretoglobin, family 1B, member 3	1,31
D830024N08Rik	RIKEN cDNA D830024N08 gene	1,31
Gm13844	predicted gene 13844	1,31
4930414L22Rik	RIKEN cDNA 4930414L22 gene	1,31
Anxa11	annexin A11 /// predicted gene 2274 /// predicted gene 2260 /// annexin A11 /// predicted gene 2274 /// predicted gene 2260	1,31
Fam76a	family with sequence similarity 76, member A	1,31
D930028M14Rik	RIKEN cDNA D930028M14 gene /// RIKEN cDNA D930028M14 gene	1,31
Gm4532	predicted gene 4532	-1,31
Gm23468	predicted gene, 23468	-1,31
Bcat2	branched chain aminotransferase 2, mitochondrial	-1,31
Fstl3	follistatin-like 3	-1,31
Ctgf	connective tissue growth factor	-1,31
A430105I19Rik	RIKEN cDNA A430105I19 gene	-1,31
Sema4d	sema domain, immunoglobulin domain (Ig), transmembrane domain (TM) and short cytoplasmic domain, (semaphorin) 4D /// sema domain, immunoglobulin domain (Ig), transmembrane domain (TM) and short cytoplasmic domain, (semaphorin) 4D	-1,31
LOC102638330	uncharacterized LOC102638330 /// predicted gene 14264	-1,31
1600029O15Rik	ribosomal protein L17 pseudogene /// ribosomal protein L17 pseudogene	-1,31
Chadl	chondroadherin-like /// chondroadherin-like	-1,31
Gm5532	predicted gene 5532 /// predicted gene 5532 /// predicted gene 5532	-1,31
Art4	ADP-ribosyltransferase 4	-1,31
BC030867	cDNA sequence BC030867	-1,31
Mmp9	matrix metallopeptidase 9	-1,31
Ranbp1	RAN binding protein 1 /// predicted gene, 25777	-1,31
Nmur1	neuromedin U receptor 1	-1,31
Gm15353	predicted gene 15353	-1,31
Cib2	calcium and integrin binding family member 2	-1,31
Adcy5	adenylate cyclase 5	-1,31
Cd83	CD83 antigen	-1,32
Tmsb15b1	thymosin beta 15b1 /// thymosin beta 15b like /// thymosin beta 15b2	-1,32
Stat2	signal transducer and activator of transcription 2	-1,32
Gm19510	predicted gene, 19510	-1,32
Snx15	sorting nexin 15	-1,32
1810010D01Rik	RIKEN cDNA 1810010D01 gene	-1,32
Olfr724	olfactory receptor 724	-1,32
Cnih1	cornichon homolog 1 (Drosophila)	-1,32
Col23a1	collagen, type XXIII, alpha 1	-1,32
2900041M22Rik	RIKEN cDNA 2900041M22 gene /// RIKEN cDNA 2900041M22 gene /// RIKEN cDNA 2900041M22 gene	-1,32
Zfp563	zinc finger protein 563 /// zinc finger protein 563	-1,32
Gm22897	predicted gene, 22897	-1,32
Ube2v1	ubiquitin-conjugating enzyme E2 variant 1	-1,32
AA987161	expressed sequence AA987161	-1,32
Gm24796	predicted gene, 24796	-1,32
Rrp7a	ribosomal RNA processing 7 homolog A (S. cerevisiae)	-1,32
Gm22198	predicted gene, 22198	-1,32
Mcur1	mitochondrial calcium uniporter regulator 1 /// mitochondrial calcium uniporter regulator 1	-1,32
Cd8a	CD8 antigen, alpha chain	-1,32
Snord100	small nucleolar RNA, C/D box 100	-1,32
Gm6253	predicted pseudogene 6253 /// gem (nuclear organelle) associated protein 6 /// predicted pseudogene 6253	-1,32
Gm3055	predicted gene 3055 /// zinc finger protein 781	-1,33
Gm23546	predicted gene, 23546	-1,33
Gm17224	predicted gene 17224 /// uncharacterized LOC102638851	-1,33
Tcrb-J	T cell receptor beta, joining region /// T cell receptor beta, variable 13-2 /// T cell receptor beta joining 1-6	-1,33
Olfr792	olfactory receptor 792	-1,33
B230307C23Rik	RIKEN cDNA B230307C23 gene /// RIKEN cDNA B230307C23 gene /// zinc finger protein 709-like	-1,33
Mkrn3	makorin, ring finger protein, 3	-1,33
Olfr875	olfactory receptor 875	-1,33
Gm24068	predicted gene, 24068	-1,33
Mir1938	microRNA 1938 /// microRNA 1938	-1,33
Gm22595	predicted gene, 22595	-1,33
Npffr1	neuropeptide FF receptor 1	-1,33
Gm11979	predicted gene 11979	-1,33
Syt2	synaptotagmin II	-1,33
Anpep	alanyl (membrane) aminopeptidase	-1,33
Trav9d-3	T cell receptor alpha variable 9D-3 /// T cell receptor alpha variable 12N-2 /// T cell receptor alpha joining 12	-1,33
Gm20472	predicted gene 20472	-1,33
Gm9796	predicted gene 9796 /// predicted gene 9796	-1,33
Ecscr	endothelial cell surface expressed chemotaxis and apoptosis regulator	-1,34
H2afb2	H2A histone family, member B2	-1,34
Stk32b	serine/threonine kinase 32B	-1,34
Nutm1	NUT midline carcinoma, family member 1	-1,34
A930004D18Rik	RIKEN cDNA A930004D18 gene /// RIKEN cDNA A930004D18 gene	-1,34
Acot3	acyl-CoA thioesterase 3 /// acyl-CoA thioesterase 3	-1,34
17473988		-1,34
Nwd2	NACHT and WD repeat domain containing 2	-1,34
Elavl4	ELAV (embryonic lethal, abnormal vision, Drosophila)-like 4 (Hu antigen D)	-1,34
Vav3	vav 3 oncogene	-1,34
Gm15478	predicted gene 15478 /// predicted gene 15478	-1,34
Ccdc23	coiled-coil domain containing 23	-1,34
Mob3a	MOB kinase activator 3A	-1,34

4930552P12Rik	RIKEN cDNA 4930552P12 gene /// RIKEN cDNA 4930552P12 gene	-1,34
Defb30	defensin beta 30	-1,34
Gper1	G protein-coupled estrogen receptor 1	-1,34
Msln	mesothelin	-1,34
LOC102641123	mitotic spindle assembly checkpoint protein MAD2A-like /// MAD2 mitotic arrest deficient-like 1	-1,34
17393960		-1,34
Gm3364	predicted gene 3364	-1,35
Igkv12-98	immunoglobulin kappa variable 12-98	-1,35
Ino80b	INO80 complex subunit B	-1,35
Grik1	glutamate receptor, ionotropic, kainate 1 /// glutamate receptor, ionotropic, kainate 1	-1,35
Rgs10	regulator of G-protein signalling 10	-1,35
Gm22072	predicted gene, 22072	-1,35
Heyl	hairy/enhancer-of-split related with YRPW motif-like	-1,35
17230327		-1,35
Slc4a8	solute carrier family 4 (anion exchanger), member 8	-1,35
LOC102635284	60S ribosomal protein L23a-like	-1,35
Itga6	integrin alpha 6	-1,35
Zfp90	zinc finger protein 90	-1,35
Slc2a8	solute carrier family 2, (facilitated glucose transporter), member 8	-1,35
Orm1	orosomucoid 1	-1,35
1700012L04Rik	RIKEN cDNA 1700012L04 gene /// predicted gene 14477 /// predicted gene 14476 /// predicted gene 14479 /// predicted gene 14482 /// predicted gene 14475 /// predicted gene 14501 /// predicted gene 14478 /// predicted gene 5382 /// predicted gene 14484 /// predicted gene 14474 /// predicted gene 14483 /// predicted gene 5132	-1,35
D4Ertd617e	DNA segment, Chr 4, ERATO Doi 617, expressed	-1,36
Zfp2	zinc finger protein 2	-1,36
Rhobtb2	Rho-related BTB domain containing 2 /// Rho-related BTB domain containing 2	-1,36
Ccdc86	coiled-coil domain containing 86	-1,36
Mir212	microRNA 212 /// microRNA 212	-1,36
Mir1981	microRNA 1981 /// microRNA 1981	-1,36
Rps28	ribosomal protein S28	-1,36
Pik3r6	phosphoinositide-3-kinase, regulatory subunit 6 /// phosphoinositide-3-kinase, regulatory subunit 6	-1,36
9330102E08Rik	RIKEN cDNA 9330102E08 gene	-1,36
Rnu3b4	U3B small nuclear RNA 4 /// U3B small nuclear RNA 2 /// U3B small nuclear RNA 1 /// U3B small nuclear RNA 3	-1,36
Poll	polymerase (DNA directed), lambda	-1,36
17274378		-1,36
Gm11772	predicted gene 11772	-1,36
Gm25092	predicted gene, 25092	-1,36
Gm26014	predicted gene, 26014	-1,36
Ngb	neuroglobin	-1,36
Zfp335os	zinc finger protein 335, opposite strand /// zinc finger protein 335, opposite strand	-1,36
Gm22728	predicted gene, 22728	-1,37
D130012P04Rik	RIKEN cDNA D130012P04 gene	-1,37
Glis1	GLIS family zinc finger 1	-1,37
Gm2799	predicted gene 2799	-1,37
1700021J08Rik	RIKEN cDNA 1700021J08 gene /// RIKEN cDNA 1700021J08 gene	-1,37
Msc	musculin /// musculin	-1,37
6430571L13Rik	RIKEN cDNA 6430571L13 gene	-1,37
4930565N06Rik	RIKEN cDNA 4930565N06 gene /// RIKEN cDNA 4930565N06 gene	-1,37
Snord49b	small nucleolar RNA, C/D box 49B /// small nucleolar RNA, C/D box 49B	-1,37
4933413G19Rik	RIKEN cDNA 4933413G19 gene	-1,37
Pet112	PET112 homolog (S. cerevisiae)	-1,37
Hcn2	hyperpolarization-activated, cyclic nucleotide-gated K+ 2	-1,37
Akap7	A kinase (PRKA) anchor protein 7 /// A kinase (PRKA) anchor protein 7	-1,37
Slco1a4	solute carrier organic anion transporter family, member 1a4	-1,37
Olfr366	olfactory receptor 366	-1,37
Gm17508	predicted gene, 17508	-1,37
Grin2c	glutamate receptor, ionotropic, NMDA2C (epsilon 3)	-1,37
Siae	sialic acid acetylesterase	-1,37
Plxna4os1	plexin A4, opposite strand 1 /// plexin A4, opposite strand 1	-1,37
B4galt7	xylosylprotein beta1,4-galactosyltransferase, polypeptide 7 (galactosyltransferase I)	-1,37
Gm24398	predicted gene, 24398	-1,37
1110034G24Rik	RIKEN cDNA 1110034G24 gene	-1,38
Gm10425	predicted gene 10425 /// exocyst complex component 3-like 4	-1,38
Gm24083	predicted gene, 24083	-1,38
Mir30c-1	microRNA 30c-1 /// microRNA 30c-1	-1,38
Kcnj11	potassium inwardly rectifying channel, subfamily J, member 11	-1,38
Ptch2	patched homolog 2	-1,38
Frat2	frequently rearranged in advanced T cell lymphomas 2	-1,38
Lrrc20	leucine rich repeat containing 20	-1,38
Nxt2	nuclear transport factor 2-like export factor 2	-1,38
Sctr	secretin receptor /// secretin receptor	-1,38
Pitpnm3	PITPNM family member 3	-1,38
Kcna5	potassium voltage-gated channel, shaker-related subfamily, member 5	-1,38
Ptpn2	protein tyrosine phosphatase, non-receptor type 2	-1,38
1700016L21Rik	RIKEN cDNA 1700016L21 gene	-1,39
Cyp4f17	cytochrome P450, family 4, subfamily f, polypeptide 17	-1,39
Gm16340	predicted gene 16340 /// predicted gene 16340	-1,39
Gm20063	predicted gene, 20063	-1,39
Gm19412	predicted gene, 19412	-1,39
Drd2	dopamine receptor D2	-1,39
Rgs19	regulator of G-protein signaling 19	-1,39
Gtf2h2	general transcription factor II H, polypeptide 2	-1,39
5430440P10Rik	RIKEN cDNA 5430440P10 gene	-1,40
1700042G15Rik	RIKEN cDNA 1700042G15 gene /// RIKEN cDNA 1700042G15 gene	-1,40
Sarm1	sterile alpha and HEAT/Armadillo motif containing 1	-1,40
Aldh1a7	aldehyde dehydrogenase family 1, subfamily A7	-1,40
Mir92b	microRNA 92b /// microRNA 92b	-1,40
Smad3	SMAD family member 3	-1,40
Naglu	alpha-N-acetylglucosaminidase (Sanfilippo disease IIIB) /// alpha-N-	-1,40

	acetylglucosaminidase (Sanfilippo disease IIIB)	
Cpsf4	cleavage and polyadenylation specific factor 4	-1,40
Plcb3	phospholipase C, beta 3	-1,40
Rmdn2	regulator of microtubule dynamics 2 /// regulator of microtubule dynamics 2	-1,40
Mir669m-1	microRNA 669m-1 /// microRNA 669m-1	-1,40
Gm19426	predicted gene, 19426 /// predicted gene, 19426	-1,40
2310061J03 Rik	RIKEN cDNA 2310061J03 gene	-1,40
Cys1	cystin 1 /// cystin 1	-1,40
Gm5045	predicted gene 5045	-1,40
LOC675947	multiple epidermal growth factor-like domains protein 6-like	-1,40
Sebox	SEBOX homeobox	-1,41
Tmem74bos	transmembrane 74B, opposite strand /// transmembrane 74B, opposite strand	-1,41
Otop1	otopetrin 1	-1,41
A730028G0 7Rik	RIKEN cDNA A730028G07 gene	-1,41
BC002059	cDNA sequence BC002059	-1,41
Pomc	pro-opiomelanocortin-alpha	-1,41
Gm26052	predicted gene, 26052	-1,41
2310069G1 6Rik	RIKEN cDNA 2310069G16 gene /// RIKEN cDNA 2310069G16 gene	-1,41
Ccbl2	cysteine conjugate-beta lyase 2	-1,41
4930479D1 7Rik	RIKEN cDNA 4930479D17 gene /// RIKEN cDNA 4930479D17 gene	-1,41
S100a4	S100 calcium binding protein A4 /// S100 calcium binding protein A4	-1,42
AU020206	expressed sequence AU020206 /// expressed sequence AU020206	-1,42
Zbtb7b	zinc finger and BTB domain containing 7B	-1,42
Samd14	sterile alpha motif domain containing 14	-1,42
Gm24218	predicted gene, 24218	-1,42
17549004		-1,42
Gm8122	predicted gene 8122	-1,42
Snrpb	small nuclear ribonucleoprotein B	-1,42
Fam53a	family with sequence similarity 53, member A	-1,42
Kctd15	potassium channel tetramerisation domain containing 15	-1,42
Rbpms	RNA binding protein gene with multiple splicing /// RNA binding protein gene with multiple splicing	-1,42
Sh3bp2	SH3-domain binding protein 2	-1,42
Zfp873	zinc finger protein 873	-1,42
G0s2	G0/G1 switch gene 2	-1,42
Col6a4	collagen, type VI, alpha 4	-1,43
Tmem42	transmembrane protein 42	-1,43
17455673		-1,43
Pddc1	Parkinson disease 7 domain containing 1	-1,43
2310040G2 4Rik	RIKEN cDNA 2310040G24 gene	-1,43
Cdc42ep4	CDC42 effector protein (Rho GTPase binding) 4 /// CDC42 effector protein (Rho GTPase binding) 4	-1,43
Akap12	A kinase (PRKA) anchor protein (gravin) 12	-1,43
4930524J08 Rik	RIKEN cDNA 4930524J08 gene /// RIKEN cDNA 4930524J08 gene	-1,43
Cthrc1	collagen triple helix repeat containing 1	-1,43
Btg1	B cell translocation gene 1, anti-proliferative	-1,43

A930017M0 1Rik	Smg-5 homolog, nonsense mediated mRNA decay factor pseudogene /// RIKEN cDNA 2310069G16 gene	-1,44
4932416H0 5Rik	RIKEN cDNA 4932416H05 gene	-1,44
Yae1d1	Yae1 domain containing 1	-1,44
Olfr605	olfactory receptor 605	-1,44
4930578M0 1Rik	RIKEN cDNA 4930578M01 gene /// RIKEN cDNA 4930578M01 gene	-1,44
D430040D2 4Rik	RIKEN cDNA D430040D24 gene /// RIKEN cDNA D430040D24 gene	-1,44
Eif3j2	eukaryotic translation initiation factor 3, subunit J2	-1,44
493340401 2Rik	RIKEN cDNA 4933404O12 gene /// RIKEN cDNA 4933404O12 gene	-1,44
Szrd1	SUZ RNA binding domain containing 1	-1,44
Map3k11	mitogen-activated protein kinase kinase kinase 11	-1,45
Plekha2	pleckstrin homology domain-containing, family A (phosphoinositide binding specific) member 2 /// predicted gene, 16933	-1,45
Gale	galactose-4-epimerase, UDP	-1,45
H2-K2	histocompatibility 2, K region locus 2 /// histocompatibility 2, K region locus 2	-1,45
Nap1l3	nucleosome assembly protein 1-like 3	-1,45
LOC102638 521	60S ribosomal protein L23a-like /// predicted gene 6096	-1,45
261004401 5Rik8	RIKEN cDNA 2610044O15 gene	-1,45
Gm19648	predicted gene, 19648	-1,45
Gm15458	predicted gene 15458	-1,45
Pramef8	PRAME family member 8	-1,45
Gm19696	predicted gene, 19696	-1,45
Gm23993	predicted gene, 23993	-1,45
Gsto2	glutathione S-transferase omega 2	-1,46
Gm4544	predicted gene 4544 /// predicted gene 4544	-1,46
Rrp15	ribosomal RNA processing 15 homolog (S. cerevisiae)	-1,46
17321622		-1,47
Slc25a33	solute carrier family 25, member 33	-1,47
Bricd5	BRICHOS domain containing 5	-1,47
Mpl	myeloproliferative leukemia virus oncogene	-1,47
Adk	adenosine kinase /// adenosine kinase	-1,47
Lzts3	leucine zipper, putative tumor suppressor family member 3	-1,47
Gm25083	predicted gene, 25083	-1,47
Gm9970	predicted gene 9970 /// predicted gene 9970	-1,47
n-R5s204	nuclear encoded rRNA 5S 204	-1,47
Rmnd1	required for meiotic nuclear division 1 homolog (S. cerevisiae)	-1,47
GENSCAN00 000030690		-1,47
Nkg7	natural killer cell group 7 sequence	-1,48
Sgpp2	sphingosine-1-phosphate phosphotase 2 /// sphingosine-1-phosphate phosphotase 2	-1,48
17549566		-1,48
Bach2	BTB and CNC homology 2	-1,48
Ghsr	growth hormone secretagogue receptor	-1,49
Pth2	parathyroid hormone 2	-1,49
Gm15706	predicted gene 15706 /// predicted gene 15706	-1,49
Ddx19b	DEAD (Asp-Glu-Ala-Asp) box polypeptide 19b	-1,49
D930015M0 5Rik	RIKEN cDNA D930015M05 gene /// RIKEN cDNA D930015M05 gene	-1,49
Gm25723	predicted gene, 25723	-1,49
AI987944	expressed sequence AI987944	-1,49

Fzd9	frizzled homolog 9 (Drosophila)	-1,49
C1galt1	core 1 synthase, glycoprotein-N-acetylgalactosamine 3-beta-galactosyltransferase, 1	-1,49
Lyz1	lysozyme 1	-1,49
Has2	hyaluronan synthase 2	-1,50
Gcnt1	glucosaminyl (N-acetyl) transferase 1, core 2	-1,50
Gm6728	predicted gene 6728	-1,50
Gm10322	predicted gene 10322 /// predicted gene 10322	-1,51
Chst13	carbohydrate (chondroitin 4) sulfotransferase 13	-1,51
Zfp937	zinc finger protein 937	-1,51
Gm24886	predicted gene, 24886	-1,52
Snord45b	small nucleolar RNA, C/D box 45B /// Rab geranylgeranyl transferase, b subunit /// small nucleolar RNA, C/D box 45B	-1,52
Tmem37	transmembrane protein 37	-1,52
Atp6v0a4	ATPase, H+ transporting, lysosomal V0 subunit A4	-1,52
Tmub2	transmembrane and ubiquitin-like domain containing 2 /// transmembrane and ubiquitin-like domain containing 2	-1,53
Gm4889	predicted gene 4889	-1,53
Hba-a2	hemoglobin alpha, adult chain 2 /// hemoglobin alpha, adult chain 1	-1,53
Gm15315	predicted gene 15315	-1,53
Gm23554	predicted gene, 23554	-1,53
NONMMUT029950		-1,54
Gm23100	predicted gene, 23100	-1,54
n-R5s183	nuclear encoded rRNA 5S 183	-1,54
Abcd1	ATP-binding cassette, sub-family D (ALD), member 1	-1,54
A630001G21Rik	RIKEN cDNA A630001G21 gene /// RIKEN cDNA A630001G21 gene	-1,55
Igkv4-73	immunoglobulin kappa variable 4-73	-1,55
Hhipl1	hedgehog interacting protein-like 1 /// hedgehog interacting protein-like 1	-1,55
Kansl2	KAT8 regulatory NSL complex subunit 2 /// KAT8 regulatory NSL complex subunit 2, pseudogene	-1,55
Gm6277	predicted gene 6277 /// predicted gene 6277	-1,56
Gm22889	predicted gene, 22889	-1,56
Gm17615	predicted gene, 17615	-1,56
Arl10	ADP-ribosylation factor-like 10 /// predicted gene, 24195	-1,56
A130010J15Rik	RIKEN cDNA A130010J15 gene	-1,56
Zfp941	zinc finger protein 941	-1,57
LOC102642252	uncharacterized LOC102642252 /// Immunoglobulin heavy chain (gamma polypeptide) /// immunoglobulin heavy constant mu /// immunoglobulin heavy chain (J558 family) /// immunoglobulin heavy variable 1-4	-1,57
Ormdl2	ORM1-like 2 (S. cerevisiae) /// predicted gene 5553	-1,57
Zkscan4	zinc finger with KRAB and SCAN domains 4	-1,57
Hist1h2af	histone cluster 1, H2af	-1,58
Slc25a15	solute carrier family 25 (mitochondrial carrier ornithine transporter), member 15	-1,58
LOC102635561	uncharacterized LOC102635561 /// predicted gene 10374	-1,58
Neurog1	neurogenin 1	-1,58
Mir2137	microRNA 2137 /// microRNA 2137	-1,58
Gna15	guanine nucleotide binding protein, alpha 15	-1,59
Olfr519	olfactory receptor 519	-1,59
Gm23099	predicted gene, 23099	-1,59
Gm22486	predicted gene, 22486	-1,60
Snord32a	small nucleolar RNA, C/D box 32A /// ribosomal protein L13A /// small nucleolar RNA, C/D box 32A	-1,60
Slc10a4	solute carrier family 10 (sodium/bile acid cotransporter family), member 4	-1,60
17220941		-1,60
Gm25650	predicted gene, 25650	-1,61
Xlr3a	X-linked lymphocyte-regulated 3A	-1,61
Gm26487	predicted gene, 26487	-1,61
1190007I07Rik	RIKEN cDNA 1190007I07 gene	-1,62
Ldhd	lactate dehydrogenase D	-1,62
NONMMUT014364		-1,62
Gm22741	predicted gene, 22741	-1,62
17399840		-1,63
Gm23437	predicted gene, 23437	-1,63
Gm5327	predicted pseudogene 5327	-1,63
AW047730	expressed sequence AW047730 /// expressed sequence AW047730	-1,63
Fam187a	family with sequence similarity 187, member A /// coiled-coil domain containing 103	-1,64
Gm6625	predicted gene 6625	-1,64
Gm24891	predicted gene, 24891	-1,64
Aph1a	anterior pharynx defective 1a homolog (C. elegans)	-1,66
Gm26066	predicted gene, 26066	-1,68
Gm25038	predicted gene, 25038	-1,68
17445451		-1,69
Atp6v1g3	ATPase, H+ transporting, lysosomal V1 subunit G3	-1,71
Sox3	SRY (sex determining region Y)-box 3	-1,75
Gm5635	predicted gene 5635	-1,78
n-R5s136	nuclear encoded rRNA 5S 136 /// nuclear encoded rRNA 5S 136	-1,79
Gm25147	predicted gene, 25147	-1,82
Rnu3a	U3A small nuclear RNA /// U3A small nuclear RNA	-1,83
Gm23567	predicted gene, 23567	-1,86
Gm23561	predicted gene, 23561	-1,86
Mir2137	microRNA 2137 /// microRNA 2137	-1,89
17542305		-1,91
Hba-a2	hemoglobin alpha, adult chain 2 /// hemoglobin alpha, adult chain 1	-1,92
Gm22696	predicted gene, 22696	-1,96
Trav9-2	T cell receptor alpha variable 9-2	-2,08
17547616		-2,24
Mir186	microRNA 186 /// microRNA 186	-2,61
Hbb-b2	hemoglobin, beta adult minor chain	-2,92